1990

Influence of strain hardening, strain aging and the Bauschinger effect on steel tubular strut load capacity

Jing Ping Lu
University of Wollongong

INFLUENCE OF STRAIN HARDENING, STRAIN AGING AND THE BAUSCHINGER EFFECT ON STEEL TUBULAR STRUT LOAD CAPACITY

A thesis submitted in fulfilment of the requirements
for the award of the degree of

Doctor of Philosophy

from

THE UNIVERSITY OF WOLLONGONG

by

JING PING LU, B.E.(Hons), M.E.(Hons)

DEPARTMENT OF CIVIL AND MINING ENGINEERING

March, 1990

DECLARATION

This is to certify that the work presented in this thesis was carried out by the author in the Department of Civil and Mining Engineering, The University of Wollongong, and has not been submitted to any other university or institute for a Degree except where specifically indicated.

JING PING LU

1990

ACKNOWLEDGEMENTS

This study was conducted in the Department of Civil and Mining Engineering, University of Wollongong. The author is indebted to Professor L.C. Schmidt, Head of the Department, her supervisor, for the close supervision, fruitful discussions, invaluable suggestions and generous help he has given for many years. The author also greatly appreciates the beneficial training in research skills given by him during the course of this study.

The experimental work was carried out in the Civil Engineering laboratories at the Universities of Wollongong and Melbourne. The author is grateful for facilities provided. Much appreciation is expressed to the entire technical staff of the laboratories for their assistance in the experimental work, in particular to Mr.Peter Morgan, Mr.R.Webb and Mr.Alan Lilleyman. The support of Tubemakers of Australia Pty Ltd. is also gratefully acknowledged.

The author held a University of Wollongong Scholarship for her PhD study. She greatly appreciates this generous grant.

The author also wishes to express her sincere gratitude to Dr.S.L.Chan (Department of Civil Engineering, Hong Kong Polytechnic) and Mr.F.G.A.Al-Bermani (Department of Civil Engineering, University of Queensland) for discussions and suggestions on computer programming.

The author is grateful to Associate Professors R.W.Upfold, Y.C.Loo and Professor Alan Hargraves for their interest in this study and encouragement.

Acknowledgement is also made to her colleagues and friends Mr.Y.H.Wu and Mr.J.G.Teng for help and encouragement.

Finally, special acknowledgement is made to her husband Wen Long Yue and her grandmother and her other family members for the understanding and encouragement during the period of this study.

ABSTRACT

A nonlinear finite element model for tracing the inelastic pre- and post-buckling load-deformation path of tubular struts has been developed. The analysis accounts simultaneously for both the geometrical and material nonlinearities. The influence of strain-unloading is included. In particular, the model takes into account a generalized stress-strain relationship and the influence of strain hardening. Several stress-strain relationships of the material are assumed with respect to as-received material, material that is prestrained in tension and fully-aged, and material that is prestrained in tension and unaged. The structure tangent stiffness matrix is obtained by using a series of transformation matrices to update the element geometry. A so-called arc-length iterative numerical procedure is combined with a modified Newton-Raphson method to obtain a solution to the incremental equations of equilibrium. The procedure has been applied to trace out the inelastic load-deflection paths of both as-received and prestrained pin-ended struts.

Material and strut tests have been performed on circular tubular sections of 60.3mm diameter and wall thickness 2.3mm. Several material effects (strain hardening, strain aging, the Bauschinger effect and residual stresses) have been included in the tests. The significant influence of these effects have been investigated by applying a two-way analysis variance to the strut test results. It has been found that the combined influence of strain aging, strain hardening and the Bauschinger effect have a dominant role in the test results referred to herein, with load capacity reductions up to 38%. Strain aging has been seen to be more significant than strain hardening for the rimming steel used in enhancing the capacity of the prestrained struts. The experimental results are also compared with the current

column design curves from ECCS, SSRC and existing and proposed Australian column curves.

By comparing the theoretical results with the experimental results of the as-received struts and the struts prestrained in tension, both fully-aged and unaged, it is shown that the developed theoretical model can accurately predict the experimental maximum loads and the post-buckling load-deflection paths of steel tubular struts.

TABLE OF CONTENTS

Chapter No. **Page No.**

TITLE PAGE..... - i -

DECLARATION..... - ii -

ACKNOWLEDGEMENT..... - iii -

ABSTRACT..... - v -

TABLE OF CONTENTS..... - vii -

LIST OF TABLES..... - xii -

LIST OF FIGURES..... - xiv-

NOTATION..... - xxiv -

LIST OF PUBLICATIONS DURING PhD STUDY..... -xxviii-

CHAPTER ONE INTRODUCTION..... 1-1

1.1 Introduction..... 1-1

1.2 Scope of Research..... 1-7

1.3 Outline of Thesis..... 1-9

CHAPTER TWO LITERATURE REVIEW..... 2-1

2.1 General..... 2-1

2.2 Definitions of Strain Hardening, Strain Aging and the Bauschinger Effect..... 2-2

2.3 Influence of Strut Load Capacity of Strain Hardening, Strain Aging, the Bauschinger Effect and Residual Stresses..... 2-6

2.4 Theoretical Solution Procedure..... 2-12

2.5 Present Research..... 2-18

CHAPTER THREE THEORETICAL DEVELOPMENT 3-1

3.1 General 3-1

3.2 Theoretical Model 3-1

3.2.1 Basic Assumptions 3-1

3.2.2 Total Potential Energy 3-5

3.2.3 Inelastic Model 3-10

3.2.4 Tangent Stiffness Matrix 3-12

3.2.5 Internal Resisting Forces 3-15

3.3 Method of Solution 3-18

3.4 An Outline of the Analysis Procedure 3-24

3.5 Justification of Computer Program 3-25

3.5.1 Comparison of Calculated Results by the Developed Program with an Elastic Analysis Solution of the Linear Bifurcation Load 3-25

3.5.2 Comparison of Calculated Results by the Developed Program with Those by a Nastran Package 3-28

3.5.2.1 Brief Introduction on Nastran Package .. 3-28

3.5.2.2 Tubular Struts Analysed Using Beam Element by Nastran Package 3-30

3.5.2.2.1 Idealised Elastic Perfectly Plastic Material 3-30

3.5.2.2.2 Generalised Elastic Plastic Material 3-30

3.5.3 Comparison of Theoretical Results with Kitipornchai and Chan (1986) 3-31

3.6 Numerical Applications 3-35

3.6.1 As-Received Struts..... 3-35
3.6.2 Struts That Are Prestrained in Tension and Fully-Aged..... 3-36
3.6.3 Struts That Are Prestrained in Tension and Unaged..... 3-37
3.6.4 Combined Results..... 3-41
3.6.5 The Effects of Strain Hardening..... 3-50
3.7 Summary..... 3-50

CHAPTER FOUR EXPERIMENTAL PROGRAM ... 4-1
4.1 General..... 4-1
4.2 Description of Material and Specimens..... 4-1
4.3 Instrumentation..... 4-7
4.4 Material Tests..... 4-17
4.4.1 Tests on As-Received Tensile and Compressive Tubes..... 4-17
4.4.2 Squash Tests on Prestrained ERW Tube and Tangent Modulus Et..... 4-20
4.4.3 Tests on Stress Relief Annealed As-Received and Prestrained ERW Tube..... 4-31
4.4.4 Strain Aging, Strain Hardening and the Bauschinger Effect..... 4-32
4.5 Strut Tests..... 4-36
4.5.1 Test Procedure..... 4-36
4.5.2 Initial Imperfections..... 4-44
4.5.3 Overall Strut Results..... 4-47
4.5.4 Discussion of Test Results..... 4-52
4.5.4.1 The Influence of Strain Hardening, Strain

Aging and the Bauschinger Effect..... 4-52
4.5.4.2 Post-Buckling Strength..... 4-62
4.5.5 Regression Results..... 4-66
4.5.6 Tangent Modulus Prediction..... 4-67
4.5.7 Comparison with Column Design Curves..... 4-72
4.5.7.1 European Column Curves..... 4-72
4.5.7.2 SSRC Column Curves..... 4-73
4.5.7.3 Existing and Proposed Australian Column Curves..... 4-73
4.6 Summary..... 4-79

CHAPTER FIVE STATISTICAL ANALYSES OF EXPERIMENTAL RESULTS OF MATERIAL EFFECTS ON STEEL TUBULAR STRUT LOAD CAPACITY..... 5-1
5.1 General..... 5-1
5.2 Basic Description of Analysis of Variance..... 5-1
5.3 Application of Analysis of Variance to Test Results..... 5-8
5.4 Discussion of Statistical Test Results..... 5-9
5.4.1 Influence of Slenderness Ratios..... 5-9
5.4.2 Influence of Strain Hardening, Strain Aging and the Bauschinger Effect..... 5-9
5.4.3 Influence of Steel Type..... 5-10
5.5 Summary..... 5-11

CHAPTER SIX COMPARISON AND DISCUSSION OF THEORETICAL EXPERIMENTAL RESULTS 6-1

6.1 General 6-1

6.2 Comparison of Theoretical and Experimental Load-Deformation Curves 6-1

6.3 Comparison of Theoretical and Experimental Maximum Column Loads 6-3

6.4 Discussion of Theoretical and Experimental Results 6-6

6.4.1 The Influence of Strain Hardening, Strain Aging and the Bauschinger Effect 6-6

6.4.2 The Influence of Initial Imperfection 6-8

6.5 Summary 6-13

CHAPTER SEVEN CONCLUSIONS AND RECOMMENDATIONS 7-1

7.1 Conclusions 7-1

7.2 Recommendations for Future Work 7-7

REFERENCES R-1

APPENDIX I DEFINITION OF MATRICES A-1

APPENDIX II EXECUTIVE CONTROL DECK, CASE CONTROL DECK AND BULK DATA DECK IN NASTRAN PACKAGE A-3

LIST OF TABLES

Table No.		Page No.
3.1	Percentage Errors vs Number of Elements	3-28
3.2	Summary of Failure and Post-Failure Condition (Theoretical Results)	3-48
4.1	ERW Tube	4-2
4.2	Material Properties of Rimming Steel	4-3
4.3	List and dimensions of Specimens for Strut Testing	4-5
4.4	Tensile Test Results	4-18
4.5	Squash Tests on As-Received ERW Tube	4-20
4.6	Squash Tests on Prestrained ERW Tube	4-22
4.7	Tangent Modulus Et	4-23
4.8	Yield Stresses and Transition Slenderness Ratios	4-48
4.9	Test Results of SRA Struts	4-49
4.10	Load Reduction of Prestrained Struts Compared with As-received Struts	4-60
4.11	Summary of Failure and Pos-Failure Condition (Experimental Results)	4-65
5.1	The Analysis of Variance Table	5-7
5.2	Observed and Critical Values of F	5-8
6.1	Comparison of Theoretical and Experimental Maximum Loads for As-Received Struts	6-4
6.2	Comparison of Theoretical and Experimental Maximum Loads for Prestrained and Fully-Aged Struts	6-5
6-3	Comparison of Theoretical and Experimental Maximum Loads for Prestrained and Unaged Struts	6-5
6.4	Load Reduction due to Initial Imperfections (from 0.0002L to 0.002L)	6-12

6.5	Magnitude of Deflections for Prestrained and Unaged Struts	6-12
6.6	Load Reduction due to the Bauschinger Effect	6-13
6.7	Combination of Initial Imperfections	6-13

LIST OF FIGURES

Figure No.		Page No.
1.1	The Sydney Football Stadium	1-1
1.2	The Avalon Aircraft Hangar in Melbourne	1-2
1.3	The Avalon Aircraft Hangar in Melbourne - at Ground Level	1-3
1.4	The Avalon Aircraft Hangar in Melbourne - Post-Tensioning Process	1-4
2.1	Stress-Strain Curves Illustrating Strain Hardening, Strain Aging & Bauschinger Effect	2-1
3.1(a)	Idealised Stress-Strain Relationship for As-Received Material	3-2
3.1(b)	Idealised Stress-Strain Relationship for Prestrained and Fully-Aged Material	3-3
3.1(c)	Idealised Stress-Strain Relationship for Prestrained and Unaged Material	3-4
3.2	Element Forces, Displacements and Coordinate Axes	3-14
3.3	Subdivision of Tube Section into Elementary Areas	3-14
3.4	Element Deformations	3-16
3.5	Flowchart for Computer Program	3-26
3.6	Convergence of the Finite Element Solution	3-32
3.7	Idealised Elastic Perfectly Plastic Stress-Strain Curve	3-32
3.8	Comparison of Theoretical Axial Load-Shortening Curves with Nastran	3-33
3.9	Arrangement of Plastic Rods	3-33
3.10	Comparison of Theoretical Axial Load-Shortening Curves	

	with Nastran - Prestrained in Tension Unaged Material	3-34
3.11	Comparison of Theoretical Axial Load-Shortening Curves with Chan and Kitipornchai (1986) and Nastran	3-34
3.12	Theoretical Curves of As-Received Struts	3-38
3.13	Post-Buckling Behaviour of Pin-ended struts	3-38
3.14	Theoretical Curves of 3% Prestrained Fully-Aged Struts	3-39
3.15	Theoretical Curves of 7% Prestrained Fully-Aged Struts	3-39
3.16	Theoretical Curves of 3% Prestrained Unaged Struts	3-40
3.17	Theoretical Curves of 7% Prestrained Unaged Struts	3-40
3.18	Theoretical Results - All Conditions	3-42
3.19	Theoretical Curves - All Conditions	3-43
3.20	Theoretical Curves - All Conditions	3-43
3.21	Theoretical Curves - All Conditions	3-44
3.22	Theoretical Curves - All Conditions	3-44
3.23	Theoretical Curves - All Conditions	3-45
3.24	Theoretical Curves - All Conditions	3-45
3.24a	Definition of σ_{peak}/σ_y and σ_{Re}/σ_y	3-51
3.25	Residual Load Capacity versus Normalised Slenderness Ratio	3-52
3.26	Percentage of Residual Load Capacity Relative to Peak Load Capacity versus Normalised Slenderness Ratio	3-52
3.27	Theoretical Curves with Variation of Es As-Received Strut	3-53
3.28	Theoretical Curves with Variation of Es	

	As-Received Strut	3-53
3.29	Theoretical Curves with Variation of Es	
	3% Prestrained Fully-Aged Strut	3-54
3.30	Theoretical Curves with Variation of Es	
	3% Prestrained Fully-Aged Strut	3-54
3.31	Theoretical Curves with Variation of Es	
	3% Prestrained Unaged Strut	3-55
3.32	Theoretical Curves with Variation of Es	
	3% Prestrained Unaged Strut	3-55
4.1	Tensile Specimens	4-4
4.2	Compressive Specimens	4-4
4.3	Reaction Loading Frame showing Actuator	
	and Transducers	4-8
4.4	Typical Closed Loop Servo - Block Diagram	4-9
4.5	Loading Frame for Stretching	4-10
4.6	Federhaf Universal Testing Machine	4-11
4.7	Extensometer	4-12
4.8	Data Acquisition / Control System	4-15
4.9	Flowchart	4-16
4.10	Tensile and Compressive Stress-Strain Curves	4-19
4.11	Typical Stress-Strain Curves for As-Received Material	4-19
4.12	Stub-Column Test - As-Received Tubes	4-24
4.13	Stub-Column Test - 3% Prestrained, Fully-Aged	4-24
4.14	Stub-Column Test - 7% Prestrained, Fully-Aged	4-25
4.15	Stub-Column Test - 3% Prestrained, Unaged	4-25
4.16	Stub-Column Test - 7% Prestrained, Unaged	4-26
4.17	Stub-Column Test Results Under Different Conditions	4-26
4.18	Tangent Modulus vs Stress - ERW Tube	

	As-Received	4-27
4.19	Tangent Modulus vs Stress - ERW Tube	
	3% Prestrained, Fully-Aged	4-27
4.20	Tangent Modulus vs Stress - ERW Tube	
	7% Prestrained, Fully-Aged	4-28
4.21	Tangent Modulus vs Stress, SRA	
	7% Prestrained, Fully-Aged	4-28
4.22	Tangent Modulus vs Stress - ERW Tube	
	3% Prestrained, Unaged	4-29
4.23	Tangent Modulus vs Stress - ERW Tube	
	7% Prestrained, Unaged	4-29
4.24	Tangent Modulus vs Stress, SRA	
	3% Prestrained, Unaged	4-30
4.25	Tangent Modulus vs Stress - ERW Tube	
	All Conditions	4-30
4.26	Strain Aging of ERW Tube - Tension/Tension,	
	Tension/Compression and Compression/Compression	4-34
4.27	Tubes on Annealing Furnace Base	4-39
4.28	Internal Furnace Cover	4-40
4.29	Outside Furnace Cover	4-41
4.30	Tubes after Annealing	4-42
4.31	Knife Edge End Support	4-43
4.32	Test Set Up	4-45
4.33	Buckling Mode	4-45
4.34	Initial Deflection	4-46
4.35	End Alignment	4-46
4.36	Strut Load Capacity versus Slenderness Ratio	4-50
4.37	Strut Test Results - Stress Axis Normalised	4-50

4.38	Normalised Critical Stress Versus Normalised Slenderness Ratio Plots of Test Results	4-51
4.39	Test Results - Stress Relief Annealed	4-53
4.40	Test Results of As-Received Struts	4-53
4.41	Test Results of 3% Prestrained Fully-Aged Struts	4-54
4.42	Test Results of 7% Prestrained Fully-Aged Struts	4-54
4.43	Test Results of 3% Prestrained Unaged Struts	4-55
4.44	Test Results of 7% Prestrained Unaged Struts	4-55
4.45	Test Results - All Conditions	4-56
4.46	Test Results - All Conditions	4-56
4.47	Test Results - All Conditions	4-57
4.48	Test Results - All Conditions	4-57
4.49	Test Results - All Conditions	4-58
4.50	Test Results - All Conditions	4-58
4.51	Test Results - All Conditions	4-68
4.52	Strut Load Capacity vs Slenderness Ratio	4-69
4.53	Normalised Critical Stress vs Normalised Slenderness Ratio	4-69
4.54	Test Results and Tangent Modulus Curves - As-Received and 7% Prestrained	4-70
4.55	Test Results and Tangent Modulus Curves - 3% Prestrained	4-70
4.56	Test Results and Tangent Modulus Curves - 7% Prestrained	4-71
4.57	Comparison of ECCS Column Curves with Test Results	4-74
4.58	Comparison of SSRC Column Curves with Test Results	4-74
4.59	Comparison of AS1250(1981) Column Curves with Test Results	4-78

4.60	Comparison of Column Curves Based on Rotter(1982) with Test Results	4-78
5.1	Normalised Test Results of 1983 and 1984 (ERW and HFW)	5-13
5.2	Combined Test Results 1983,1984 and 1987 (ERW and HFW)	5-14
5.3	Test Results of As-Received and Prestrained Unaged Strut	5-14
5.4	Test Results of As-Received Fully-Aged Struts	5-15
5.5	Test Results of All Struts Prestrained in Tension and Fully-Aged	5-15
6.1	Comparison of Theoretical and Experimental Curves - As-Received Struts	6-15
6.2	Comparison of Theoretical and Experimental Curves - As-Received Struts	6-15
6.3	Comparison of Theoretical and Experimental Curves - As-Received Struts	6-16
6.4	Comparison of Theoretical and Experimental Curves - As-Received Struts	6-16
6.5	Comparison of Theoretical and Experimental Curves - As-Received Struts	6-17
6.6	Comparison of Theoretical and Experimental Curves - As-Received Struts	6-17
6.7	Comparison of Theoretical and Experimental Curves - 3% Prestrained, Fully-Aged	6-18
6.8	Comparison of Theoretical and Experimental Curves - 3% Prestrained, Fully-Aged	6-18
6.9	Comparison of Theoretical and Experimental Curves	

	- 3% Prestrained, Fully-Aged	6-19
6.10	Comparison of Theoretical and Experimental Curves	
	- 3% Prestrained, Fully-Aged	6-19
6.11	Comparison of Theoretical and Experimental Curves	
	- 3% Prestrained, Fully-Aged	6-20
6.12	Comparison of Theoretical and Experimental Curves	
	- 3% Prestrained, Fully-Aged	6-20
6.13	Comparison of Theoretical and Experimental Curves	
	- 7% Prestrained, Fully-Aged	6-21
6.14	Comparison of Theoretical and Experimental Curves	
	- 7% Prestrained, Fully-Aged	6-21
6.15	Comparison of Theoretical and Experimental Curves	
	- 7% Prestrained, Fully-Aged	6-22
6.16	Comparison of Theoretical and Experimental Curves	
	- 7% Prestrained, Fully-Aged	6-22
6.17	Comparison of Theoretical and Experimental Curves	
	- 7% Prestrained, Fully-Aged	6-23
6.18	Comparison of Theoretical and Experimental Curves	
	- 7% Prestrained, Fully-Aged	6-23
6.19	Comparison of Theoretical and Experimental Curves	
	- 3% Prestrained, Unaged	6-24
6.20	Comparison of Theoretical and Experimental Curves	
	- 3% Prestrained, Unaged	6-24
6.21	Comparison of Theoretical and Experimental Curves	
	- 3% Prestrained, Unaged	6-25
6.22	Comparison of Theoretical and Experimental Curves	
	- 3% Prestrained, Unaged	6-25
6.23	Comparison of Theoretical and Experimental Curves	

	- 3% Prestrained, Unaged	6-26
6.24	Comparison of Theoretical and Experimental Curves	
	- 3% Prestrained, Unaged	6-26
6.25	Comparison of Theoretical and Experimental Curves	
	- 7% Prestrained, Unaged	6-27
6.26	Comparison of Theoretical and Experimental Curves	
	- 7% Prestrained, Unaged	6-27
6.27	Comparison of Theoretical and Experimental Curves	
	- 7% Prestrained, Unaged	6-28
6.28	Comparison of Theoretical and Experimental Curves	
	- 7% Prestrained, Unaged	6-28
6.29	Comparison of Theoretical and Experimental Curves	
	- 7% Prestrained, Unaged	6-29
6.30	Comparison of Theoretical and Experimental Curves	
	- 7% Prestrained, Unaged	6-29
6.31	Comparison of Theoretical and Testing Results	6-30
6.32	Comparison of Theoretical and Experimental	
	Maximum Loads As-Received and 7% Prestrained	6-31
6.33	Comparison of Theoretical and Experimental	
	Maximum Loads 3% Prestrained	6-31
6.34	Theoretical Results with Different Initial Imperfections	
	As-Received	6-32
6.35	Theoretical Results with Different Initial Imperfections	
	Pre.3%, Unaged	6-32
6.36	Theoretical Axial Load-Deflection Curves with Varying	
	Initial Out-of-Straightness - As-Received Struts	6-33
6.37	Theoretical Axial Load-Deflection Curves with Varying	
	Initial Out-of-Straightness - As-Received Struts	6-34

6.38	Theoretical Axial Load-Deflection Curves with Varying Initial Out-of-Straightness - As-Received Struts	6-35
6.39	Theoretical Axial Load-Deflection Curves with Varying Initial Out-of-Straightness - As-Received Struts	6-36
6.40	Theoretical Axial Load-Deflection Curves with Varying Initial Out-of-Straightness - As-Received Struts	6-37
6.41	Theoretical Axial Load-Deflection Curves with Varying Initial Out-of-Straightness - As-Received Struts	6-38
6.42	Theoretical Axial Load-Deflection Curves with Varying Initial Out-of-Straightness - 3% Prestrained Unaged Struts	6-39
6.43	Theoretical Axial Load-Deflection Curves with Varying Initial Out-of-Straightness - 3% Prestrained Unaged Struts	6-40
6.44	Theoretical Axial Load-Deflection Curves with Varying Initial Out-of-Straightness - 3% Prestrained Unaged Struts	6-41
6.45	Theoretical Axial Load-Deflection Curves with Varying Initial Out-of-Straightness - 3% Prestrained Unaged Struts	6-42
6.46	Theoretical Axial Load-Deflection Curves with Varying Initial Out-of-Straightness - 3% Prestrained Unaged Struts	6-43
6.47	Theoretical Axial Load-Deflection Curves with Varying Initial Out-of-Straightness - 3% Prestrained Unaged Struts	6-44
6.48	As-Received Struts	6-45
6.49	3% Prestrained Unaged Struts	6-45

6.50 Theoretical Axial Load-Deflection Curves with Both Initial Out-of-Straightness and Load Eccentricity 6-46

6.51 Theoretical Axial Load-Deflection Curves with Both Initial Out-of-Straightness and Load Eccentricity 6-47

NOTATION

a	= Modifying function,
A	= Area,
A_e	= Area of elastic core,
AR	= As-received,
b	= Calibration factor,
[B]	= Strain / displacement matrix,
B_ω	= Bimoment,
[C1],[C2]	= Transformation matrices,
c	= A constant,
Con.	= Condition,
D_i	= The axial deflection read from micrometer for calibration,
E	= Young's modulus,
EA	= Axial rigidity,
ECCS	= The European Convention for Constructional Steelwork,
EI_x, EI_y	= Flexural rigidity about the x and y axes,
EI_w	= Warping rigidity,
ERW	= Electric Resistance Welded,
Es	= Strain hardening modulus,
E_t, E_T,E_X	= Tangent modulus in inelastic range, see Fig.3.1(c)
F_A,F_B	= Observed F values in F test,
$F_{A0.05}$,$F_{B0.05}$	= Critical F values for 5 percent significance level,
FA	= Fully - aged,
$\{F_e\}$,$\{F_e'\}$	= Nodal force vectors (equations 3.12 and 3.13a),
$\{F\}_i$	= Total applied force vector,
GJ	= St. Venant torsional rigidity,

HFW	= Hot fusion welded,
I_d, I_{j-1}	= Desired number of iterations and the number of iterations for convergence in the (j-1)th cycle,
$[K_G]$,$[K_L]$	= Geometric stiffness and linear stiffness matrices of an element,
$[K_T]$	= Tangent stiffness matrix of a member,
L	= Length of a member,
L_e	= Length of an element,
L/r, λ	= Slenderness ratio,
$(L/r)_T$, λ_T	= Transition slenderness ratio (value at which the Euler critical stress equals the yield stress of the material),
LVDT	= Linear variable deflection transducer,
Mx,My,Mz	= Internal resisting moments,
M_{x1},M_{x2}	= End moments at ends 1 and 2 of an element,
NA	= Unaged,
n	= Number of elementary areas,
n1	= Number of readings in calibration,
O.D.	= Outside diameter,
P	= Axial load,
Pcr	= Buckling load,
P_y	= Squash load,
Q_x,Q_y	= Shear forces,
R	= Wagner effect,
$\{r\}_i$	= Total displacement vector,
$R_{t0.5}$	= 0.5% total elongation proof stress,
SHR	= Strain hardening ratio,
S_o	= Original cross-sectional area within the gauge length,
SRA	= Stress relief annealing,

SSA, SSB = Between sample sums of squares,

SSE = Error sum of squares,

$SSRC$ = The Structural Steel Research Council,

TOL = The convergence tolerance,

u, v, w = The lateral displacement, transverse displacement and axial displacement,

$u_o, v_o,$ = Initial deformations,

u_m, v_m, w_m = End displacements,

Vi = Output voltage from HP computer,

$\bar{x}$ = Grand mean,

$\bar{x}_{i.}$ = Mean of the sample from the ith population, see eq.(5.3),

$\bar{x}_{.j}$ = Mean of the sample from the jth population, see eq.(5.3),

α_{x1}, α_{x2} = Total rotations at ends 1 and 2 of an element,

α_i, β_j = Effects of the two variables considered in a two-way analysis of variance test,

$\beta_x, \beta_y, \beta_\alpha$ = monosymmetry parameters of the cross section (equations (3.2), (3.3) and (3.4)),

ε = Strain,

ε_y = Yield strain,

ε_s = Proportional strain,

ε_x = Strain defined in the range between the proportional and yield strain,

ε_{peak} = Strain at peak (ultimate) stress,

ε_{pi} = Irreversible plastic strain,

$\{\phi_m\}$ = Linear displacement function (equation 3.9),

ϕ_x = Average curvature,

$\{\psi_m\}$ = Hermite polynomials (equation 3.10),

μ_x = The rigid body rotation,

θ = Angle of twist,

θ_{x1}, θ_{x2} = The relative rotations at ends 1 and 2 of an element with respect to the deflected chord,

σ = Stress,

σ^2 = Common variance,

σ_{cr} = Buckling stress (Critical stress),

σ_{peak}/σ_y = Normalised maximum load capacity,

σ_{Re}/σ_y = Normalised residual load capacity,

σ_s = Proportional stress,

σ_x = Stress defined in the range between the proportional and yield stress,

σ_y = Yield stress,

σ_u = Ultimate stress (Maximum stress),

δ_o = Initial imperfection (Initial lateral deflection),

δ, δ_p = Lateral deflection and lateral deflection at peak load,

γ_1, γ_2 = Equation 3.56,

Δ = Axial shortening,

$\underline{\Delta}$ = Vector of nodal deflection,

ΔA = Elementary area,

$\{\Delta F_a\}$ = Arbitrary referenced load increment vector,

$\{\Delta F\}_R$ = Unbalanced force vector,

$\{\Delta r_a\}$ = Incremental displacement due to $\{\Delta F_a\}$,

$\{\Delta r\}_R$ = Incremental displacement due to the residual force $\{\Delta F\}_R$,

ΔL = Arc-length,

$\Delta\lambda_i$ = Load mutiplier,

π_p = Total potential energy,

η = Imperfection parameter,

LIST OF PUBLICATIONS DURING PhD STUDY

1. Lu, J.P., Guo, Z.T. and Chen, S.F.(1988) " Buckling of I-beam columns", Journal of Structural Engineering, ASCE., Vol.114, No.9, Sep., pp.2109-2118.

2. Schmidt, L.C. and Lu, J.P. (1988) " Procedures for determining the stability of space truss system, Proceedings of 11th ASCMSM, University of Auckland, New Zealand, pp.301-305.

3. Schmidt, L.C., Lu.J.P. and Morgan, P.R. (1989) " The influence on steel tubular strut load capacity of strain hardening, strain aging and Bauschinger effect", Journal of Constructional Steel Research, Vol.14, No.2, pp.107-109.

4. Schmidt, L.C., Cook, G.and Lu, J.P. (1989) " Effect of brittle-type slip behaviour in friction grip joints", Proceedings of International Conference, I.A.B.S.E. Moscow.

5. Schmidt, L.C., Wu, Y.H. and Lu, J.P. (1989) " Effect of tectonic stress on the stability of slopes", Proceedings of Second Large Open Pit Mining Conference, Latrobe Valley, Victoria, April, pp.217-220.

6. Schmidt, L.C., Wu, Y.H. and Lu, J.P. (1989) " Application of non-tension elastic-plastic finite element model to stability analysis of masonry structures", STRUCENG, Structural Engineering, Numerical and Experimental Analysis, Los Angeles/USA, 9-11 August.

7. Schmidt, L.C., Lu, J.P. and Morgan, P.R. " Material effects - statistics of steel tube struts ", submitted for publication.

8. Schmidt, L.C. and Lu, J.P. " Tests of stress-relief-annealed steel tubular struts", submitted for publication.

CHAPTER ONE

INTRODUCTION

1.1 INTRODUCTION

Information on the inelastic behaviour and buckling performance of tubular members is essential for a realistic assessment of strength and risk in off-shore and spatial structures. Cylindrical tubular members are the most important components in off-shore structures for various reasons: e.g., they minimize hydrodynamic forces, have great torsional rigidity, offer local strength against impact loading, and minimize the outside surface subject to corrosion. Above all, they have the same buckling strength in all directions, both locally and overall.

Steel tubular members are also widely used in the modern buildings. One of the many examples is " The Sydney Football Stadium " shown in Fig.1.1. Another example is " The Avalon Aircraft Hangar in Melbourne " (see Fig.1.2), which was built using the Strarch concepts. The trusses, which are prefabricated in segments, and assembled on site at ground level (Fig.1.3), are then the whole structure is stressed into shape by a post-tensioning process (Fig.1.4).

In the production of metal structural members the material can pass through an additional variety of processes subsequent to those used in the production of the parent material. These processes may enhance certain properties, but may reduce others. For example, the application of cold work may increase the tensile yield strength but reduce the ductility of a mild steel, while the thermal treatment

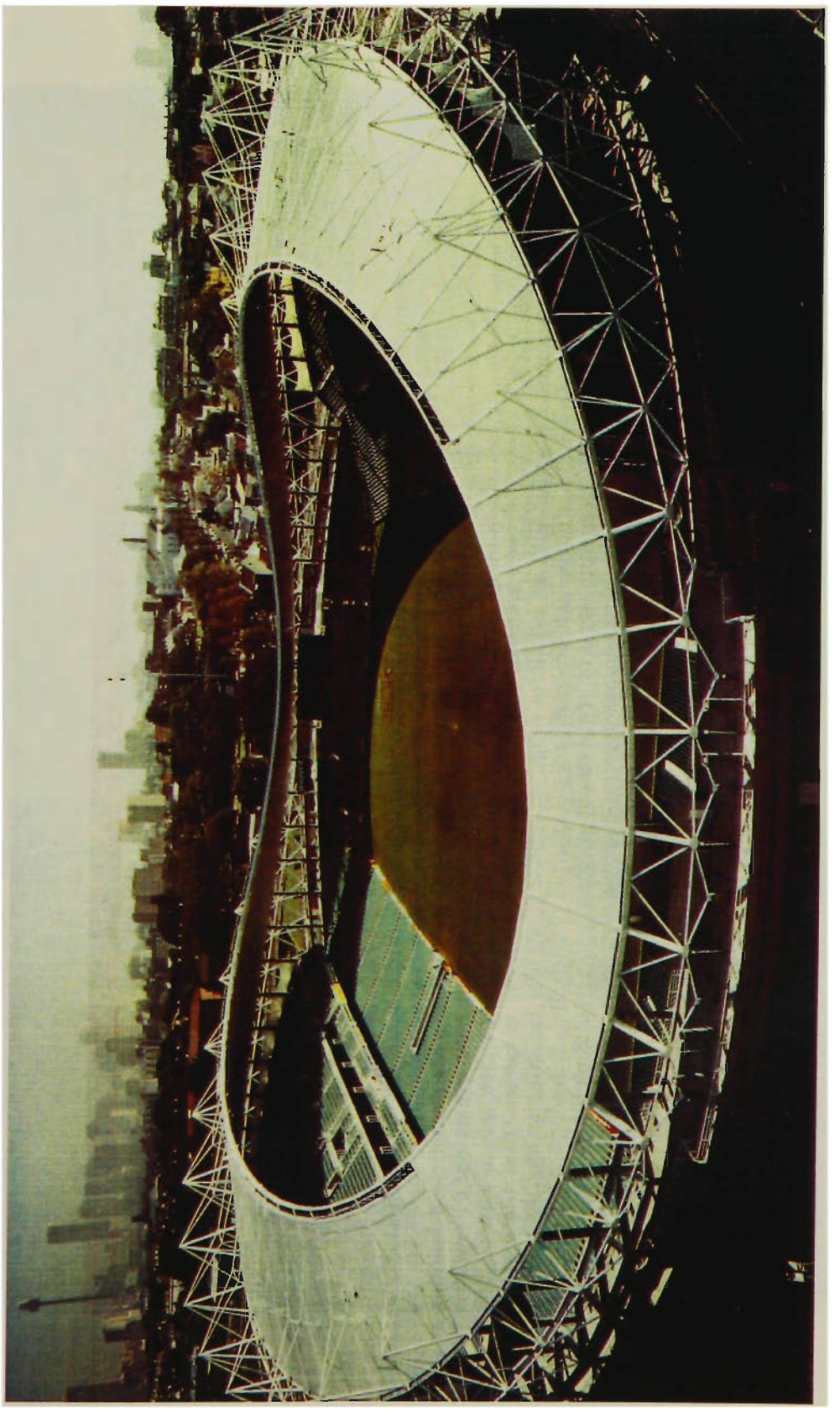

Fig.1.1 The Sydney Football Stadium

Fig.1.2 The Avalon Aircraft Hangar in Melbourne

Fig.1.3 The Avalon Aircraft Hangar in Melbourne - at Ground Level

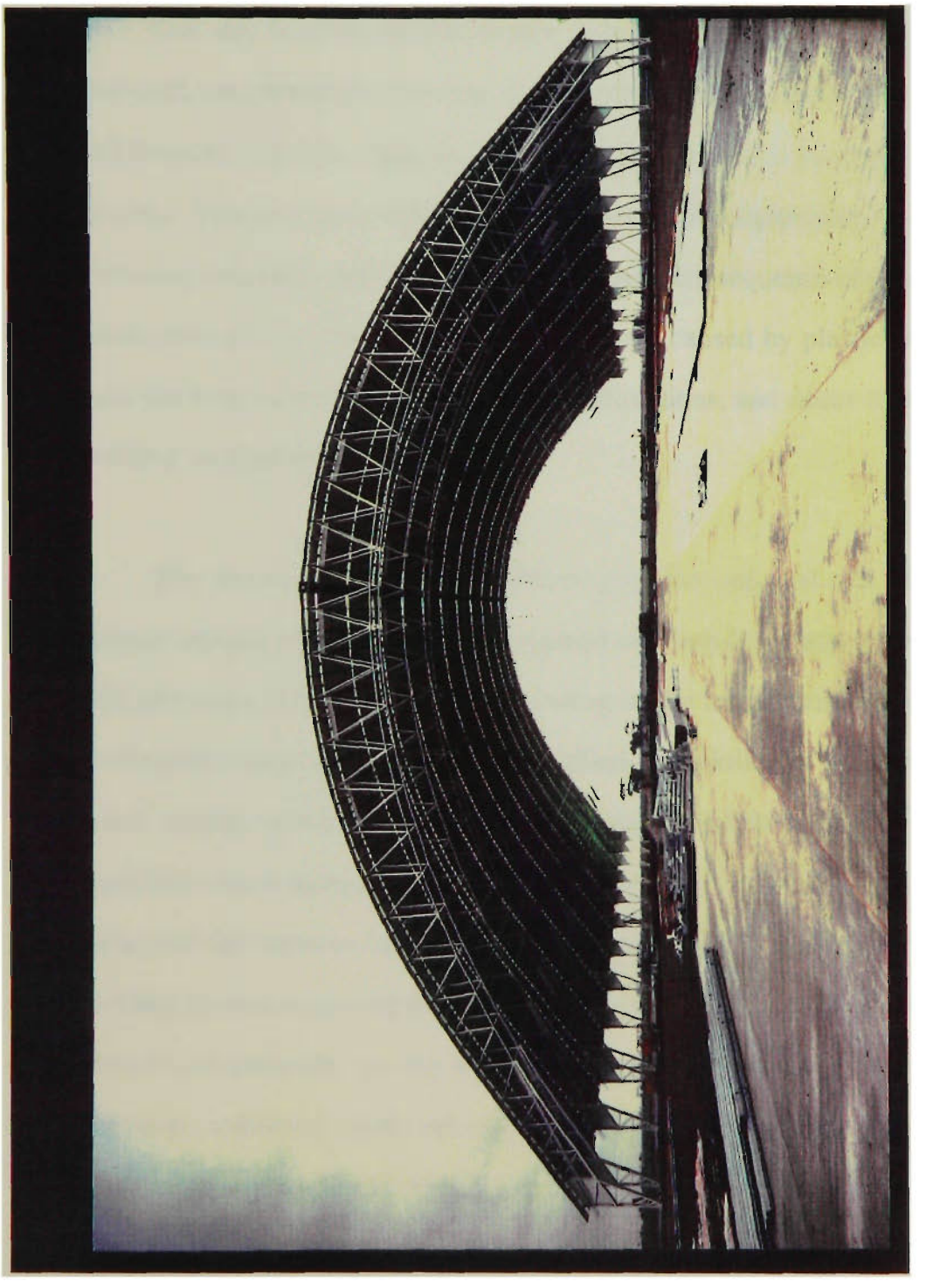

Fig.1.4 The Avalon Aircraft Hangar in Melbourne
- Post-Tensioning Process

of annealing may lower the yield strength but improve the ductility of a previously cold worked member.

One way in which circular tubular members are manufactured is by a process that cold straightens the flat strip from preformed coils, passes the strip through roll formers, and then welds the edges together by an electric-resistance welding process. This process is followed by further roll straightening to overcome the distortion caused by the welding operation. As a consequence of these steps in the production process, residual stress patterns are caused by plastic deformation in both the longitudinal and circumferential directions, and occur together with the welding residual stresses.

The processes of cold straightening of the coil and roll forming into a circular section cause the steel to be strained well into the plastic range; strain aging will take place slowly or quickly depending on the temperature and can be related to the type of steel used, whether fully-killed, semi-killed or rimmed. Fully-killed steels display virtually no strain aging capacity, whereas rimming steels offer significant strain aging. Semi-killed steels have an intermediate tendency for strain aging and fall between fully-killed and rimmed steels in this regard. Owing to the welding process occurring after these operations, strain aging probably takes place almost immediately, as the temperature of the material rises significantly. However, additional plastic straining occurs in the final roll straightening operation and further strain aging is probably complete. Depending on the type of mild steel used in the tube production process, an enhanced yield point may result, offsetting to some extent the effects of the residual stresses. For example, a rimmed steel is more sensitive to a strain aging gain in strength than a fully killed steel in which no strain aging is displayed.

Tubular members are often cold formed during fabrication, and they may also be cold formed during erection. In service such members may be subjected to overload, and therefore yielding, under quasi-static conditions. If stress reversal should occur then the material of the member suffers a change in its structural properties; rarely will these changes be beneficial. In some cases, suppliers of material modify the properties of members by additional cold work; usually the tensile strength is enhanced. Cold forming or straining never causes an increase, but usually a decrease in yield strength during loading in the opposite direction from the initial straining. This reduction is referred to as the Bauschinger effect, which is interactive with both strain aging and strain hardening effects during strut loading. A caution is necessary here, as designers often consider the tensile yield stress as the only significant material property in the determination of member strength. Under stress reversal into the compressive stress range, the properties of members can be modified significantly. Allowance needs to be made for this effect.

The purpose of this thesis is to analyse and study the influence of strain hardening, strain aging, the Bauschinger effect, initial geometric imperfections and residual stresses on strut load capacity by theoretical analysis and experimental investigation.

1.2 SCOPE OF RESEARCH

Referring to previous investigations, which are reviewed in Chapter two, the current research principally concerns the following areas :

(1) establishing a mathematical model of tubular strut behaviour based on the finite element method.

(2) establishing a numerical algorithm and its program to study the tubular strut behaviour.

(3) applying the developed theoretical model to numerical examples of structural members.

(4) reporting the details of the material and strut tests used to investigate the influence of strain aging, strain hardening and the Bauschinger effect.

(5) comparing the theoretical and experimental results and giving the general discussions.

(6) summarizing the research work conducted and making conclusions and recommendations for future work.

The strut tests are performed under eight different conditions :

(i) Two sets of as-received struts (series 1) (Here, "two sets" consists of twelve struts with six different lengths , each length including two struts);
(ii) Two sets of 3% prestrained fully aged struts (series 2) ;
(iii) Two sets of 3% prestrained but unaged struts (series 3) ;
(iv) Two sets of 7% prestrained fully aged struts (series 4) ;
(v) Two sets of 7% prestrained but unaged struts (series 5) (For series 1 to series 5, strut lengths are between 750 and 2998mm) ;
(vi) Two sets of stress relief annealed 3% prestrained but unaged struts

(series 6) ;

(vii) Two sets of stress relief annealed 7% prestrained fully aged struts (series7) ;

(viii) One set of stress relief annealed as-received struts (series 8).

(For series 6, series 7 and series 8, strut lengths are between 750 and 1875mm).

1.3 OUTLINE OF THESIS

There are seven Chapters in the thesis presented in order to furnish the primary objective proposed in Section 1.1.

Chapter One introduces the research project, in which the objective and the scope of the research are highlighted.

Previous research on strut behaviour determined from both theoretical analysis and experimental investigations is reviewed in Chapter Two, in which the importance and the required areas of the current research are indicated.

In Chapter Three, a mathematical model of tubular strut behaviour based on the finite element method is developed. The model includes both material and geometrical nonlinearities. Three stress-strain relationships are assumed with respect to the as-received struts, the struts that are prestrained in tension and fully-aged, and the struts that are prestrained in tension and unaged . A numerical algorithm and its program are established. The developed theoretical model is applied to numerical examples of structural members, and some parametric studies are carried out. The numerical results presented are also compared with results obtained from a commercial computer package and from other workers.

The details of the material and strut tests on the influence of strain hardening, strain aging and the Bauschinger effect are reported in Chapter Four. Regression analyses are used to provide an unbiased trend in the strut test results. The load capacities of all struts are predicted using the tangent modulus method based on the compressive load-deformation plot of the stub column tests. The experimental results are also compared with current column design curves, ECCS, SSRC, and existing and proposed Australian column curves.

The significant influence of material effects such as strain aging, strain hardening and the Bauschinger effect on strut load capacity is investigated by applying a two-way analysis of variance test in Chapter Five.

Chapter Six discusses the comparison of the theoretical and experimental results.

Chapter Seven presents conclusions of the research work and recommendations for future work.

CHAPTER TWO

LITERATURE REVIEW

2.1 GENERAL

Strut load capacity not only relates to variables such as initial imperfections, slenderness ratio, and yield strength, but also to variables such as material type and the process of production. Although the research on strut stability has been carried out for many years and significant achievements have been made both in theoretical analyses and experimental investigations, there are few papers on the influence on strut load capacity of strain hardening, strain aging and the Bauschinger effect. But in practical structures using steel tubular members, the members are often cold formed during fabrication, and may also be cold formed during erection. Cold forming or straining always causes a decrease in yield strength (although this decrease may be very small for some steels) during loading in the opposite direction from the initial straining. This reduction is referred to as the Bauschinger effect, which is interactive with both strain aging and strain hardening effects during strut loading. It is important, therefore, to analyze and study the practical influence on strut load capacity of strain hardening , strain aging and the Bauschinger effect. Pilot studies in this area have been carried out by Pavlovic and Stevens (1981), and Morgan and Schmidt (1985).

2.2 DEFINITIONS OF STRAIN HARDENING, STRAIN AGING AND THE BAUSCHINGER EFFECT

"Strain hardening" is the term used to define the increase in strength with increasing strain as plastic deformation or flow occurs beyond the yield point (Morgan and Schmidt, 1985) . That is, when a steel specimen is loaded in the plastic range, unloaded, and immediately reloaded in the same direction, the yield strength of the mild steel is increased up to the point where the specimen was unloaded. This phenomenon is described as strain hardening. According to Polakowski's view(1966), as strain-hardening is a permanent property only at a temperature less than about 35% to 40% of the absolute melting temperature, it is said to result from cold-work or cold-deformation. Fig. 2.1 shows stress-strain curves that illustrate significant aspects of the strain hardening, strain aging and the Bauschinger effect (Morgan and Schmidt, 1985). Path ABCD includes the strain hardening effect; path ABCDQ includes strain hardening and the Bauschinger effect; path ABCEFGHR includes strain hardening, strain aging and the Bauschinger effect. Curves labeled C', D', and H' are reflected reverse images of the corresponding parts of the virgin curve, and are included as reference curves (Morgan and Schmidt, 1985).

The Bauschinger effect can be described in terms of three parameters: strain, stress or strain energy as discussed by Abel et al.(1972), who explained that the principal causes are believed to be associated with elastic stress and/or anisotropy in the resistance to dislocation motion. The Bauschinger energy parameter appears to offer the best measure as a single parameter which evaluates the magnitude of the Bauschinger effect (Abel et al., 1972). The Bauschinger effect involves not only the initial yield strength, but also the entire stress-strain curve after prestraining . The density of mobile dislocations created

by prestrain seems to be the most important factor affecting the magnitude of the Bauschinger effect. Rolfe et al.(1968) analyzed the effect of the state-of-stress and the yield criterion on the Bauschinger effect by a series of test results. As different amounts of prestraining were applied in tension or in compression before stress reversal, the tests included the influence of strain hardening. Bauschinger loss on load reversal was observed whether the prestraining was in tension or in compression, and this effect depended on the particular strain offset used to determine yield strength. It was further observed that moduli measured from the reverse loading curve were sensitive to the prestrain condition. As these moduli are the basis for the Tangent or Reduced Modulus strut capacity predictions the stress history during the manufacture of steel struts is seen to be important. The permanent compressive strain in the transverse direction (resulting from tensile prestraining in the longitudinal direction) increased the compressive yield strength(strain hardening) and decreased the tensile yield strength (Bauschinger effect). No mention was made of the effect of strain aging in Rolfe's work (1968).

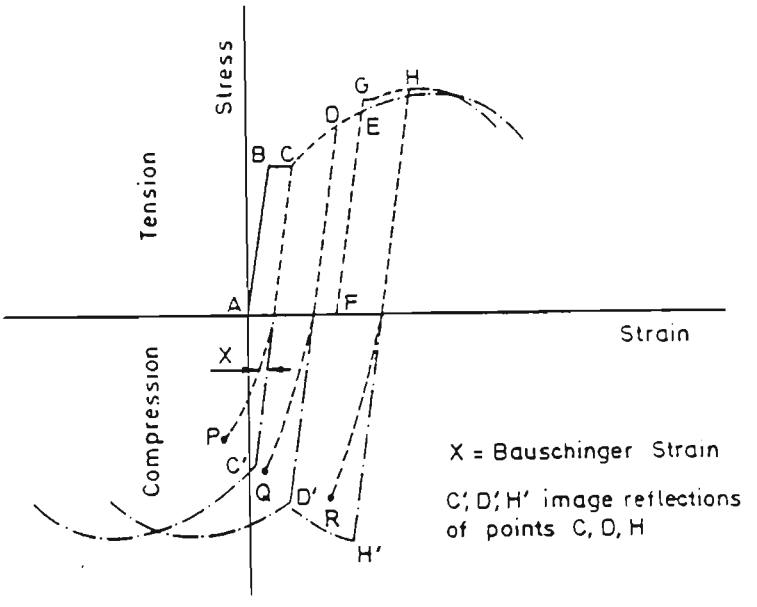

Fig.2.1 Stress-Strain Curves Illustrating Strain Hardening, Strain Aging & Bauschinger Effect

"Strain aging " is the term used to describe any increase in strength or reappearance of a discontinuous yield phenomenon occurring on reloading in the same direction of strain as that applied by the initial inelastic load. Strain aging is considered (Baird, 1963) to be due to the migration of carbon and nitrogen atoms to dislocations causing locking. Other changes also follow from the strain aging phenomenon. The discontinuous yield phenomenon normally returns, the ultimate tensile strength may be increased, and the elongation to fracture may be reduced. Baird (1963) has given an explanation of the effects as a multistage process. The first stage is the formation of atmospheres of carbon and nitrogen around the dislocations caused by the prestraining. As a consequence, the yield stress increases and a reduction occurs in the elongation at the lower yield stress. The second stage occurs when precipitates form along the dislocations; the yield stress continues to rise, the elongation at lower yield remains constant, but the ultimate tensile stress increases, and the elongation to fracture is reduced. A final stage may be reached when over aging occurs, especially at higher temperatures. The yield stress will fall and the ultimate tensile stress may decrease as the elongation to fracture increases.

The amount of tensile prestrain seems to have only a small effect on the change in yield stress produced by subsequent aging when in the same strain direction, but with higher prestrains it markedly increases the plastic elongation at the lower yield stress and increases the ultimate tensile stress. As discussed by Baird (1963), aging is sensitive to temperature and time . The principal effect of increasing the aging temperature is to accelerate the approach to the fully aged condition.

Chajes et al.(1963) have discussed at length the effects of cold-stretching flat sheets of steel with regard to the variables considered herein .

They showed that the effects of the cold work were directional. The Bauschinger effect was observed in the longitudinal direction, together with an inverse effect in a direction normal to the direction of straining. After an initial inelastic tensile strain, straining in tension longitudinally causes an increase in tensile yield strength, but causes a reduction in compressive yield strength. In the transverse direction the opposite occurs; the compressive yield strength increases, but the tensile yield strength decreases. Chajes et al.(1963) referred to this effect as an "Inverse Bauschinger Effect". Such effects have been discussed also by Pascoe (1971). Another detailed investigation on the effects of inelastic transverse bending on the longitudinal strength values for one type of steel, including the effects of strain aging , has been carried out by Karren and Gohil (1975) . Three types of tensile and compressive tests were conducted on a hot-rolled light-gage steel to investigate the corner yield strength and the influence of strain aging for different a/t (inside radius/thickness) ratios.

Pascoe (1971) reported tensile and compressive tests on high-yield low-alloy steel prestrained in tension to different extents. The tests included material orientation relative to prestrain direction as a variable, and the tests enabled the interaction of Bauschinger effect and strain hardening to be observed. The Bauschinger loss (at all reverse load yield definitions less than about 0.60% offset) heavily outweighed the gain in strength owing to strain hardening and strain aging. Unfortunately no mention was made of strain aging nor test timing, and yet from the stress-strain plots presented strain aging has probably made a significant contribution to increased strength. The author, in a series of related tests, again did not mention the influence of strain aging, comments being restricted to the strong influence of the Bauschinger effect on yield strength and modulus of elasticity. The small amounts of prestrain (less than 1%) meant that parts of the test pieces may have reached the initiation of strain hardening, while

other parts were still elastic. Difficulties are therefore caused in the interpretation of some of the reversed loading tests because of this discontinuity of the strain in the Luder strain region, but the small prestrains should eliminate strain hardening as a variable.

2.3 Influence on Strut Load Capacity of Strain Hardening, Strain Aging, the Bauschinger Effect and Residual Stresses

Turning attention to the strut as a structural element, limited work has been reported which includes these effects. Paris (1956) conducted an extensive series of tests on 13mm square pin-ended mild-steel struts which had been prestrained in tension; tangent-modulus column theory and double-modulus theory were employed to predict the collapse loads of prestrained structural steel columns; Paris reached the conclusion that the previous tensile yield considerably reduced the buckling capacity of the struts (up to 50%) and the tangent-modulus column theory was a conservative criterion. The reduction was due to the Bauschinger effect. No mention was made of the existence or influence of strain aging and steel type.

Bouwkamp(1975) carried out axial load tests on seamless and electric-welded line-pipes with slenderness ratios between 40 and 120. The test results agreed reasonably well with predicted load values using the tangent-modulus expression. It was found that local plastic buckling caused a drastic reduction of the post buckling strength. Results indicated that an offshore tower under lateral loads could deform under ultimate conditions significantly more than a linear elastic analysis would indicate, thus increasing the earthquake resistance.

Perry and Chilver (1976) investigated the statistical variation of buckling strengths of a series of as-received strut tests on rectangular strip with various slenderness ratios from 40 to 220. Attention was restricted to the influence of geometric imperfections within the strut length, the material used being the same throughout. The same end fittings were used for all tests. The variation of maximum strength was found to be dependent on slenderness ratios, with the greatest scatter of maximum strength occurring in the region of the slenderness ratio where there was a transition from elastic to plastic buckling. A method of obtaining design curves was proposed, based on the probability of failure.

The effect of prior flexural prestrain on the stability of structural steel columns was studied by Pavlovic and Stevens (1981). By investigating the properties of mangled bars, that is bars which had been deliberately deformed in cyclic flexure so as to reduce initial geometric imperfections, the authors indicated that the prior large bending deformations might cause a significant reduction in the buckling stress of a mild steel strut subjected to direct compression . The potential dangers were highlighted of a situation which might arise when a severely deformed element was straightened and then subjected to loading conditions which would be regarded as safe for a previously undeformed element. The influence of strain hardening was almost excluded by restricting prestrains to about 2%, but the effect of strain aging can only be conjectured as the time elapsing between prestraining and final testing was not stated.

Chen and Ross(1977) investigated experimentally the magnitude and distribution of longitudinal and circumferential residual stresses in fabricated steel tubular columns. Stub-column tests and the strength and behaviour of 10 full-scale fabricated cylindrical columns of medium slenderness ratios of 48 and 70 were investigated. It was concluded that theoretical ultimate load analysis based

on the tangent modulus theory of an initially straight column underestimated the strength of fabricated tubular members. Except for the shortest columns, these variations were from 8% to 16%. It appeared that the transition from general plastic yielding to a local buckling type of failure occurred at a diameter -to-thickness ratio (D/t) of about 60 for all slenderness ratios tested.

Smith et al. (1981) described a theoretical and experimental investigation of the effects of collision damage, in the form of elasto-plastic lateral bending and local indentations, on the stiffness and strength of tubular steel bracing members. Full-scale tests were carried out on two pairs of nominally identical braces obtained from the BP West Sole Platform following twelve years in service . One tube from each pair was tested to collapse under compressive load in an initially undamaged condition while the second was tested to collapse following application of simulated collision damage, thus providing a direct indication of damage effects. Four tests on small-scale tubes representing as closely as possible the full-scale experiments were also performed. It was concluded that, provided care was taken to simulate full-scale geometry as closely as possible and to obtain material with representative and uniform yield strength tests on the small-scale tubes, the model tests provided a satisfactory means of investigating damage effects in braces and other tubular members such as pipelines. The test results were found to correlate satisfactorily with theoretical analysis.

Based on a yield line collapse mechanism of the dented shell, Taby and Moan (1981) presented a simplified theoretical model of a damaged tubular member subjected to axial compression. Consequent eccentricity of the load in the dented portion of the member was accounted for and the ultimate strength was evaluated. The post-ultimate strength behaviour was traced based on a large deflection formulation and a plastic hinge inserted at the middle of the dented portion. An

extensive experimental study was carried out, and satisfactory agreement was obtained when compared with the results of analysis.

Belvin (1984) investigated buckling and vibration characteristics of pretensioned structures through analyses and tests of a stayed column. Modal vibration tests to determine the lateral modes of vibration of a stayed column and static axial compression tests to determine the column's buckling and post-buckling behaviour were performed. Effects of stay tension levels and vibration-load interaction were presented. Two finite element models were used to analyze the column, a three-dimensional frame using NASTRAN. Results indicated premature buckling of the column due to vibration-load interaction and nonlinear oscillations due to stay slackening. Post-buckling behaviour of the column was unusual because of stay slackening and results in a post-buckling restoring force of less than the bifurcation buckling load.

Camotim and Roorda (1985) carried out an analytical and experimental study of a column model, in order to investigate the influence of residual stresses in plastic buckling, namely, at the lowest bifurcation load and the corresponding post-buckling behaviour. Initial geometrical imperfections were also taken into account and a sensitivity analysis was performed, in which the combined effect of residual stresses and initial geometrical imperfections on the strength and maximum load supported by the structure was studied. Two elastic-plastic stress-strain relations were considered, with linear and nonlinear strain-hardening respectively. An experiment simulating the behaviour of the model was conducted. It was concluded that the presence of residual forces significantly affected the buckling behaviour of the model in the plastic range. Furthermore, this effect might be detrimental or beneficial, in the sense of reducing or

increasing the strength respectively, depending on the compression or tension of the constitutive relation considered.

Material and strut tests, including fully aged specimens, on both as-received and prestrained material have been performed (Schmidt and Morgan, 1984; Morgan and Schmidt, 1984). In these tests, two cross-sections were selected to demonstrate variations in the influence of strain hardening, strain aging and the Bauschinger effect : a rectangular solid section 25mm by 12mm of 250 grade semi-killed steel, and a circular tube 60.3mm outside diameter by 2.9mm wall thickness of 200 grade semi-killed steel.

The material test results showed that the percentage increase of strength achieved in both tensile and compressive tests was greater for the rectangular sections than the circular sections for similar elongations and was greater under compressive testing owing to the changes of geometry during squashing of the short specimens. The strut test results showed that the level of prestraining (3% to 7%) of the rectangular section struts had a small effect on strut strength. The influence of strain aging seemed to be significant, especially in the region of the transition length for the struts. The prestrained struts had a lower load capacity than the as-received struts in the structurally significant range of slenderness ratios, 60-150. The reduction in modulus was seen to be the most significant factor for strut stability. The larger the amount of tensile prestrain the lower the value of E_T (Tangent modulus) for an intermediate axial stress range. This effect is reversed for the higher stress ranges ($\sigma > 325$ MPa). The influence of strain aging is highly significant; full aging furnishes the highest values of E_T in the intermediate to higher stress range, for a given value of prestrain.

Strut capacity after repeated tests to failure was investigated (Morgan and Schmidt, 1986). The tests were performed for as-received and tensile prestrained steel struts of tubular section which were Hot Fusion Welded (HFW) and Electric Resistance Welded (ERW) . Failed struts were straightened to a defined tolerance and then retested, the cycle being followed several times. For the tensile prestrained ERW struts the capacity changes observed were small and the variations appeared almost to be random owing to the degree of straightness actually achieved. The capacity of tensile prestrained HFW struts changed significantly on reloading cycles. The overall changes varied with slenderness ratio from a loss of 9% for slender struts to a gain of 52% for the shorter struts. The HFW strut capacity increases were greater than those of the ERW struts because of its higher SHR (Strain Hardening Ratio) when these struts were axially loaded to collapse, then straightened and retested in subsequent load cycles. The HFW struts have been shown to have significant load capacity, often exceeding the initial load capacities. The ability of tubular steel struts to carry increased load on load cycles after the first depends on slenderness ratio but also on the tube material having a high SHR. Strain aging has a significant effect on the reload capacity of steel tubular struts made from rimming or semi-killed steels. With uncertainty about the plastic deformations applied to steel tube during manufacture, the influence of strain aging, of strain hardening, and of the Bauschinger effects, the load capacity of tubular struts made from steel , is worthy of further study.

Key and Hancock (1985) described an experimental investigation of the strength and behaviour of Australian-produced cold-formed SHS (square hollow sections). The tests consisted of concentrically and eccentrically loaded pin-ended columns at four different overall slenderness ratios, stub columns, material property determination and imperfection measurement. The sections tested had

plate width to thickness ratios varying from 29 to 38. The test results were compared with existing and proposed design curves , both Australian and European. An allowance for local buckling of sections with slender plate elements using the Q factor approach had been suggested by the authors.

2.4 THEORETICAL SOLUTION PROCEDURE

To analyse theoretically the effects mentioned above on strut load capacity, the theoretical model must include both geometrical and material nonlinearity . In addition, the post-buckling behaviour needs to be tracked(analysed), as the characteristics of the post-limit-point behaviour of the structure can be related to its imperfection sensitiveness. In order to determine the pre- and post-buckling behaviour of the structure, the nonlinear load-deflection path has to be followed. The conventional Newton-Raphson procedure may have difficulty in surpassing the limit point on the load deflection curve where the tangent stiffness matrices approach singularity. The iterative process may then fail in the neighbouring region of the limit point. It is necessary to employ a more powerful iterative procedure to trace the load-deflection curve beyond the critical point.

The arc-length method technique has been independently introduced by Riks (1972 and 1979) and Wempner (1971). Both authors limit the load step by a constraint equation; that is, the generalized "arc length" of the tangent at a converged point of the load-displacement curve is fixed to a prescribed value. Then the iteration path follows a "plane" normal to the tangent path. The Newton-Raphson method is not often used with the finite element method, the modified Newton-Raphson method (m.N-R) being generally preferred (Zienkiewicz,1977). When using the m.N-R procedure, the tangent stiffness matrix is neither re-formed nor re-factorized at each iteration but is, instead, held

fixed. Even having substituted the m.N-R method for the N-R procedure, Riks' technique is still not suitable for use with the standard finite element method, because the direct simultaneous solution of relevant equations destroys the symmetric banded nature of the equilibrium equations on their own (with a loading parameter λ taken as a constant). The technique has been then modified by Crisfield(1981) and Ramm(1981), so that it is suitable for use with the finite element method. In addition to the "constant-arc-length " the step size may be scaled by relating the number of iterations used in the previous step to a desired value. If material nonlinearities are involved smaller load steps should be defined to avoid drifting. Whenever a negative element in the triangularized matrix is encountered unloading is initiated.

Bergan et al. (1978) use the "current stiffness parameter ", to predict the position of the local maximum or minimum. They then suppress the equilibrium iterations in the neighbourhood of the extreme (limit) point and reverse the sign of the load following a change in the sign of the determinant of the tangent stiffness matrix. The suppression of the equilibrium iterations dictates the provision of very small load increments close to the limit point and also leads to a local drift from equilibrium.

Powell and Simons (1981) described a solution strategy for the analysis of nonlinear structures. The strategy was a simple extension of existing Newton-type procedures, and was applicable to both geometric and material nonlinearity. A few examples, covering several different types of structural behaviour, were described.

Bathe et al.(1983) presented an algorithm for the automatic incremental solution of nonlinear element equations in static analysis. The procedure used two

different constraints depending on the response and load level considered; i.e., the spherical constant arc-length and a constant increment of external work. It was designed to calculate the pre- and post-buckling collapse response of general structures. Eigensolutions for calculating the linearized buckling response were also discussed.

Szilard (1985) presented a solution strategy and algorithm for finite element non-linear stability analysis of elastic structures, employing the total Lagrangian formulation and applying an incremental Newton-Raphson procedure. The technique was referred to as an energy balancing technique. It was said that this energy based line-search technique drastically reduced or even eliminated the equilibrium iterations required by the conventionally used Newton-Raphson methods, and was especially effective for tracing the post-limit-path of large structures.

The theoretical inelastic behaviour of tubular columns and beam-columns has been studied extensively by Hays and Santhanan (1979), Supple and Collins (1982), and notably by Chen and his co-workers (Han and Chen,1983; Sugimoto and Chen, 1985; Toma and Chen, 1983). Most of the earlier analytical methods presented on the inelastic biaxial bending of beam-columns ignored the influence of strain unloading (Saleeb and Chen, 1981) and so could not predict with accuracy the post-buckling behaviour.

Smith et al. (1979) investigated the buckling strength and post-collapse behaviour of tubular bracing members including damage effects by using incremental finite element methods. The influence of initial deflection and residual stresses were considered. By applying incremental end-shortening displacements instead of loads, it is possible in many cases to carry analysis well into the post-

collapse range without numerical difficulty. However, the authors found that, for some columns, the incremental stiffness matrix K was found to become non-positive definite just after the peak load was reached and the solution procedure broke down. In such cases, a static post-collapse load-shortening curve was computed by incrementing lateral displacement, say at mid-length on the column with end-shortening displacements unrestrained and with axial force as an undetermined parameter. Compression tests were also carried out on a series of 16 tubes representing off-shore steel bracing members at about 1/4 scale so as to provide experimental confirmation of theoretical results, referring particularly to post-collapse behaviour and the performance of damaged members.

The recent works by Chen and his co-workers (1983 and 1985) incorporated the strain-unloading influence into inelastic studies of tubular columns. The numerical methods used are the so called finite segment method (FSM) and the influence coefficient method(ICM). These methods rely on first deriving accurate moment-axial force-curvature (M-P-ϕ) and moment-axial force-strain (M-P-ε) relationships for the particular cross section. A series of approximate functions is then selected to represent the M-P-ϕ and M-P-ε curves, and is used in a numerical procedure for tracing the post-buckling curve.

Han and Chen (1983) presented a numerical procedure combining the finite segment method with the influence coefficient method for the cyclic inelastic analysis of steel tubular beam-columns with symmetrical support and loading conditions. The hysteretic loops for cyclic behaviour of struts, which were obtained by an analysis based on the doubly symmetric model of general stress-strain relationships, showed good agreement with test results as a whole.

Toma and Chen (1983) studied the behaviour of fabricated tubular steel beam-columns for the entire range of monotonic loading up to the ultimate load including the post-buckling branch of unloading, using the so-called assumed deflection method. The mathematical models were developed based on different combinations of assumed deflection shape with moment-curvature relationships. In the approach described, equilibrium was established only at a critical section of a beam-column using closed form analytical expressions for the moment-curvature-thrust relationship of a fabricated tube. By analysing a considerable amount of data obtained, it was concluded from the numerical study that initial imperfection (out-of-straightness), lateral load at mid-span, and bending moment at the ends affect the behaviour of a beam-column in a similar manner. As these values increased, the ultimate strength was reduced significantly while their associated load-deflection or load-shortening relations became flatter.

Based on the Finite Segment Method, Sugimoto and Chen (1985) developed a computer model to study the post-buckling, post-peak, and cyclic behaviour of beam-columns and frames, using generalised cyclic stress-strain relationships and an automatic load control technique. But there were limitations for this model. These are the limitations on the length of the beam-columns with a post-buckling branch and on the analysis of the post-fully plastified branches in tensile loading, where no elastic rigidity can be expected. Convergence difficulties were encountered when analyzing short beam-columns where post-buckling behaviour was expected (effective slenderness ratios less than 70).

More recently, Chan and Kitipornchai(1986) investigated the inelastic post-buckling behaviour of beam-columns of circular hollow section. A finite element technique was employed to study the geometric and material nonlinearities by continuously updating the geometry of the element and by modifying the element

stiffness for plasticity (the idealized elastic perfectly plastic stress-strain model was assumed), taking into account the influence of strain unloading. Incremental equilibrium equations were formulated in an updated Lagrangian framework. The iterative arc-length technique (Crisfield, 1981) was employed to trace the pre- and the post-buckling load-deflection paths. Moment-axial-force-curvature relationships was not needed in the analysis but only the fundamental stress-strain relationship of the material was required. Kitipornchai et al. (1987) modified the method proposed (Chan and Kitipornchai, 1986) and studied the geometric and material nonlinear large deflection behaviour of structures comprising thin-walled rectangular hollow sections. The influence of various types of residual stress, initial geometrical imperfections, load eccentricity and yielding of material were incorporated in the analysis. The idealized elastic perfectly plastic stress strain relationship was assumed, strain hardening was neglected, and the effects of strain unloading were included.

Based on the second order kinematic field, Hasegawa et al.(1987) developed an inelastic finite displacements formulation of thin-walled members, using the theorem of virtual work. The general stiffness equation of linearized finite displacement formulated is in a similar form as in the case of elastic material, with additional block stiffness expressions appearing due to the nonlinearity of the material. The block stiffness expressions are in terms of area integrals involving axial stress, and tangent moduli for axial and shear stress, which correspond to the stress resultants, Young's and shear moduli respectively for elastic material. The numerical examples analysed showed that the effect of shear stress resulting from the equilibrium with axial stresses towards the member axis was significant, and thus it should be incorporated in the yield condition, even though the shear deformation itself was neglected in the incremental formulations of beam mechanics.

Very recently, Chan (1988) developed a new geometric and material non-linear analysis procedure for framed structures using a solution algorithm of minimizing the residual displacements. As the aim of an iterative process is to eliminate the residual displacements due to the unbalanced forces, an efficient solution scheme should attempt to minimize these unbalanced displacements, instead of using the geometric or energy constraints. Chan's minimum residual displacement method adopted this philosophy and followed the shortest path to achieve convergence.

2.5 PRESENT RESEARCH

Following previous experimental investigations on the influence of material effects on tubular steel strut capacity (Schmidt and Morgan, 1986; Morgan and Schmidt, 1986), the experimental work conducted herein is confined to prestraines not more than 7%, and differentiates between unaged and fully-aged material. The influence of prior axial prestrain will be investigated for the behaviour of a simple structural element, the pin-ended strut.

As an appropriate theoretical model considering the influence of strain aging, strain hardening and the Bauschinger effect, does not appear to be readily available at present , the current research will establish a mathematical model of tubular strut behaviour, where these related material effects are deliberately included.

CHAPTER THREE

THEORETICAL DEVELOPMENT

3.1 GENERAL

A mathematical model of tubular strut behaviour based on the finite element method is developed in this chapter. The model includes both material and geometrical nonlinearities. Details of the algorithm are described, using three different stress-strain relationships. Numerical examples of structural members are presented using the computer model.

3.2 THEORETICAL MODEL

3.2.1 Basic Assumptions

The basic assumptions adopted in the research are the following:

1. Based on the observation of material behaviour, the stress-strain relationship of the steel for as-received material is approximated by a bilinear curve, as shown in Fig.3.1 (a); the stress-strain relationship of the steel for material that is prestrained in tension and fully aged is approximated by a trilinear curve, as shown in Fig.3.1 (b); the stress-strain relationship of steel for material that is prestrained in tension and unaged is approximated by a quadrilinear curve, as shown in Fig.3.1(c).

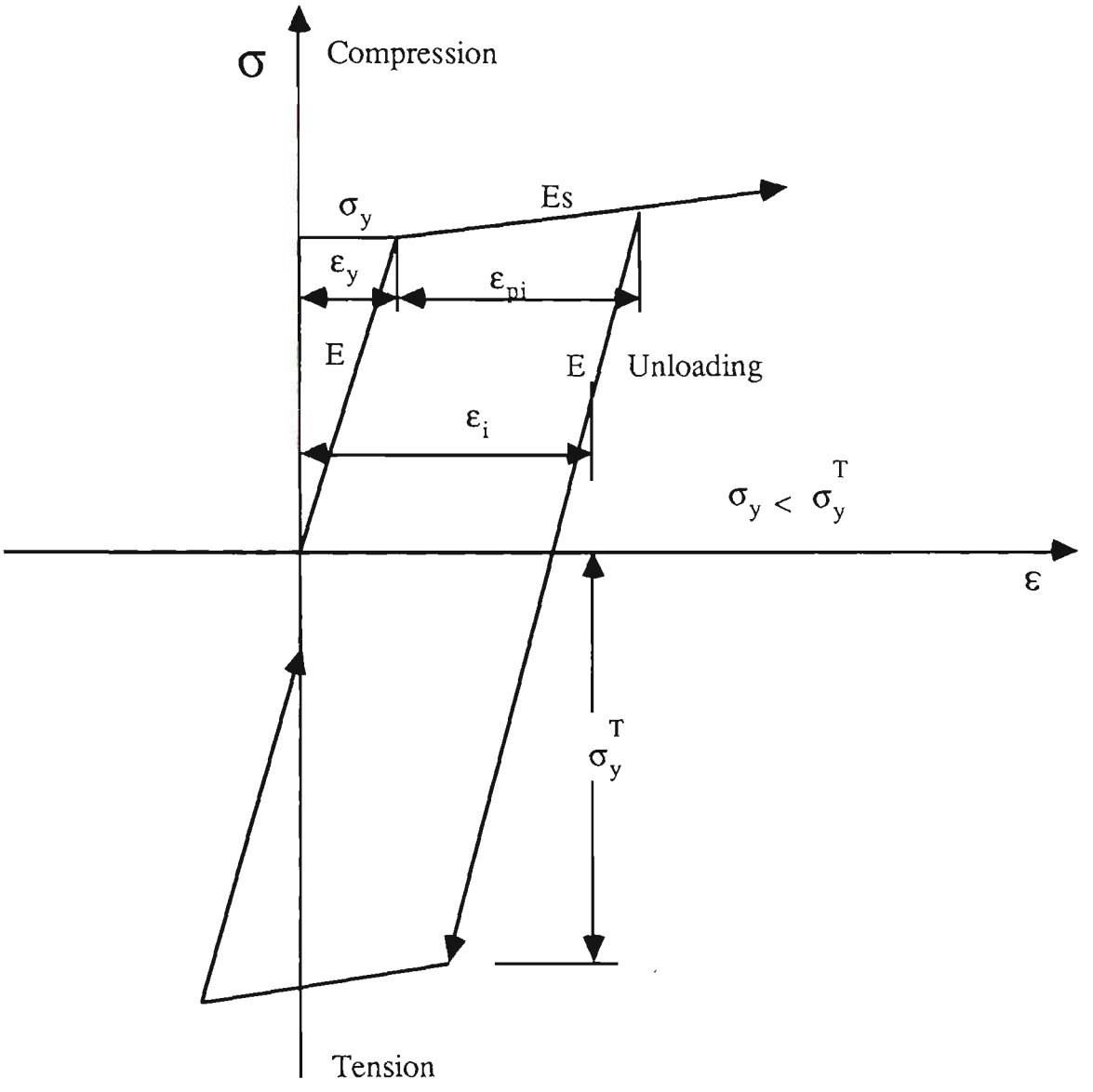

Fig.3.1(a) Idealised Stress-Strain Relationship
For As-Received Material

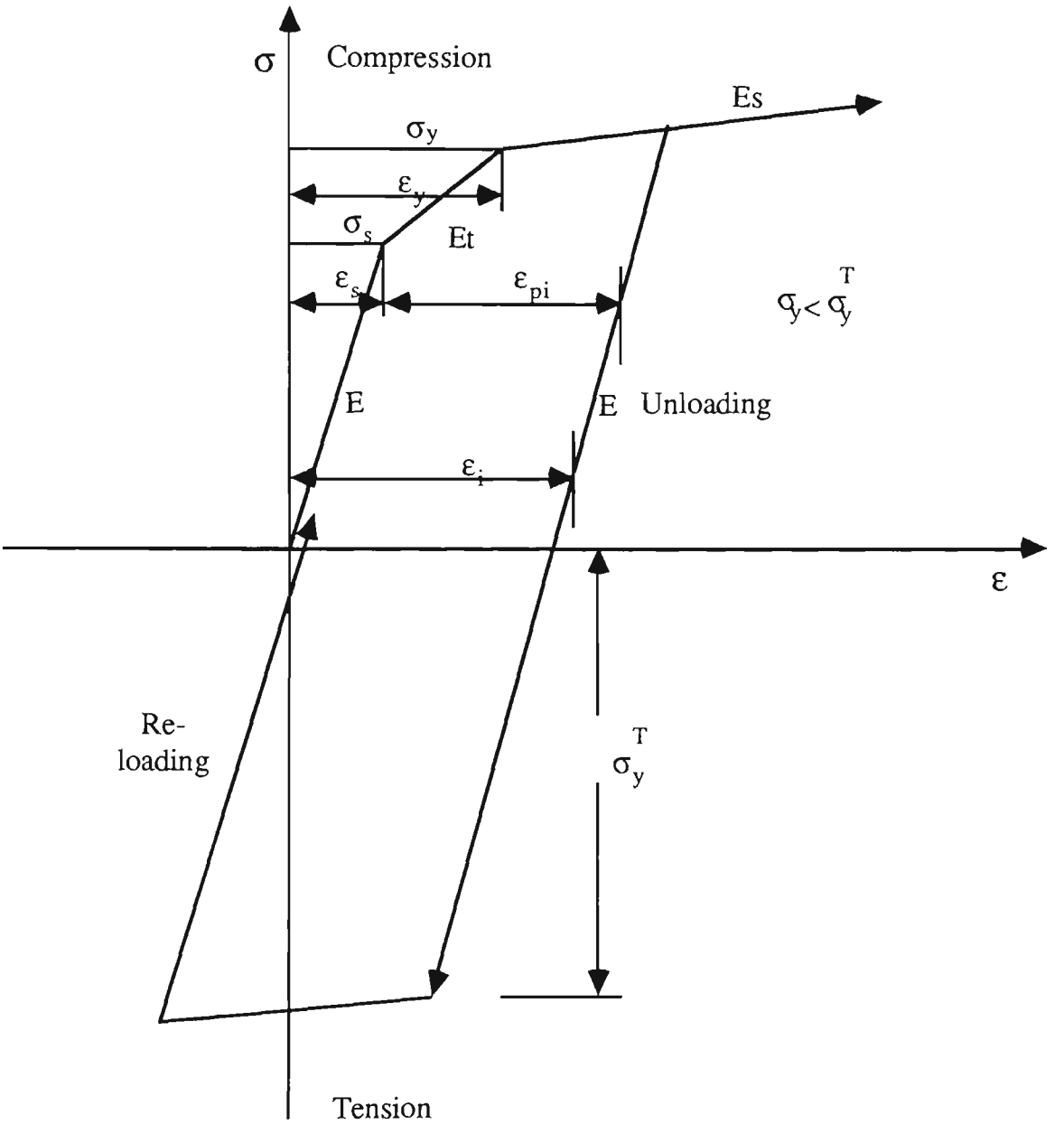

Fig.3.1 (b) Idealised Stress-Strain Relationship for Prestrained and Fully-Aged Material

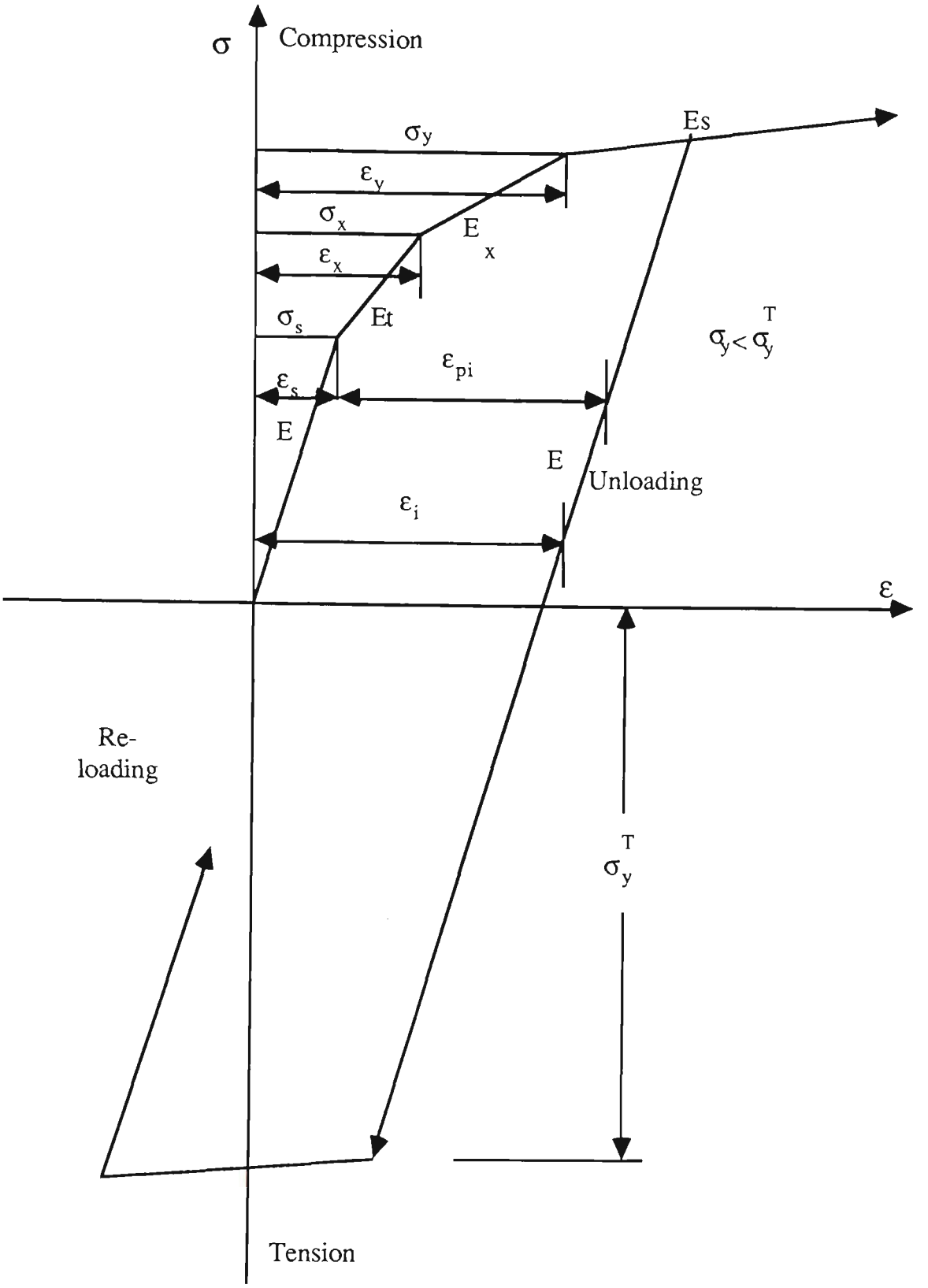

Fig.3.1(c) Idealised Stress-Strain Relationship
For Prestrained and Unaged Material

2. Strain hardening is considered, and allowance is made for recovery of elastic stiffness of yielded fibres which experience strain-reversal. It is assumed that the modulus in the strain-hardening region is approximately 1/70th of the elastic modulus for as-received material; 1/30th of the elastic modulus for the material that is prestrained in tension and fully-aged; 1/15th of the elastic modulus for the material that is prestrained in tension and unaged.

3. Bauschinger effect is considered.

4. Plane sections before deformation remain plane after deformation.

5. Yielding is governed by direct stress only. Shear strains due to bending are not considered.

6. Strains are small but displacements and rotations can be arbitrarily large.

7. Local buckling does not occur.

3.2.2 Total Potential Energy

The total potential energy of an element of length L_e of a general thin-walled cross-section (see Fig.3.2) adopted in this thesis is as follows (Lu et al., 1983):

$$\pi_p = \frac{1}{2}\int_{L_e} [EA(\frac{\partial w}{\partial z})^2 + EI_y[\frac{\partial^2(u-u_0)}{\partial z^2}]^2 + EI_x[\frac{\partial^2(v-v_0)}{\partial z^2}]^2 + EI_w[\frac{\partial^2(\theta-\theta_0)}{\partial z^2}]^2$$

$$+ GJ[\frac{\partial(\theta-\theta_0)}{\partial z}]^2$$

$$- P(\frac{\partial u}{\partial z})^2 - P(\frac{\partial v}{\partial z})^2 + M_x\beta_x(\frac{\partial \theta}{\partial z})^2 + M_y\beta_y(\frac{\partial \theta}{\partial z})^2 + B_\omega\beta_\omega(\frac{\partial \theta}{\partial z})^2 + R(\frac{\partial \theta}{\partial z})^2$$

$$- 2Py_0(\frac{\partial u}{\partial z})(\frac{\partial \theta}{\partial z}) - 2M_x\beta_x(\frac{\partial \theta}{\partial z}) + 2Px_0(\frac{\partial v}{\partial z})(\frac{\partial \theta}{\partial z}) + 2M_y\beta_y(\frac{\partial v}{\partial z})(\frac{\partial \theta}{\partial z})$$

$$+ (Q_x\beta_y + Q_y\beta_x + B_\omega\beta_\omega)\theta(\frac{\partial \theta}{\partial z}) + 2Q_x\frac{\partial v}{\partial z}\theta - 2Q_y\frac{\partial v}{\partial z}\theta]\, dz$$

$$- [Pw + Q_xu + Q_yv - M_y(\frac{\partial u}{\partial z}) - M_x(\frac{\partial v}{\partial z}) + M_z - B_\omega(\frac{\partial \theta}{\partial z})]_0^{L_\epsilon} \qquad (3.1)$$

where EA=axial rigidity; EI_x, EI_y = flexural rigidity about the x and y axes, respectively; EI_w = warping rigidity ; GJ = St.Venant torsional rigidity; $R = \int_A \sigma r^2 dA$, σ = total stress; $r^2 = (x-x_0)^2 + (y-y_0)^2$; B_α = bimoment; x_0, y_0 = ordinates of the shear centre; u,v,w and θ = the lateral displacement, transverse displacement, axial displacement, and angle of twist about the shear centre of a deformed member, respectively; u_0, v_0 and θ_0 = initial deformations; and the terms of β_x, β_y and β_α are given by

$$\beta_x = \frac{\int_A y(x^2+y^2)\, dA}{I_x} - 2y_0 \qquad (3.2)$$

$$\beta_y = \frac{\int_A x(x^2+y^2)\, dA}{I_y} - 2x_0 \qquad (3.3)$$

$$\beta_\omega = \frac{\int_A \omega(x^2+y^2)\,dA}{I_\omega} \qquad (3.4)$$

A linear displacement function for w and a cubic displacement function for u, v and θ are assumed. The displacement in an element is represented by the nodal displacements at the ends as

$$w(z) = \{\phi_m\}^T \{w_m\} \qquad (3.5)$$

$$u(z) = \{\psi_m\}^T \{u_m\} \qquad (3.6)$$

$$v(z) = \{\psi_m\}^T \{v_m\} \qquad (3.7)$$

$$\theta(z) = \{\psi_m\}^T \{\theta_m\} \qquad (3.8)$$

where u_m, v_m, w_m and θ_m are end displacements and angle of twist of the element , respectively;

$$\{\phi_m\} = [(1-\frac{z}{L_e}) \quad \frac{z}{L_e}]^T \qquad (3.9)$$

and $$\{\psi_m\} = [(1-3(\frac{z}{L_e})^2+2(\frac{z}{L_e})^3) \quad (-z+2\frac{z^2}{L_e} - \frac{z^3}{L_e^2}) \quad (3(\frac{z}{L_e})^2-2(\frac{z}{L_e})^3) \quad (\frac{z^2}{L_e} - \frac{z^3}{L_e^2})]^T$$

(3.10)

The equilibrium equations of one element of length L_e can be derived by using the Rayleigh-Ritz method.

$$\begin{bmatrix} EA[T1] & 0 & 0 & 0 \\ 0 & EI_x[S1]-P[N1] & 0 & \begin{matrix} Px_0[N1]+M_{y1}[S2]^T \\ +\Delta M_y[N2]^T+Q_x[N1] \end{matrix} \\ 0 & 0 & EI_y[S1]-P[N1] & \begin{matrix} -Py_0[N1]-M_{x1}[S2]^T \\ -\Delta M_x[N2]^T-Q_y[N1] \end{matrix} \\ 0 & \begin{matrix} Px_0[N1]+M_{y1}[S2] \\ +\Delta M_y[N2]+Q_x[N1] \end{matrix} & \begin{matrix} -Py_0[N1]-M_{x1}[S2] \\ -\Delta M_x[N2]-Q_y[N1] \end{matrix} & \begin{matrix} EI_w[S1]+GJ[N1]-R[N1] \\ +\beta_x M_{x1}[S2]+\beta_x \Delta M_x[N2] \\ +\beta_y M_{y1}[S2]+\beta_y \Delta M_y[N2] \\ +\beta_\omega M_\omega[N1] \\ +(Q_x\beta_y+Q_y\beta_x+\beta_\omega M_\omega)[T2] \end{matrix} \end{bmatrix} \begin{Bmatrix} w_m \\ v_m \\ u_m \\ \theta_m \end{Bmatrix} = \{F_e\} \qquad (3.11)$$

where $\Delta M_x = M_{x1} + M_{x2}$, $\Delta M_y = M_{y1} + M_{y2}$ and matrices [N1], [N2], [S1], [S2], [T1] and [T2] are given in the Appendix I. $\{F_e\}$ = nodal force vector, given by (3.12).

$$\{F_e\} = \begin{Bmatrix} \begin{Bmatrix} N_{x1} \\ N_{x2} \end{Bmatrix} \\ EI_x[S1]\{v_0\} + \begin{Bmatrix} Q_{y1} \\ M_{x1} \\ Q_{y2} \\ M_{x2} \end{Bmatrix} \\ EI_y[S1]\{u_0\} + \begin{Bmatrix} Q_{x1} \\ M_{y1} \\ Q_{x2} \\ M_{y2} \end{Bmatrix} \\ EI_w[S1]\{\theta_0\} + GJ[N1]\{\theta_0\} + \begin{Bmatrix} M_{z1} \\ B_{\omega 1} \\ M_{z2} \\ B_{\omega 2} \end{Bmatrix} \end{Bmatrix} \tag{3.12}$$

For the in-plane stability problem considered in this thesis, the equation (3.11) is simplified as

$$\begin{bmatrix} EA[T1] & 0 \\ 0 & EI_x[S1]\text{-}P[N1] \end{bmatrix} \begin{Bmatrix} w_m \\ v_m \end{Bmatrix} = \{F_e'\} \tag{3.13}$$

$$\{F_e'\} = \begin{Bmatrix} \begin{Bmatrix} N_{x1} \\ N_{x2} \end{Bmatrix} \\ EI_x[S1]\{v_0\} + \begin{Bmatrix} Q_{y1} \\ M_{x1} \\ Q_{y2} \\ M_{x2} \end{Bmatrix} \end{Bmatrix} \tag{3.13a}$$

$$[K_T]_e \{\Delta r_e\} = \{\Delta F'_e\} \qquad (3.14)$$

where $[K_T]_e = [K_L + K_G]_e$, and K_L and K_G are the linear and the geometric stiffness matrices of an element, respectively.

3.2.3 Inelastic Model

In any structural analysis, the stress-strain law is essential. The state of stress in each fibre of each element is examined. Where the total stress exceeds the yield value, the fibre adopts a modulus from either of the following two different stress-strain curves:

(a) zero modulus in the next incremental solution, in accordance with an elastic-perfectly plastic stress-strain curve, or

(b) a reduced modulus derived from a numerically defined stress-strain curve of any prescribed shape.

In the elastic-plastic range, because of the shift in the centroid of the remaining elastic core caused by the partial yielding of the member, it is necessary to calculate the geometrical properties of the elastic core numerically by subdividing the cross section into elementary areas, according to the updated stress distribution.

The direct stress at an arbitrary point on a cross section of an element is a function of its strain history. The relationship is not unique but is path dependent, and follows the unloading path laws. Generalized stress, σ_i and strain ε_i of an

arbitrary point in a cross section may be expressed as one of the following three cases:

1. As-received material (See Fig.3.1(a))

$$\sigma_i = E\,\varepsilon_i \qquad \text{for} \qquad |\varepsilon_i| < |\varepsilon_y| \tag{3.15}$$

or $$= \sigma_y + (\varepsilon_i - \varepsilon_y)\,E_s \quad \text{(loading)} \quad \text{for} \quad |\varepsilon_i| \geq |\varepsilon_y| \tag{3.16}$$

or $$= E\,(\varepsilon_i - \varepsilon_{pi}) \quad \text{(unloading)} \tag{3.17}$$

$$\varepsilon_{pi} = \varepsilon_{max} - (\varepsilon_y + (\varepsilon_{max} - \varepsilon_y)E_s / E) \tag{3.18}$$

2. Prestrained fully aged material (See Fig.3.1(b))

$$\sigma_i = E\,\varepsilon_i \qquad \text{for} \qquad |\varepsilon_i| < |\varepsilon_s| \tag{3.19}$$

or $$= \sigma_s + (\varepsilon_i - \varepsilon_s)\,E_t \quad \text{(loading)} \quad \text{for} \quad |\varepsilon_s| \leq |\varepsilon_i| < |\varepsilon_y| \tag{3.20}$$

or $$= \sigma_y + (\varepsilon_i - \varepsilon_y)\,E_s \quad \text{(loading)} \quad \text{for} \quad |\varepsilon_y| \leq |\varepsilon_i| \tag{3.21}$$

or $$= E\,(\varepsilon_i - \varepsilon_{pi}) \quad \text{(unloading)} \tag{3.22}$$

$$\varepsilon_{pi} = \varepsilon_{max} - (\varepsilon_{sn} + (\varepsilon_{max} - \varepsilon_y)E_s / E) \tag{3.23}$$

where $\varepsilon_{sn} = \sigma_y / E$.

3. Prestrained Unaged Material (See Fig.3.1(c))

$$\sigma_i = E\,\varepsilon_i \qquad \text{for} \qquad |\varepsilon_i| < |\varepsilon_s| \tag{3.24}$$

or $$= \sigma_s + (\varepsilon_i - \varepsilon_s)\,E_t \quad \text{for} \quad |\varepsilon_s| \le |\varepsilon_i| < |\varepsilon_x| \tag{3.25}$$

or $$= \sigma_x + (\varepsilon_i - \varepsilon_x)\,E_x \quad \text{for} \quad |\varepsilon_x| \le |\varepsilon_i| < |\varepsilon_y| \tag{3.26}$$

or $$= \sigma_y + (\varepsilon_i - \varepsilon_y)\,E_s \quad \text{(loading)} \quad \text{for} \quad |\varepsilon_y| \le |\varepsilon_i| \tag{3.27}$$

or $$= E\,(\varepsilon_i - \varepsilon_{pi}) \qquad \text{(unloading)} \tag{3.28}$$

$$\varepsilon_{pi} = \varepsilon_{max} - (\varepsilon_{sn} + (\varepsilon_{max} - \varepsilon_y)E_s / E) \tag{3.29}$$

where $\varepsilon_{sn} = \sigma_y / E$.

The incremental stress-strain relationship can be found by a variation of the above equations. In the elastic range ($|\varepsilon_i| < |\varepsilon_y|$ or $|\varepsilon_i| < |\varepsilon_s|$), and on the unloading and re-loading paths ($|\sigma_i| < |\sigma_y|$ and $|\varepsilon_i| > |\varepsilon_y|$), and $\delta\sigma_i = E\,\delta\,\varepsilon_i$.

In the inelastic range ($|\varepsilon_i| > |\varepsilon_s|$), $\delta\sigma_i = E_t\,\delta\varepsilon_i$ or $\delta\sigma_i = E_x\,\delta\varepsilon_i$ or $\delta\sigma_i = E_s\,\delta\varepsilon_i$, depending on the inelastic model used.

3.2.4 Tangent Stiffness Matrix

The incremental finite element method for a problem having geometric nonlinearity requires that equilibrium equations must be written with respect to the current deformed geometry. Therefore element-to-member transformations must

account for the geometric change. A system of moving nodal co-ordinates is employed so that updating of the structural geometry is achieved simply by adjusting the angular orientation of elements relative to the nodes' previously updated position.

In the elastic-plastic range , due to the shift in the centroid of the remaining elastic core caused by the partial yielding of the member, the applied load which was concentric before yielding now becomes eccentric . Basic geometrical properties required for the evaluation of the element tangent matrix (shown in equation (3.14)) are the cross-sectional area, A , and the second moment of area I_X, which are calculated numerically by subdividing the cross-section into elementary areas, n, (see Fig.3.3), depending on the accuracy required.

$$A_e = \sum_{1}^{n} \Delta A_i \qquad (3.30)$$

$$I_{xe} = \sum_{1}^{n} Y_i^2 \Delta A_i \qquad (3.31)$$

in which A_e is the area of the elastic core, and y_i is the coordinate of the centroid of the elementary area ΔA_i. The elementary area ΔA_i is calculated by $\Delta A_i = \frac{E_T}{E}(\frac{A}{n})$ or $\Delta A_i = \frac{E_x}{E}(\frac{A}{n})$ or $\Delta A_i = \frac{E_s}{E}(\frac{A}{n})$ depending on which inelastic model is used (see **3.2.3 Inelastic Model**).

For each applied load increment, a corresponding displacement increment may be calculated based on the tangent stiffness relationship. At the end of each load cycle, the displacement increment is added to give accumulated total displacements, and the geometric properties of the elements including the load eccentricity due to the shift in the position of the centroid is updated.

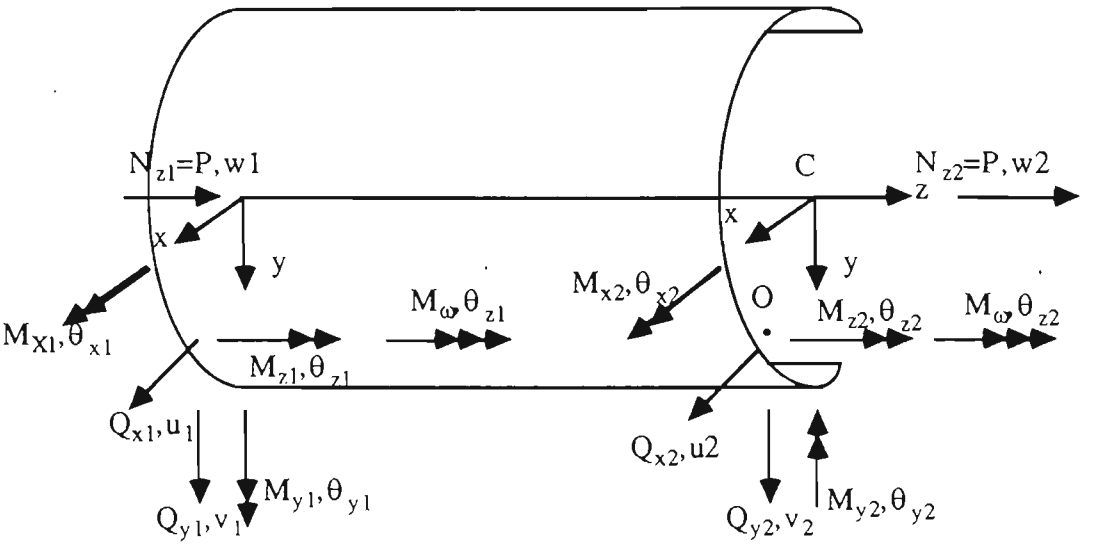

Fig.3.2 Element Forces, Displacements and Coordinate Axes

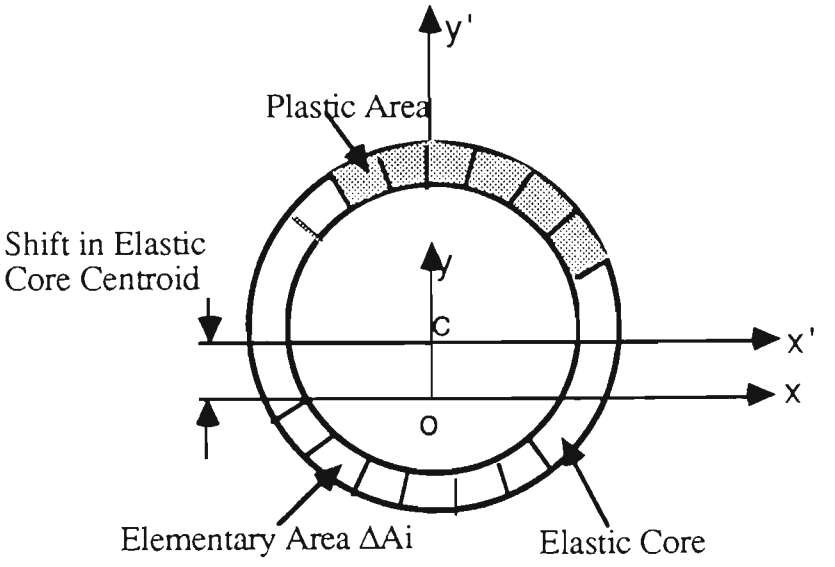

Fig.3.3 Subdivision of Tube Section into Elementary Areas

The tangent stiffness matrix $[K_T]$ of the member is obtained by assembling updated the stiffness of all the elements, i.e.,

$$[K_T] = \sum_{1}^{m} [C_1][C_2][K_L + K_G]\left[C_2^T\right]\left[C_1^T\right] \qquad (3.32)$$

where m is the number of elements, $[C_1]$ is the transformation matrix relating the local coordinate axes x, y to the global coordinate axes x, y , and $[C_2]$ is the transformation matrix accounting for the load eccentricity (Kitipornchai and Chan, 1987). Matrix $[C_1]$ may be found in standard texts (see for example, Gere et al., 1965).

The incremental equilibrium equations may be expressed by the linearized stiffness expression ,

$$\{\Delta F\} = [K_T]\{\Delta r\} \qquad (3.33)$$

where $\{\Delta F\}$ is the incremental nodal force vector and $\{\Delta r\}$ is the incremental displacement vector.

3.2.5 Internal Resisting Forces

Based on the updated accumulated deflections, the internal displacements of the two nodes of an element can be found. Fig.3.4 shows a deformed position of an element in the yz plane. The relative rotations θ_{x1} and θ_{x2} at ends 1 and 2 with respect to the deformed chord can be expressed as :

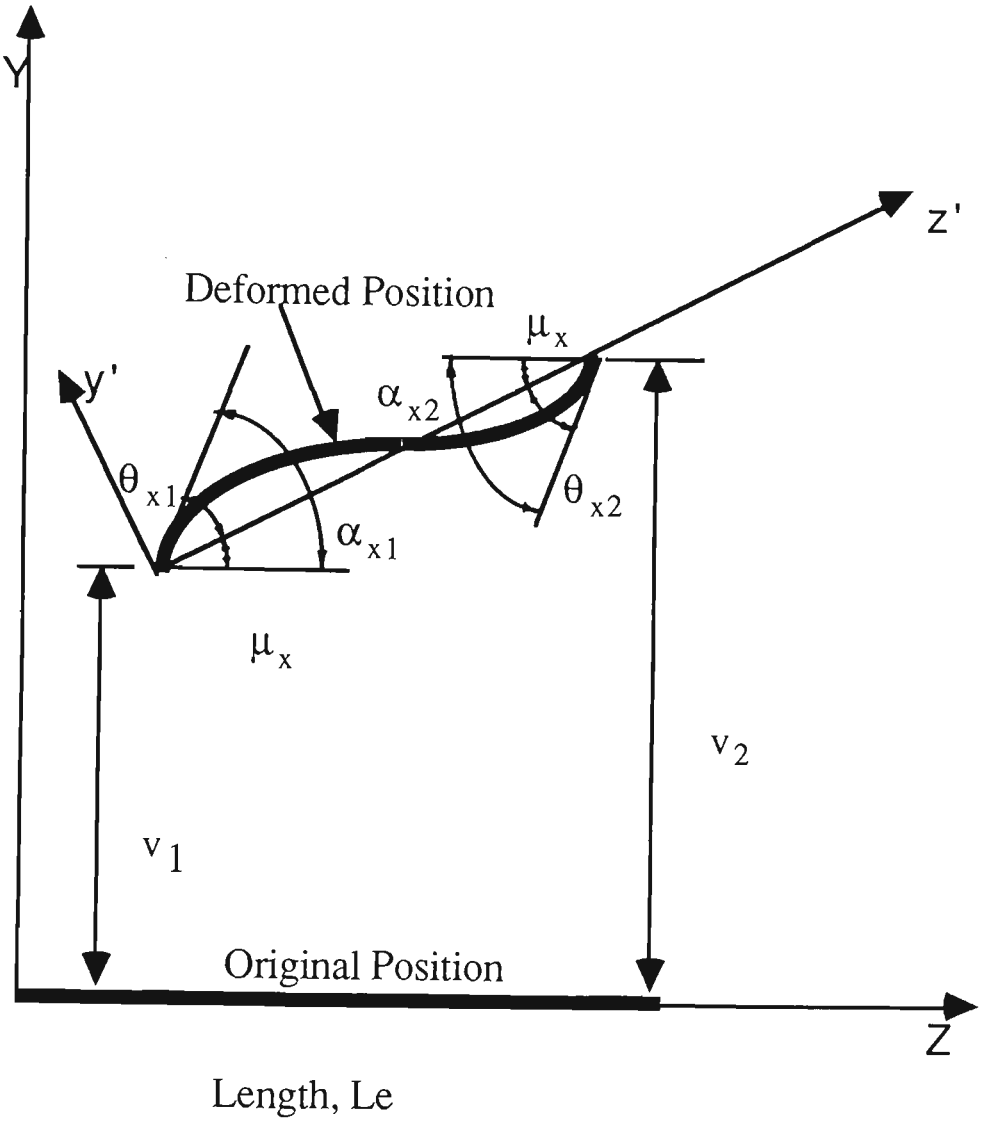

Fig.3.4 Element Deformations

$$\theta_{x1} = \alpha_{x1} - \mu_x \qquad (3.34)$$

and $$\theta_{x2} = \alpha_{x2} - \mu_x \qquad (3.35)$$

in which μ_x is the rigid body rotation and α_{x1}, α_{x2} are the total rotations at ends 1 and 2,

$$\mu_x = \sin^{-1}\left(\frac{v_2 - v_1}{L_e}\right) \qquad (3.36)$$

where v_1, v_2 are the displacements in the y direction of ends 1 and 2, and L_e is the original length of the element.

The average curvature, ϕ_x, of the element may be calculated :

$$\phi_x = \frac{1}{L_e}(\theta_{x2} - \theta_{x1}) \qquad (3.37)$$

The total direct strain at the centre of any elementary area ΔA_i may be expressed in the sum of the axial and bending strain components :

$$\varepsilon_i = \frac{P}{E\,A} + \phi_x\, y_i' \qquad (3.38)$$

in which P is the applied axial force, y_i' is the y' coordinate of the centre of the elementary area ΔA_i, ϕ_x is the curvature about the principal x' axis. Substituting the total strain ε_i into Equations (3.15) to (3.17) or (3.19) to (3.22) or (3.24) to (3.26), the total stress, σ_i, at any point is obtained.

The total resisting forces for an element may be summed over the entire cross-section :

$$P = \sum_{i=1}^{n} \sigma_i \Delta A_i \qquad (3.39)$$

$$M_x = \sum_{i=1}^{n} \sigma_i y_i' \Delta A_i \qquad (3.40)$$

A linear variation of moments along the length of the element is assumed. The moment M_x may be taken as an average of the two end moments, M_{x1} and M_{x2} ,

$$M_x = \frac{1}{2}(M_{x2} - M_{x1}) = \sum_{i=1}^{n} \sigma_i y_i' \Delta A_i \qquad (3.41)$$

The end moments M_{x1} and M_{x2} can be determined according to the ratio of the end moments in terms of the end rotations, θ_{x1} and θ_{x2} ,

$$\frac{M_{x1}}{M_{x2}} = \frac{2\theta_{x1} + \theta_{x2}}{\theta_{x1} + 2\theta_{x2}} \qquad (3.42)$$

3.3 METHOD OF SOLUTION

As mentioned in Chapter 2 (Literature Review), the conventional Newton-Raphson procedure may have difficulty in surpassing the critical points on the load deflection curve when the tangent stiffness matrix approaches singularity. The

iterative process may then fail in the neighbouring region of the limit point. Therefore, a more powerful procedure needs to be chosen to overcome these shortcomings. In the present study, the arc-length method (Crisfield, 1981) is used to trace the pre- and post-critical load deflection path.

In the arc-length method, the load increment is not going to be chosen arbitrarily, rather it is determined under an arc-length constraint equation.

For an arbitrary referenced load increment vector $\{\Delta F_a\}$, the tangent displacement vector may be calculated as

$$\{\Delta r_a\} = [K_T]^{-1} \{\Delta F_a\} \qquad (3.43)$$

At the ith iteration within the jth load cycle, the incremental displacement due to residual forces is given by

$$\{\Delta r\}_R = [K_T]^{-1} \{\Delta F\}_R \qquad (3.44)$$

in which $\{\Delta r\}_R$ is the incremental displacement due to the residual force $\{\Delta F\}_R$,

$$\{\Delta F\}_R = \int_V [B]^T [\sigma] \, dv - \{F\} \qquad (3.45)$$

$\{\Delta F\}_R$= Unbalanced force vector

$\{F\}$ = Applied force vector

[B] = Strain / displacement matrix

[σ] = Internal stress of the structure

The accumulated displacement increment, $\{\Delta r\}_i^j$, after the ith iteration in the jth cycle is given by

$$\{\Delta r\}_i^j = \{\Delta r\}_{i-1}^j + \Delta\lambda_i\{\Delta r_a\} + \{\Delta r\}_R \qquad (3.46)$$

in which $\Delta\lambda_i$ is the load multiplier to be determined . Imposing the arc-length constraint condition, the arc-length ΔL is specified.

$$\{\Delta r\}_i^T\{\Delta r\}_i = \Delta L^2 \qquad (3.47)$$

For the first iteration of jth load cycle

$$\{\Delta r\}_0^j = \{\Delta r\}_R = 0 \qquad (3.48)$$

So

$$\Delta L^2 = \{\Delta r\}_1^T\{\Delta r\}_1 \qquad (3.49)$$

Substituting equations (3.46) and (3.48) into (3.49) , we obtain

$$\Delta\lambda_1 = \frac{\Delta L}{\sqrt{\{\Delta r_a\}^T\{\Delta r_a\}}} \qquad (3.50)$$

For the second and subsequent iteration, equation (3.47) becomes,

$$\left[\{\Delta r\}_{i-1}^{j} + \Delta\lambda_i\{\Delta r_a\} + \{\Delta r\}_R\right]^T\left[\{\Delta r\}_{i-1}^{j} + \Delta\lambda_i\{\Delta r_a\} + \{\Delta r\}_R\right] = \Delta L^2 \qquad (3.51)$$

This equation can be written as

$$A\,\Delta\lambda_i^2 + B\,\Delta\lambda_i + C = 0 \qquad (3.52)$$

in which

$$A = \{\Delta r_a\}^T\{\Delta r_a\} \qquad (3.53)$$

$$B = 2[\{\Delta r\}_{i-1}^{j} + \{\Delta r\}_R]^T\{\Delta r_a\} \qquad (3.54)$$

$$C = [\{\Delta r\}_{i-1}^{j} + \{\Delta r\}_R]^T[\{\Delta r\}_{i-1}^{j} + \{\Delta r\}_R] - \Delta L^2 \qquad (3.55)$$

The two roots of this scalar quadratic equation will be designated $\Delta\lambda_{i1}$ and $\Delta\lambda_{i2}$. To avoid "doubling back " on the original load/deflection path, the " angle " between the incremental displacement vector, Δr_{i-1} before the present iteration, and the incremental vector, Δr_i after the current iteration within jth load cycle should be positive. The "angles" γ_1 and γ_2 are given by

$$\gamma_1 = \Delta r_{i,1}^T \Delta r_{i-1} \quad , \quad \gamma_2 = \Delta r_{i,2}^T \Delta r_{i-1} \qquad (3.56)$$

The appropriate root for $\Delta\lambda_{i1}$ or $\Delta\lambda_{i2}$ is that one which gives a positive angle. However, if both angles are positive, then that one closer to the linear solution, equation (3.57), should be chosen.

$$\Delta\lambda_i = -\frac{C}{B} \qquad (3.57)$$

Once $\Delta\lambda_i$ is determined , the displacement increments from the current iteration and the total applied force can be determined :

$$\{\Delta r\}_i^j = \{\Delta r\}_{i-1}^j + \Delta\lambda_i\{\Delta r_a\} + \{\Delta r\}_R \qquad (3.58)$$

The total displacement $\{r\}_i$ and the total applied force, $\{F\}_i$, are

$$\{r\}_i = \{r\}_{i-1} + \{\Delta r\}_i \qquad (3.59)$$

$$\{F\}_i = \{F\}_{i-1} + \Delta\lambda_i\{\Delta F_a\} \qquad (3.60)$$

The total resisting forces and moments of each element obtained from equations (3.39) to (3.42) are transformed to the global coordinate axes and summed to give the total resisting forces and moments of the member. These forces are then compared with the external applied forces to obtain an out-of-balance force, which must be dissipated so as to satisfy equilibrium. The iterative process ceases when the convergence tolerances (equations 3.61 and 3.62) are satisfied.

If an incremental solution strategy based on iterative methods is to be effective, realistic criteria should be used for the termination of the iterative process. At the end of each iteration, the solution obtained should be checked to see whether it has converged within preset tolerances or whether the iteration is diverging. The following convergence criteria have been adopted in this study.

$$\frac{\|\Delta F_R\|}{\|F\|} = <TOL \qquad (3.61)$$

$$\|\Delta F_R\| = \sqrt{\Delta F_R^T D \Delta F_R^{-1}} \text{ and } \quad \|F\| = \sqrt{F^T D F^{-1}} \qquad (3.62)$$

Where ΔF_R and F are out-of-balance force and total applied force vectors, D is a diagonal matrix containing the leading diagonal elements of the tangent stiffness matrix (at the beginning of the load increment). The convergence tolerance, TOL, of equation (3.61) is set to 0.5% to 1%.

The present formulation uses the variable arc-length method (Ramm, 1981) in which the arc-length is modified by

$$\Delta L_j = \Delta L_{j-1} \sqrt{\frac{I_d}{I_{j-1}}} \qquad (3.59)$$

in which ΔL_j and ΔL_{j-1} are the arc-lengths for the jth and (j-1)th load increment cycles, I_d is the desired number of iterations and I_{j-1} the number of iterations for convergence in the (j-1)th cycle. That is, if the required number of iterations for each cycle is kept constant, this procedure will automatically lead to smaller arc-lengths in the areas of the most severe non-linearity, and longer lengths when the response is nearly linear.

It is known that the stability of a network is established if the stiffness matrix is positive-definite. Alternatively, the sign of the determinant of the stiffness matrix can be used as an indicator of stability; positive for stability, negative for instability. However, Bergan et al. (1978) and Ramm (1981) pointed out that the requirement of a positive determinant is a necessary but insufficient condition for a stable state equilibrium. Strictly, a condition of positive work is required, such as that given by the triple product $\underline{\Delta}^T K \underline{\Delta} > 0$ where $\underline{\Delta}$ is the vector of nodal deflections and K is the stiffness matrix. Under this condition the stiffness matrix is determined as being positive definite.

As a practical working tool, the criterion based on the determinant check seems to be satisfactory for most situations. Therefore, in this study, the maximum or buckling load of the strut is detected by the negative value in the determinant of the tangent stiffness matrix. When this occurs, a negative load increment is used to trace out the unloading path, and iteration is suppressed and the load increment is further reduced to prevent possible divergence to an incorrect equilibrium path. At this stage, the total equilibrium equation is used only to estimate the magnitude of the drifting-off error.

3.4 AN OUTLINE OF THE ANALYSIS PROCEDURE

An outline of the analysis procedure is summarized as follows:

1. Select a basic load increment as the reference load ΔF_a, thus defining the arc-length ΔL in the first step (equation 3.49).
2. In any step :
   a) Solve the equilibrium equations for ΔF_a and linearly scale the load and displacements to produce the arc-length ΔL. This step determines $\Delta\lambda_1$.

b) Adjust the step size to the desired number of iterations I_c , e.g. $\sqrt{\frac{I_d}{I_{j-1}}}$.

c) Check the sign of determinant of the triangularized matrix for unloading .

3. a) Determine the out-of-balance forces ΔF_R .

b) Solve for the out-of-balance forces ΔF_R to determine the incremental displacements Δr_R .

4. Use constrained equation (3.50) or (3.52) to determine the load multiplier.

5. Update the load level and the displacement field.

6. Repeat steps 3-5 until the desired accuracy is achieved.

7. Reformulate the stiffness matrix and start a new step by returning to step 2.

3.5 JUSTIFICATION OF COMPUTER PROGRAM

Based on the above described procedure, a computer program in Fortran 77 has been written. Fig.3.5 shows the flowchart for the program. Before applying the program, it is necessary to carry out feasibility and accuracy checks of the program in both the elastic and inelastic ranges.

3.5.1 Comparison of Calculated Results by the Developed Program with an Elastic Analytical Solution of the Linear Bifurcation Load

Consider a pin-ended steel tubular strut of length 149mm, outside diameter 60.3mm , wall thickness 2.3mm, second moment of area 17.65mm^4, and Young's modulus 203 GPa as an example. The Euler critical load is calculated as follows:

$$P_{cr} = \pi^2 EI/L^2 = 157.5 \text{ KN}$$

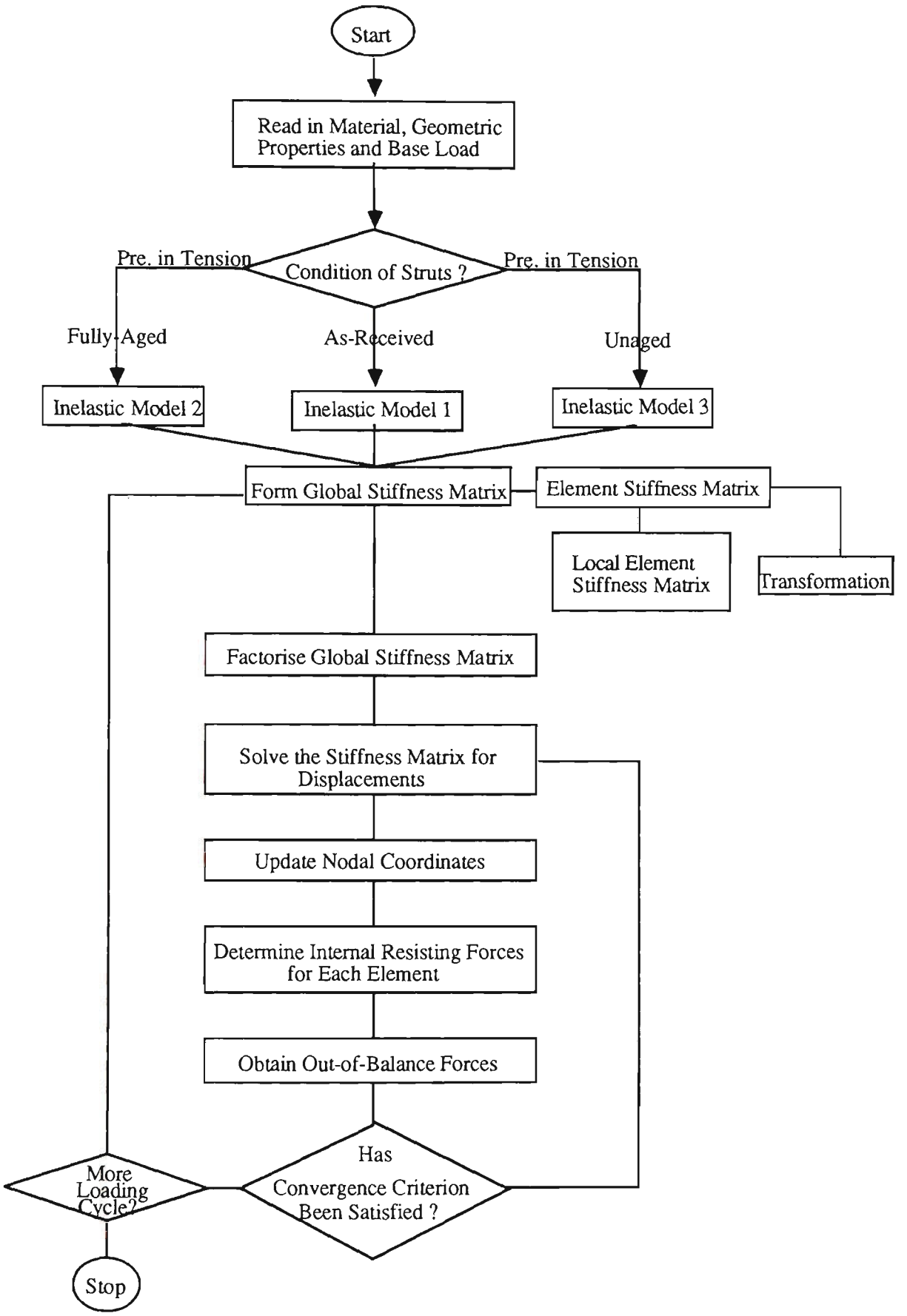

Fig.3.5 Flowchart for Computer Program

The bifurcation buckling loads in the elastic range, calculated by using the computer program described above, and according to the different number of elements used, are determined as follows. The elements are of equal length.

P_{cr1} = 172.0 KN (one element used, whole length of the strut)

P_{cr2} = 160.0 KN (two elements used)

P_{cr4} = 156.3 KN (four elements used)

P_{cr6} = 156.5 KN (six elements used)

P_{cr8} = 156.8 KN (eight elements used)

P_{cr10} = 157.0 KN (ten elements used)

P_{cr12} = 157.0 KN (twelve elements used)

Compared with the Euler load, the percentage errors with respect to the number of elements adopted are shown in Table 3.1.

The curve of error percentage versus number of elements is plotted in Fig.3.6. It can be seen that ten elements are sufficient to model the pin-ended strut with good accuracy.

Table 3.1 Percentage Errors vs Number of Elements

No. of Elements	Percentage Errors %
1	9.14
2	1.53
4	0.85
6	0.69
8	0.45
10	0.37
12	0.37

3.5.2 Comparison of Calculated Results by the Developed Program with Those by a NASTRAN Package

3.5.2.1 Brief Introduction on NASTRAN Package

Nastran is a finite element digital computer program for structural analysis that is intended for general use. It has been designed according to two classes of criteria. The first class relates to functional requirements for the solution of an extremely wide range of large and complex problems in structural analysis with high accuracy and computational efficiency, which are met by developing advanced mathematical models of the physical phenomena and incorporating their computational algorithms into the program. The second class of criteria relates to the operational and organizational aspects of the program .

The Nastran deck consists of three parts:

(1) Executive Control Deck - controlling the fundamental functions.

(2) Case Data Deck - controlling the input and output functions.

(3) Bulk Data Deck - containing all of the required data.

The primary Nastran input medium is the Bulk Data card. These cards are used to define the structural model and the various pools of data which may be selected by Case Control at execution time.

For nonlinear problems, the solution method provided in Nastran are biased towards the "almost linear" problems; if the nonlinear effects are second-order or localized, the nonlinear solution efficiency and user interaction approach the linear case.

The solution sequence Sol.66 in Nastran provides static solutions for both large displacement and material nonlinearities. The primary solution operations in Solution 66 are controlled with NLPARM Bulk Data Card. The three primary operations are (1) applied load increments, (2) internal force equilibrium error limits, and (3) element stiffness matrix updates.

The goal in the Nastran nonlinear static analysis capability of Sol 66 is to simulate a specific physical structure undergoing a specific load history. Nonlinear structural solutions are typically obtained from a trial and error search procedure for a particular loading or displacement increment. The search procedure starts from a particular stress and position state and terminates when the basic equations are satisfied within a known tolerance.

3.5.2.2 Tubular Struts Analysed Using Beam Element by Nastran Package

3.5.2.2.1 Idealised Elastic Perfectly Plastic Material

An elastic ideally-plastic stress-strain curve as shown in Fig.3.7 is used to study the nonlinear behaviour of pin-ended struts. Ten beam elements are used for the pin-ended struts. The load-displacement plots from Nastran results are shown in Fig.3.8. The load-axial shortening curves calculated from the computer program developed herein are shown in Fig.3.8 as well. It can be seen that the agreement between two curves is reasonably good.

In the Nastran Package, the BEAM element has been modified to provide plastic hinges at the ends of an otherwise elastic element. This element is intended for collapse analysis in frameworks with loads at the joints, and materials with a small degree of work hardening. The flexibility of the plastic hinge is based upon eight idealised rods at each end, chosen to match the total area and second moments of area of the cross-section. The spacing of the rods in the equivalent cross-section is shown in Fig.3.9. It needs to be noted that to trace the unloading path, the enforced displacements are used instead of the applied loads for achieving a first estimate of the solution . The problem may be restarted with boundary constraint changes. The details of Executive Control Deck, Case Control Deck and Bulk Data Deck used in this example are given in Appendix II.

3.5.2.2.2 Generalised Elastic Plastic Material

Stress-strain curves for a generalised elastic plastic material are shown in Fig.3.1(c). Convergence difficulties were encountered when using the Nastran

Package in the neighbouring region of the limit point, no matter how small the displacement increments used. The load-axial shortening plot from the Nastran results using ten elements is shown in Fig.3.10 . For comparison, the results using the developed computer program are also plotted in Fig.3.10. It can be seen that the difference between the two curves are very significant. It should be noted that strut buckling occurs far before the plastic hinge forms. For struts which are prestrained and unaged, the material reaches the proportional strength at a relatively low load, but has not reached the yield strength. Therefore, the material still has the ability to withstand further load until buckling occurs (the ultimate load is reached). In this case, the NASTRAN beam element model which provides plastic hinges at the ends of an otherwise elastic element is not relevant as a model for strut stability with this kind of material.

3.5.3 Comparison of Theoretical Results with Kitipornchai and Chan (1986)

In the inelastic range, the buckling loads of tubular struts, including both material and geometrical nonlinearity, are only available for comparison purposes for an idealised elastic-perfectly-plastic material .

Fig.3.11 shows the axial load-axial shortening relations derived from the computer program developed herein for pin-ended tubular struts (D=45" and t=0.09375") having slenderness ratios, L/r, of 80, 120 and 160, and with initial imperfections, δ_0/L, of 0.001; ten elements were used for the length of the struts. The computer results were also obtained from the Nastran Package using ten elements for the strut length, and from Chan's results that used twelve elements for the strut length in the finite element method. These results are shown in Fig.3.11. It is seen that the agreement of all the results is excellent. The excellent

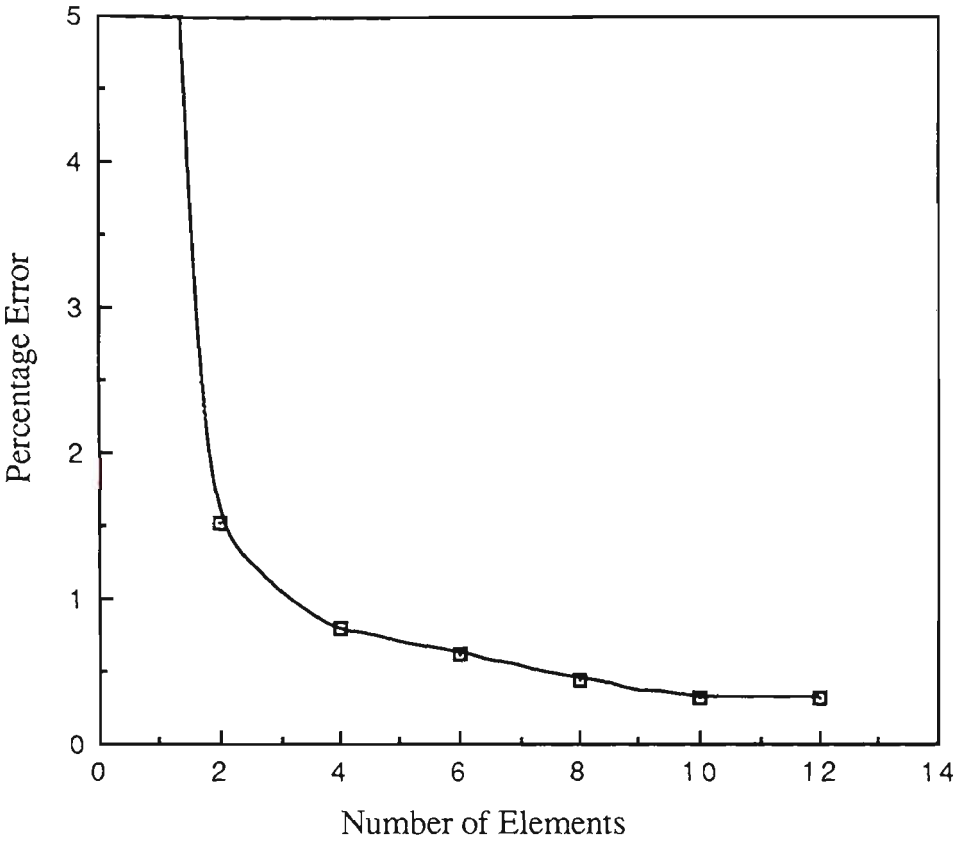

Fig.3.6 Convergence of the Finite Element Solution

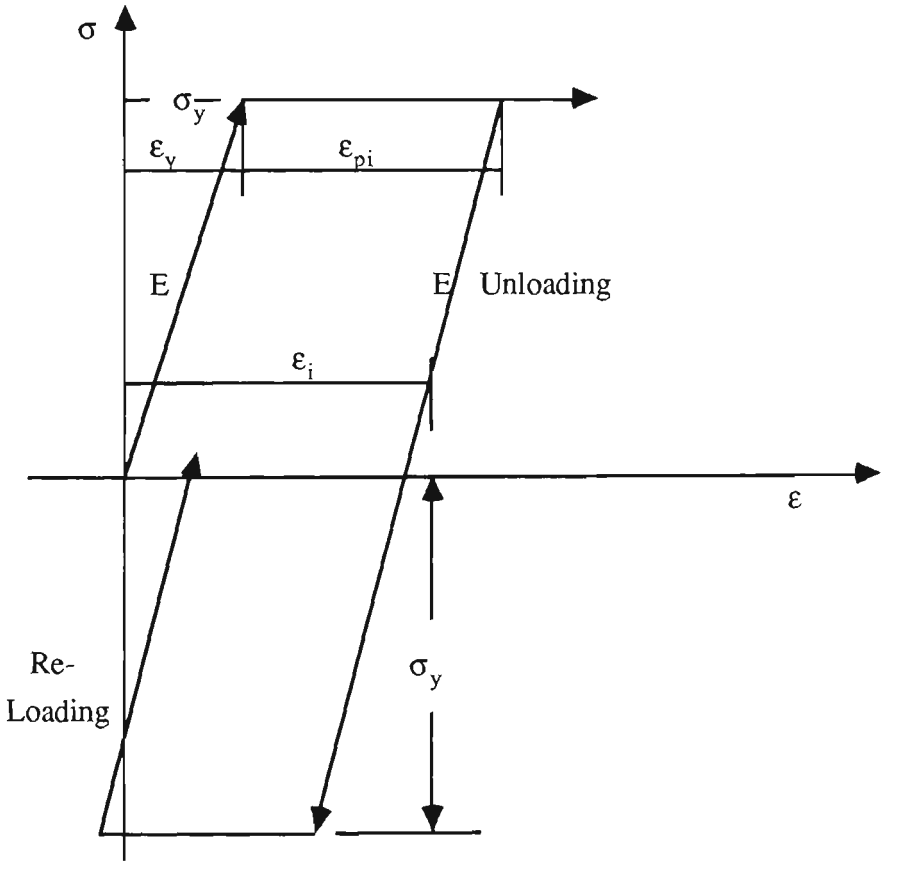

Fig.3.7 Idealised Elastic Perfectly Plastic Stress-Strain Curve

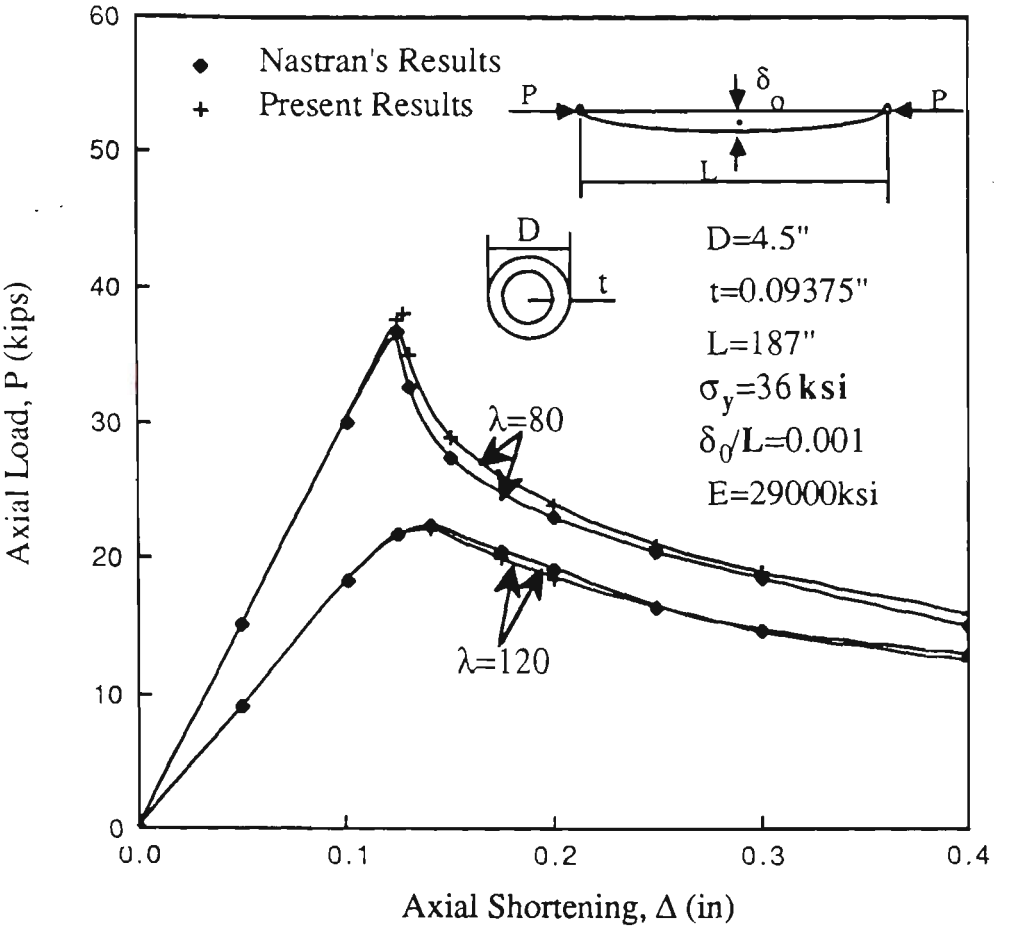

Fig.3.8 Comparison of Theoretical Axial Load-Shortening Curves with Nastran

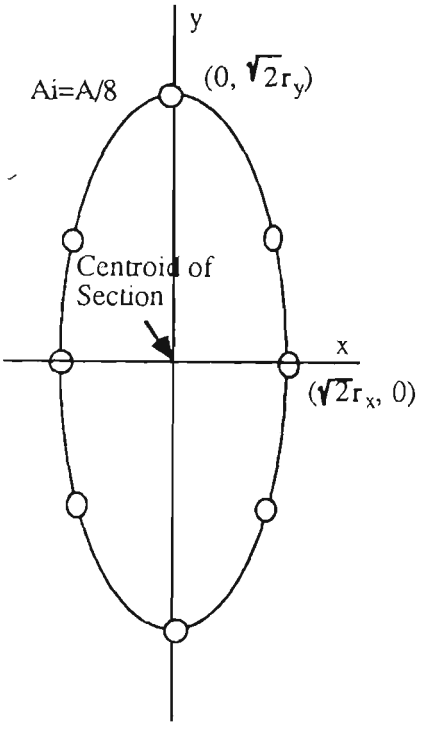

x,y are principal axes.

$$r_x=\sqrt{\frac{I_y}{A}};\ r_y=\sqrt{\frac{I_x}{A}}$$

Fig.3.9 Arrangement of Plastic Rods

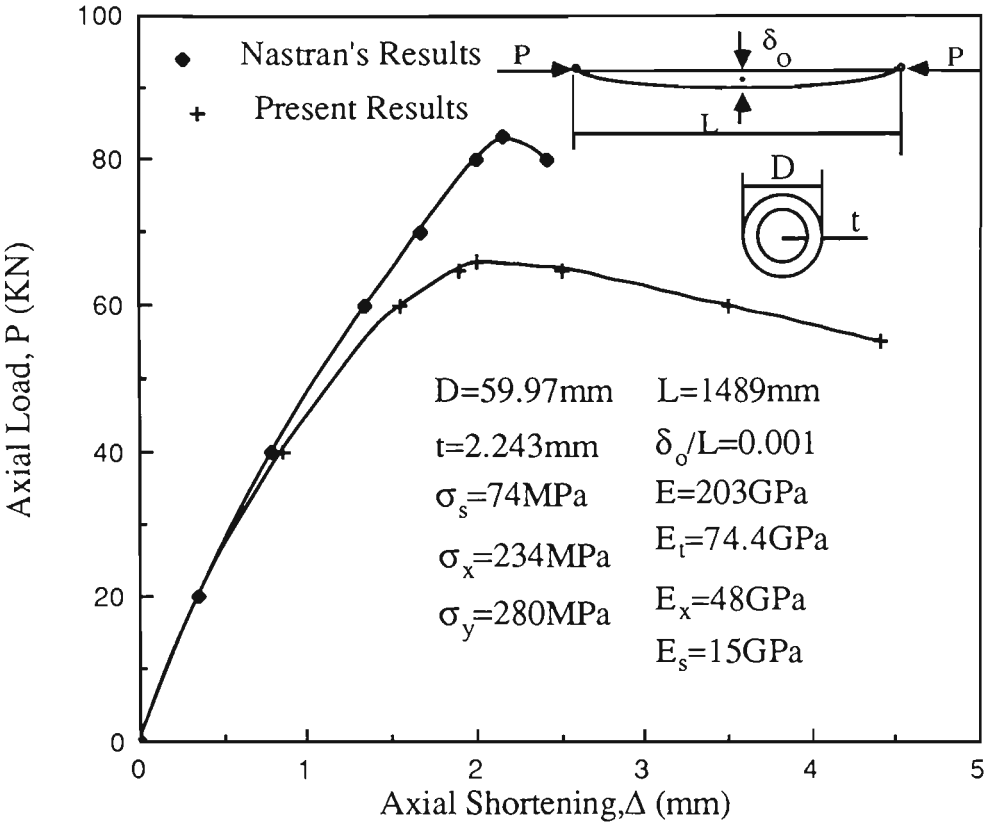

Fig.3.10 Comparison of Theoretical Axial Load-Shortening Curves with Nastran -Prestrained in Tension Unaged Material

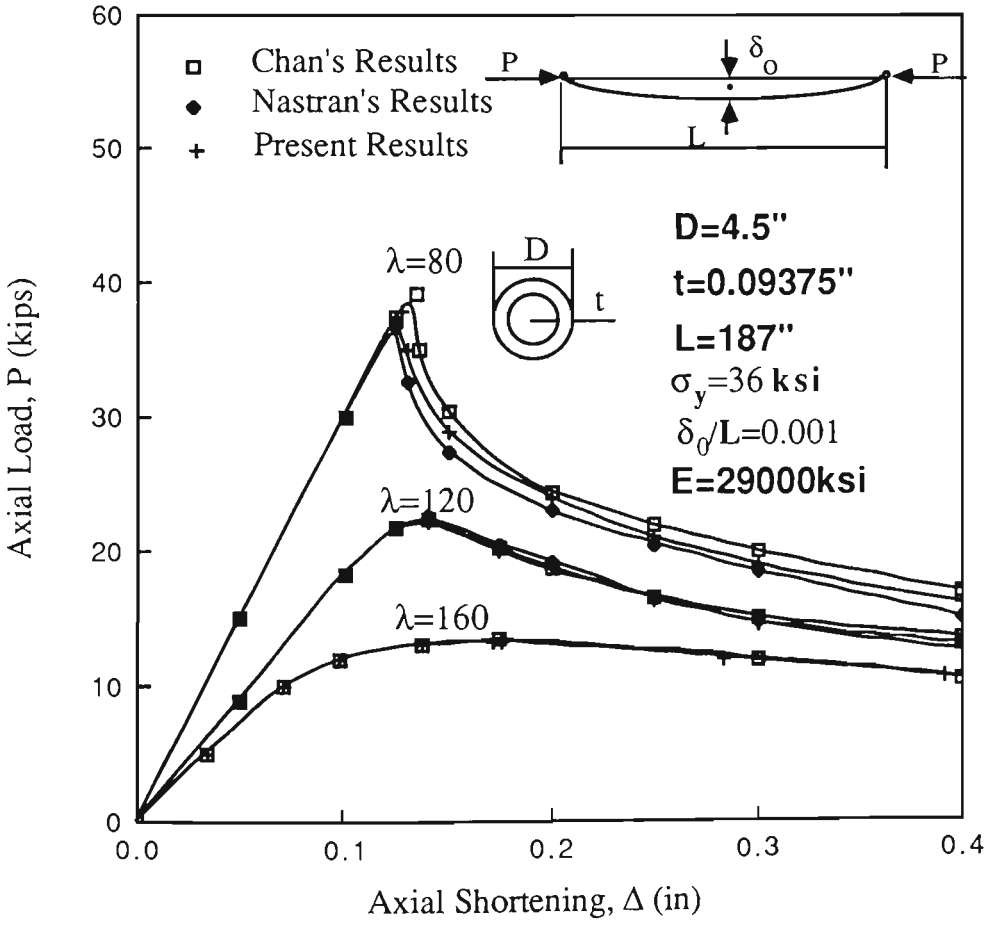

Fig.3.11 Comparison of Theoretical Axial Load-Shortening Curves with Chan and Kitipornchai (1986) and Nastran

agreement with both the Nastran and Chan's results confirms the accuracy of the present theory.

3.6 NUMERICAL APPLICATIONS

The pre-buckling and post-buckling load-deflection paths of pin-ended steel tubular struts of different slenderness ratios have been obtained using the proposed approach. For comparative purposes, the specific dimensions of the tubes were chosen for the numerical studies so that results could be compared directly with the experimental results (A detailed comparison of theoretical results with respect to the experimental results is undertaken in Chapter 6). The detailed numerical results are described in the following sections according to the following categories : as-received struts, struts that are prestrained in tension and fully-aged, struts that are prestrained in tension and unaged, and combined results.

3.6.1 As-Received Struts

Based on the described procedure, the inelastic post-buckling behaviour of pin-ended struts of different slenderness ratios for as-received struts have been studied. Six slenderness ratios, were considered, namely λ = 36, 55, 73, 91, 110 and 146. The stress-strain relationship shown in Fig.3.1(a) was assumed. The values of the Young's modulus, E, of 203 GPa, modulus Es of 3 GPa, and yield stress σ_y of 315 MPa, were used.

Fig.3.12 presents the critical stress and axial strain curves normalised with respect to the yield stress / strain for pin-ended tubular struts (D=60.3mm and t=2.3mm) with an initial imperfection, δ_0/L, 0.0015 for slenderness ratios, λ =

36 and 55; 0.001 for λ = 73; 0.0005 for λ = 91, 110 and 150. Ten elements were used for the total strut length. Note that the yield stress and strain are obtained from stub-column tests and the different initial imperfections with respect to the corresponding experimental specimens were assumed herein.

From Fig.3.12, it can be seen that the strut load capacities decrease with increasing slenderness ratios. Struts of slenderness ratios of 36 and 146 follow a comparatively flat post-buckling curve, while struts in between show a rapid load shedding post-buckling behaviour. Note that the so-called rapid load shedding post-buckling behaviour is most sensitive near the peak load area, and after a certain deformation range, the post-buckling behaviour follows a similar trend for all struts, independently of slenderness ratios. It is appropriate at this point to introduce a boundary curve, and therefore the post-buckling behaviour can be understood according to the two differently defined zones. This phenomenon is illustrated schematically in Fig.3.13. Apart from the strain hardening behaviour of stub columns, there are three types of post-buckling behaviour in zone A, namely (I) gentle (moderate) load shedding, (II) rapid load shedding, (III) ductile behaviour. In zone B, the post-buckling behaviour follows one trend, i.e., (I) gentle load shedding.

3.6.2 Struts That Are Prestrained in Tension and Fully-Aged

Based on the stress-strain curves assumed in Fig.3.1(b), the critical stress and the axial strain curves, normalised with respect to yield stress / strain for struts that are prestrained in tension and fully-aged with different prestrains 3% and 7%, are shown in Fig.3.14 and Fig.3.15, respectively. The specific dimensions listed in Table.4.3 are used. The dimensions of specimens for strut testing are presented in Table 4.3 (in Chapter four, Experimental Program). To

stress the difference between the as-received and prestrained struts, the initial deflections adopted are the same as those for the as-received struts. Material properties were, E=203 GPa, E_t = 35 GPa, E_s = 7 GPa, σ_s = 285 MPa, σ_y = 327 MPa. The six slenderness ratios considered are : λ = 36, 55, 73 (74), 92, 110 (111) and 147.

Comparing Figs. 3.14 and 3.15 with Fig.3.12, it is seen that the behaviour of struts that are prestrained in tension and fully-aged is similar to that of the as-received struts. The description presented in the earlier section is applicable here.

3.6.3 Struts That Are Prestrained in Tension and Unaged

The stress-strain relationship assumed in Fig.3.1(c) is used to trace pre- and post-buckling load and axial shortening curves for struts that are prestrained in tension and unaged. Material properties adopted were E=203 GPa, E_t= 74.4 GPa, E_x=48 GPa, E_s=15 GPa, σ_s=74 MPa. σ_x=234 MPa and σ_y=280 MPa. The initial deflections assumed are the as same as those for the as-received struts to emphasize the different characters between the as-received and prestrained struts. The six slenderness ratios considered are : λ = 36, 55, 73, 91, 110 and 147. The critical stress and axial strain curves normalised with respect to yield stress / strain for struts that are prestrained in tension and unaged are shown in Figs.3.16 and 3.17 for different prestrains of 3% and 7%, respectively. Referring to the zones defined in Fig.3.13, it can be seen that the post-buckling behaviour follows the trend classified in zone B, i.e., (I) gentle (moderate) load shedding.

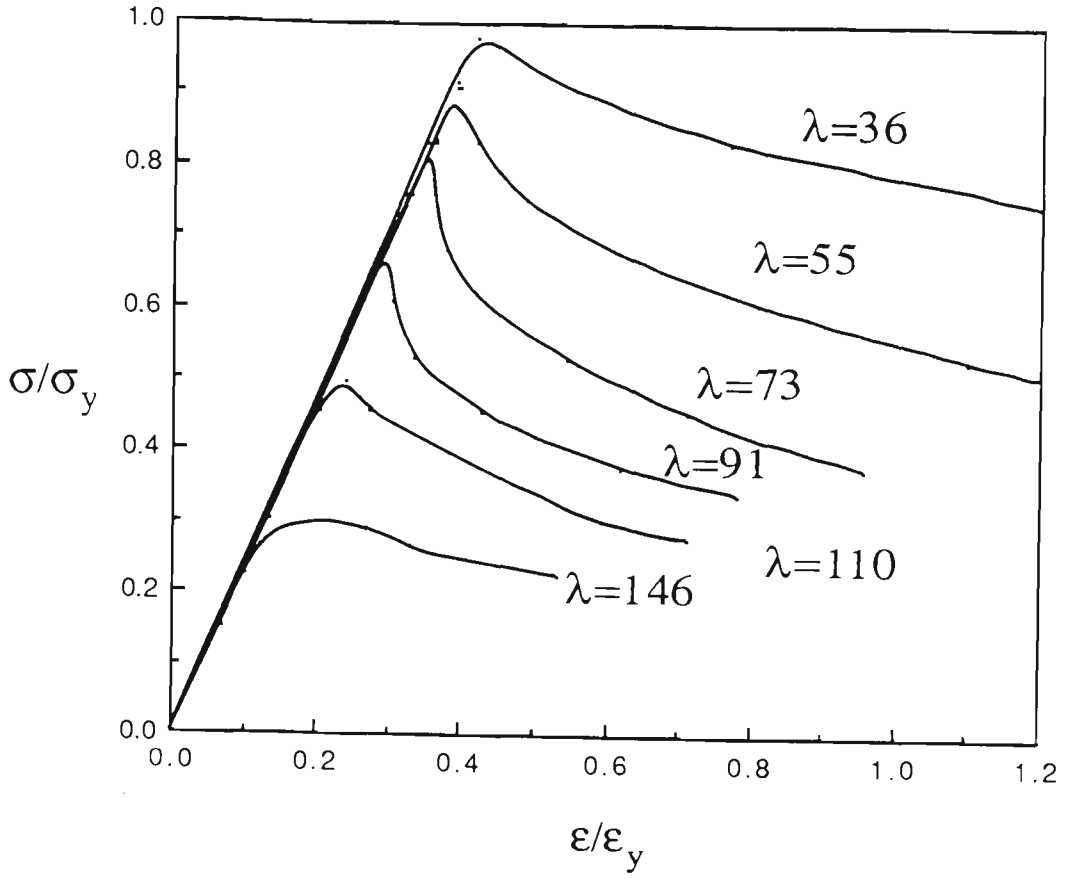

Fig.3.12 Theoretical Curves of As-Received Struts

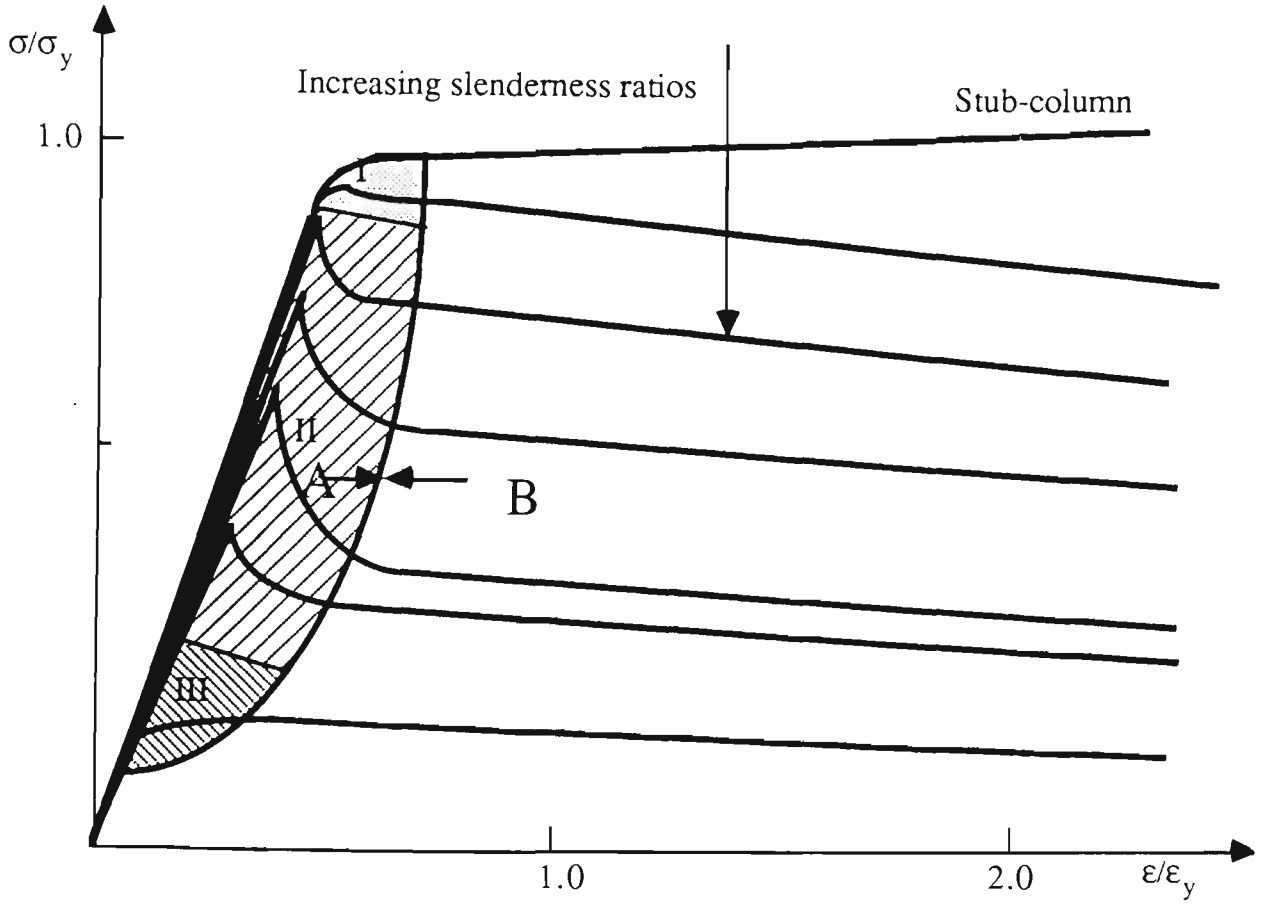

Fig.3.13 Post-buckling Behaviour of Pin-ended Struts

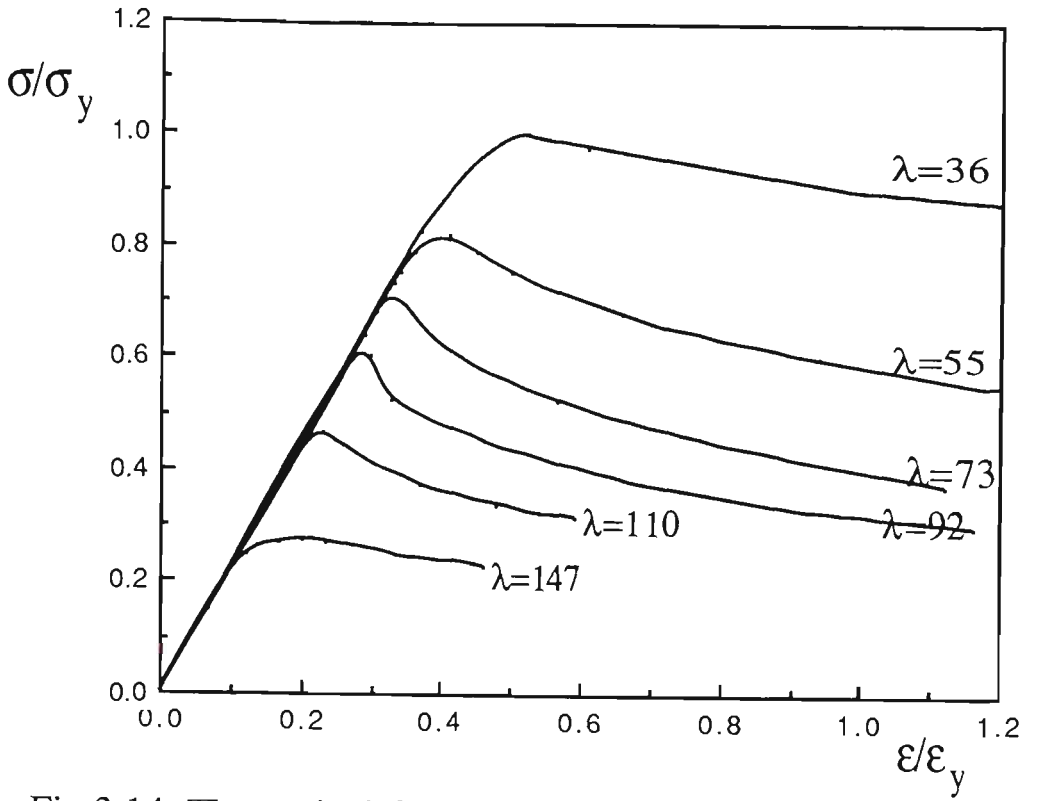

Fig.3.14 Theoretical Curves of 3% Prestrained Fully-Aged Struts

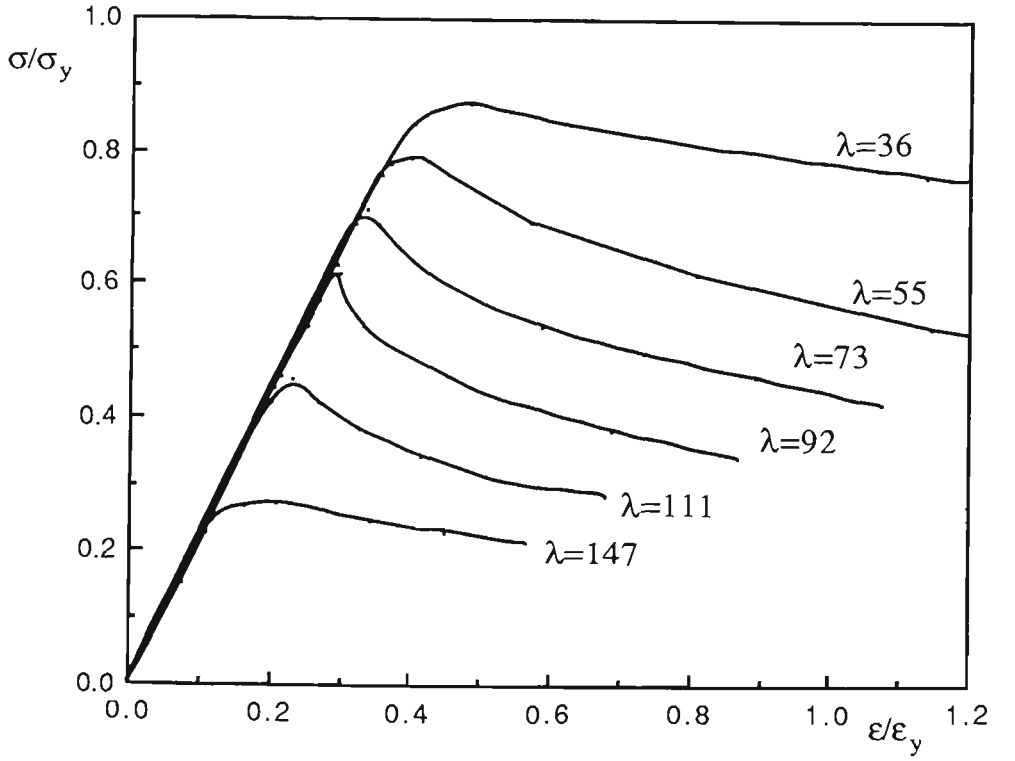

Fig.3.15 Theoretical Curves of 7% Prestrained Fully-Aged Struts

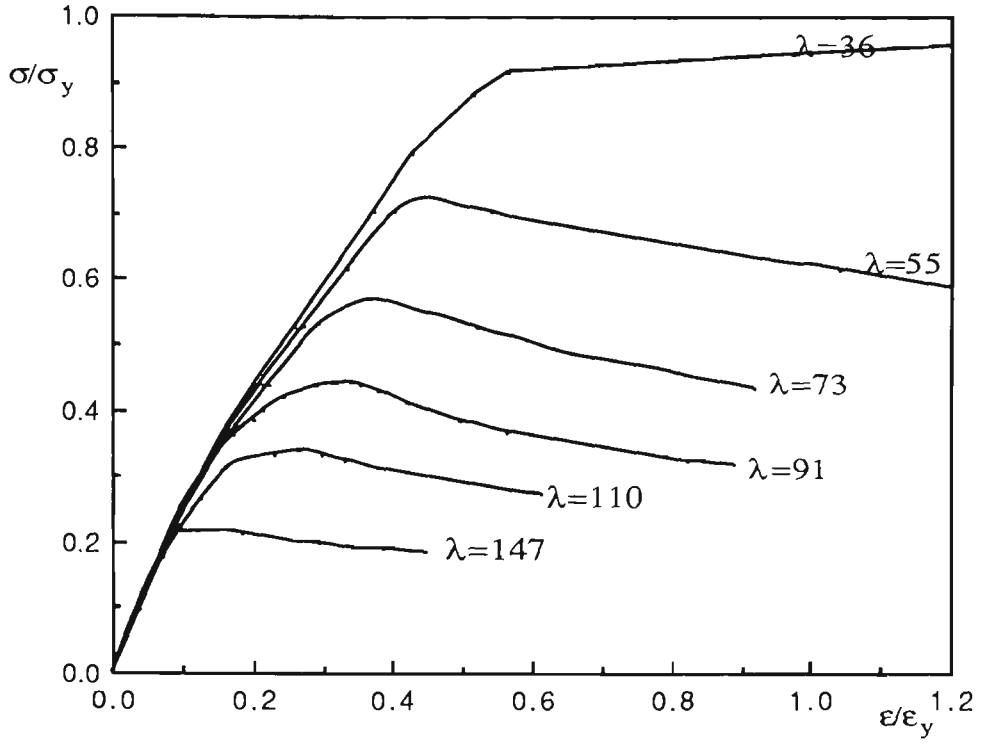

Fig.3.16 Theoretical Curves of 3% Prestrained Unaged Struts

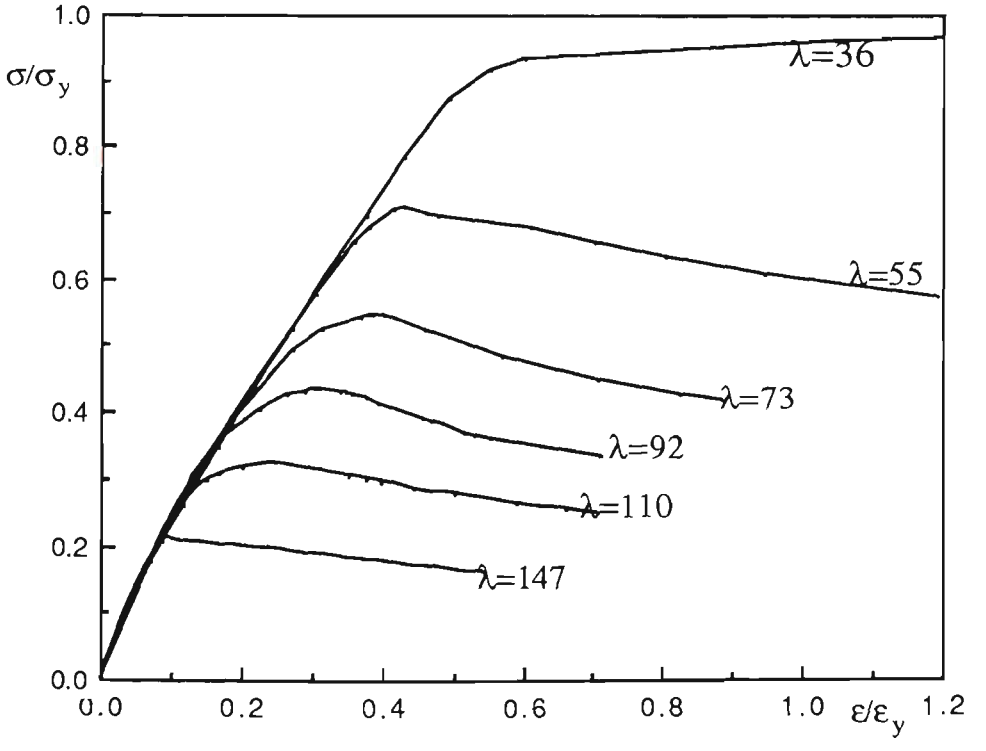

Fig.3.17 Theoretical Curves - 7% Prestrained Unaged Struts

3.6.4 Combined Results

Based on the calculated results, the theoretical results, for the maximum average stress of both as-received struts and struts that are prestrained in tension, versus slenderness ratios are presented in Fig.3.18. Note that the theoretical results have been normalised with respect to both the yield stress and the transition slenderness ratio (The transition slenderness ratio is defined as the value at which the Euler critical stress equals the yield stress of the material).

The theoretical average stress versus average strain curves, normalised with respect to the yield stress / strain of the as-received struts and the struts that are prestrained in tension, are plotted in Figs.3.19 to 3.24 for different slenderness ratios. Regarding the struts that are prestrained in tension and fully-aged, it can be seen that the strut behaviours are similar to those for as-received struts. As for the struts that are prestrained in tension and unaged, a significant discrepancy between these results and the as-received struts exists near the peak load area, but the curves eventually cluster around those of the as-received struts in the post-buckling range.

From these figures, the difference in load capacities for different conditions is clearly seen. All the prestrained struts have lower capacities than the corresponding as-received struts. This loss of load capacity is due to the Bauschinger effect on load reversal. Strain aging reduces this reduction.

Based on the observation of the material behaviour it is found that following plastic tensile prestrains the Bauschinger rounding is revealed on load reversal, and it has the effect of reducing the 0.2% offset stress, reducing or eliminating a

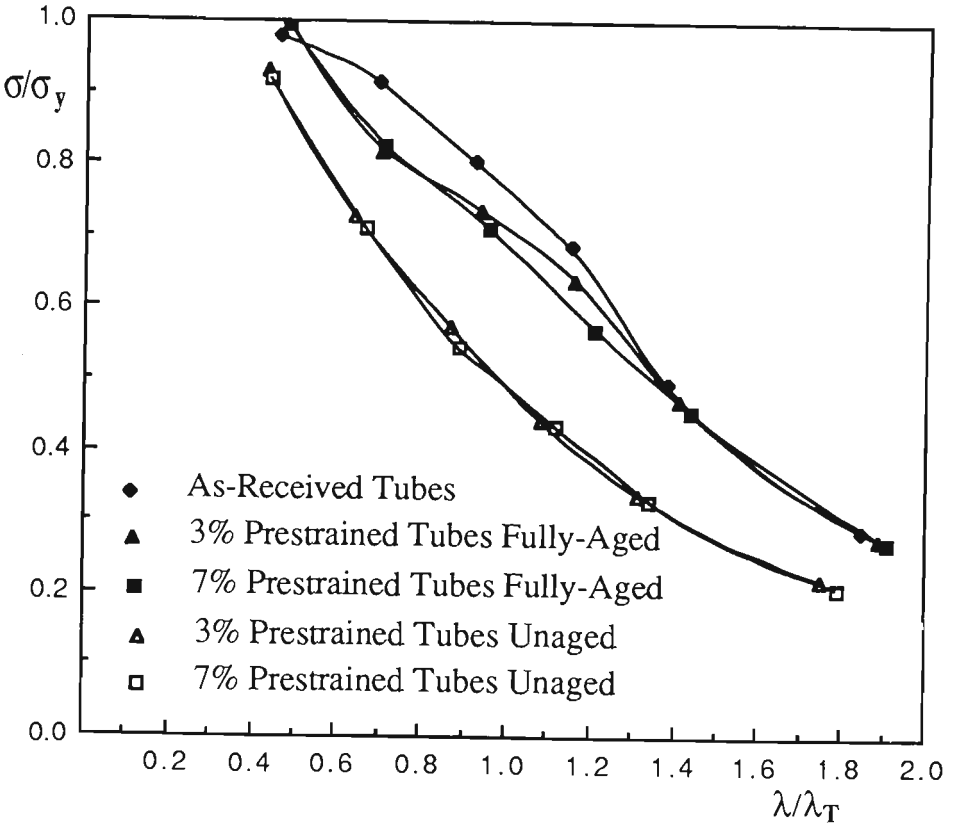

Fig.3.18 Theoretical Results - All Conditions

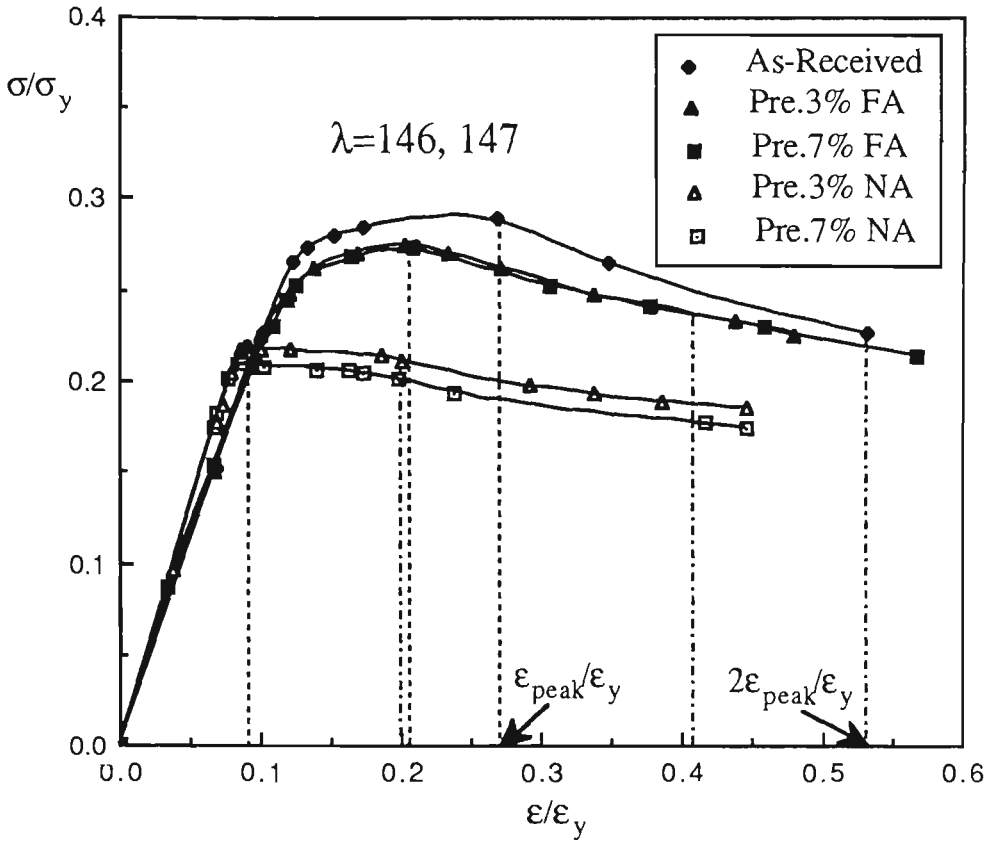

Fig.3.19 Theoretical Curves - All Conditions

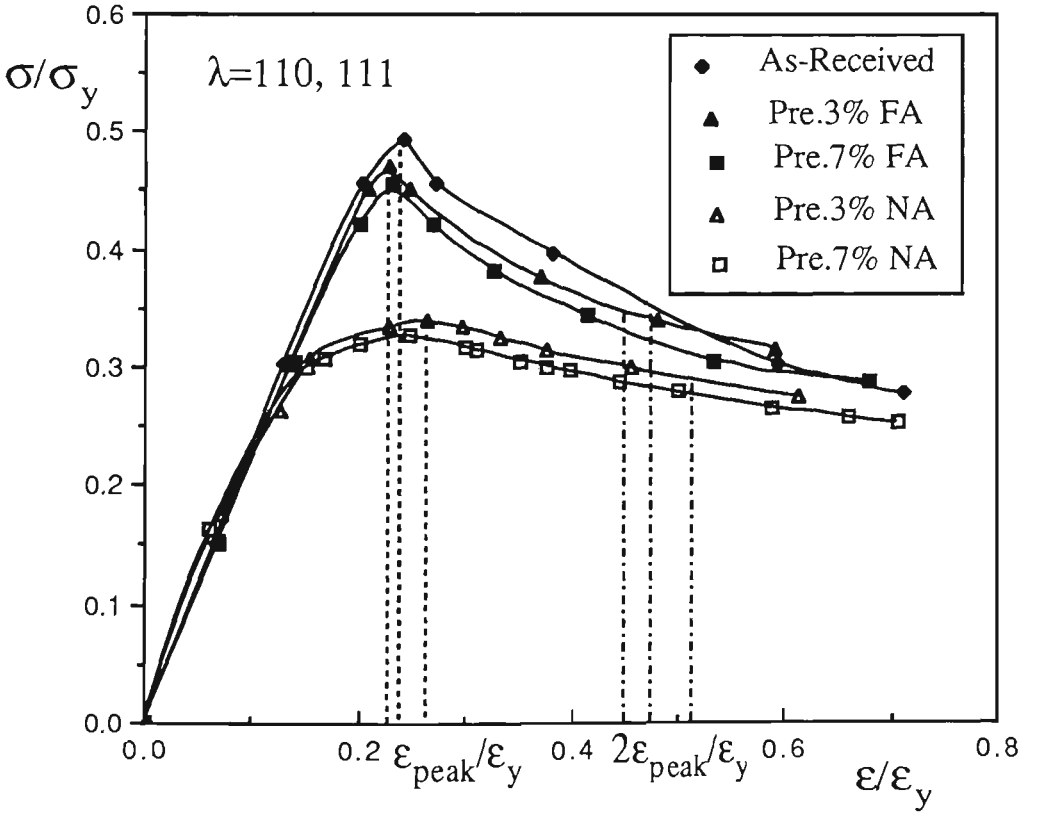

Fig.3.20 Theoretical Curves - All Conditions

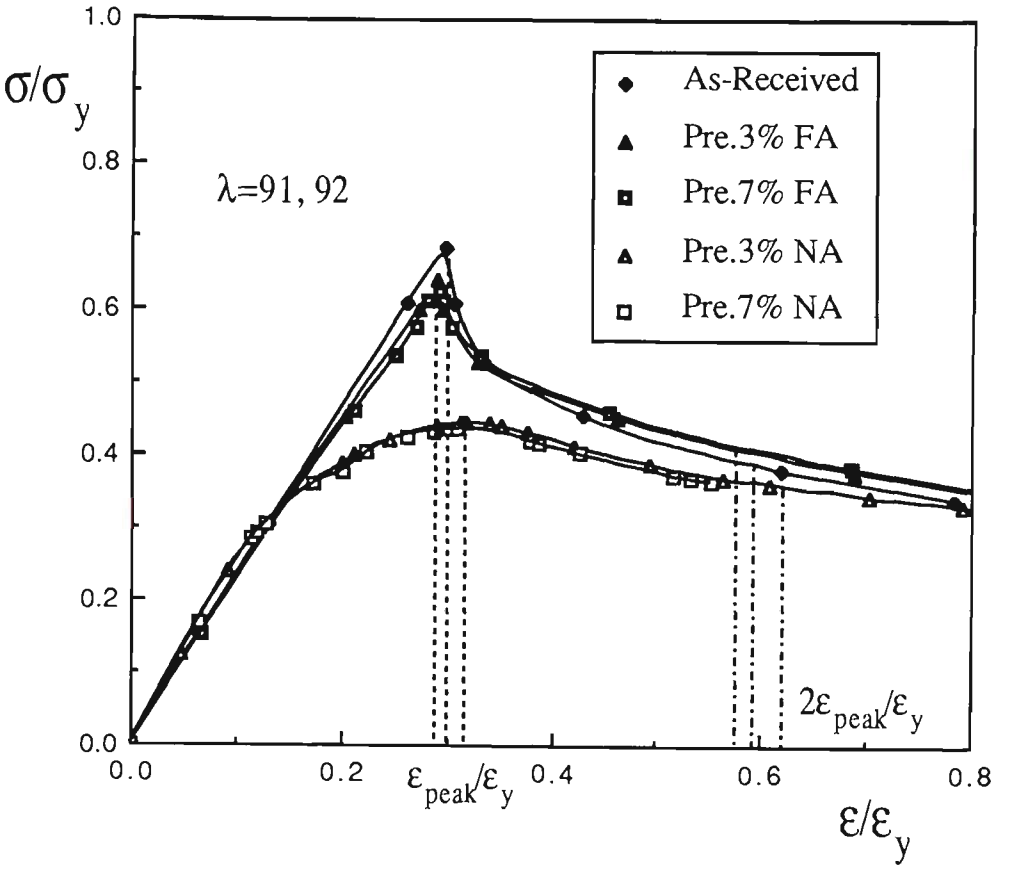

Fig.3.21 Theoretical Results - All Conditions

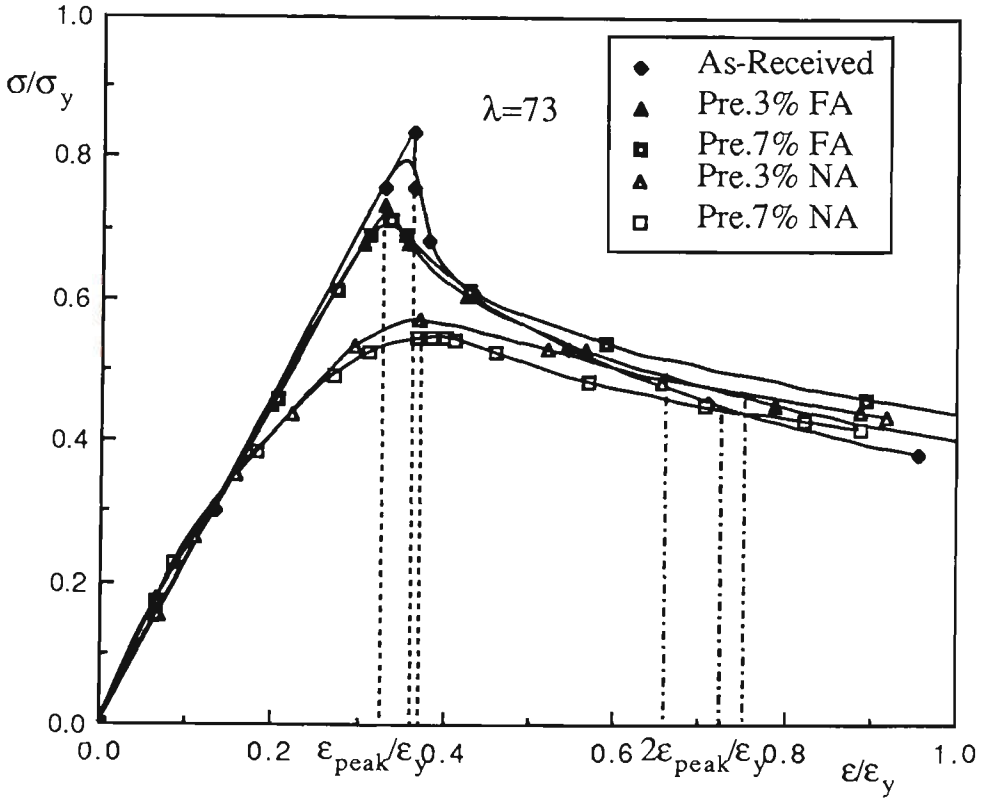

Fig.3.22 Theoretical Curves - All Conditions

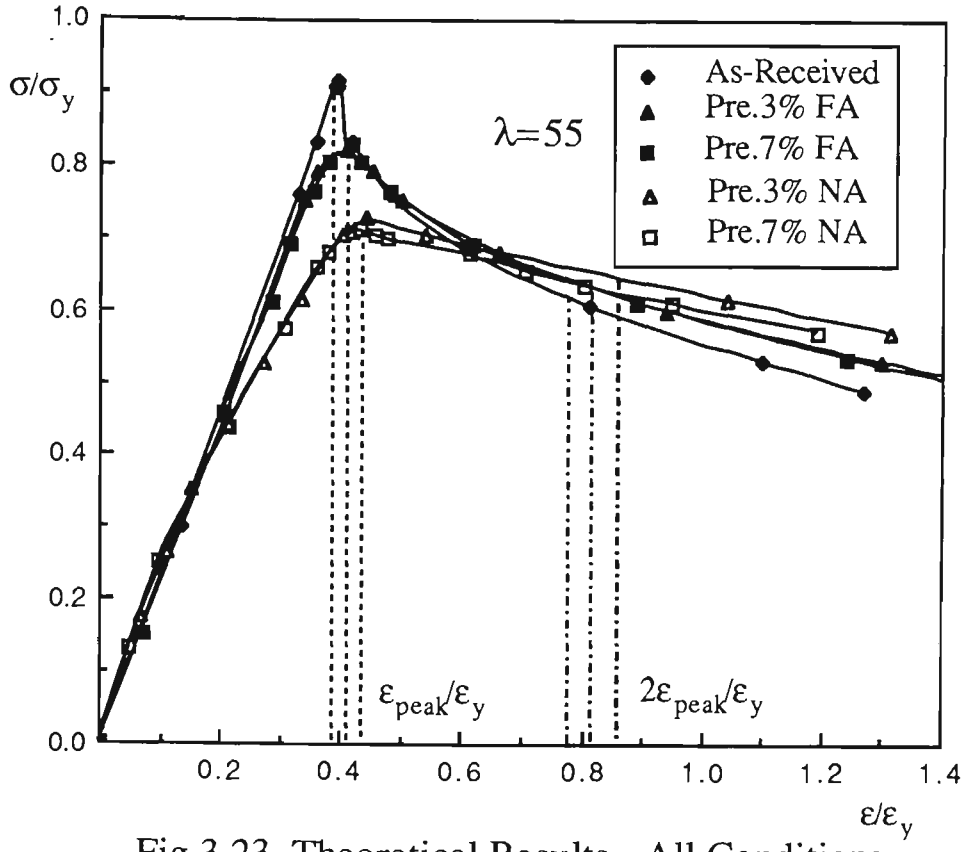

Fig.3.23 Theoretical Results - All Conditions

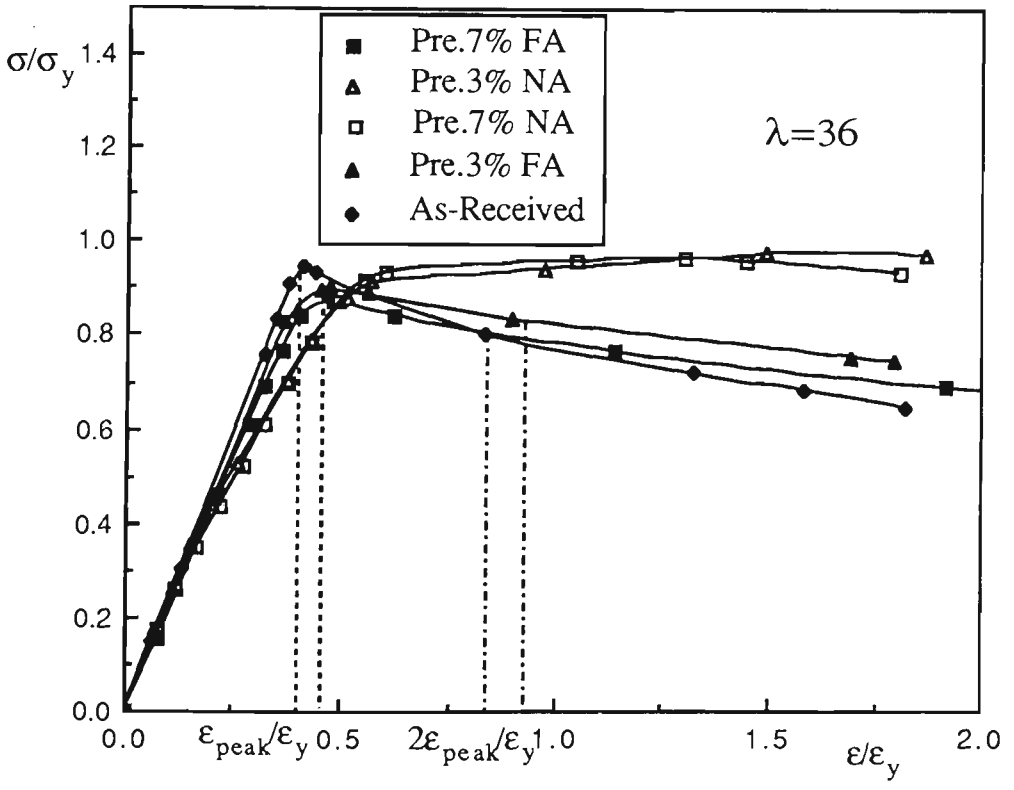

Fig.3.24 Theoretical Results - All Conditions

proportional limit, and changing the peak load capacity of the as-received tube. In other words, the Bauschinger rounding reduces the tangent modulus in compression markedly, which in turn leads to a significant reduction of strut load capacity. The influence of strain aging and strain hardening reduces this reduction. The three stress-strain relationships of the steel assumed with respect to the as-received, prestrained in tension and fully-aged and prestrained in tension and unaged material, reflect these effects .

Further details concerning strain hardening, strain aging and the Bauschinger effect will be discussed in the following chapters.

Compared with the as-received struts and the struts that are prestrained in tension and fully-aged (see Figs.3.20-3.24), the piecewise linear stress-strain model assumed for the material that is prestrained in tension and unaged (referring to Fig.3.1(c)) gives the following results for the strut analysis: (I) greater nonlinearity prior to buckling is manifested; (II) a much lower buckling load is furnished; (III) the post-buckling load drop with increasing axial shortening is much less marked.

To better understand and quantify the post-buckling behaviour, nominally, comparisons are made of the curves at peak strains ($\varepsilon_{peak}/\varepsilon_y$) and double peak strains ($2\,\varepsilon_{peak}/\varepsilon_y$) to intersect the curves respresenting different strut conditions. With respect to the as-received struts, the struts which are prestrained in tension and fully-aged, and the struts which are prestrained in tension and unaged respectively (Figs.3.19-3.24), the points of intersection between ordinates at $2\varepsilon_{peak}/\varepsilon_y$ with the normalized critical stress vs axial strain curves can be referred to as the residual load capacity (σ_{Re}/σ_y) after buckling, as afterwards the post-buckling behaviour is ductile. Note that for prestrained struts the vertical lines are

only drawn for struts which are prestrained to 3%, as the difference in the curves between 3% and 7% prestrained struts is small.

Table 3.2 gives details of the maximum load capacity and the residual load capacity. The post-buckling loads drop dramatically (29% - 44%) for the as-received struts with slenderness ratios λ=55–110, and as expected the drop reduces with slenderness ratios smaller λ=36 (14%) and larger λ=146 (20%). This phenomenon is identical with the three types of post-buckling behaviour discussed in Section 3.5.1, viz. (I) gentle load shedding (II) rapid load shedding, and (III) ductile behaviour.

For the struts which are prestrained in tension and fully-aged, the post-buckling load drop is similar to that of the as-received struts. That is, the post-buckling loads drop more dramatically for struts with λ=55–110 (23% - 36%) than with λ=36 (8%) and λ=147 (11%).

The post-buckling load drop for the struts that are prestrained in tension and unaged, which belongs to the type of gentle load shedding behaviour, is much less (9% - 18%) for all the slenderness ratios (λ=36 – 147) compared with the as-received struts and the struts that are prestrained in tension and fully-aged.

Figs.3.19 - 3.24 and Table 3.2 also indicate the significant post-buckling load capacities of the struts after reaching the ultimate load, 56% to 86% of maximum load capacities for the as-received struts, 64% to 92% of maximum load capacities for the struts prestrained in tension and fully-aged, and 82% to 91% of maximum load capacities for struts prestrained in tension and unaged.

Table 3.2 Summary of Failure and Post-Failure Condition (Theoretical Results)

λ	Condition	σ_{peak}/σ_y	σ_{Re}/σ_y	$\sigma_{Re}/\sigma_{peak}$ %	$\frac{\sigma_{peak}-\sigma_{Re}}{\sigma_{peak}}$ %
36	AR	0.95	0.81	86	14
	FA	0.90	0.83	92	8
	NA	0.98	-	-	-
55	AR	0.92	0.61	66	34
	FA	0.82	0.63	77	23
	NA	0.73	0.65	89	11
73 (74)	AR	0.80	0.45	56	44
	FA	0.74	0.49	66	34
	NA	0.57	0.47	82	18
91 (92)	AR	0.69	0.39	57	43
	FA	0.64	0.41	64	36
	NA	0.44	0.36	82	18
110 (111)	AR	0.49	0.35	71	29
	FA	0.47	0.34	72	28
	NA	0.34	0.29	85	15
146 (147)	AR	0.29	0.23	80	20
	FA	0.28	0.24	89	11
	NA	0.23	0.21	91	9

FA=Fully-Aged. NA=Unaged, AR=As-Received.

σ_{peak}=Maximum load capacity, σ_{Re}=Residual load capacity.

σ_{peak}/σ_y and σ_{Re}/σ_y are defined in Fig.3.24a.

Fig.3.25 summarizes the previously defined residual load capacity versus normalised slenderness ratio curves for both as-received and prestrained struts. Although the curves are not very regular, it can be expected that the trend of the curves gives some insight into the residual load capacity. Compared with Fig.3.18 which shows the ultimate load capacity versus normalised slenderness ratio curves, it is sen that two figures follow a similar trend, but the difference in residual load capacity between the struts which are prestrained in tension and fully-aged and the struts which are prestrained in tension and unaged is smaller.

Fig.3.26 gives the percentage residual load capacity relative to peak load capacity versus normalised slenderness ratio curves for both as-received and prestrained struts. It is noted that the percentage residual load capacities are the lowest in the transition slenderness ratio range, and become higher towards the larger or smaller slenderness ratios. Among the three curves, the struts prestrained in tension and unaged furnish the highest percentage residual load capacities, the struts prestrained in tension and fully-aged are below these, and the as-received struts furnish the least percentage residual load capacities. Even though the as-received struts furnish the lowest percentage residual load capacities, nevertheless these capacities are highly significant (61% to 88%) of maximum load capacities.

3.6.5 The Effects of Strain Hardening

After buckling, the strains in the inelastic region of the struts can become very large and therefore the present theoretical model considers the influence of strain hardening on the elasto-plastic behaviour of the tubular struts. To check the sensitivity of the post-buckling behaviour to various amplitudes of strain hardening modulus Es, struts of slenderness ratios λ=36 and 73 are studied herein with variation of strain hardening modulus Es.

The results of analyses are shown in Figs.3.27 and 3.28 for as-received struts, Figs.3.29 and 3.30 for struts that are prestrained to 3% in tension and fully-aged , and Figs.3.31 and 3.32 for struts that are prestrained to 3% in tension and unaged. The sensitivity of load capacity to various amplitudes of strain hardening modulus Es is clearly seen in the post-buckling range. It is seen that the strut strength and the behaviour of post-buckling at slenderness ratio of λ=36 is more sensitive to the value of Es than those at λ=73. In fact, at a slenderness ratio of λ=73, the difference owing to various values of Es is only seen in the post-buckling range.

3.7 SUMMARY

A nonlinear finite element model for tracing the inelastic post-buckling load-deformation path of tubular struts is developed. The analysis accounts simultaneously for both the geometrical and material nonlinearities. The influence of strain-unloading is included. In particular, the model takes into account a generalised stress-strain relationship which includes the influence of strain hardening. The structure tangent stiffness matrix is obtained by using a series of transformation matrices to update the element geometry. The so-called arc-length

iterative numerical procedure is used to obtain a solution to the incremental equations of equilibrium.

The procedure has been applied to trace out the inelastic load-deflection paths of pin-ended struts with varying slenderness ratios and initial geometrical imperfections for both as-received and prestrained struts. Results obtained compared very well with available analytical results such as those from Kitipornchai and Chan(1986), and the Nastran Computer Package (1982).

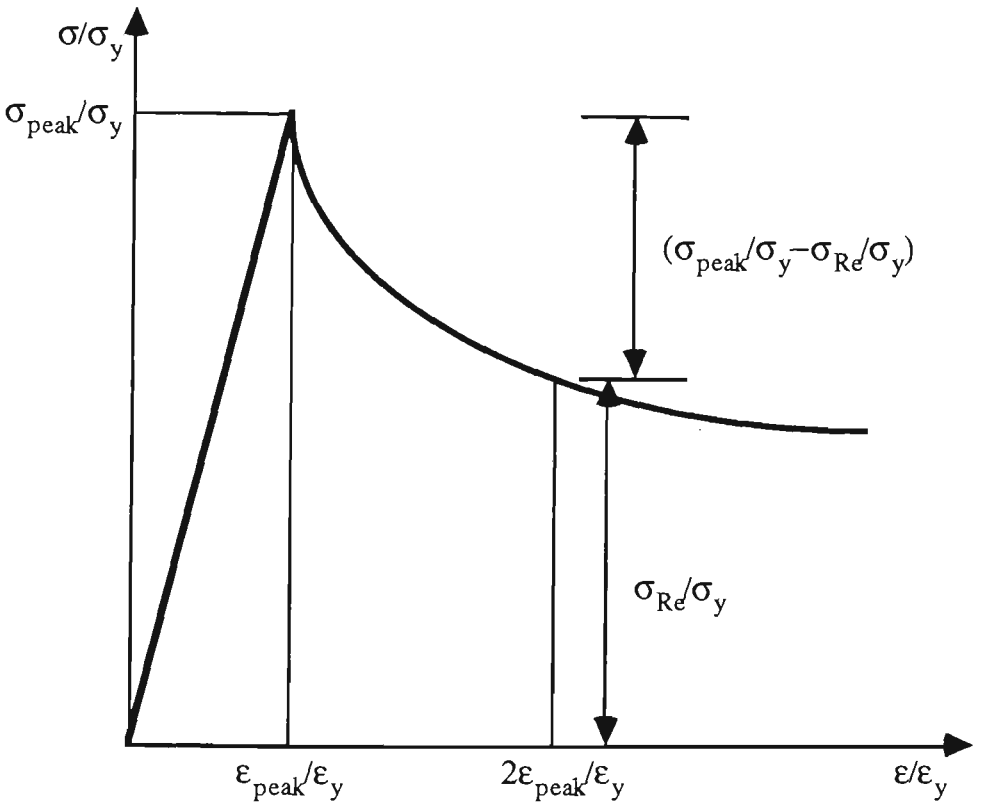

Fig 3.24a Definition of σ_{peak}/σ_y and σ_{Re}/σ_y

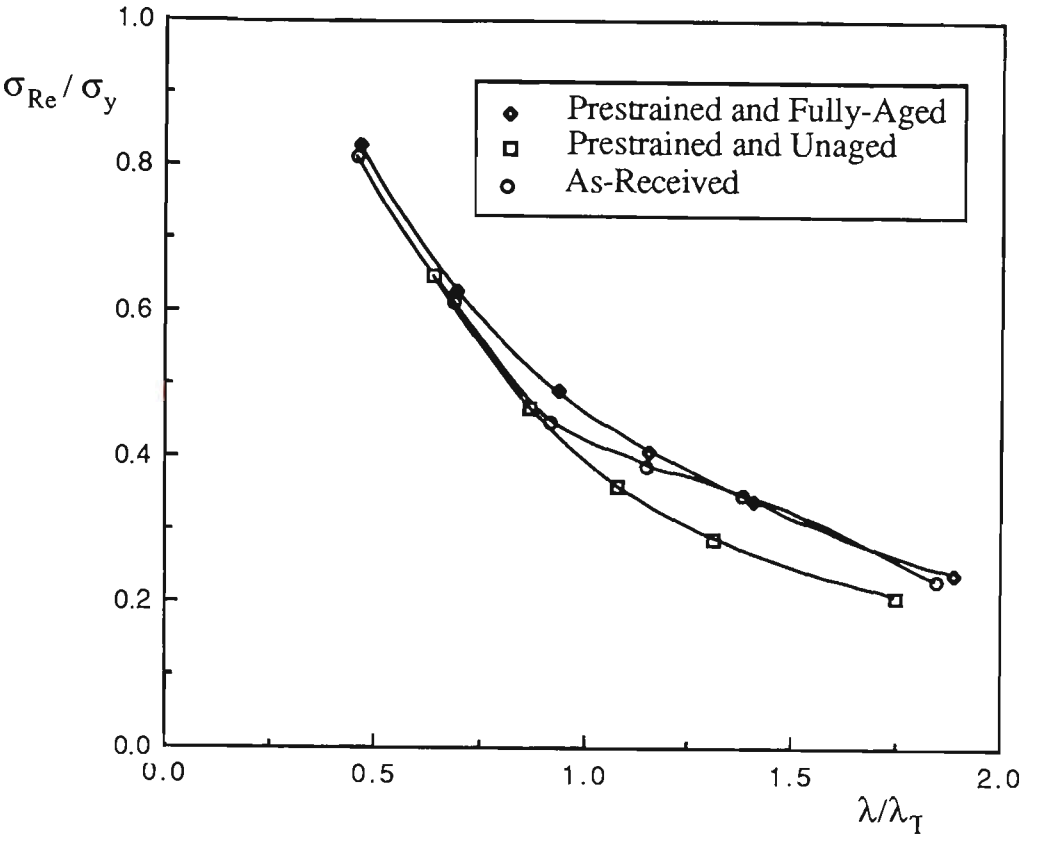

Fig.3.25 Residual Load Capacity versus Normalised Slenderness Ratio

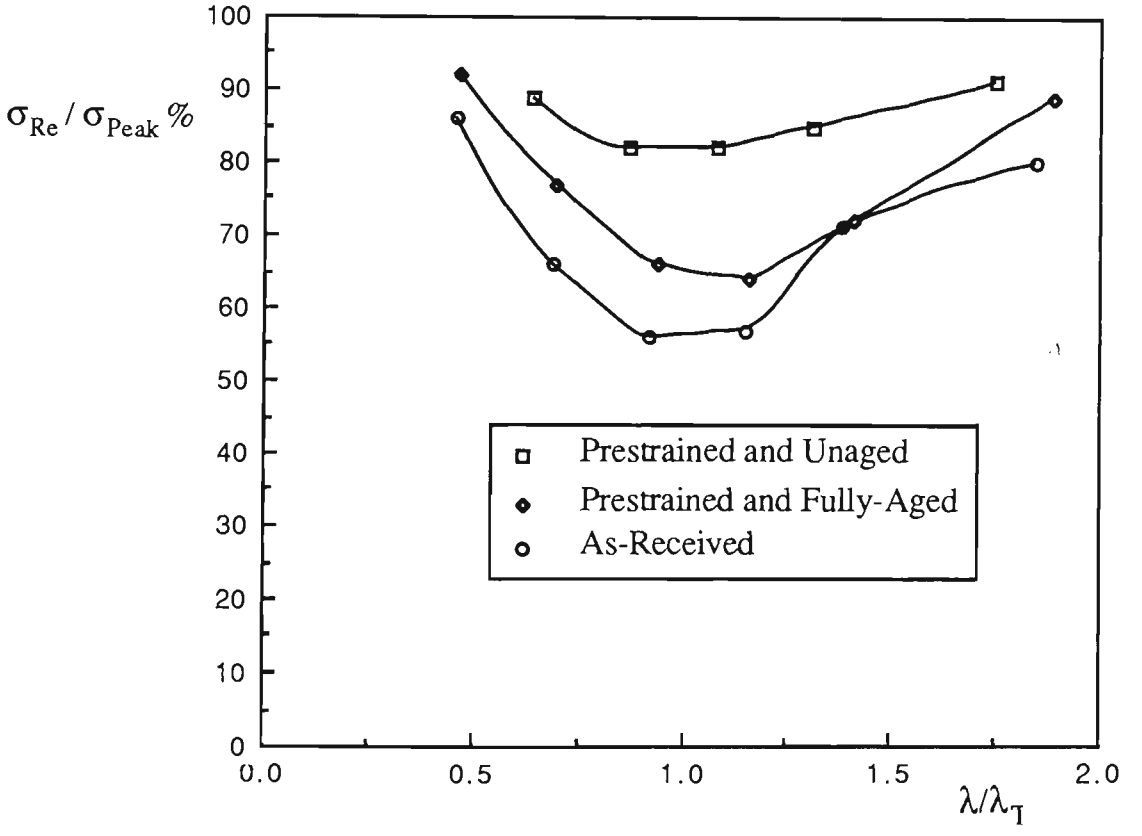

Fig.3.26 Percentage of Residual Load Capacity Relative to Peak Load Capacity versus Normalised Slenderness Ratio

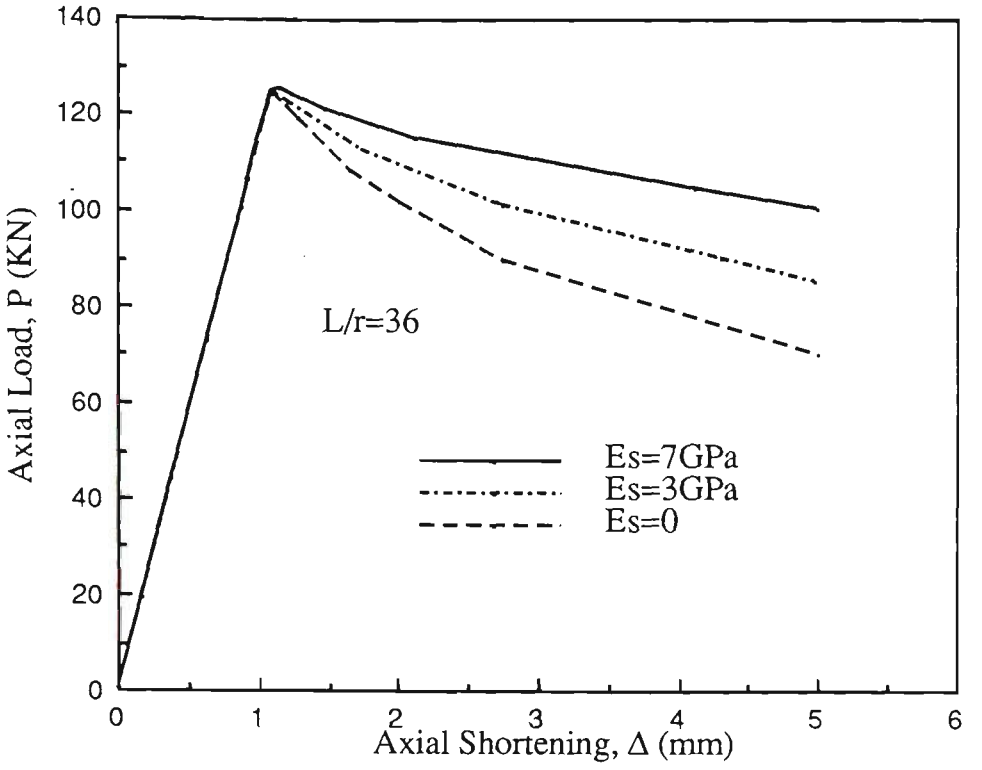

Fig.3.28 Theoretical Curves with Variation of Es
As-Received Strut

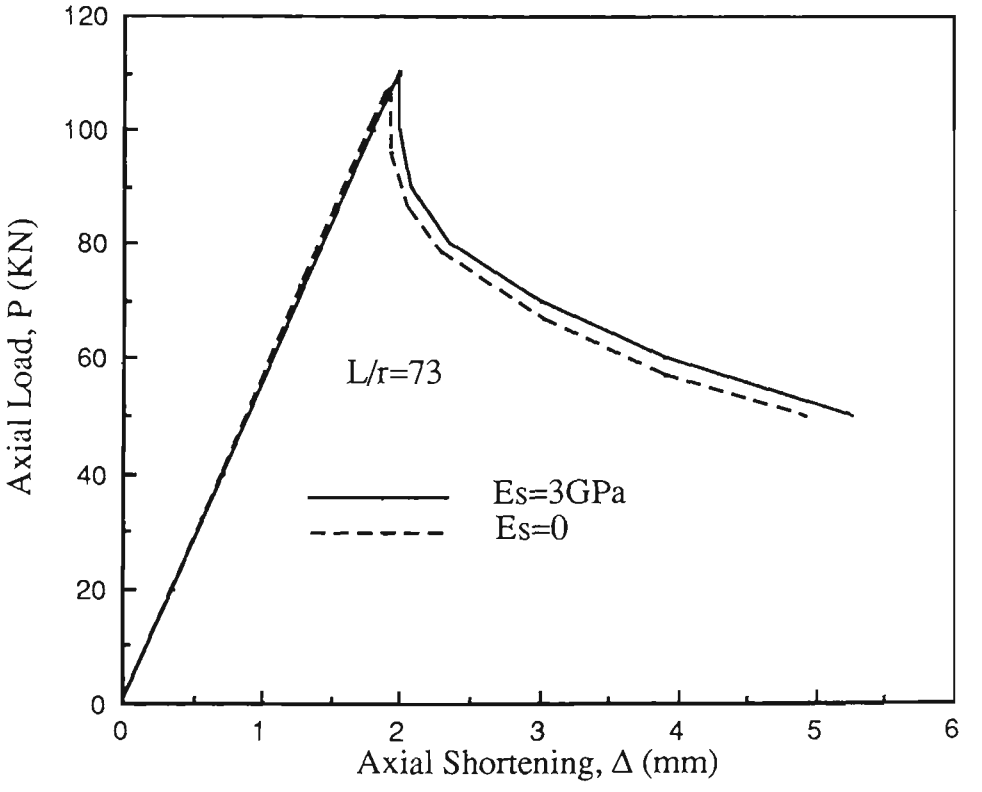

Fig.3.27 Theoretical Curves with Variation of Es
As-Received Strut

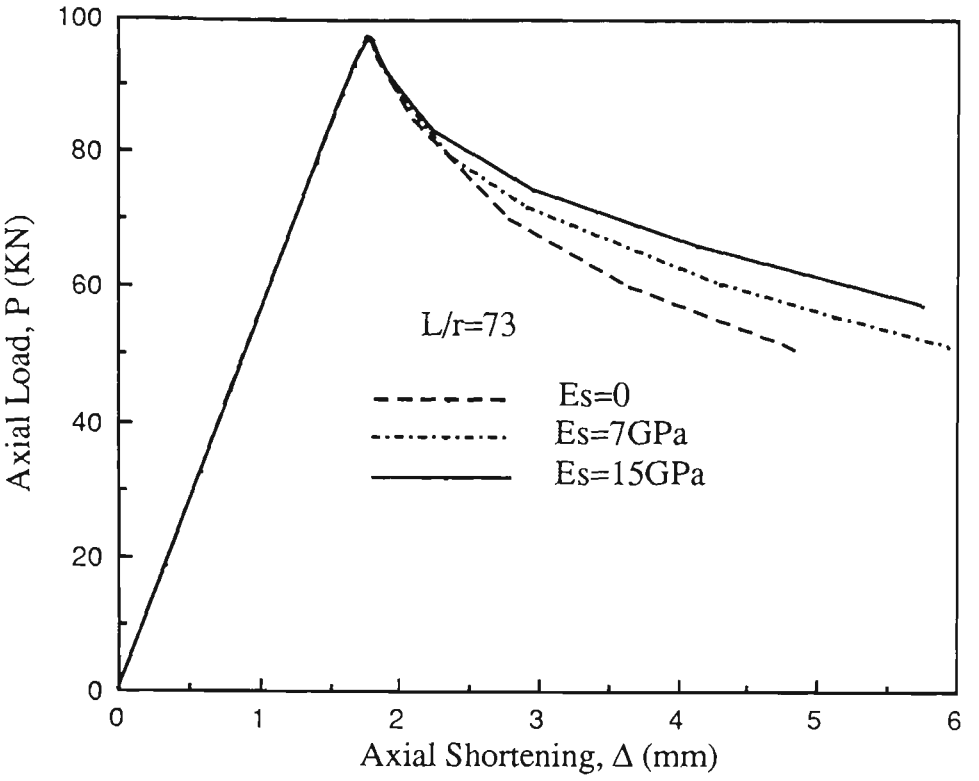

Fig.3.29 Theoretical Curves with Variation of Es
3% Prestrained Fully-Aged Strut

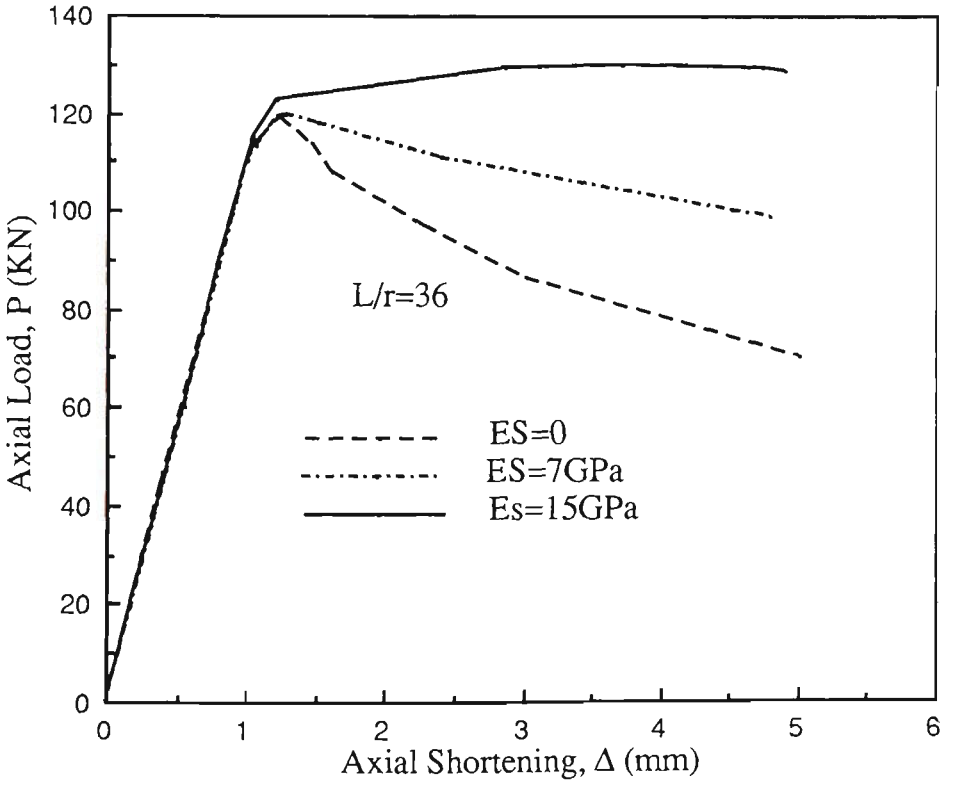

FiG.3.30 Theoretical Curves with Variation of Es
3% Prestrained Fully-Aged Strut

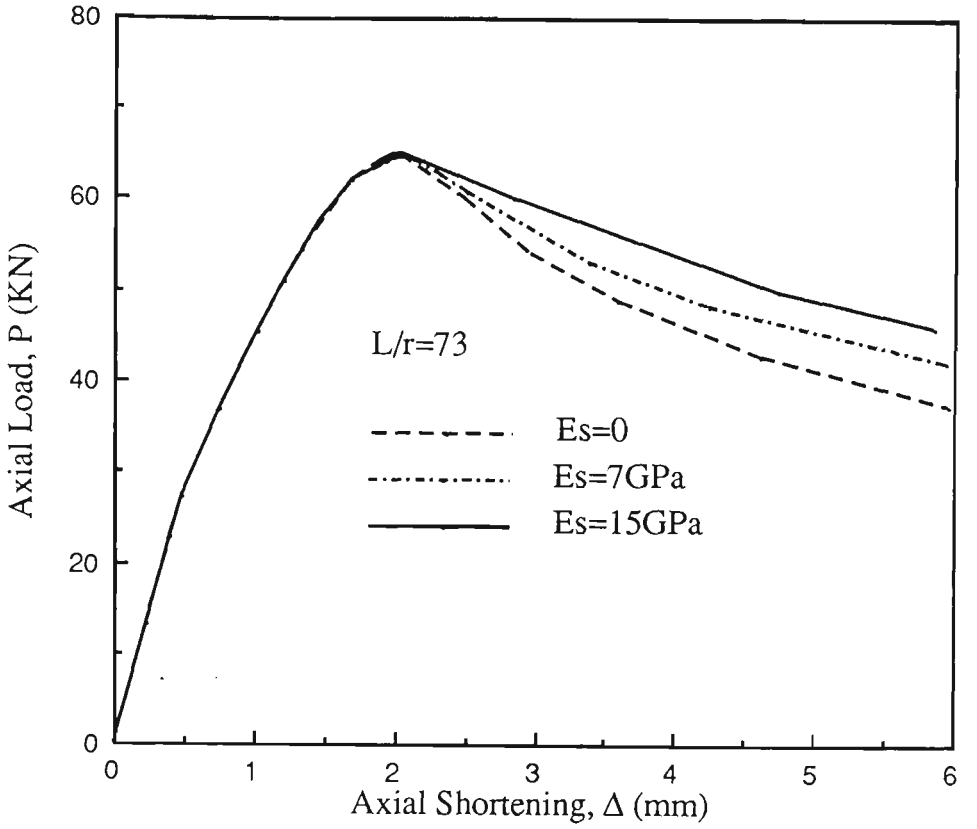

Fig.3.31 Theoretical Curves with Variation of Es
3% Prestrained Unaged Strut

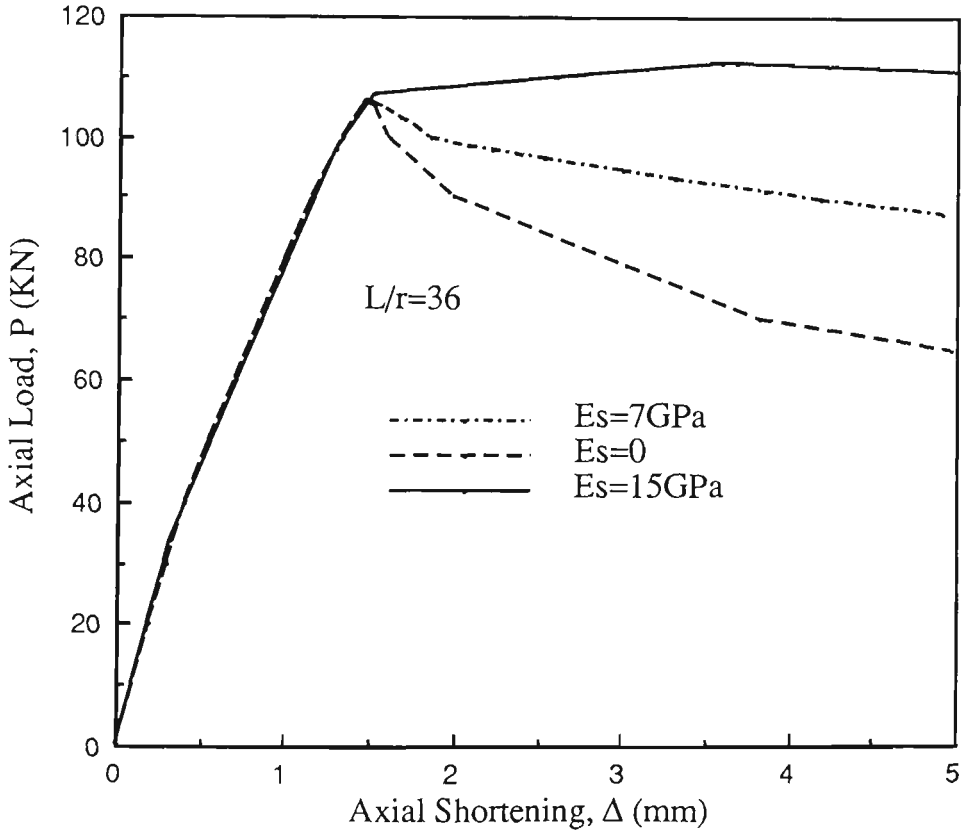

Fig.3.32 Theoretical Curves with Variation of Es
3% Prestrained Unaged Strut

CHAPTER FOUR

EXPERIMENTAL PROGRAM

4.1 GENERAL

To furnish basic data in the elastic and inelastic ranges, material tests have been conducted under tensile and compressive loading, including the influence of strain aging, strain hardening and the Bauschinger effect.

In order to determine the influence of strain aging, strain hardening and the Bauschinger effect on strut load capacity, 85 pin-ended steel tubular strut tests have been carried out under different conditions.

On the basis of the least-squares criterion, regression analyses were used to provide an unbiased trend in the strut test results. A comparison is made between the observed strut load capacities and the theoretical results that were predicted using the simple tangent modulus method. The experimental results are also compared with current column design curves from various international codes of practice.

4.2 DESCRIPTION OF MATERIAL AND SPECIMENS

The material used in the tests was a hot-rolled low-carbon rimming steel. It had an essentially uniform fine equiaxed grain structure with a grain size of approximately 9μm; the rim had a much larger grain size of approximately 55μm.

The tubular cross section had an outside diameter 60.3mm and wall thickness 2.3mm. The tubes were manufactured by cold-forming and seamed by the Electric Resistance Welding (ERW) process. The chemical analysis and mechanical properties of the ERW tube are presented in Table 4.1 .

All the specimens used in this research were rolled from one of the three heat numbers shown in Table 4.1. Tensile tests of the material were performed by Tubemakers of Australia Limited on 25.4mm wide strips cut from tube from the beginning, middle and end of the coil from which the donated specimens were made. The tensile test results are shown in table 4.2 . Each test piece was artificially aged for 20 minutes at between 150^0c and 200^0c. Testing was in accordance with AS1391, straining rate A (A is the conventional straining rate), using $R_{t0.5}$ ($R_{t0.5}$=0.5% total elongation proof stress) as reported yield strength and elongation was reported on a gauge length of $5.65\sqrt{S_o}$ (S_o=original cross-section area within the gauge length), using BS3894 Part 1 as a basis of conversion from an actual gauge length of 50mm.

Table 4.1 ERW Tube

Electric Resistance Welded (ERW) tube manufactured from multi-slit rimming steel. O.D.=60.3mm, Wall thickness=2.3mm.

	% of Element by Mass								
Heat No.	C	P	Mn	Si	S	Ni	Cr	Mo	Cu
6675111	0.045	0.012	0.31	0.005	0.012	0.022	0.014	0.002	0.008
7669841	0.055	0.012	0.3	0.005	0.013	0.024	0.012	0.003	0.016
8173381	0.06	0.013	0.25	0.005	0.007	0.021	0.015	0.002	0.013

Table 4.2 Material Properties of Rimming Steel

Location of Coil	Yield strength	Ultimate Strength	$\frac{\sigma_y}{\sigma_u}$	Elongation
	$\sigma_{y(MPa)}$	σ_u (MPa)		%
Beginning	351	366	0.96	36
Middle	357	383	0.93	38
End	356	382	0.93	33
Average	355	377	0.94	36

Tensile and squash tests of the forms detailed in Fig.4.1 and Fig.4.2 have been conducted to furnish basic data in the elastic and inelastic ranges under tensile and compressive loading .

Tensile specimens were tubes of 0.6m length with 12mm thick end plates to facilitate gripping in the testing machine. Compressive specimens were cylinders of 200mm length and will be referred to as squash cylinders (stub-columns). The ends of the stub-columns were machined to provide intimate contact with the platens of the servo-controlled testing machine.

Table 4.3 gives the list and dimensions of specimens supplied for strut testing. The slenderness ratios of the specimens range from 36 to 150 . The effective lengths of the struts were measured between two knife edges.

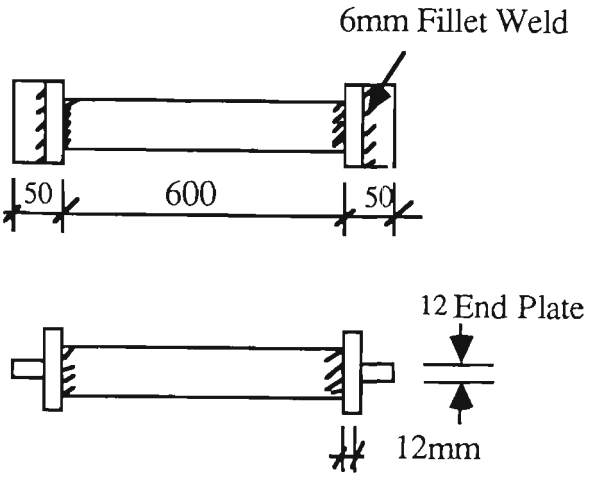

Fig.4.1 Tensile Specimens

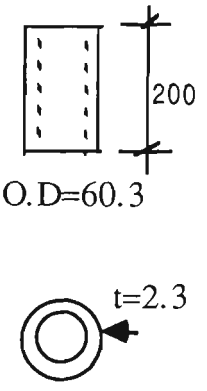

Fig.4.2 Compressive Specimens

Table 4.3 List and Dimensions of Specimens for Strut Testing

No.	Length(L) mm	L/r ratio	Outside Diameter D mm	Thickness t mm	Condition	Max.Dev.from Straightness mm	δ_o/L	Initial Ovality $\frac{Dmax - Dmin}{Dmean}$
1	2998	146				1.50	0.0005	
2	2998	146				2.00	0.0007	
3	2247	110				1.60	0.0007	
4	2247	110				1.12	0.0005	
5	1870	91	60.3	2.3	AR	0.70	0.0004	
6	1872	91				0.94	0.0005	
7	1496	73				1.50	0.0010	
8	1496	73				1.48	0.0010	
9	1122	55				0.85	0.0008	
10	1122	55				0.30	0.0003	
11	746	36				1.12	0.0015	
12	742	36				1.14	0.0015	
13	2986	147	59.75	2.252		1.50	0.0005	0.0067
14	2983	147	59.64	2.257		1.80	0.0006	0.0047
15	2235	110	59.69	2.255	PRE	0.44	0.0002	0.0064
16	2235	110	59.77	2.25	3%	0.50	0.0002	0.0050
17	1862	92	59.81	2.251	FA	0.50	0.0003	0.0067
18	1860	91	59.81	2.259		5.58	0.0030	0.0067
19	1866	92	59.71	2.254		0.70	0.0004	0.0034
20	1485	73	59.88	2.247		0.35	0.0002	0.0084
21	1487	73	59.84	2.248		0.30	0.0002	0.0033
22	1112	55	59.80	2.250		0.30	0.0003	0.0050
23	1112	55	59.78	2.251		0.60	0.0005	0.0034
24	737	36	59.92	2.245		0.30	0.0004	0.0033
25	737	36	59.92	2.245		0.40	0.0005	0.0050
26	2984	147	59.73	2.253		1.00	0.0003	0.0062
27	2985	147	59.69	2.253		1.00	0.0003	0.0027
28	2233	110	59.63	2.271		1.89	0.0009	0.0160
29	2236	110	59.80	2.249	PRE	1.20	0.0005	0.0060
30	1862	91	59.84	2.248	3%	0.30	0.0002	0.0033
31	1862	91	59.96	2.243	NA	0.50	0.0003	0.0083
32	1489	73	59.97	2.243		0.30	0.0002	0.0067
33	1486	73	59.83	2.249		0.20	0.0001	0.0017
34	1111	54	59.90	2.245		0.30	0.0003	0.0033
35	1111	55	59.78	2.251		0.30	0.0003	0.0033
36	737	36	60.02	2.241		0.30	0.0004	0.0033
37	739	36	60.02	2.241		0.30	0.0004	0.0033
38	2944	147	58.88	2.218	PRE	0.82	0.0003	0.0039
39	2941	147	58.98	2.213	7%	0.50	0.0002	0.0142
40	2215	111	58.71	2.209	FA	1.50	0.0007	0.0155
41	2213	111	58.71	2.209		1.35	0.0006	0.0078
42	1837	93	58.19	2.227		2.10	0.0011	0.0086
43	1839	92	58.85	2.200		1.00	0.0005	0.0034

Table 4.3 List and Dimensions of Specimens (continued)

44	1474	74	58.76	2.204		1.10	0.0008	0.0051
45	1471	74	58.76	2.204	PRE 7%+	1.20	0.0008	0.0034
46	1096	55	58.92	2.197	FA	0.50	0.0005	0.0007
47	1095	55	58.92	2.197		0.10	0.0007	0.0007
48	901	45	59.32	2.182		0.60	0.0006	0.0051
49	901	45	59.05	2.192		0.70	0.0008	0.0017
50	900	45	59.15	2.188		0.70	0.0008	0.0068
51	732	37	57.83	2.200		1.10	0.0015	0.0590
52	717	36	59.15	2.188		0.40	0.0006	0.0132
53	2940	147	58.71	2.286		1.10	0.0004	0.0085
54	2952	148	58.71	2.217		0.99	0.0003	0.0060
55	2208	110	59.01	2.204		0.70	0.0003	0.0270
56	2213	111	58.71	2.209		0.55	0.0003	0.0034
57	1838	92	58.43	2.217		1.40	0.0008	0.0017
58	1839	91	59.22	2.185		1.50	0.0008	0.0051
59	1471	73	59.05	2.192		0.60	0.0004	0.0051
60	1471	73	59.06	2.192		1.00	0.0007	0.0034
61	1098	55	58.89	2.199	PRE 7%	0.70	0.0006	0.0101
62	1096	55	58.95	2.196	+ NA	0.60	0.0006	0.0101
63	722	36	58.78	2.203		0.70	0.0010	0.0120
64	718	36	58.91	2.198		0.30	0.0004	0.0112
65	1839	92	58.59	2.210		0.80	0.0004	0.0034
66	1839	92	58.62	2.220	SRA	0.93	0.0005	0.0010
67	1470	74	58.67	2.212	PRE 7%	0.90	0.0006	0.0017
68	1470	74	58.81	2.206	+ FA	1.42	0.0010	0.0051
69	1096	55	58.74	2.206		0.76	0.0007	0.0027
70	1096	55	58.80	2.207		1.10	0.0010	0.0024
71	723	36	58.98	2.197		0.76	0.0011	0.0007
72	722	36	58.92	2.198		0.74	0.0010	0.0058
73	1862	92	59.59	2.259		0.60	0.0003	0.0017
74	1862	92	59.63	2.257		1.26	0.0007	0.0013
75	1488	73	59.59	2.258	SRA	0.90	0.0006	0.0017
76	1488	74	59.65	2.256	PRE 3%	0.86	0.0006	0.0010
77	1112	55	59.68	2.255	+ NA	1.46	0.0013	0.0020
78	1111	55	59.73	2.253		1.03	0.0009	0.0020
79	736	36	59.74	2.258		0.70	0.0010	0.0013
80	735	36	59.77	2.251		0.54	0.0007	0.0007
81	1870	91				0.50	0.0003	
82	1495	73				0.22	0.0001	
83	1499	73	60.3	2.3	AR	0.20	0.0001	
84	1120	55				0.50	0.0004	
85	745	36				0.60	0.0008	

AR=As-Received, PRE=Prestrained in Tension, FA=Fully-aged, NA=Unaged.
SRA=Stress Relief Annealed, δ_o/L as defined in Fig.4.34

4.3 INSTRUMENTATION

All the tests (including both material and struts up to 1875mm long for both prestraining and compression) were performed in a 50 tonne capacity closed loop hydraulic testing system (Instron machine) with controlled rates of ram travel. This machine typically consists of three major units : a) a reaction loading frame; b) an electronic control console; c) a hydraulic power pack.

The servo-hydraulic loading frame and closed loop servo - block diagram are shown in Fig.4.3 and Fig.4.4 respectively. Within servo hydraulic testing systems, energy is transmitted to the specimen using high pressure hydraulic fluid acting on a double sided piston (actuator). The actuator is mechanically coupled to the specimen through a reaction loading frame (see Fig.4.3).

Prestraining for longer struts (L=2233mm to 2998mm) were performed in a floor rig using prestressing jacks, and extensions were measured with steel tapes over the total strut length . A photograph of the loading frame is shown in Fig.4.5. Buckling test for longer struts were carried out in a Mohr and Federhaf Universal testing machine, as shown in Fig.4.6.

In addition to load and apparent extension , by obtaining a load-deformation plot from the Instron machine, to check elastic moduli, and permit other more detailed calculations, some test specimen contractions were measured. An extensometer of gauge length 100mm (see Fig.4.7) was mounted centrally with respect to the length of the material test specimen, and specimen contraction was recorded with a Linear Variable Deflection Transducer by a Hewlett Packard 3054A Data Acquisition Automatic Control System , as shown

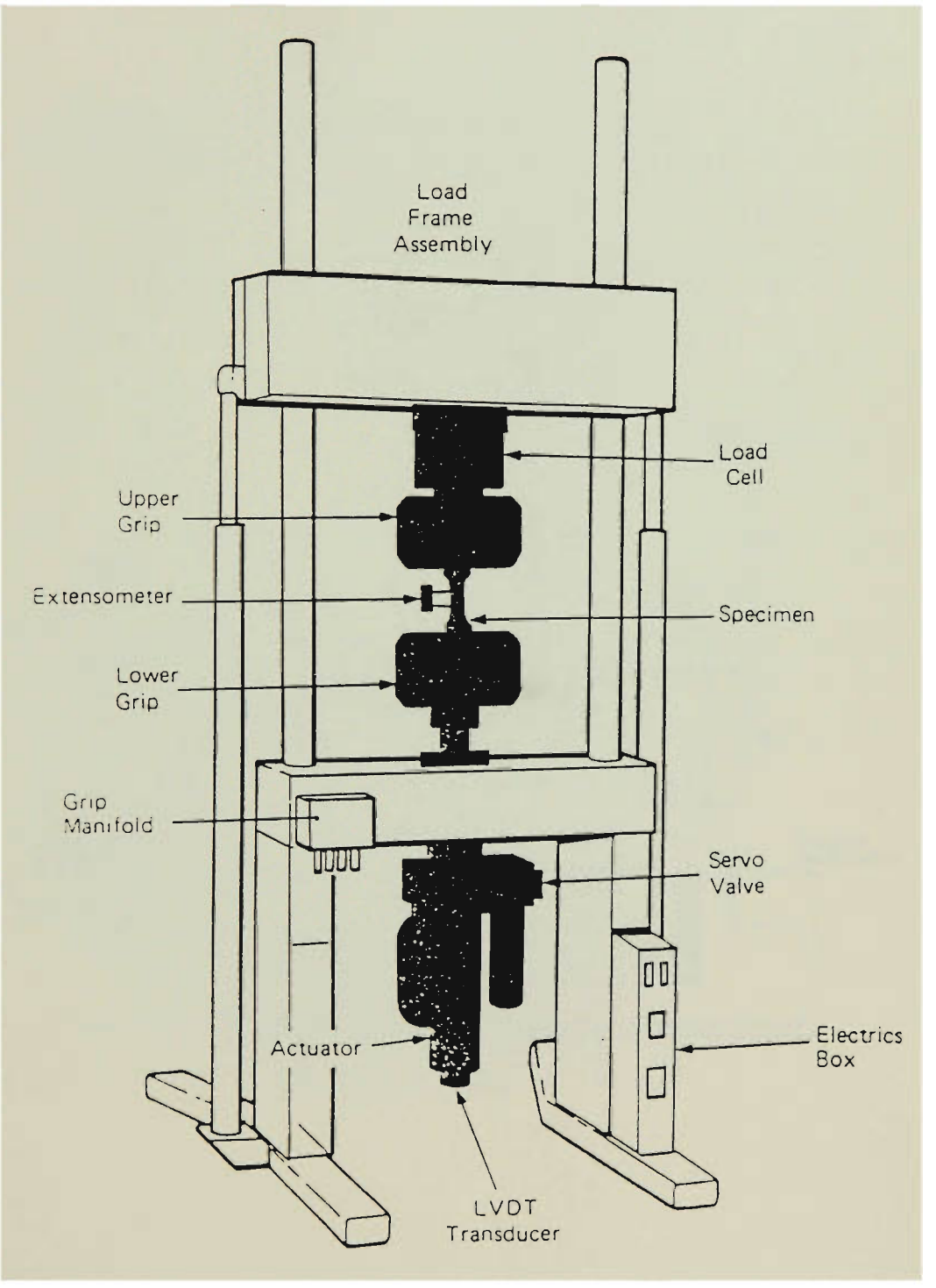

Fig.4.3 Reaction Loading Frame showing Actuator and Transducers

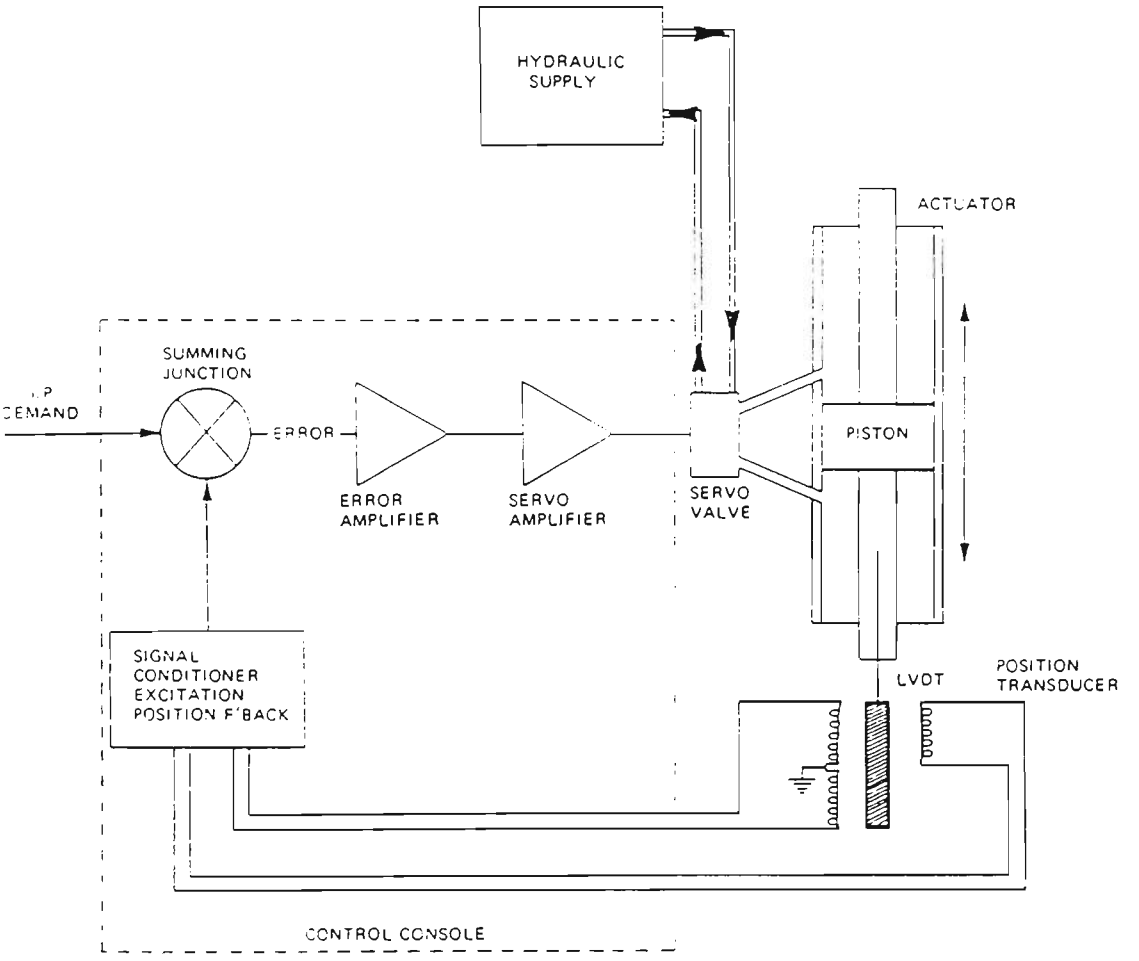

Fig.4.4 Typical Closed Loop Servo - Block Diagram

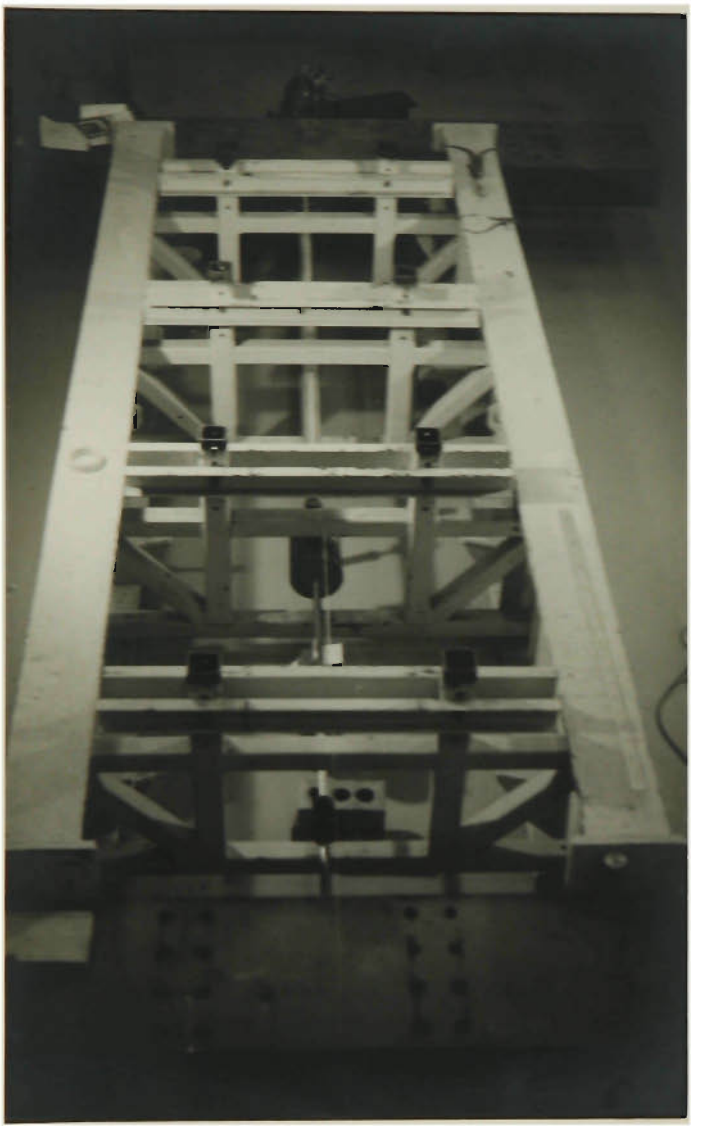

Fig.4.5 Loading Frame for Stretching

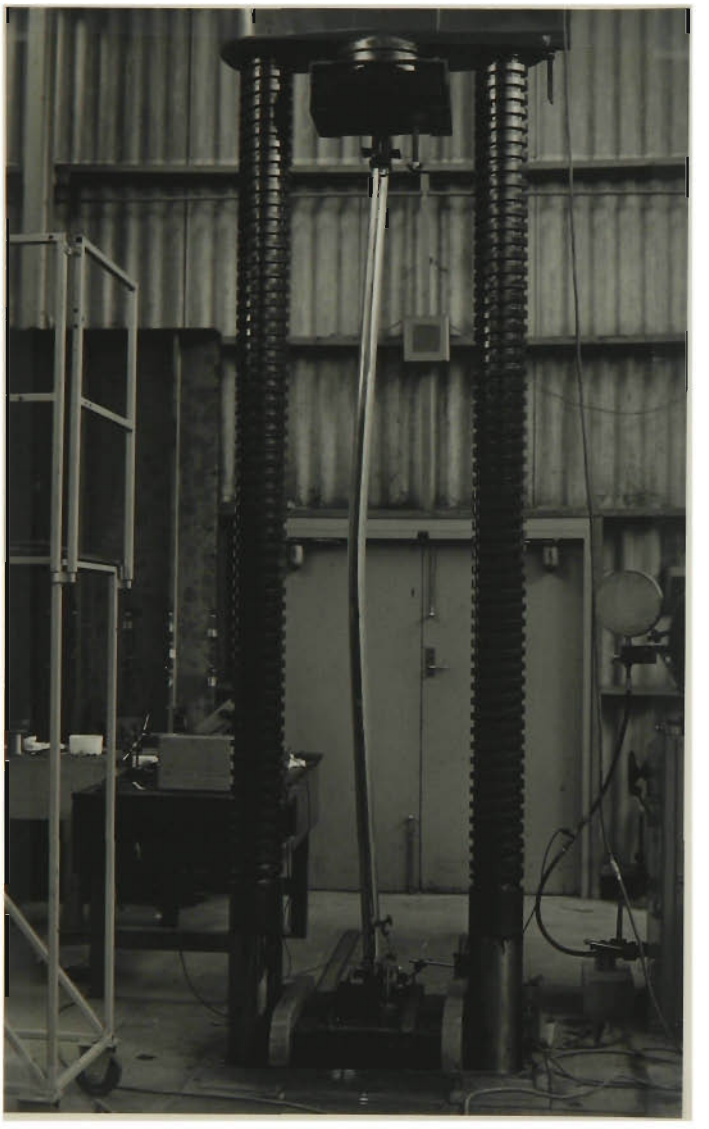

Fig.4.6 Mohr & Federhaf Universal Testing Machine

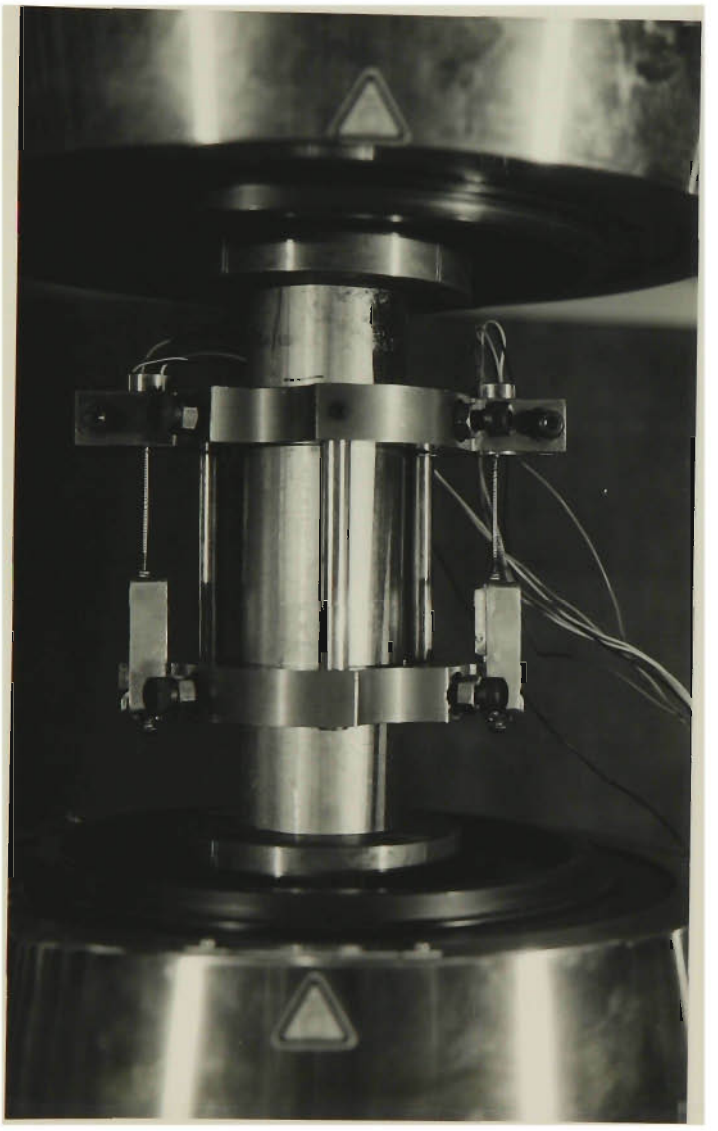

Fig.4.7 Extensometer

in Fig.4.8. Two readings were taken at locations 180 degrees apart in plan around the longitudinal axis of the tube. The Data Acquisition Control System consists of two transducers used for converting displacements to voltage signals, a computer HP 9826 which is a controller of the system, and a data acquisition control system HP 3054A which contains a system Mainframe 3497A used for connecting the HP 3456A to voltage sources and a voltmeter HP 3437A, and which is interfaced via a HP-IB cable to the 9826 computer.

All devices on the bus were given a unique address, and the bus was under the control of the 9826 computer. The 3497 accepted inputs, through a variety of input modules, and was connected directly to either the 3437 or 3456 voltmeter. Commands were sent down the bus to the 3054 to tell it to read an input channel. While this channel is being read, a voltmeter is told to measure the voltage on its input. This value is then transferred, via the Bus, to the computer where it is stored/processed.

The Data Acquisition / Control Unit is the instrument that provides the analog multiplexing, digital monitoring, and control functions using plug-in assemblies. Analog signals switched by the 3497A are connected to either the 3456A Digital Voltmeter for measurement.

The Digital Voltmeter is a HP high accuracy, high resolution Voltmeter - an essential instrument for low level measurements. It is an extremely versatile DVM offering variable precision, variable speeds, and noise rejection through integration and guarding.

The System Voltmeter is a 3 1/2 digit high speed sampling voltmeter which provides precision timed sample and hold readings. It can perform a variety of

tasks from scanning DC inputs to AC waveform analysis. High speed scanning is provided by a hardware synchronization between the 3437A and the 3497A. Repetive signals with frequency components up to 1 MHz and low frequency transients longer than 1 ms can be rapidly digitized and analyzed.

The 9826s Desktop Computer needed to automate the 3054A System consists of the following:

1) 9826A Desktop computer with 64k bytes user read/write memory,
2) Two 256k byte memory cards (98256A),
3) 98611A Option 655 BASIC Soft Operating System with extended Soft BASIC System,
4) 98615A Option 655 Pascal Soft Operating System.

More details about the system are given in HP Manuals (1982).

The system program was written in HP-enhanced Basic Language. Fig.4.9 shows the flowchart for computer programming .

The measurement from the HP computer contains random errors in the output signals . In order to minimize these errors such as instrumental errors , the fluctuation of power supply , environmental noise , and so on , sixty readings were recorded in every scan and the average of these readings was taken as the final result of this scan .

Before testing , it was necessary to calibrate each of the transducers used in the experiment. The linear regression formulae employed to calculate the calibrated factors are as follows :

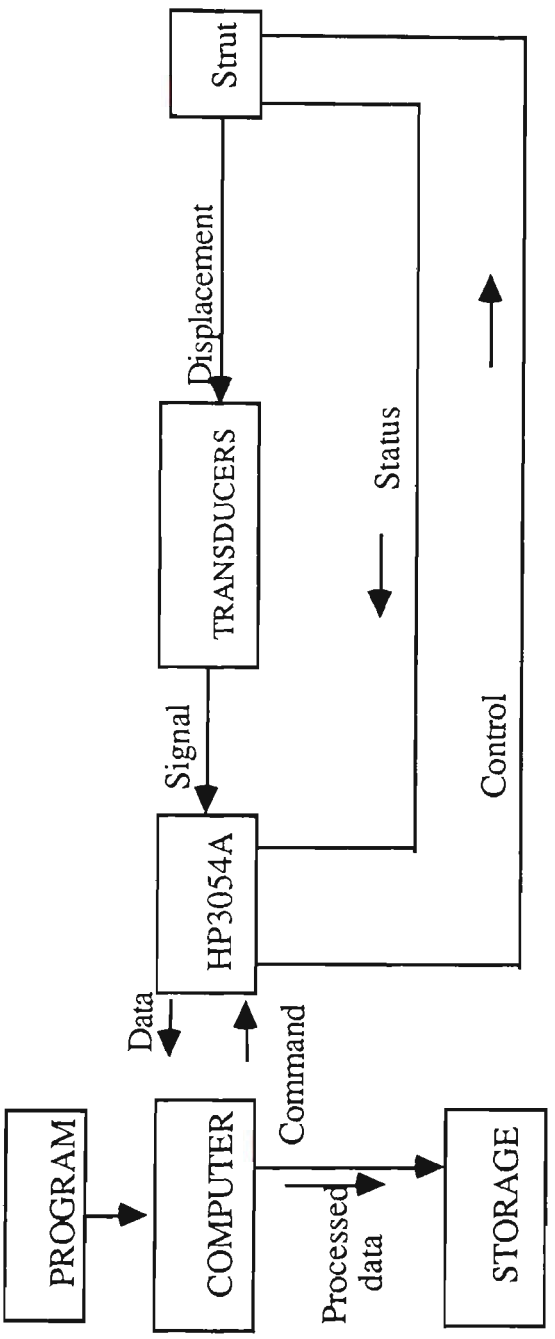

Fig.4.8 Data Acquisition/Control System

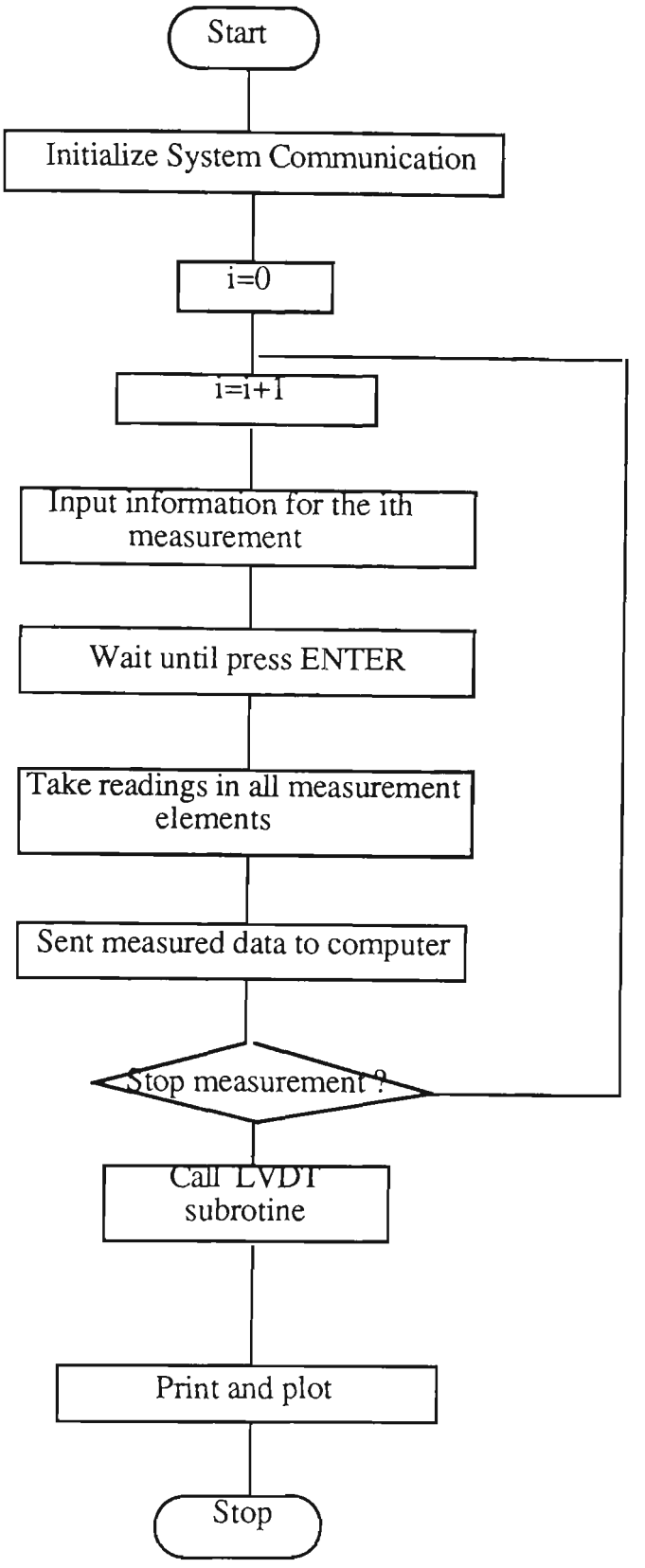

Fig.4.9 Flowchart

$$D = bV \qquad (4.1)$$

$$b = \frac{\sum_{i=1}^{n1} D_i V_i - \frac{1}{n1}\left(\sum_{i=1}^{n1} D_i\right)\left(\sum_{i=1}^{n1} V_i\right)}{\sum_{i=1}^{n1} V_i^2 - \frac{1}{n1}\left(\sum_{i=1}^{n1} V_i\right)^2} \qquad (4.2)$$

Where

D_i = the axial deflection read from micrometer for calibration,

V_i = output voltage from HP computer,

n1 = number of readings , b = calibration factor .

4.4 MATERIAL TESTS

4.4.1 Tests on As-received Tensile and Compressive Tubes

The results of the tensile and squash tests on as-received tubes are listed in Table 4.4 and Table 4.5 in which reference is made to the significant levels of the idealised stress-strain curves of Fig.4.10 .

Table 4.4 Tensile Test Results

Test No.	M KN	A KN	ε%	B KN	Con.	C KN	$\frac{C-B}{C}$%	$\frac{M-A}{A}$%	$\sigma_{0.2}$ MPa	σ_u MPa
A1	139	135	0.9	139	FA	142	2	3.1	322	
A2	139	132	1	139	NA	139	0	5.6	314	
A3	138	128	1.2	138	FA	150	8.7	7.8	305	
A4	153	133	7	152				15.1	318	365
A5	154	132	7	153				16.4	316	367
A6	151	133	3	151				13.5	318	
A7	155	133	7	155				16.5	318	370
A8	155	133	7	154				16.8	318	371
A9	152	133	3	152				14.5	317	
A10	149	134	3	149				11.4	319	
A11	154	131	7	152				17.7	313	368

The typical material stress-strain curves in tension and compression for as-received material is shown in Fig.4.11 . As there is no clearly defined yield point the 0.2% offset figure is adopted as a yield value. The average result of all six squash tubes is 315 MPa., of all eleven tensile tubes is 318 MPa. The average value of elasticity modulus E is 203 GPa .

The tests of stub columns, which were comparatively short specimens, provided the load-axial shortening behaviour of the column cross-section without introducing the possibility of overall instability (column buckling) influencing results. Therefore, the tests directly reflect the influence of both the residual stress distribution and the variation in yield stress on column strength.

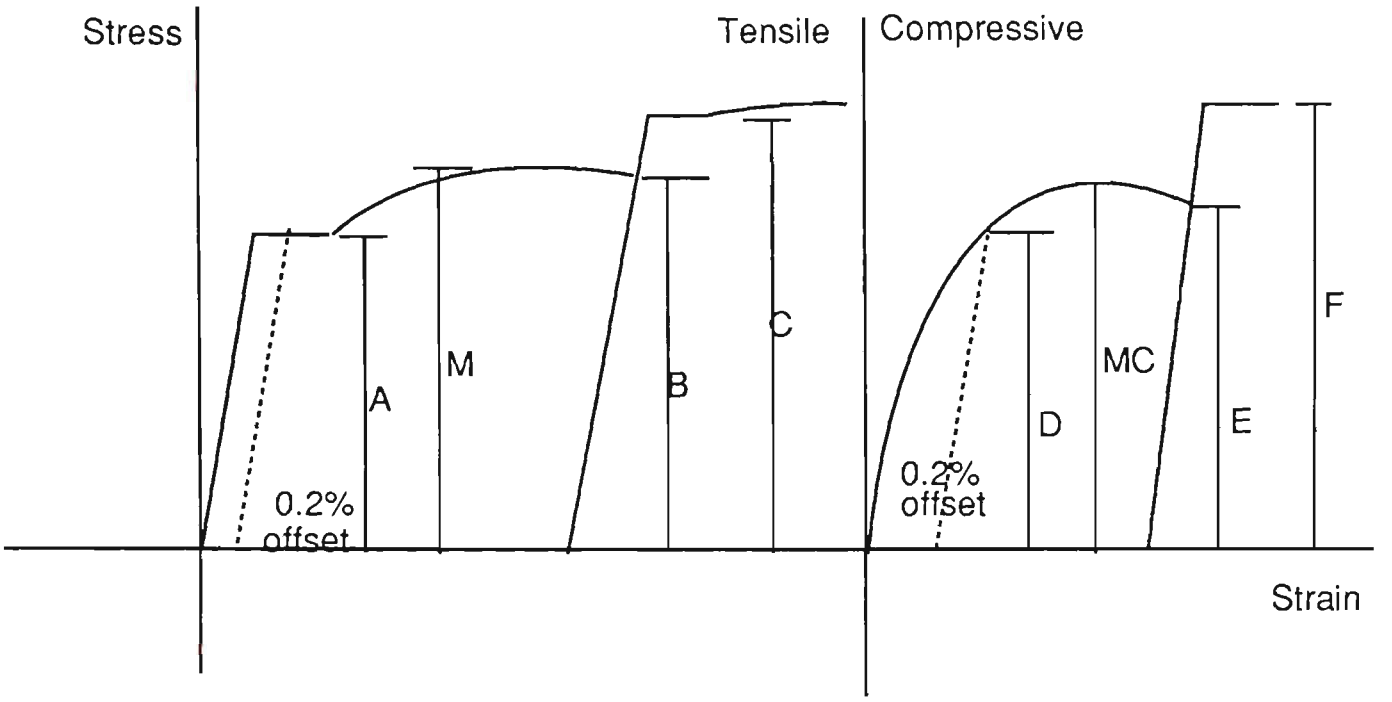

Fig.4.10 Tensile and Compressive Stress-Strain Curves

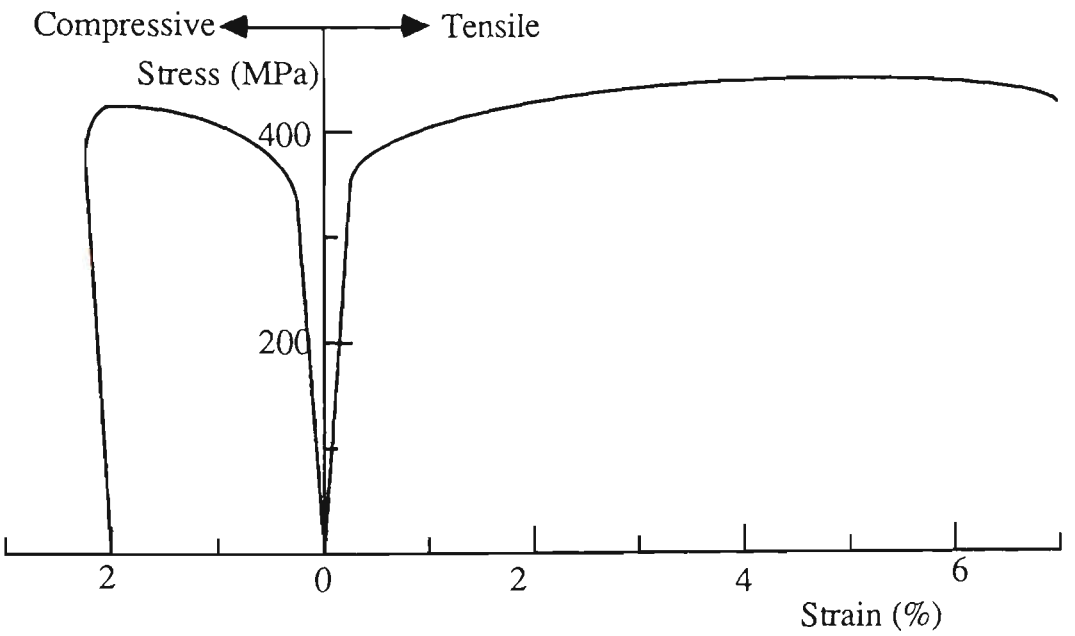

Fig.4.11 Typical Stress-Strain Curves for As-Received Material

Table 4.5 Squash Tests on As-received ERW Tube
(Tubes B1-B3 recompressed)

Test No.	M KN	A KN	ε%	B KN	Con.	C KN	$\frac{C-B}{C}$%	$\frac{M-A}{A}$%	$\sigma_{0.2}$ MPa	σ_u MPa	E GPa
B1	153	132	7.4	53.5	FA	55.3	3.4	16.6	314	366	
B2	152	132	3.2	143	FA	150	4.8	15.4	315	363	
B3	153	133	7.5	52	FA	53.7	3.3	15.3	317	366	
B4	159	133						15.1	317		207
B5	159	133						14.8	317		210
B6	152	132						15.1	315	363	203
B7	152	132						14.8	315	362	192
B8	151	131						15.4	313	361	202

4.4.2 Squash Tests on Prestrained ERW Tube and Tangent Modulus Et

The axial squash tests were carried out on 200mm length (length three times the diameter) cut from the tube prestrained in tension to 3% and 7% respectively. To determine the effect of aging, different aging treatments were applied (after initial prestraining in tension in the inelastic range) before loading in the opposite direction(compressing). The aging treatments applied to different tests were , (a) varying times at ambient temperature, or (b), 2 hours at 100^0C. Specimens FF and GG had been prestrained in tension to 3% and 7% respectively, followed by full aging, and were then cut into cylinders and then tested in compression. Specimens, EE and DD, which had been prestrained in tension to 3% and 7% respectively, were tested in compression shortly after the prestraining to exclude strain aging. The facts of interest were any increase in the

load level following aging, and any evidence of a yield point and different load extension characteristics after aging.

The load-deformation data of the stub-column tests are presented in Figures 4.12 to 4.16 for as-received struts, 3% prestrained in tension and fully-aged struts, 7% prestrained in tension and fully-aged struts, 3% prestrained in tension and unaged struts, and 7% prestrained in tension and unaged struts, respectively. The combined load-deformation data of the stub-column tests normalised with respect to yield stress/strain (Yield stress was defined as the 0.2% offset stress of the squash tests) are given in Fig.4.17.

Table 4.6 summarizes the results of squash tests on the prestrained ERW tube . Some values of the tangent modulus Et from corresponding compressive load-deflection curves are presented in Table 4.7 .

Following plastic tensile prestrains, Bauschinger rounding is revealed on load reversal; it has the effect of reducing the 0.2% offset stress (for prestrained and unaged tubes), reducing or eliminating a proportional limit, and changing the peak load capacity of stub columns made from the as-received tube. This change depends on the relative influence of strain hardening and strain aging on the tests, all of which affect the tangent modulus.

As tangent modulus calculations are useful in predicting strut load capacities this effect has been highlighted by plotting Tangent Modulus (E_T) against Stress (σ) on Fig.4.25. In this series of tests seven classes of behaviour have been observed, depending on the tensile prestrain , aging treatment and residual stresses. The variation of tangent modulus with stress has been found to be

significantly different for each class of test , as is shown separately on figures 4.18 to 4.24, and in combination on Fig.4.25.

Table 4.6 Squash Tests on Prestrained ERW Tube

Test No.	A KN	Strain %	B KN	Con.	D KN	$\frac{D-A}{A}$ %	M_c KN	E KN	Con.	F KN	% $\frac{F-E}{E}$	% $\frac{M_c-D}{D}$	% $\frac{\sigma_{D0.2}-\sigma_{A0.2}}{\sigma_{A0.2}}$
BB	132	3	151	AR									
BB1				PS+1D	117	-11	148	141	PS+NA	141	0	2.6	-10.5
BB2				PS+1D	120	-9	149	135	PS+FA	148	9.3	24.8	-8.3
BB3				PS+FA	133	1.1	154	124	PS+FA	127	2.4	15.8	1.9
DD	133	7	154	AR									
DD1				PS+NA	116	-13	146	140				25.3	-10.4
DD2				PS+NA	115	-14	144	140				25.4	-11
DD3				PS+NA	113	-15	145	140				28.4	-13.2
EE	134	3	151	AR									
EE1				PS+NA	114	-15	148	146				29.6	-14.7
EE2				PS+NA	116	-14	147	143				26.7	-13.1
EE3				PS+NA	111	-17	147	141				31.7	-16.3
FF	132	3	150	AR									
FF1				PS+FA	133	0.4	154	145				16.6	0.95
FF2				PS+FA	133	0.8	154	146				15.4	1.6
FF3				PS+FA	133	0.8	153	128				15.3	1.6
GG	131	7	152	AR									
GG1				PS+FA	130	0.8	154	145				18.5	1.6
GG2				PS+FA	131	0	155	146				18	2.6
GG3				PS+FA	131	0	154	148				17.8	2.2

PS = Prestrained in tension , NA = No strain aging , AR= As-received, Con.=Condition.

FA = Fully strain aged (Full aging is defined as aging at 100^0c for 2 hours).

The symbols (M,A,B,C,D,MC,E and F) used in the Table Headings are defined on Fig.4.10.

For struts fabricated from the tube size chosen for study, the intermediate slenderness ratio corresponds to an ultimate stress range varying from about 110-310 MPa, as derived from a stress versus slenderness ratio plot. In this significant range of axial stress the as-received tube(Fig.4.18) had the highest value for E_T , whereas the stress relief annealed (SRA) tube (Fig.24) had the lowest value. This result is expected and is clearly seen in Fig.4.25.

The results show that aging can have a significant influence on the tangent modulus. The 3% prestrained and fully aged curve is well above that for the 3% prestrained but unaged curve in the same stress range, as is shown in Fig.4.25.

Table 4.7 Tangent Modulus Et

Condition	Stress(MPa) vs Modulus(GPa)									
AR	σ	239	250	263	275	286	310			
	Et	192	145	102	69	23	4.62			
Pre.3%	σ	73.75	147	172	196	221	245	282	295	307	327
FA	Et	193.8	189	179	146	145	100	47	34	21	11
Pre.7%	σ	102	154	205	230	256	281	293	306	320	332
FA	Et	199	164	155	112	78.2	51.9	35	26.3	20.9	14.3
Pre.3%	σ	98.3	122.7	171.8	196.4	220.9	245.5	257.8	277.2	289.5	306.8
NA	Et	125.5	89.9	82.1	65.6	48.9	33.8	27.3	20.9	14.6	10.9
Pre.7%	σ	49.8	74.76	99.72	124.3	149.3	174.4	199.4	249.6	298.7	323.7
NA	Et	115	110	106	82.2	76.5	62.8	50.9	32.6	14	7.6

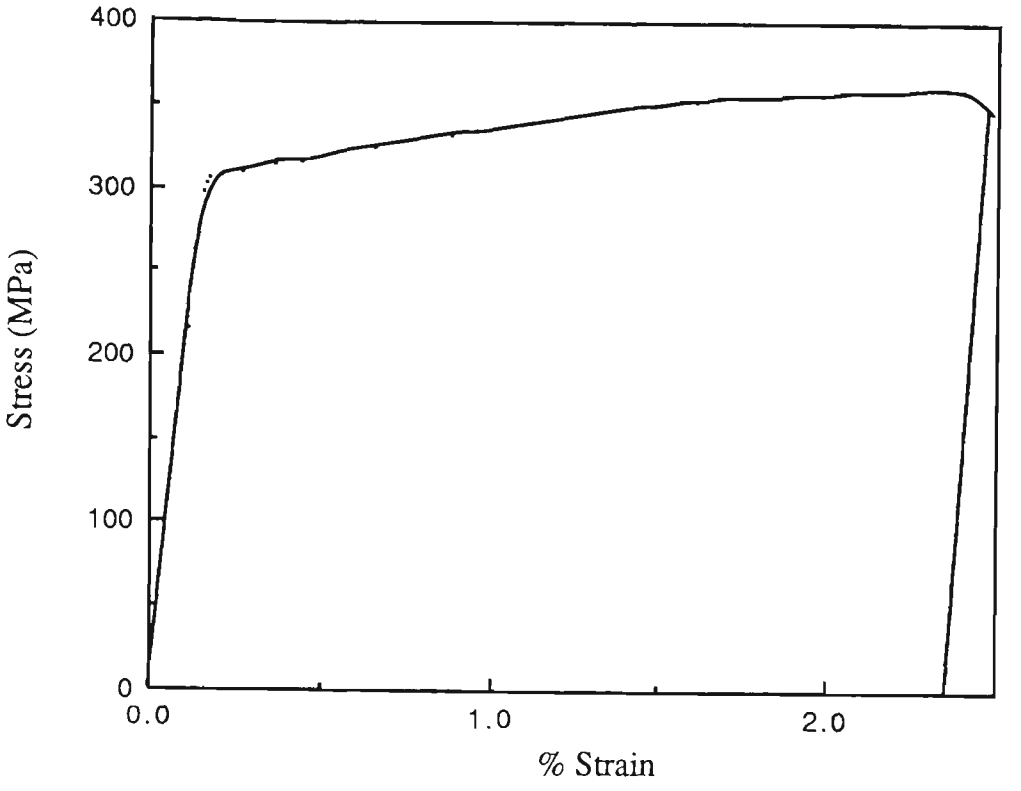

Fig.4.12 Stub-Column Test - As-Received Tubes

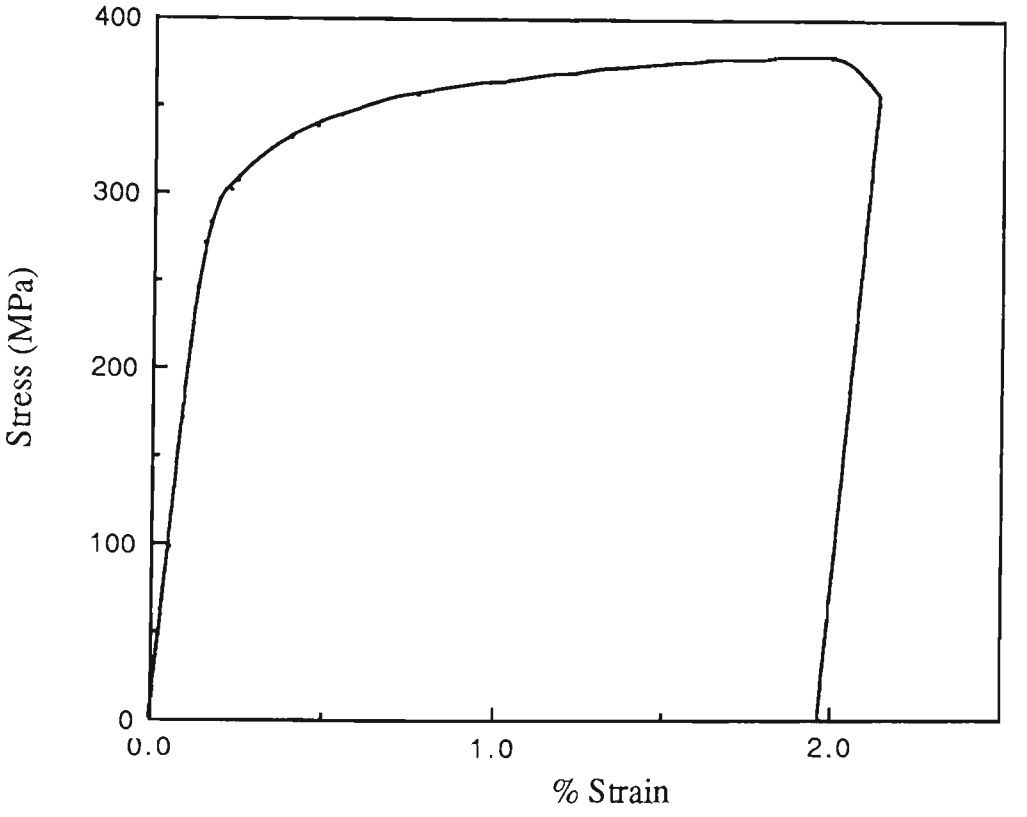

Fig.4.13 Stub-Column Test - 3% Prestrained, Fully-Aged

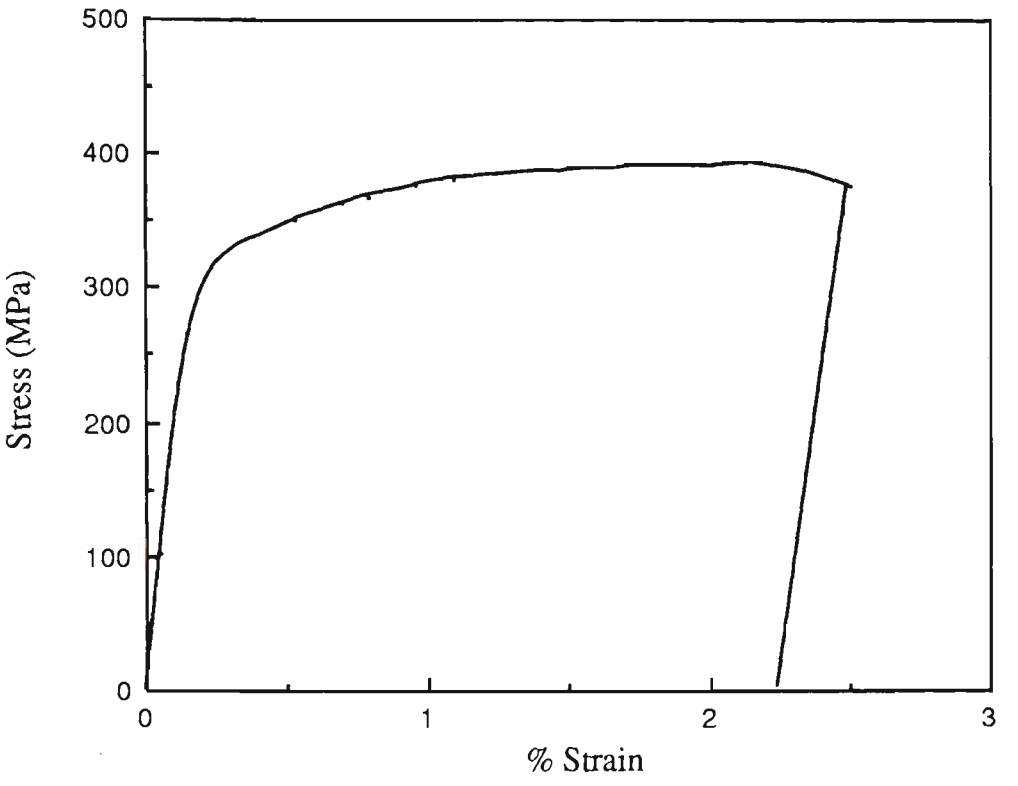

Fig.4.14 Stub-Column Test - 7% Prestrained, Fully-Aged

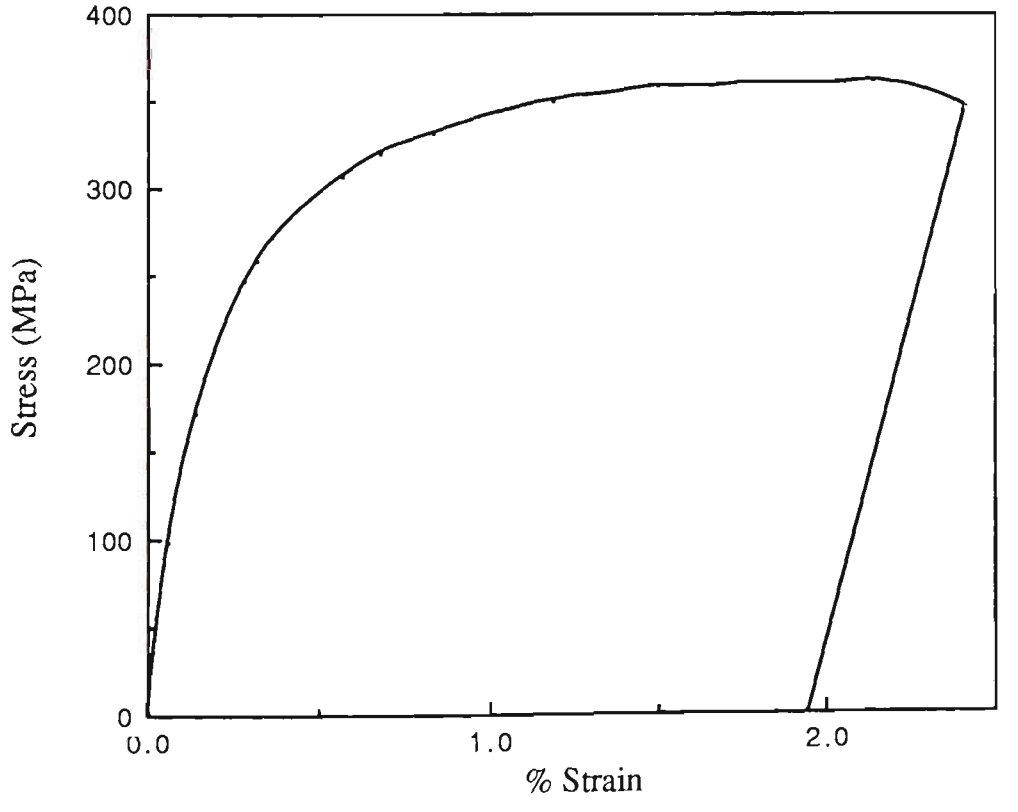

Fig.4.15 Stub-Column Test - 3% Prestrained, Unaged

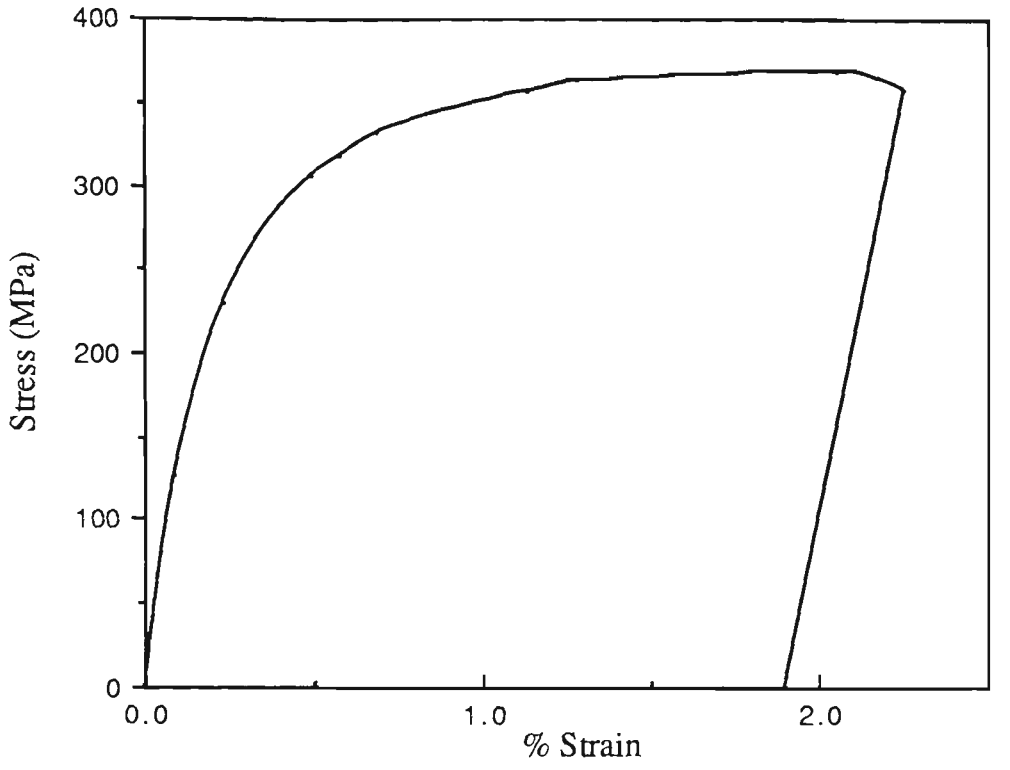

Fig.4.16 Stub-Column test - 7% Prestrained, Unaged

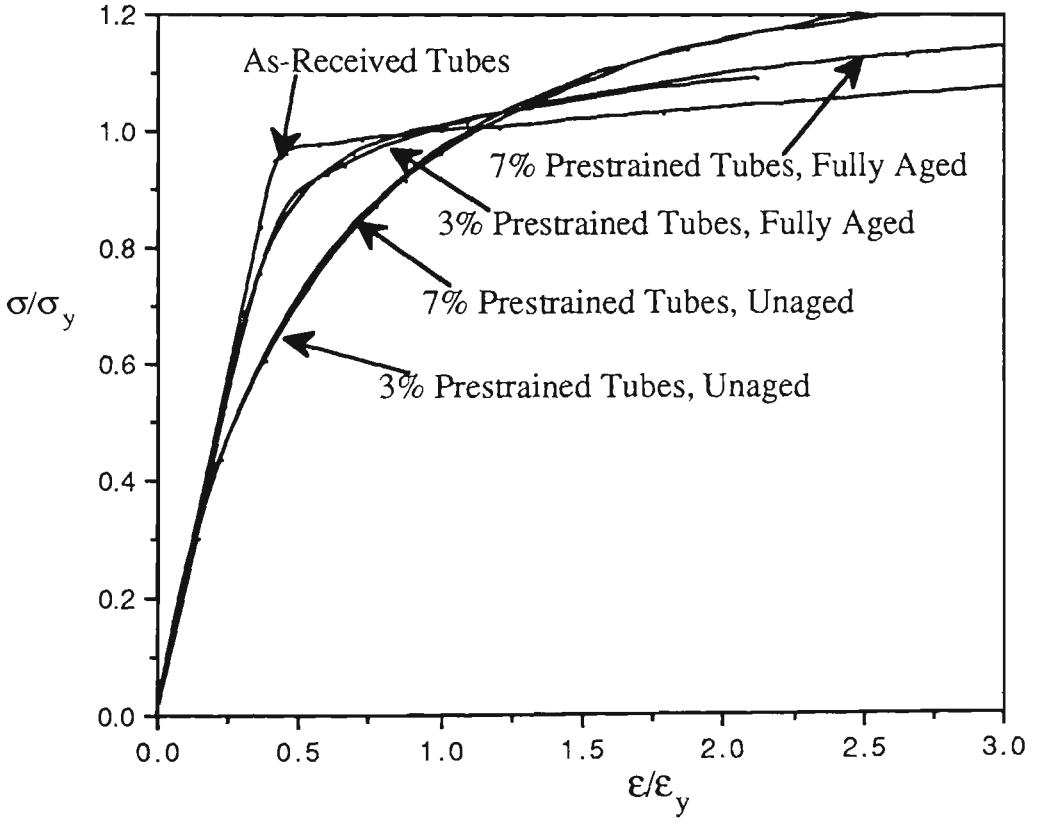

Fig.4.17 Stub-Column Test Results Under Different Conditions

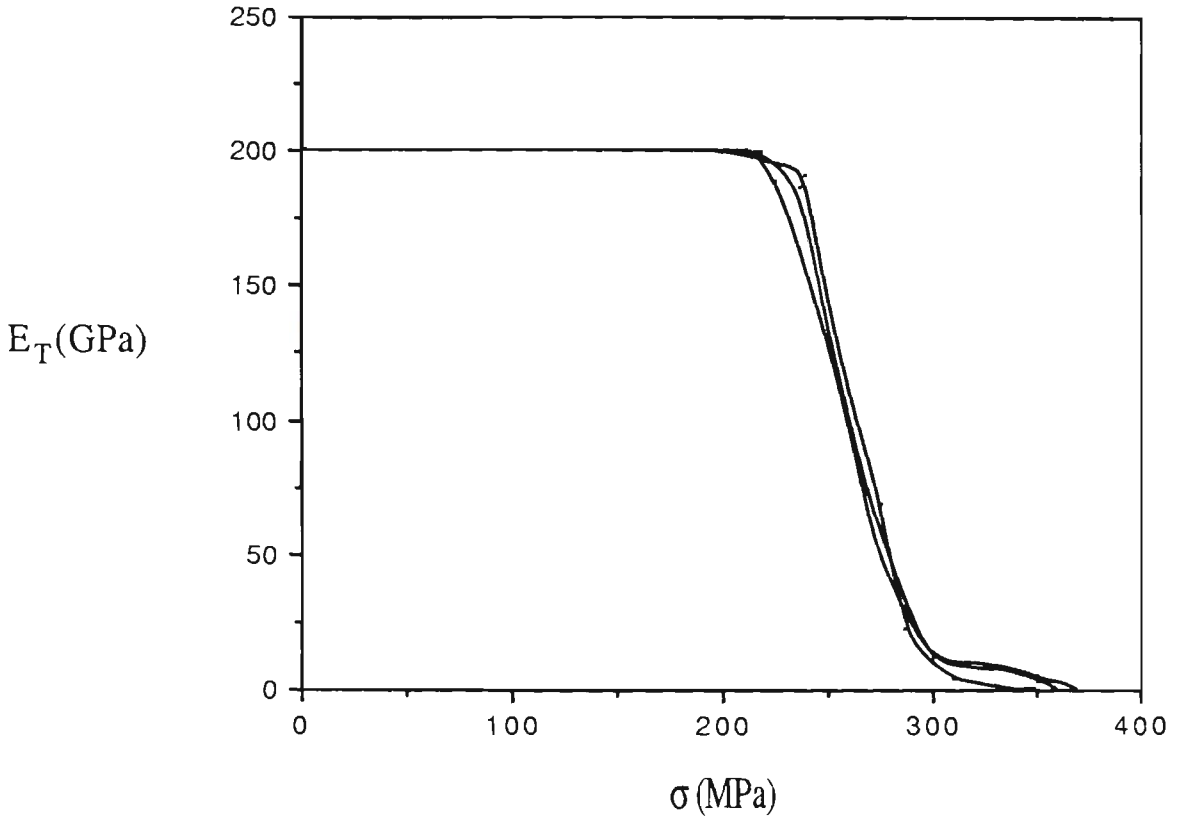

Fig.4.18 Tangent Modulus vs Stress - ERW Tube As-Received

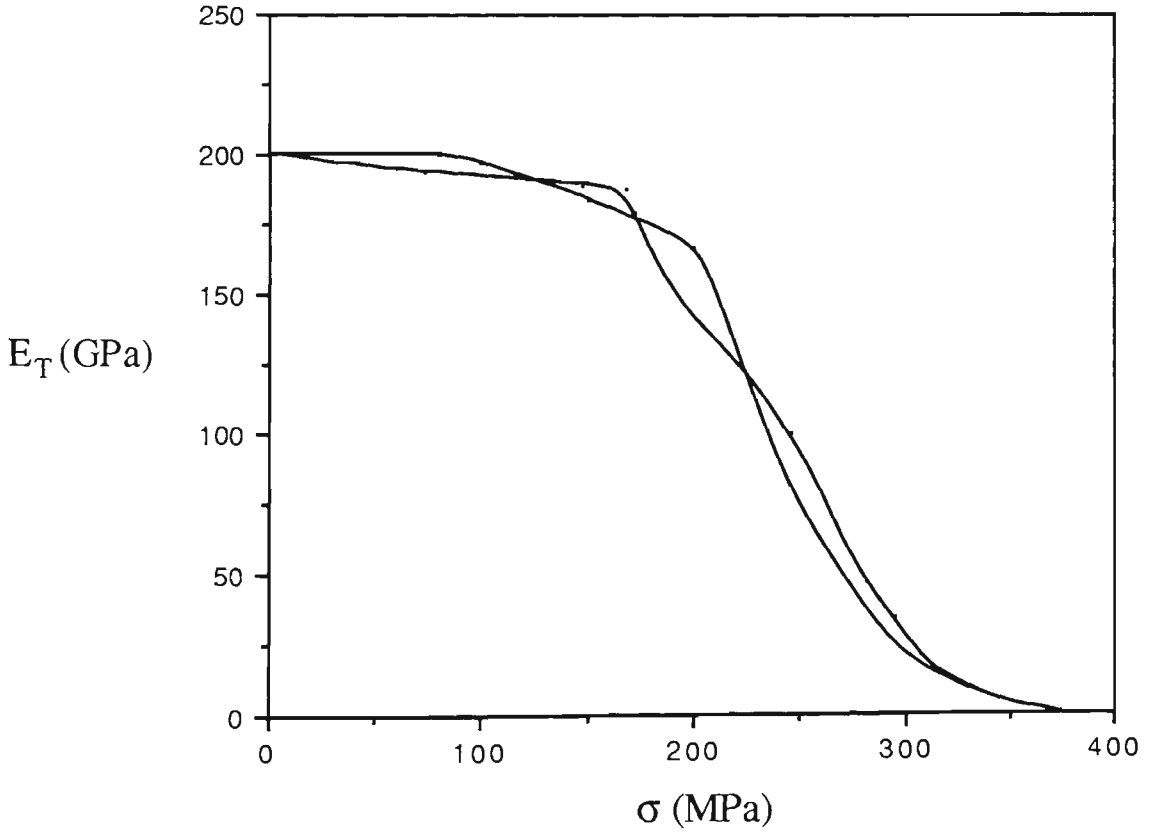

Fig.4.19 Tangent Modulus vs Stress - ERW Tube 3% Prestrained, Fully-Aged

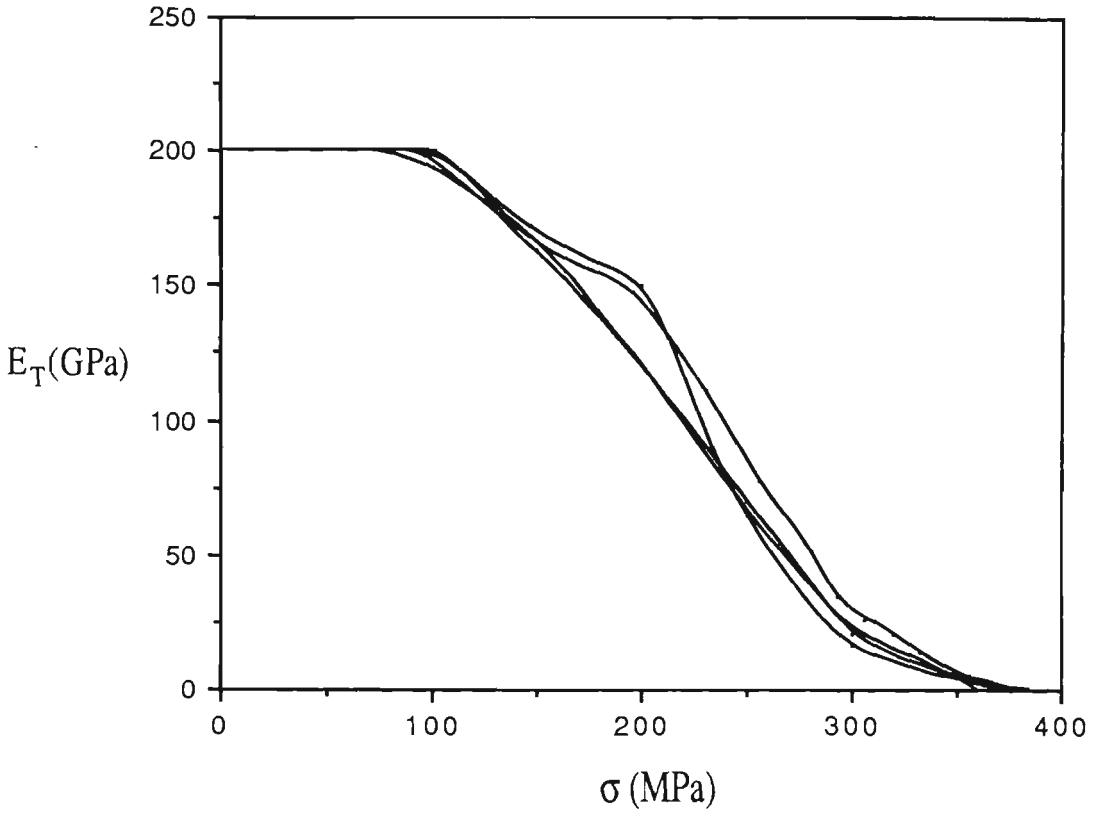

Fig.4.20 Tangent Modulus vs Stress - ERW Tube
7% Prestrained, Fully-Aged

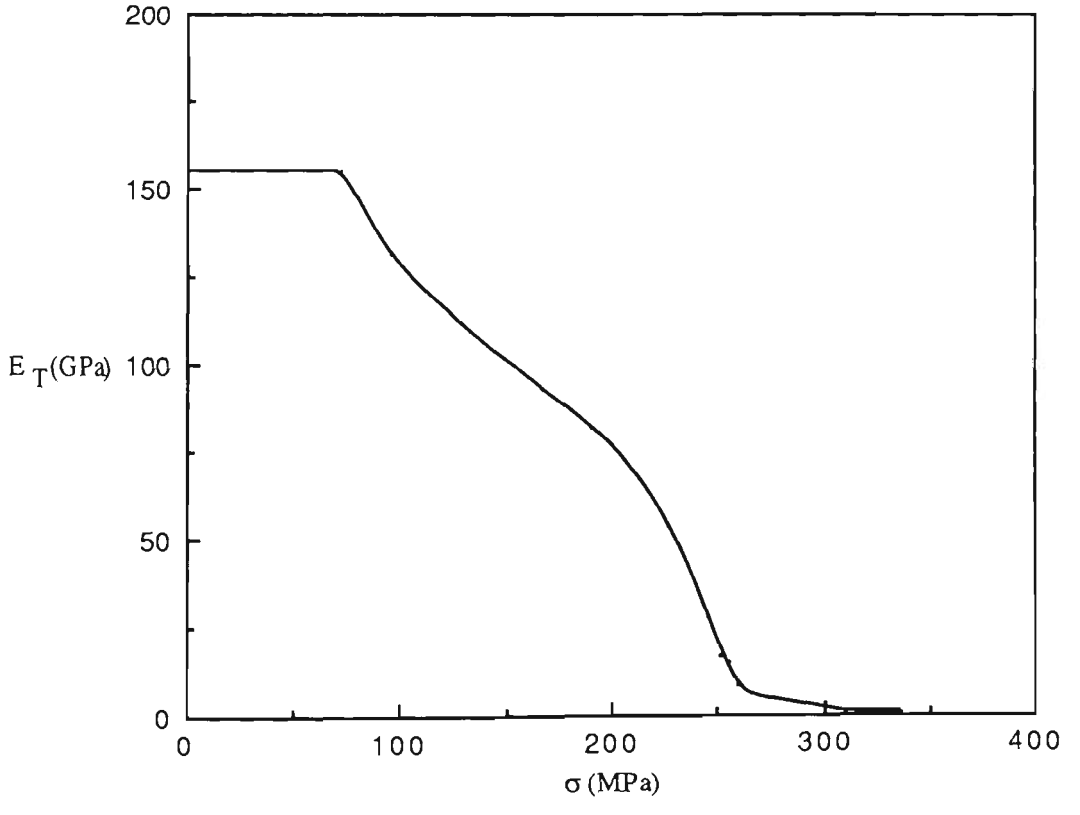

Fig.4.21 Tangent Modulus vs Stress, SRA
7% Prestrained, Fully-Aged

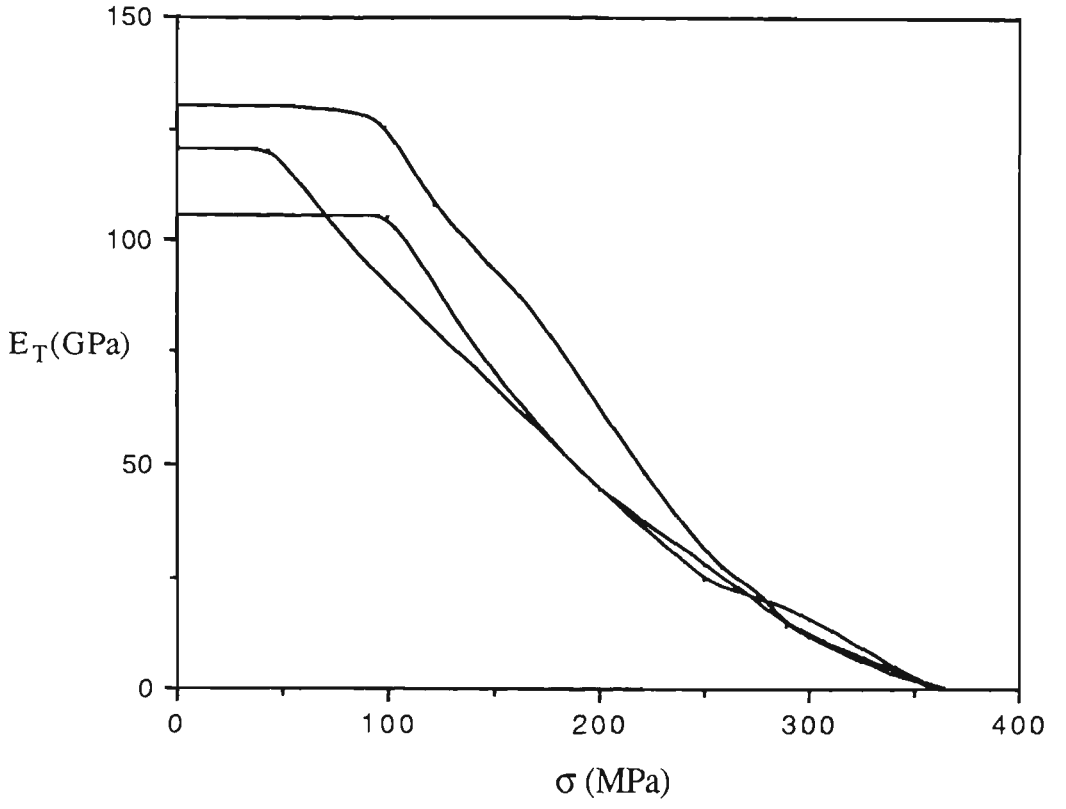

Fig.4.22 Tangent Modulus vs Stress - ERW Tube
3% Prestrained, Unaged

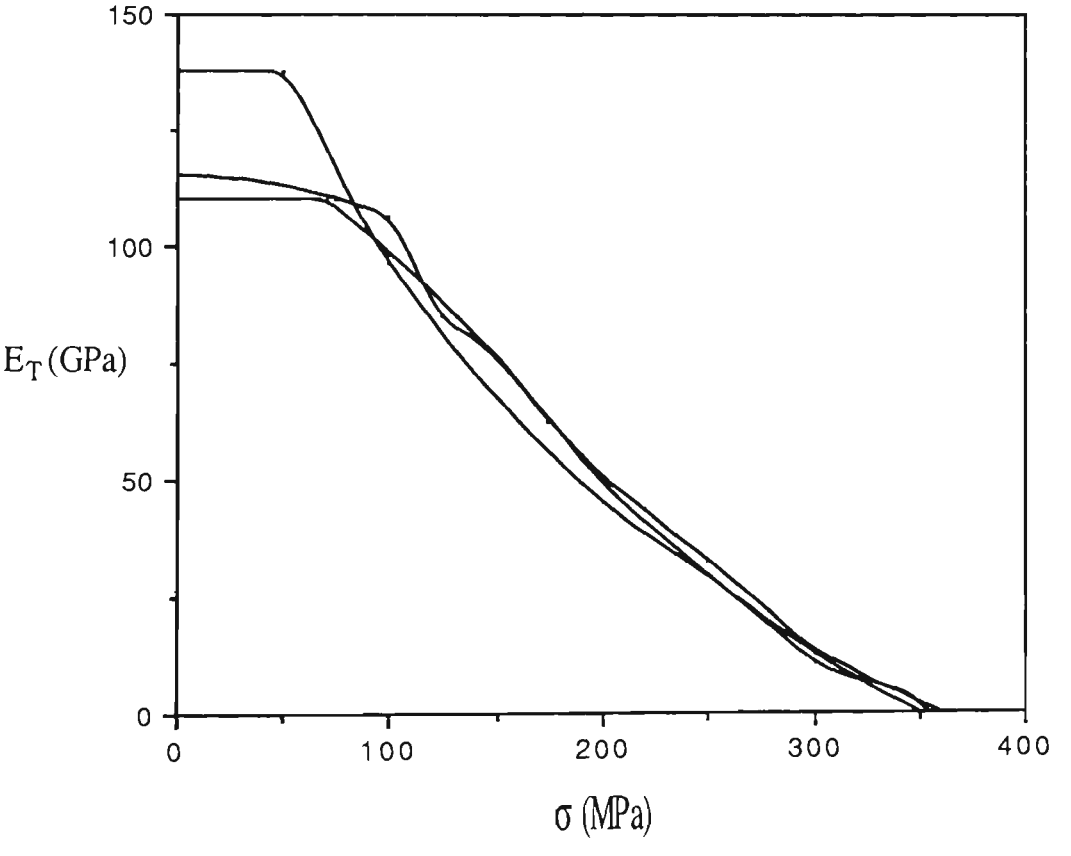

Fig.4.23 Tangent Modulus vs Stress - ERW Tube
7% Prestrained, Unaged

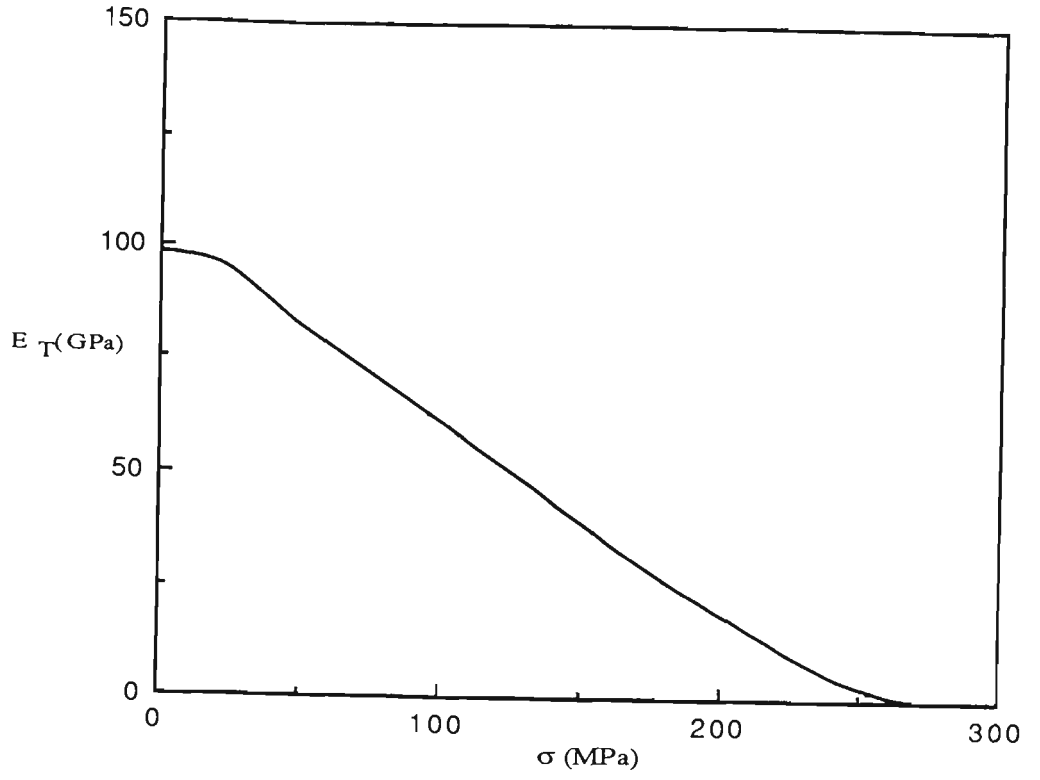

Fig.4.24 Tangent Modulus vs Stress, SRA
3% Prestrained, Unaged

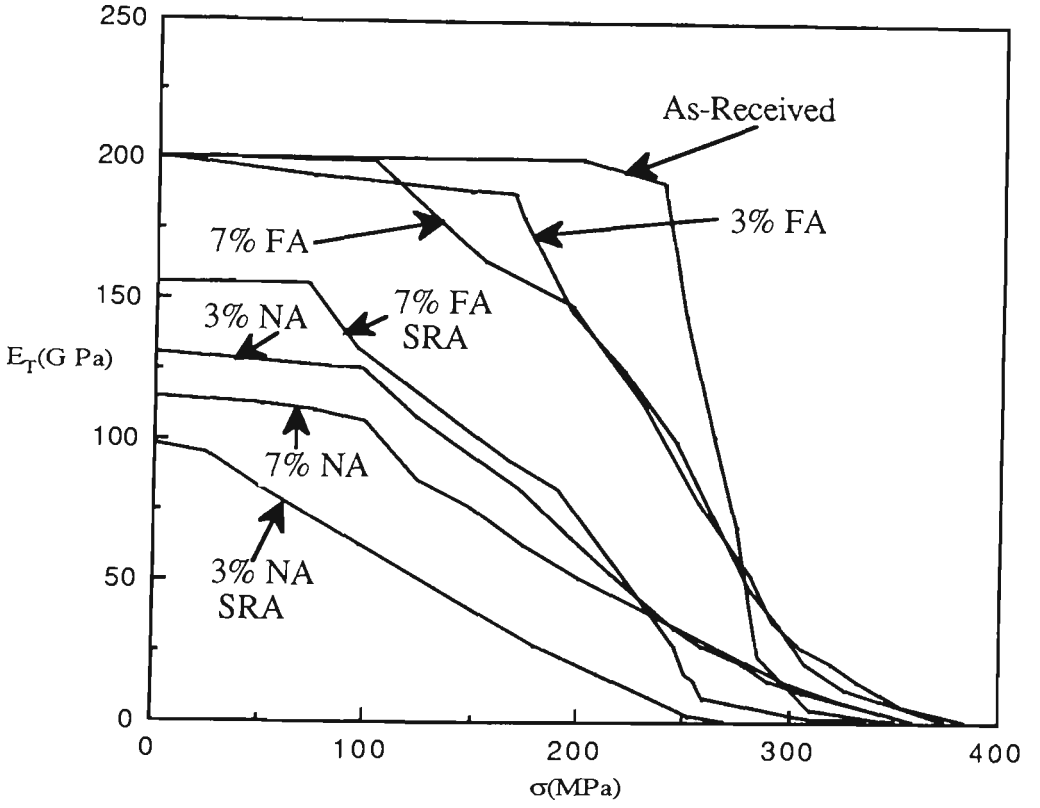

Fig.4.25 Tangent Modulus vs Stress - ERW Tube
All Conditions

It is clear that for a stress level of 315MPa struts made of materials treated in the five different ways would have significantly different load capacities. The variation of tangent modulus with stress is highly sensitive to each factor, as is the load capacity of struts made from appropriately prepared materials. Although the calculation of the slope of the stress versus strain curves, in order to obtain E_T, involves a loss of accuracy, nevertheless the relative influences of the variables can be clearly seen.

4.4.3 Tests on Stress Relief Annealed As-Received and Prestrained ERW Tube

A stress relief annealing treatment (SRA) was performed in a furnace at 650^0C in an inert atmosphere (nitrogen) for 30 minutes, followed by air cooling. This result was expected from such a short time sub-critical annealing treatment. The only change would be relief of the residual stresses set up during the tubemaking process.

Nine stub-column tests of SRA tubes (three were stress relief annealed as-received; five were stress relief annealed and 7% prestrained and fully-aged; one was stress relief annealed and 3% prestrained and unaged) were conducted to furnish basic data in the elastic and inelastic ranges. The material tests were performed in a 50 tonne capacity servo-hydraulic testing machine. Stub-columns were cylinders of 200mm length (length three times the diameter) cut from the SRA as-received tubes and SRA tubes prestrained in tension to 3% and 7%. The 3% prestrained stub-columns were tested unaged, whereas the 7% prestrained stub-columns were tested in the fully aged condition. The ends of squash

cylinders were machined to provide intimate contact with the platens of the Instron testing machine.

Compared with the stress-strain curves from the as-received stub-columns which had no clearly defined yield plateau, the well-defined yield plateau of the stress-relief-annealed as-received stub-columns indicated that residual stresses set up during the tubemaking process existed. Young's modulus dropped dramatically in the flat stress-strain curve range (Luder's plateau) in which the stress-strain gradient was apparently zero. The clearly defined yield stress of the stress-relief-annealed as-received stub-columns was 274 MPa.

As there was no clearly defined yield point for prestrained stub-columns the 0.2% offset figure is adopted as a yield value. The yield stress obtained from the SRA 3% and unaged squash tests was 216MPa, and 247 MPa from the 7% fully aged squash tests.

4.4.4 Strain Aging , Strain Hardening and the Bauschinger Effect

Full details of the strain hardening available in ERW tube at different elongations is given on Fig.4.12 and in Table 4.4. There is an average strain hardening enhancement of the yield stress of approximately 16% right up to the peak load capacity at about 6-7% elongation. At lower strains the increase is slightly less; 5% at 1% strain. It will be appropriate at this point to define a Strain Hardening Ratio (SHR) as the ratio of the as-received ultimate to yield tensile stresses. For the ERW tube the strain hardening ratio for the as-received tube was 1.15.

Whether the steel was able to be aged or not was determined by reloading several of the tensile and compressive test specimens several times after different amounts of time had elapsed. Typical load deflection curves are presented on Fig.4.26 . As well as these elapsed time tests at ambient temperature, several tensile tests were performed followed by full aging and immediate reload, then further reload cycles were performed after a range of elapsed time at ambient temperature. Further tests were also carried out to check the influence of strain aging after load reversal from tension to compression; details are given in Table 4.6. It was observed that strain aging occurred when loading was continued after a delay at ambient temperature (approximately 23^0 c) (one day for specimens BB1 and BB2), or full aging defined as aging at 100^0 C for 2 hours , whether the direction of strain was forward or reversed . Full aging was performed by placing specimens in a oven at 100^0c.

It was found that the reduction of material strength due to the Bauschinger effect on strain reversal occurred for all the tensile prestrained and unaged tubes, and the Bauschinger effect was interactive with both strain aging and strain hardening. Strain hardening of the ERW tube had relatively little influence on Bauschinger loss, due to its low strain hardening capacity , having a SHR (strain hardening ratio) of 1.15 . The different tensile prestrains of 3% and 7% were used to test the influence of strain hardening. Under fully-aged conditions, as tensile prestrain increases, the compressive strength (as measured by 0.2% offset stress and maximum stress) increases but the non-linearity of the load-deformation plot occurs at lower levels. As tensile prestrain increases from 3% to 7% , under an unaged condition , the average difference of yield strength is only 4.4% ; under a fully-aged condition , the difference was even less (only 1.8%).

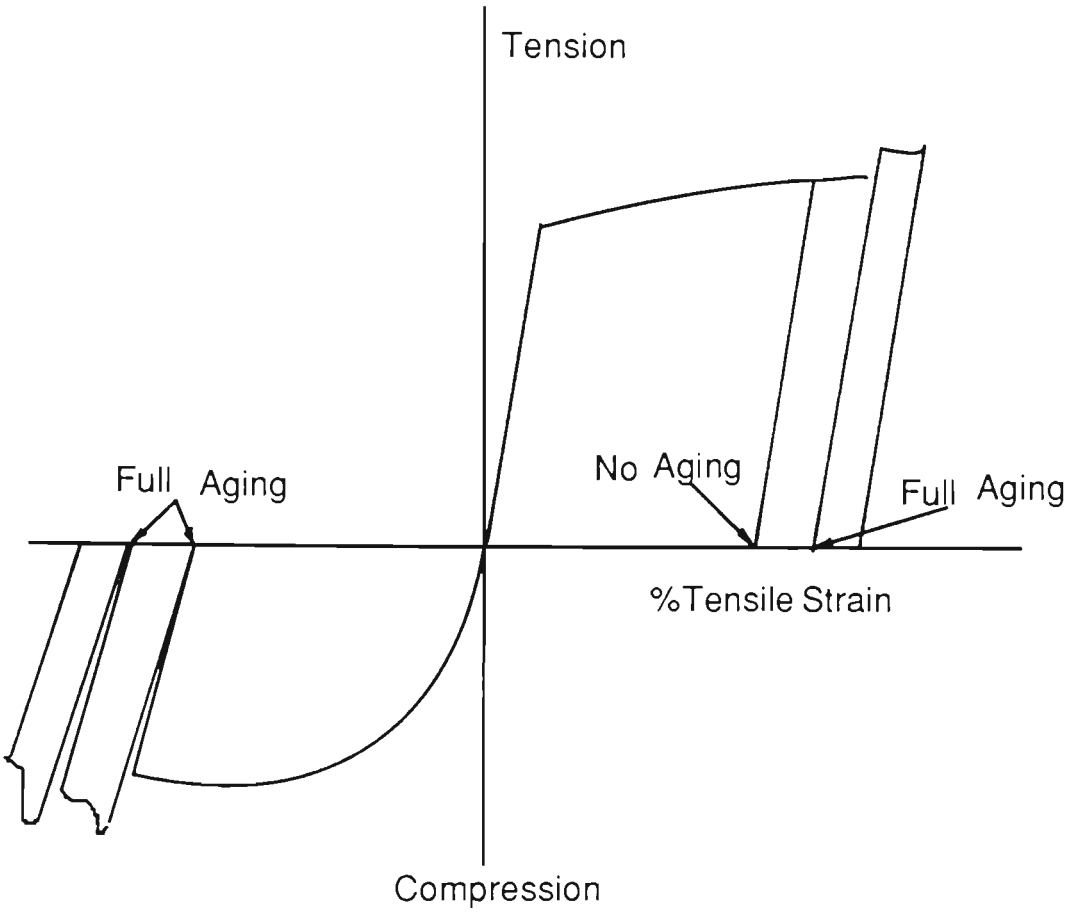

Fig.4.26 Strain Aging of ERW Tube - Tension/Tension, Tension/Compression and Compression/Compression

For squash cylinders of ERW tubes that were prestrained in tension and fully-aged a reduction of capacity did not always occur. This effect indicates that Bauschinger loss does not always outweigh the combined strength gains due to strain hardening and strain aging. Comparing the amount of Bauschinger loss under different conditions indicates that strain aging is a more dominant factor than strain hardening; in the experimental work reported herein (remembering that the ERW tube is a rimming steel) strength reductions were only recorded in the case of load reversal for tubes that were prestrained in tension and unaged . This effect was true of prestrains of 3% and 7% that were used in the test program.

As mentioned earlier, the influence of strain aging on Bauschinger loss was significant . Whether aging occurred over an extended time at ambient temperatures, or was accelerated in a oven (two hours at 100^0c), the influence on Bauschinger loss was clear. It should be observed that this result is true for rimming (ERW tube) and semi-killed (HFW tube, Morgan and Schmidt , 1985). The loss should be more significant for fully-killed steels which display virtually no strain aging capability. Specimens prestrained 3% and 7% and fully aged gain strength while the same prestrain, but with no aging , lead to strength reductions of about 10% - 16% (compared with the as-received strength) upon load reversal .

All of the factors mentioned above affect the tangent modulus significantly , which in turn has a great influence on the stability of struts .

4.5 STRUT TESTS

4.5.1 Test Procedure

In order to determine the influence of strain aging, strain hardening, residual stress and the Bauschinger effect on strut load capacity, 85 pin-ended strut tests have been carried out under eight different conditions:

1) Two sets of as-received struts (series 1) (Here, "two sets" consists of twelve struts with six different lengths , each length including two struts) ;
2) Two sets of 3% prestrained fully aged struts (series 2) ;
3) Two sets of 3% prestrained but unaged struts (series 3) ;
4) Two sets of 7% prestrained fully aged struts (series 4) ;
5) Two sets of 7% prestrained but unaged struts (series 5) (For series 1 to series 5, strut lengths are between 750 and 2998mm) ;
6) Two sets of stress relief annealed 3% prestrained but unaged struts (series 6) ;
7) Two sets of stress relief annealed 7% prestrained fully aged struts (series 7) ;
8) One set of stress relief annealed as-received struts (series 8) (For series 6, series 7 and series 8 strut lengths are between 750 and 1875mm).

The fully aged condition was realized by keeping the prestrained struts in a water bath of boiling water for 2 hours. Temperatures were recorded during the time. Prior tests have shown that this time is satisfactory for the specimens used. The prestrain value of 3% was chosen to ensure that the steel was uniformly strained beyond the value at which strain hardening occurred over the entire length (approximately 1.4%). The value of 7% was chosen so as to

generate the near-peak load capacity of each member without causing excessive geometric change of cross section. The effects due to the degree of strain hardening should be illustrated by choice of these significantly different values.

A stress relief annealing treatment was performed in a furnace at 650^0C for 30 minutes, followed by air cooling. Fig.4.27 shows the tubes hanging in the stand which is located on the annealing furnace base. The stable triangle frame stand was designed to withstand the weight of the tubes at the high temperature (650^0C) and 12mm square diagonal members were used to stabilize the stand. All the specimen tubes had a 6mm hole drilled at one end plate to prevent a high pressure built up inside the tube caused by the high temperature , and the specimens were hung vertically so that they did not deform (distort) laterally at the annealing temperature(650^0C). From Fig.4.27, the thermocouple attached to the tube is seen on the right hand side of the tube stand for temperature recording. Fig.4.28 shows the internal cover which is used to isolate specimens from direct contact with the annealing furnace. Fig.4.29 shows the outside furnace cover in position ready for firing, while Fig.4.30 shows the tubes and stand after removal from the furnace.

Prior to the production of some of the struts the tube was stretched (prestrained) to a defined percentage elongation. Prestraining for struts up to 1875 mm long was carried out in a closed loop hydraulic testing machine. Longer struts were extended in a floor rig using prestressing jacks, and extensions were measured with steel tapes over the total strut length.

In order to allow the strut end plates to connect tightly with the 70 degree knife edges , and to prevent the end plates from rotating during loading ,

wedges were fixed when each strut was preloaded to about 10%-15% of the expected peak load , as shown in Fig.4.31 .

All the tests for which the struts were up to 1875mm long, were performed in a 50 tonne capacity servo - hydraulic testing machine . All these tests were carried out at controlled rates of ram travel of 0.005mm per second during loading up to peak load , then 0.05mm per second while following the unloading curve of the struts. In all cases load-axial shortening plots with a LVDT (7DCDT-3000) by the Instron machine and with a LVDT (7DCDT - 1000) by the Hewlett Packard 3054A Data Acquisition Automatic Control System were recorded. Two readings were taken at locations 180 degrees apart in plan around the longitudinal axis of the tube. The longer strut tests were carried out in a hydraulic universal testing machine . A loading rate was used of 7KN per minute up to peak load, followed by 30KN per minute for unloading behaviour. Loads were recorded on the vertical axis of an x-y plot from a pressure transducer fixed in the pressure line of Testing Machine. A pair of dial gauges was fixed between the lower and upper platens to measure the axial shortening between the two knife edges. These axial deflections were recorded on the horizontal axis of an x-y plot .

All the struts failed in an overall instability buckling mode. Local buckling of the tube wall occurred only for specimens with low slenderness ratios and in the post-collapse range when the load was about 45% of the peak load. It was noticed that for stress-relief-annealed as-received specimens, the local buckling of tube wall in the localised region of the strut, when the Luders bands developed, occurred in the post-buckling range for all the slenderness ratios tested (λ=36, 55, 73 and 91), which was possibly due to the dramatic drop of Young's modulus in the Luder's plateau.

Fig.4.27 Tubes on Annealing Furnace Base

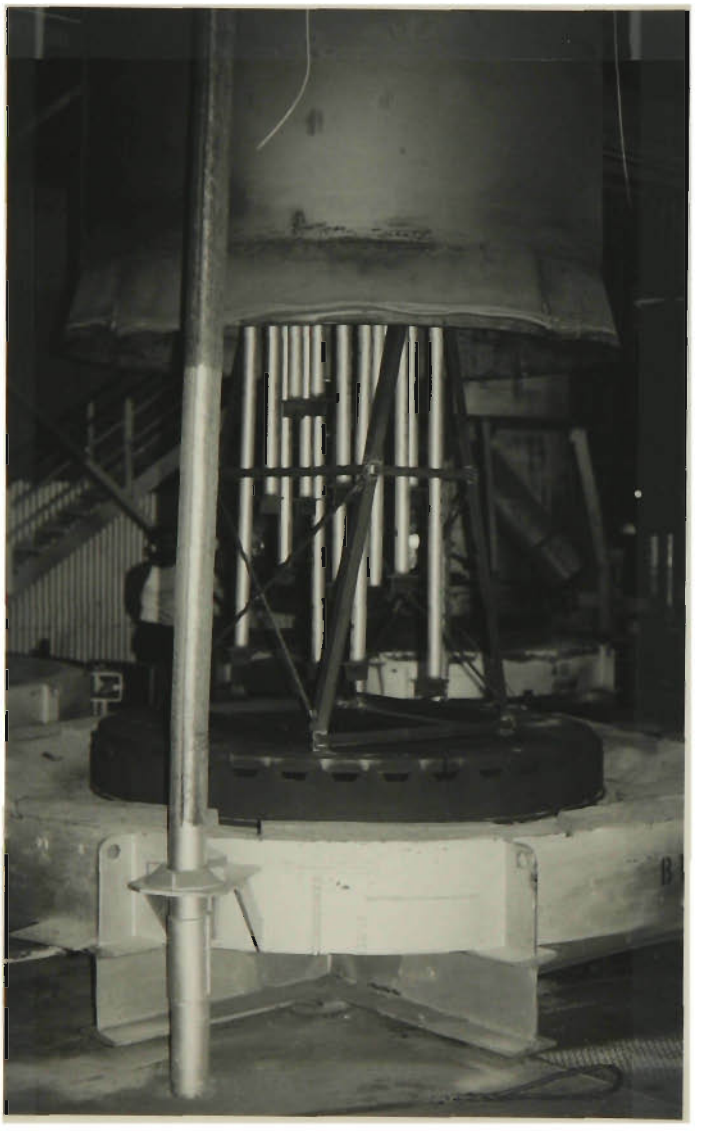

Fig.4.28 Internal Furnace Cover

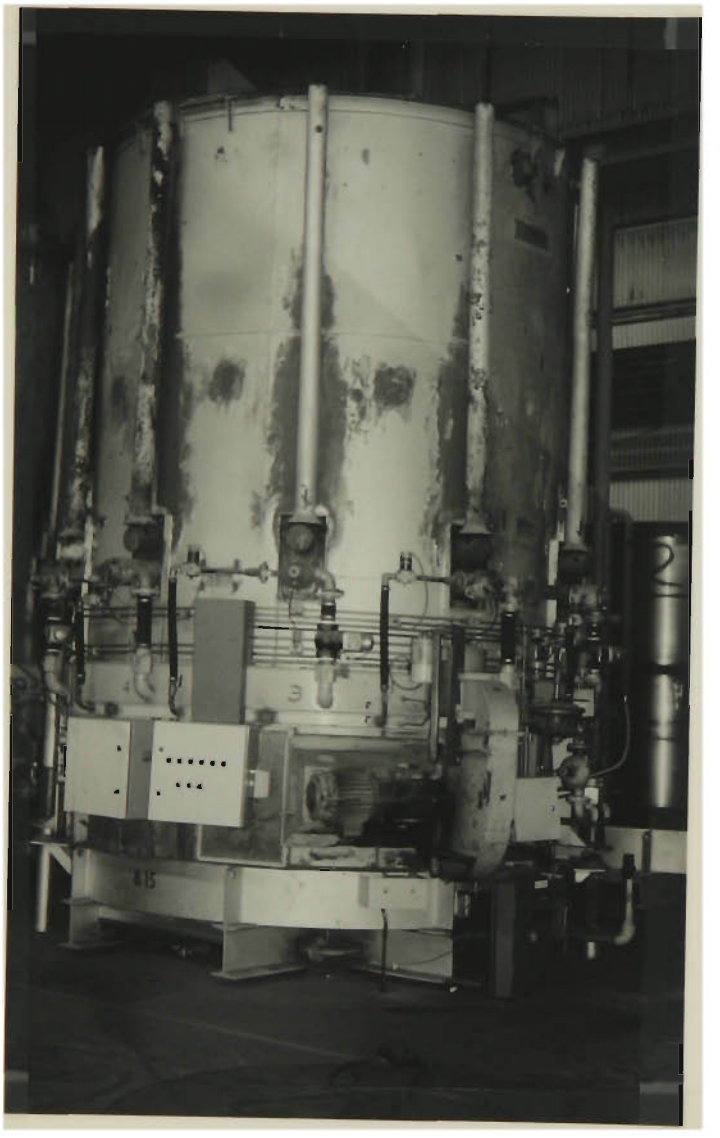

Fig.4.29 Outside Furnace Cover

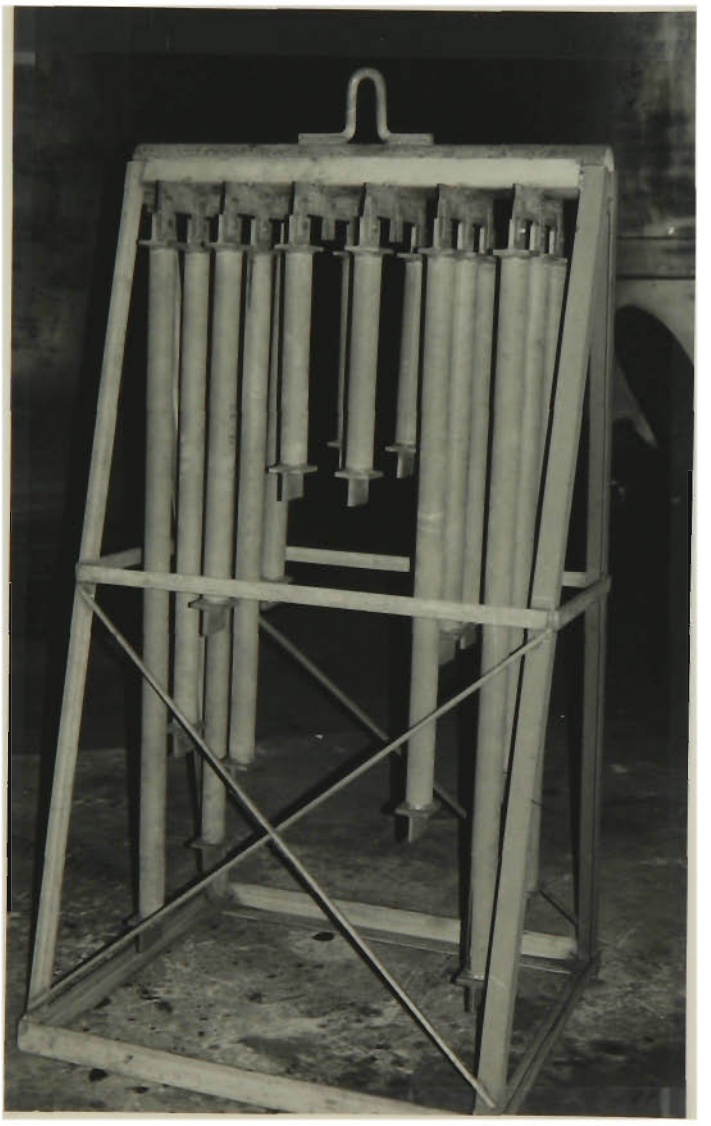

Fig.4.30 Tubes after Annealing

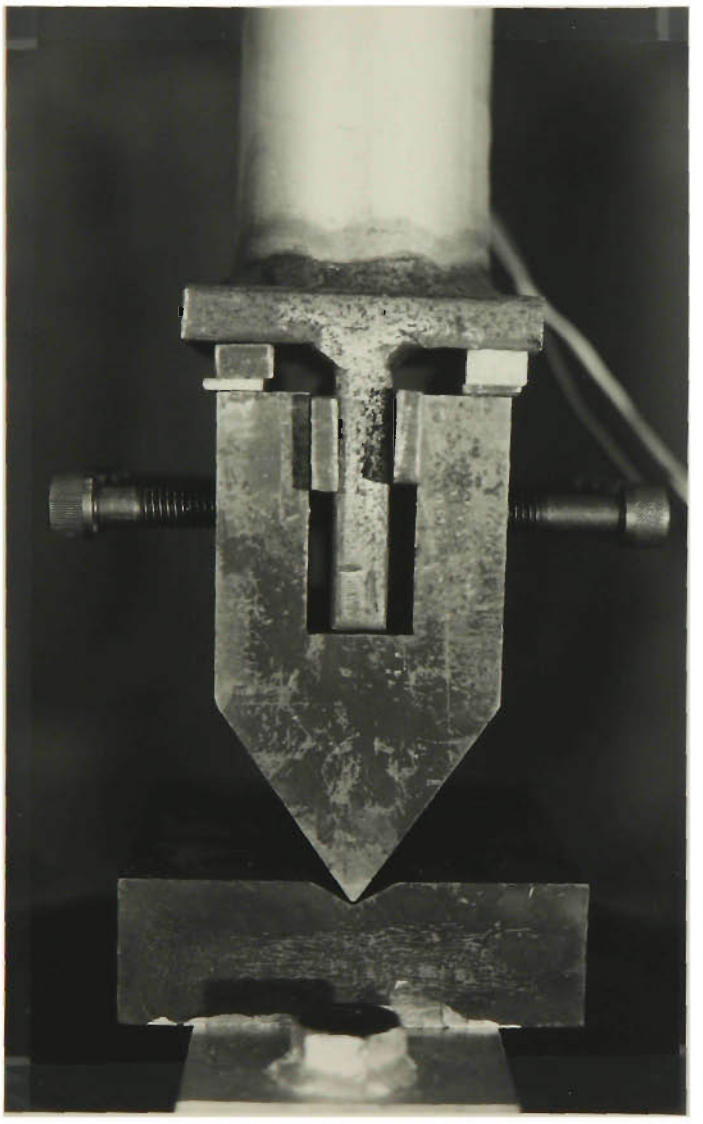

Fig.4.31 Knife Edge End Support

Fig.4.32 shows a typical specimen prior to testing, while Fig.4.33 shows the same specimen after testing -- a typical buckling mode of failure.

4.5.2 Initial Imperfections

Before testing , measurements of the out-of-roundness (Deviations from circularity (ovality)), based on diameter measurements, characterized as (Dmax - Dmin)/Dmean and the out-of-straightness were made (see Table.4.3 and Fig.4.34). It was found that , in general , there was less than 1% difference between two perpendicular diameters at positions along the strut length . The initial out-of-straightness of the test specimens was less than 0.0015L (L is the effective length of the strut, measured between the two end knife edges) for both as-received struts and prestrained struts (except for one specimen, No.18, where the maximum initial out-of-straightness at middle of the strut length was as large as 5.58mm, due to the accidental machine reversal after the prestraining cycle, the δ_o/L was 0.003).

Fig.4.34 defines the out-of-straightness δ_o for a pin-ended strut. It should be noted that with the limitation of the facilities used the measured maximum out-of-straightness δ_o was not very accurate. Nevertheless, these measurements can still be used as a reference. The end alignment was ensured using a height gauge and vernier calipers until the two end knife edges and the longitudinal center line referred to a machined base were in the same line within the tolerance of 0.0015L (see Fig.4.35). The line of action of the axial load was always through the line that was the center line of the two knife edges. The load eccentricity was then better controlled.

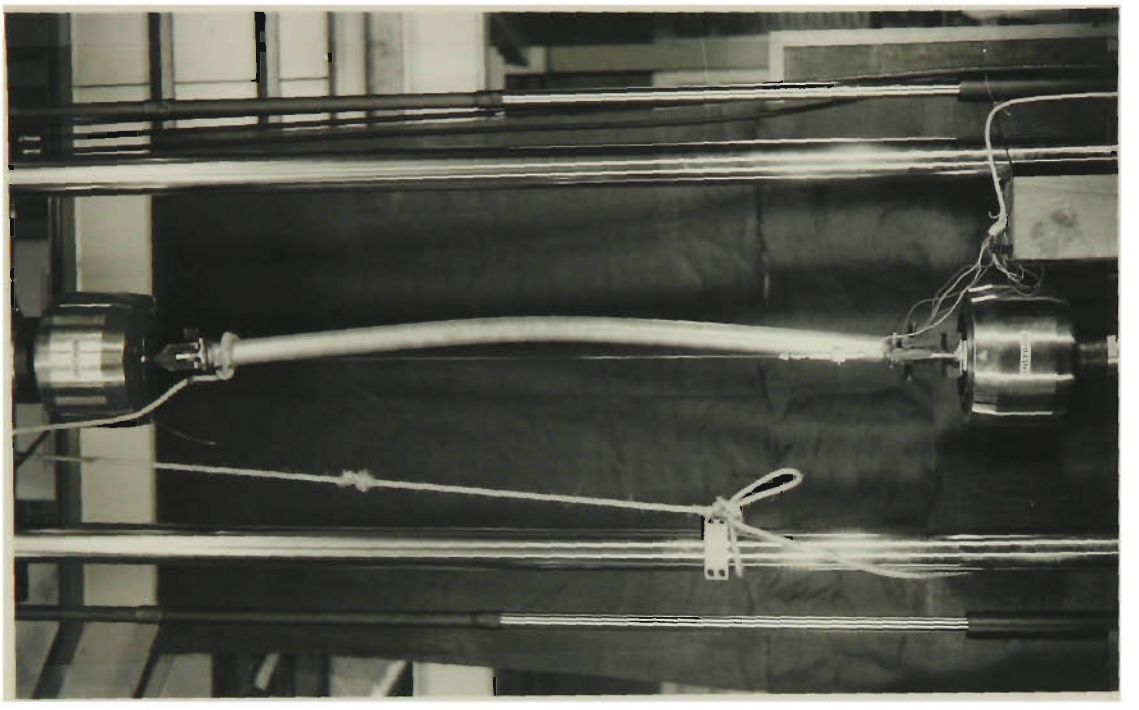

Fig.4.33 Buckling Mode

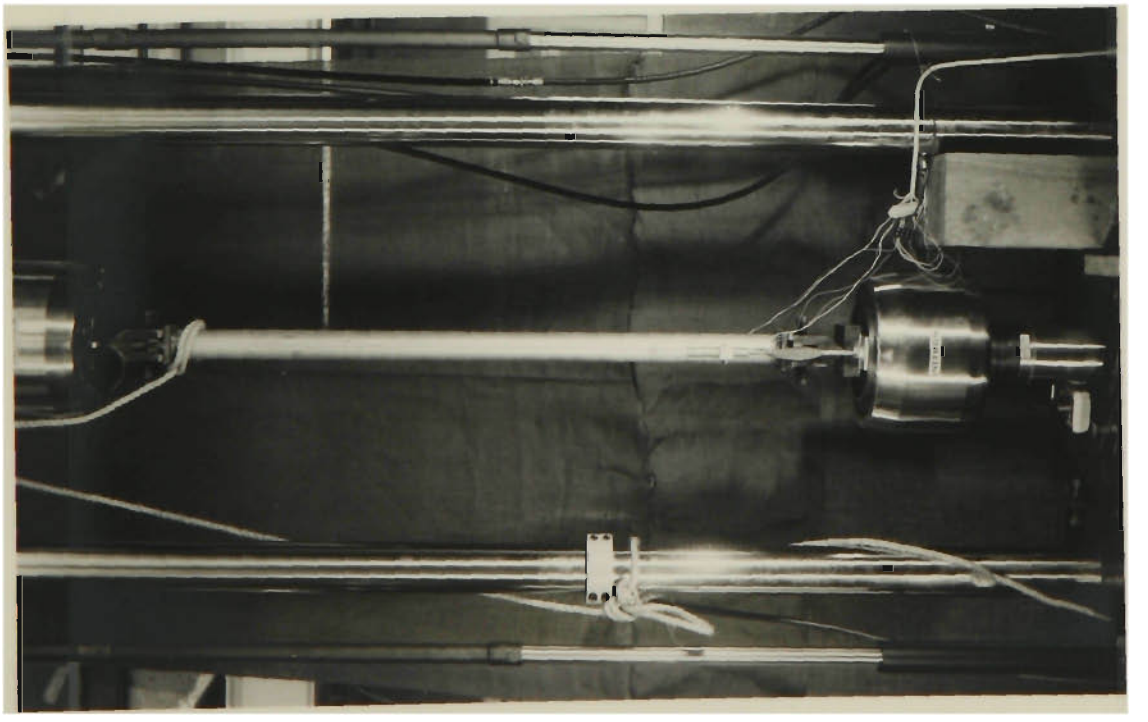

Fig.4.32 Test Set Up

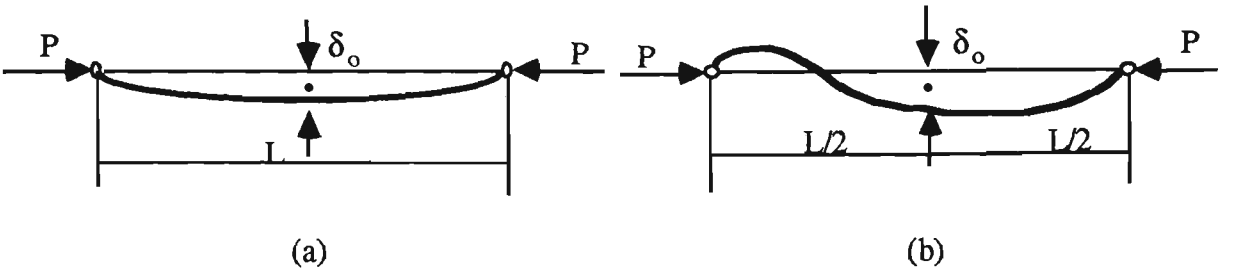

Fig.4.34 Initial Deflection

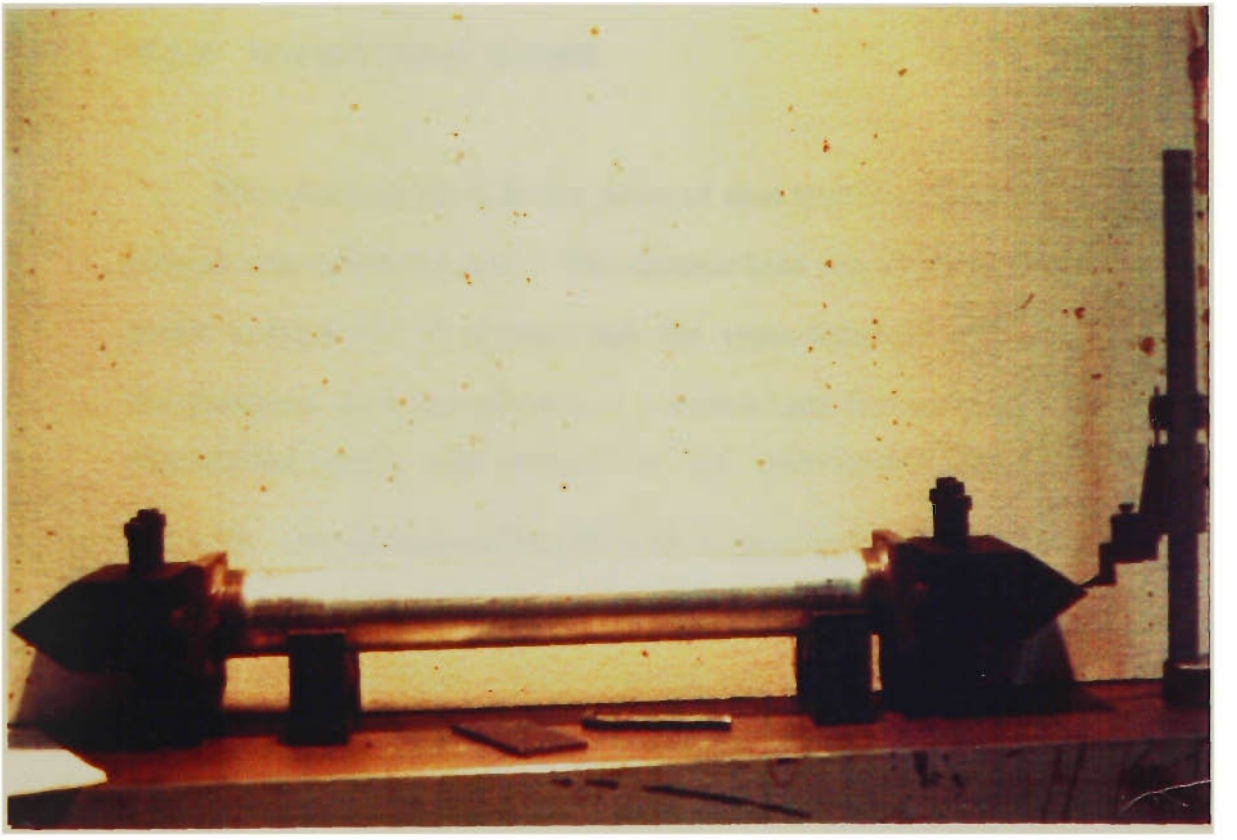

Fig.4.35 End Alignment Measurement

The replication of the strut tests and the subsequent results should indicate the significance of the initial out-of-straightness of the test specimens, as the difference between the ultimate load capacities for the same slenderness ratio should be small if the effect of the out-of-straightness and the eccentricity of loading is small within the given tolerance. With identical treatments, the geometrical imperfection will be slightly different; the variation in results will furnish some indication of the significance of this variable.

4.5.3 Overall Strut Results

The results of the first five series of strut tests mentioned before have been plotted with different scales . The ultimate load versus the slenderness ratio are given in Fig.4.36. It is noted that the cross-sectional area changes due to the prestrain, so a comparison in a normalised format is more reasonable . Normalised results with respect to the corresponding σ_y are given in Fig.4.37, and normalised results with respect to both the yield stress and the transition slenderness ratio (the transition slenderness ratio is defined as that value at which the Euler critical stress equals the yield stress of the material.) in Fig.4.38 . The supplementary test results of three specimens for 7% prestrained and fully-aged tubes (λ=45) are also included in Figs.4.36-4.38. Because of the prestraining, there were significant area reductions from the as-received material. Use was made, therefore, of the reduced area in determining critical stresses and in determining the slenderness ratios. In addition, the yield stress (σ_y) used in the normalisation procedure required definition. In this study, the 0.2% offset figure has been adopted as a yield value. It was also noticed that the cross section changes among the tubes for the same prestrain (say 7%) were small enough to use the average area to calculate the transition slenderness ratios. Table 4.8 shows the yield stresses used for each strut series , and the transition slenderness ratios.

Table 4.8 Yield Stresses and Transition Slenderness Ratios

Test Series	Material Condition	σ_y (MPa) (compression)	$(L/r)_T$
1	As-received	315	79.16
2	Pre.3% in Tension FA	319	78.63
3	Pre.3% in Tension NA	273	85.03
4	Pre.7% in Tension FA	320	78.59
5	pre.7% in Tension NA	280	83.96
6	SRA Pre.7% FA	247	89.4
7	SRA Pre.3% NA	216	95.6
8	SRA As-Received	274	85.51

The ultimate load withstood by each SRA test specimen is listed in Table 4.9 (the data were not sufficient to plot curves as presented for the first five series test results). To cater for the change of cross-section and of the length of the struts because of prestraining, normalised results with respect to both stress and the transition slenderness ratios are given in Table 4.9 as well. The test results of the SRA as-received and the SRA prestrained struts are presented in Fig.4.39. For comparative purposes, the test results of the prestrained struts and the as-received struts, but without the SRA treatment , are also plotted in Fig.4.39.

Table 4.9 Test Results of SRA Struts

Specimen No.	Material Condition *	λ	P (Kn)	λ/λ_T	σ/σ_y
1	SRA, 7% FA	36	95.9	0.40	0.98
2	SRA, 7% FA	36	93.7	0.40	0.97
3	SRA, 7% FA	55	87.1	0.61	0.90
4	SRA, 7% FA	55	84.7	0.61	0.87
5	SRA, 7% FA	74	83.3	0.82	0.86
6	SRA, 7% FA	74	82.8	0.82	0.85
7	SRA, 7% FA	92	70.5	1.03	0.73
8	SRA, 7% FA	92	70.0	1.03	0.73
9	SRA, 3% NA	36	84.1	0.38	0.96
10	SRA, 3% NA	36	81.5	0.38	0.93
11	SRA, 3% NA	55	69.5	0.57	0.79
12	SRA, 3% NA	55	72.0	0.57	0.82
13	SRA, 3% NA	74	63.2	0.77	0.72
14	SRA, 3% NA	73	54.4	0.77	0.62
15	SRA, 3% NA	92	43.5	0.96	0.50
16	SRA, 3% NA	92	48.4	0.96	0.55
17	SRA, AR	36	109.2	0.42	0.95
18	SRA, AR	55	113.0	0.64	0.98
19	SRA, AR	73	107.5	0.85	0.94
20	SRA, AR	73	107.4	0.85	0.94
21	SRA, AR	91	92.86	1.06	0.81

* : FA=Fully-aged, NA=Unaged, AR=As-Received.

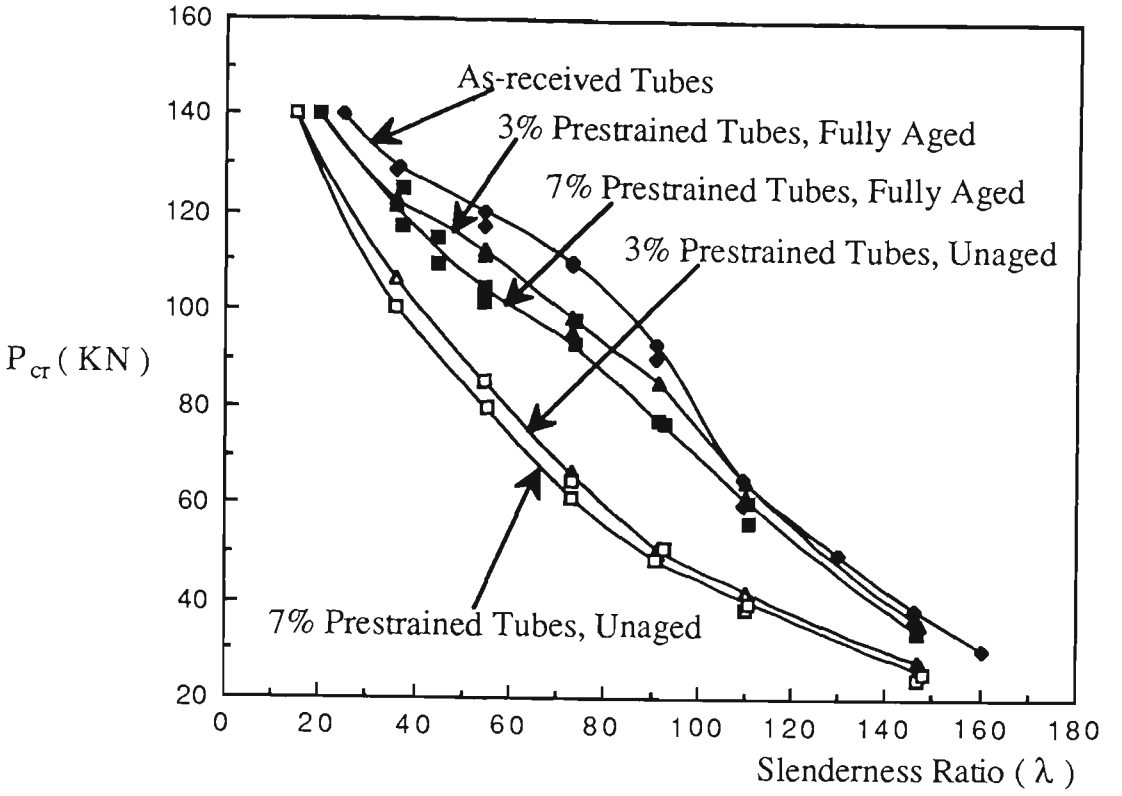

Fig.4.36 Strut Load Capacity versus Slenderness Ratio

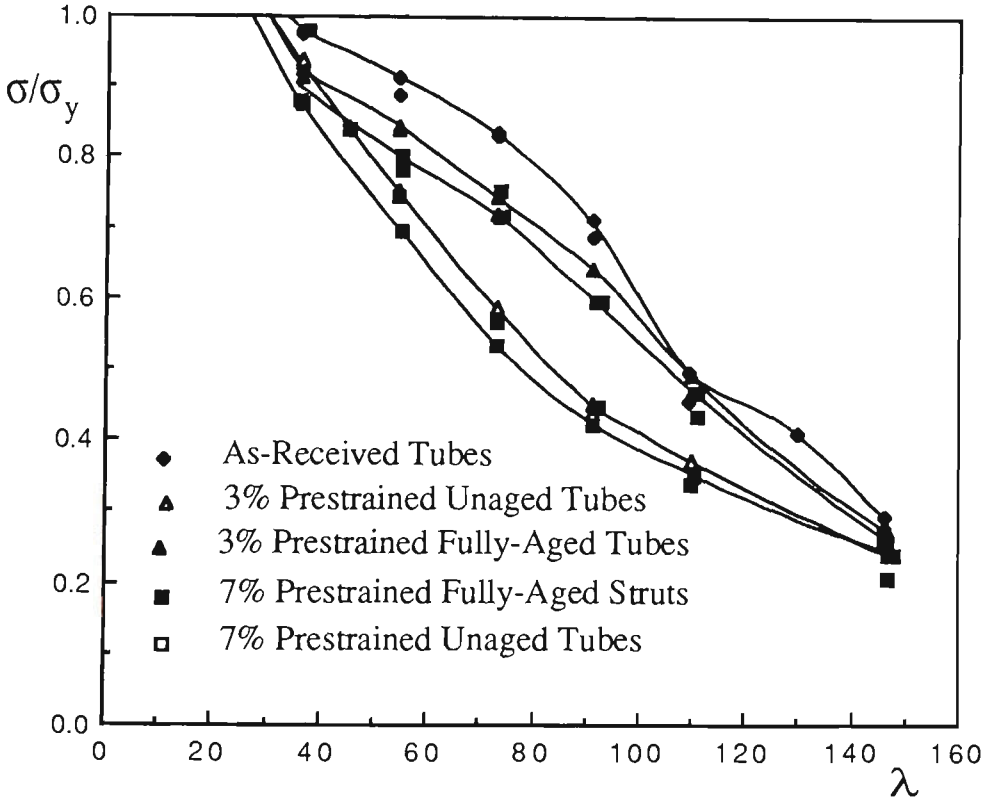

Fig.4.37 Strut Test Results - Stress Axis Normalised

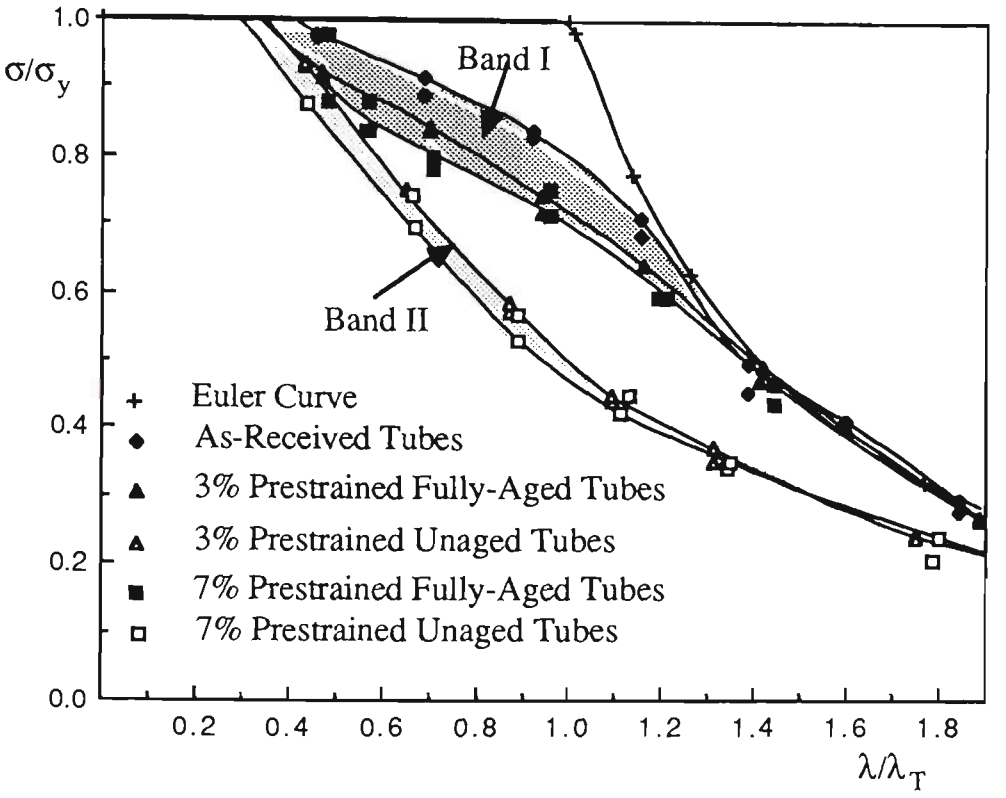

Fig.4.38 Normalised Critical Stress Versus Normalised Slenderness Ratio Plots of Test results

Experimental load-shortening curves for different slendernesses, normalised with respect to yield stress/strain, are superimposed on the stub-column curves in Fig.4.40 for as-received struts, Fig.4.41 for 3% prestrained in tension and fully-aged struts, Fig.4.42 for 7% prestrained in tension and fully-aged struts, Fig.4.43 for 3% prestrained in tension and unaged struts, and Fig.4.44 for 7% prestrained in tension and unaged struts. It can be seen that the stub-column curves form the top envelop curves and all other curves with different slenderness ratios fell below.

The load-shortening curves normalised with respect to yield stress/strain, of the first five series of strut test results, are plotted in Fig.4.45 for slenderness ratio λ=146(147), Fig.4.46 for λ=110(111), Fig.4.47 for λ=91(92), Fig.4.48 for λ=73(74), Fig.4.49 for λ=55 and Fig.4.50 for λ=36.

4.5.4 Discussion of Test Results

4.5.4.1 The Influence of Strain Hardening, Strain Aging and The Bauschinger Effect

The most significant result is the difference in load capacities for the different conditions. From Fig.4.36, in the structurally more significant range of slenderness ratios (50-110), the buckling load is reduced by up to 42% for struts prestrained 3% in tension and 43% for struts prestrained 7% with no aging . However, under the fully aged condition , the reduction is less,being 11% for 3% prestrained struts , and 14% for 7% prestrained struts .

It is noted that the cross-sectional area changes due to the prestrain, so a comparison in a normalised format is more reasonable. As shown in Fig.4.38, at

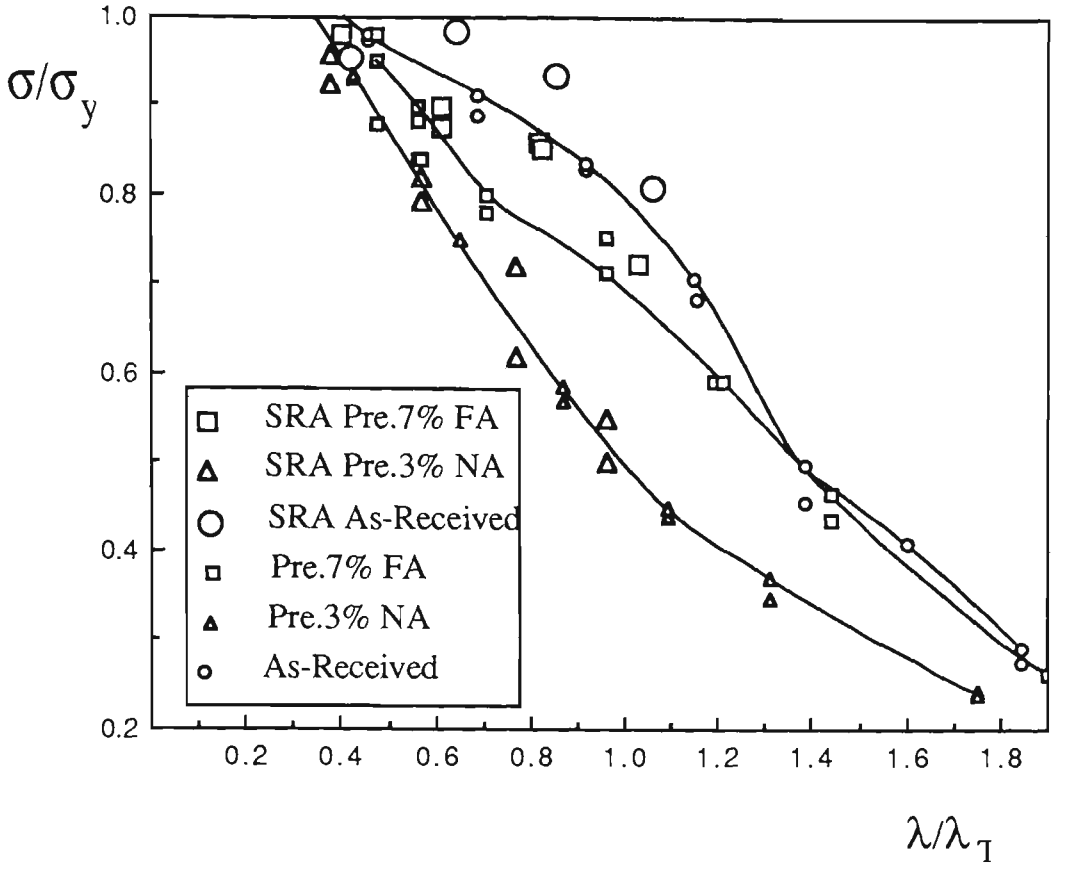

Fig.4.39 Test Results - Stress Relief Annealed

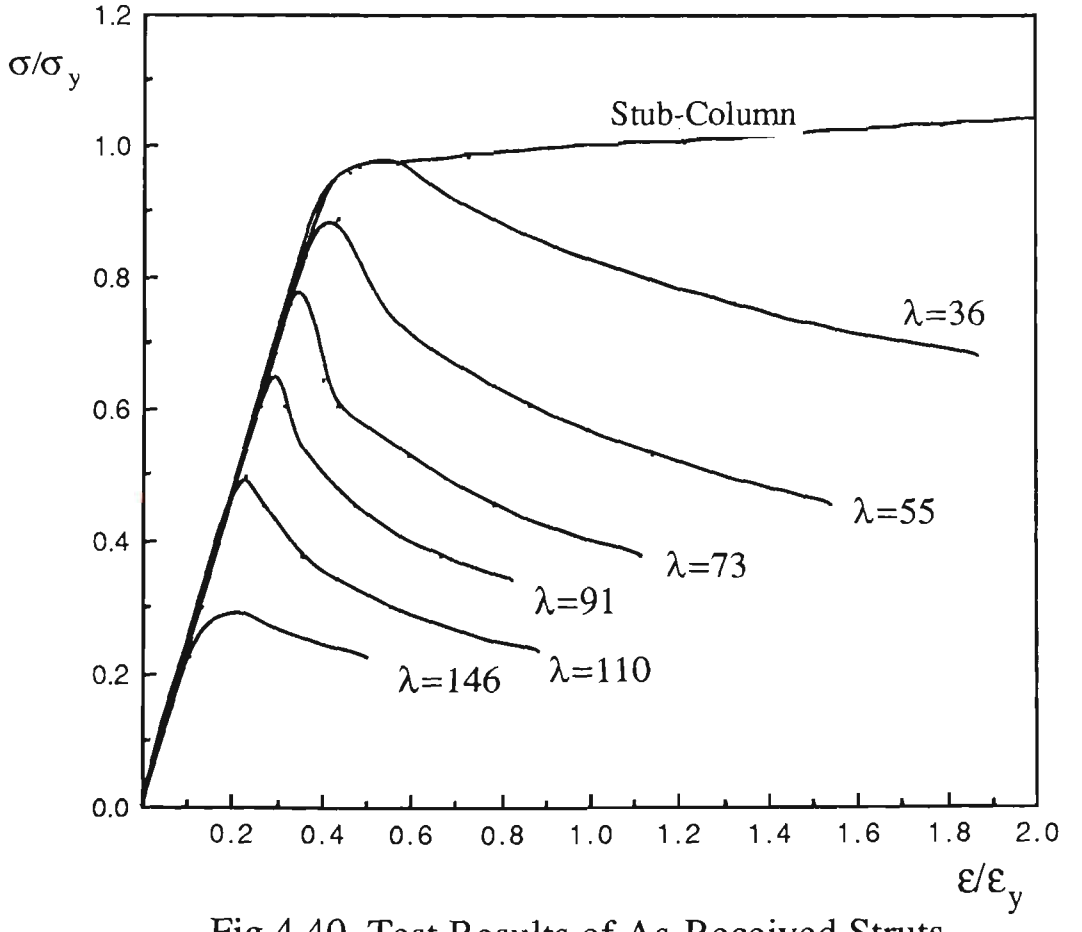

Fig.4.40 Test Results of As-Received Struts

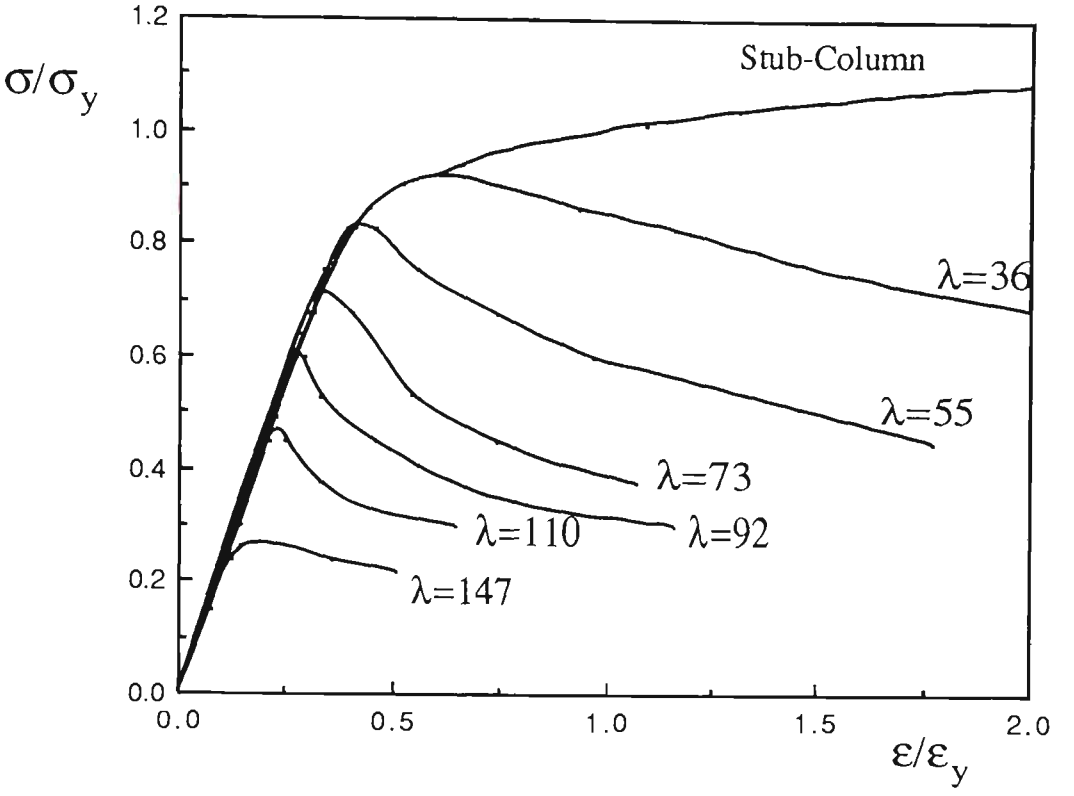

Fig.4.41 Test Results of 3% Prestrained Fully-Aged Struts

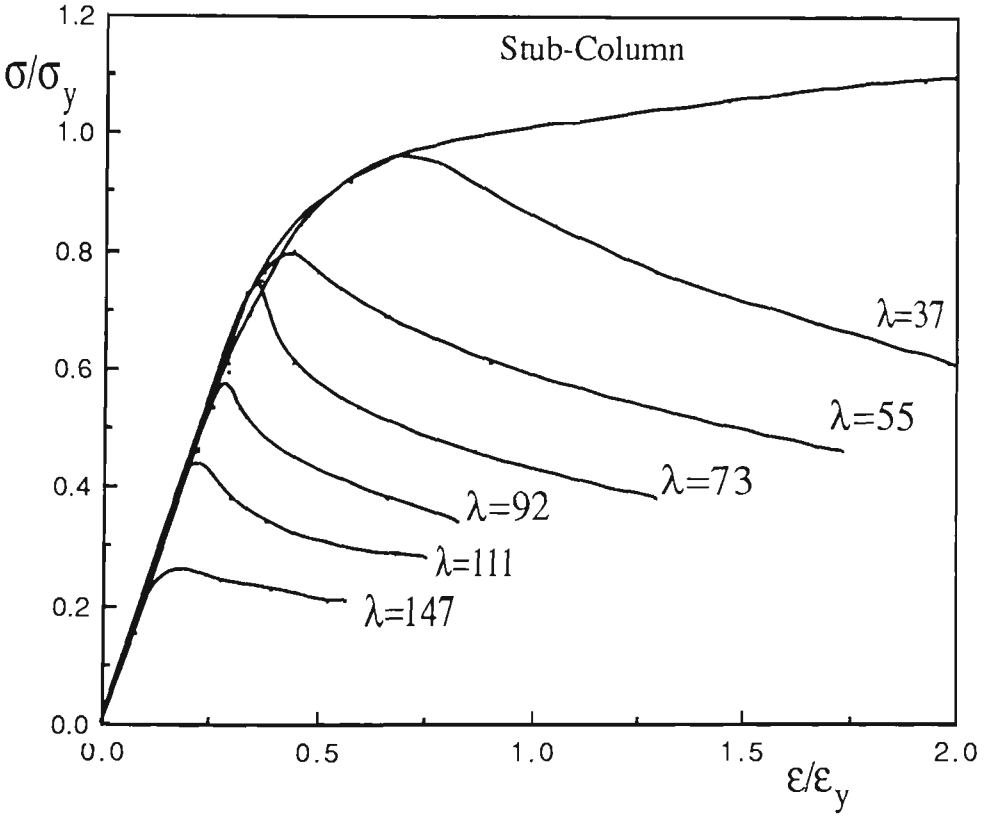

Fig.4.42 Test Results of 7% Prestrained Fully-Aged Struts

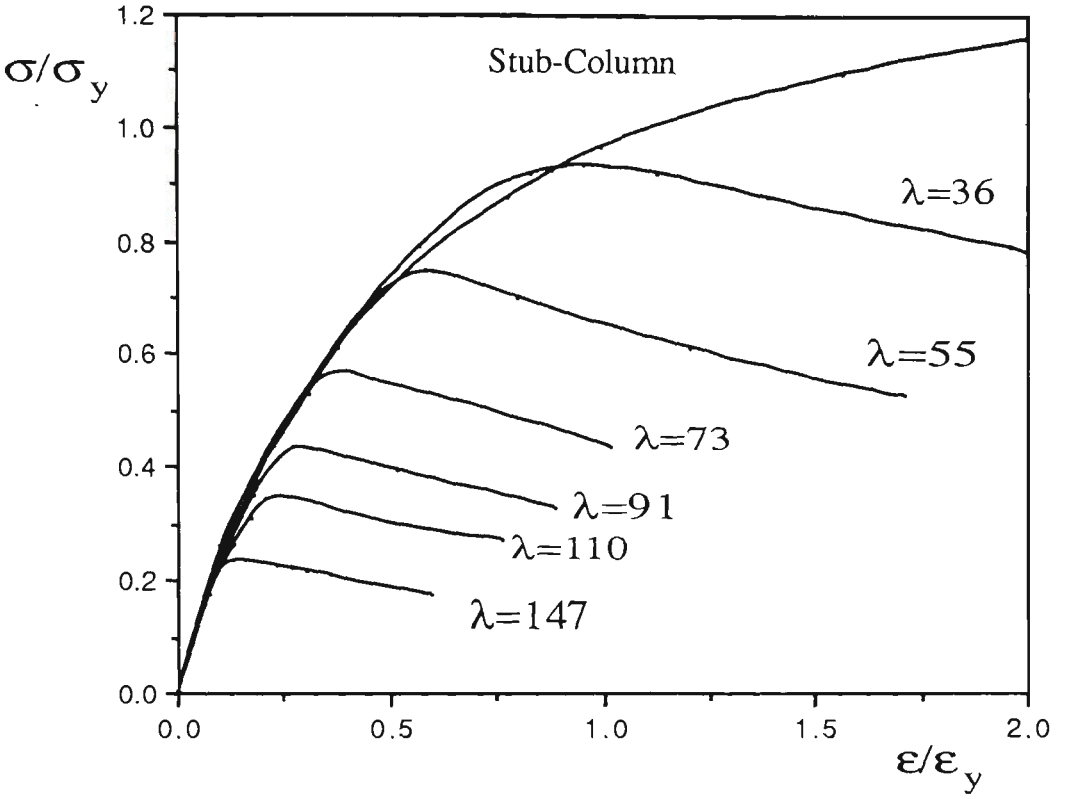

Fig.4.43 Test Results of 3% Prestrained Unaged Struts

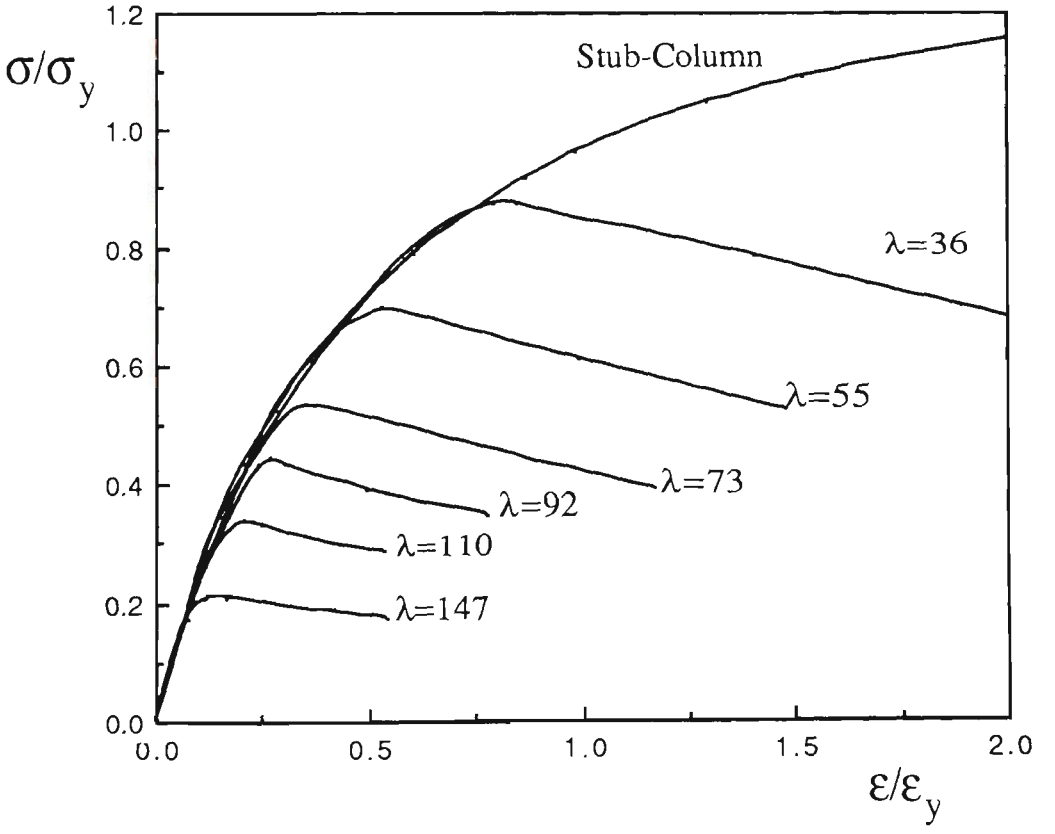

Fig.4.44 Test Results of 7% Prestrained Unaged Struts

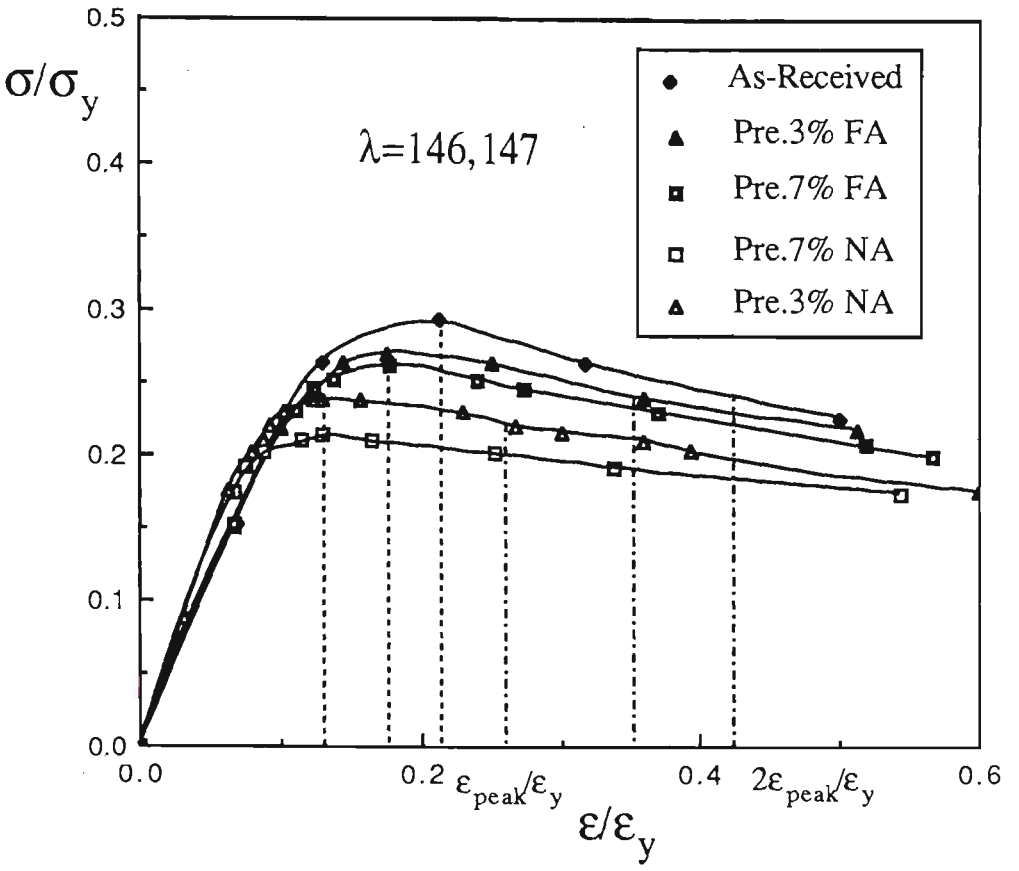

Fig.4.45 Test Results - All Conditions

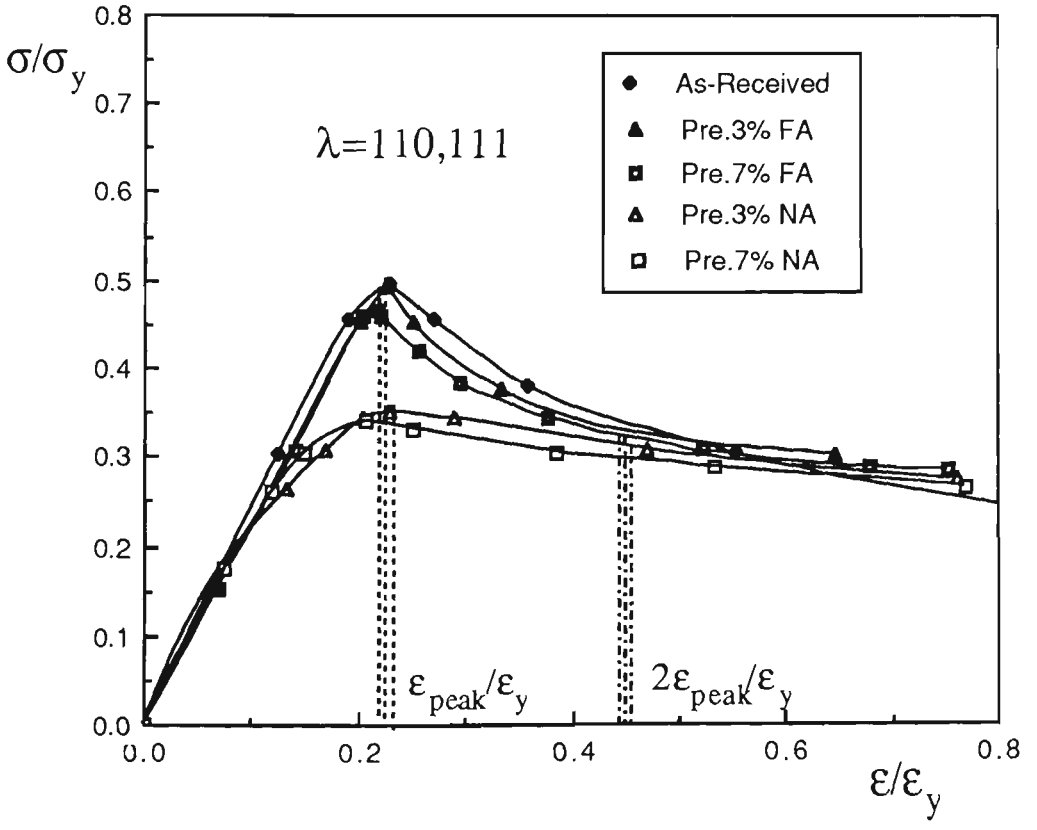

Fig.4.46 Test Results - All Conditions

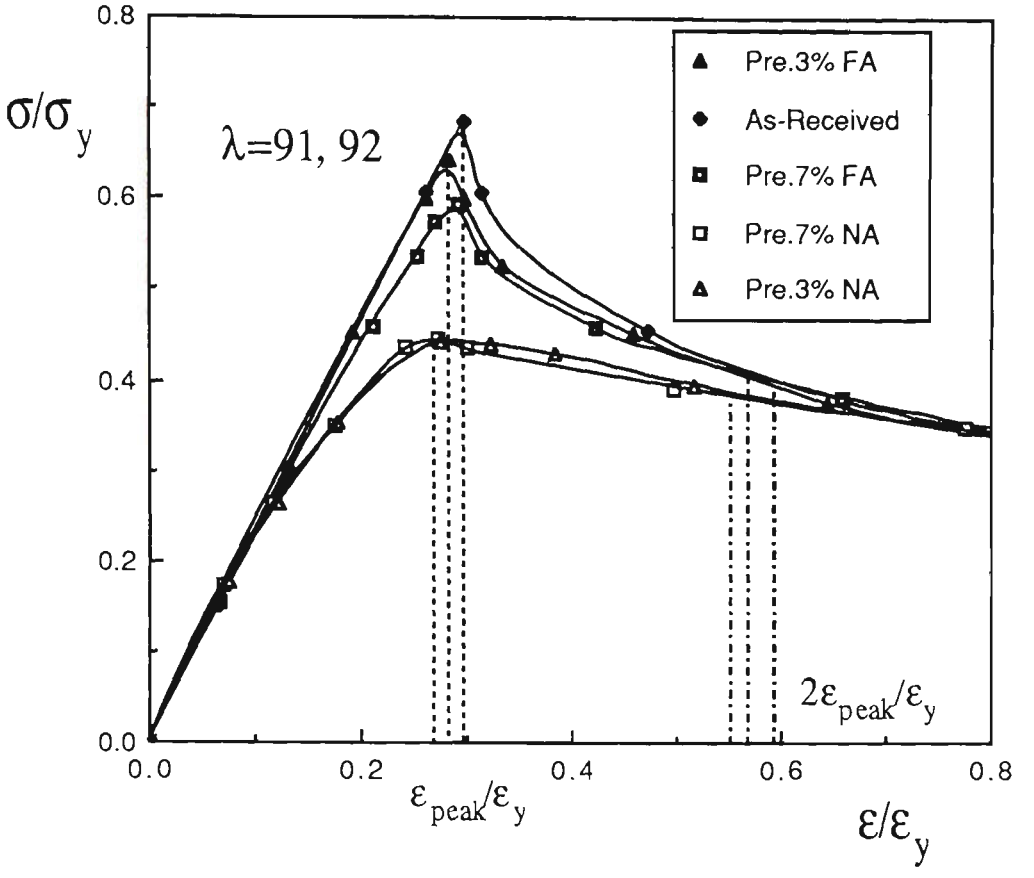

Fig.4.47 Test Results - All Conditions

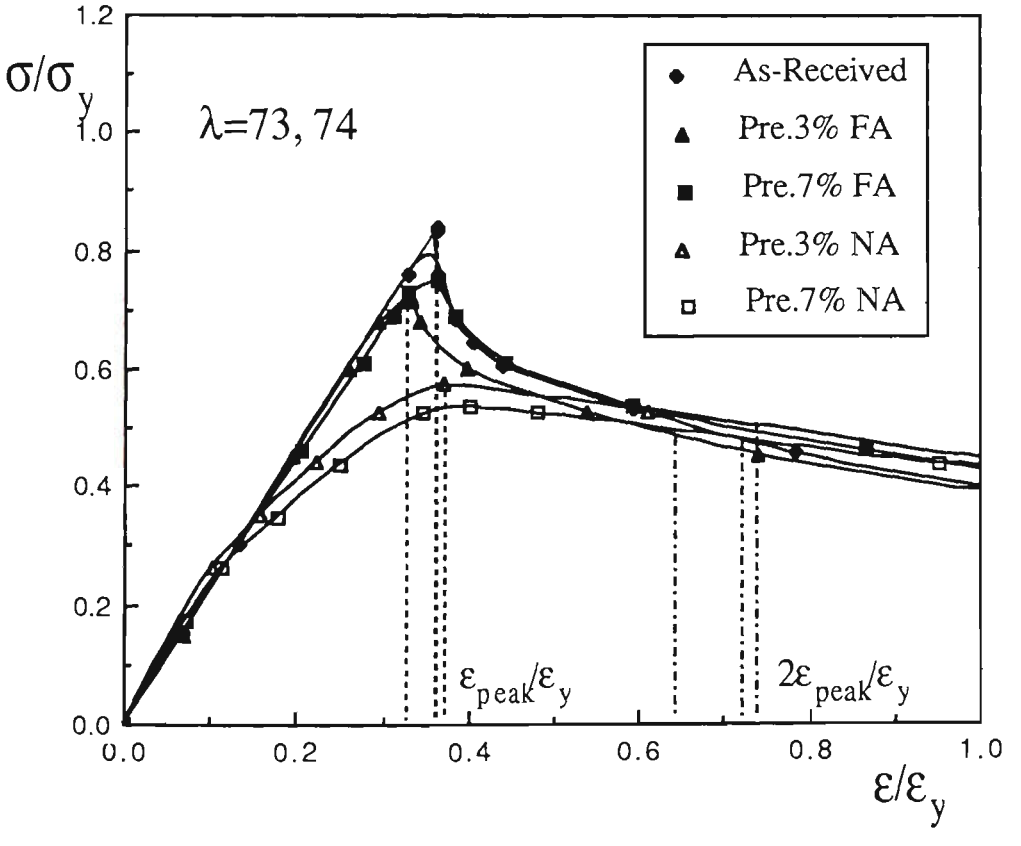

Fig.4.48 Test Results - All Conditions

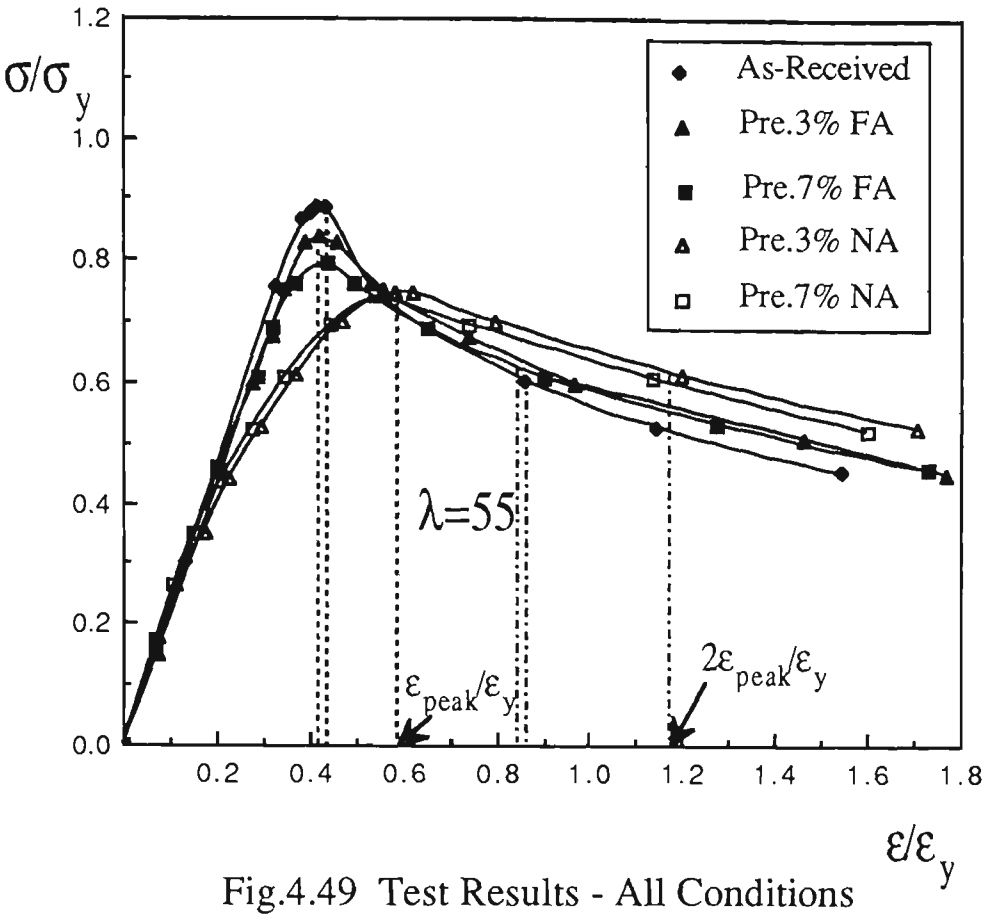

Fig.4.49 Test Results - All Conditions

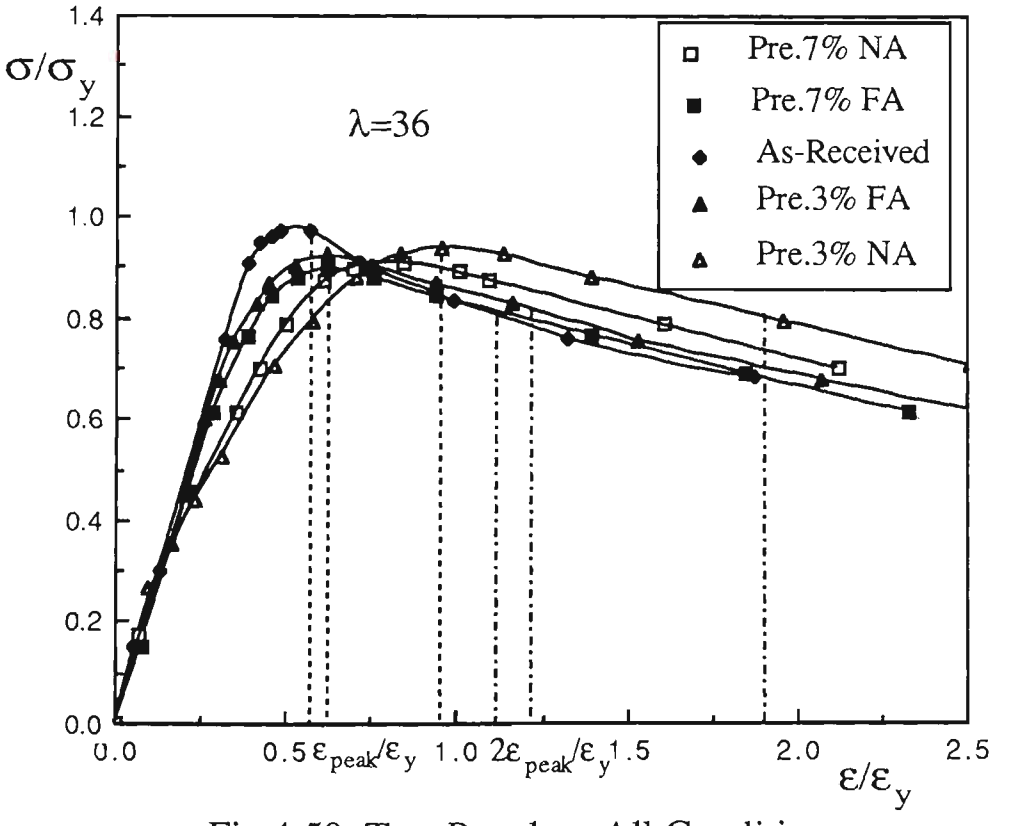

Fig.4.50 Test Results - All Conditions

very high slenderness ratios, the curve of 3% prestrained and full-aged tubes was slightly above the as-received tubes. For all other cases the prestrained struts had lower capacities than the corresponding as-received struts. That is, the loss of strut load capacity due to the Bauschinger effect on load reversal occurs for all the struts prestrained in tension (3% and 7%), whether fully aged or not aged , and this loss is more sensitive to strain aging than strain hardening. The potential strength gains due to strain hardening had been outweighed by the combined effects of strain aging (beneficial) and the Bauschinger effect (deleterious).

Two distinct bands of test results are evident in Fig.4.38; an upper band of virgin tests and prestrained struts with strain aging (series 1, series 2 and series 4), a lower band of prestrained struts without strain aging (series 3 and series 5).

The influence of strain aging on load capacity changes with different L/r values. The reduction compared with that for the as-received struts is shown in Table 4.10.

The measure of strain hardening propensity used herein was the strain hardening ratio which was 1.15 for the ERW tube. The struts made from prestrained tube had different 0.2% offset stress levels depending on the amount of prestrain, strain aging and the strain hardening ratio. At slenderness ratios significantly below the transition length, prestrained strut load capacities above the as-received yield squash level were possible even with no strain aging; whether or not such levels were achieved depended on the relative influence of strain hardening and the other two effects considered herein, strain aging and the Bauschinger effect. The results of the steel tubular strut tests in Fig.4.38 indicate that the level of prestraining (3% to 7%) has a small effect on strut load capacity made from material with a low SHR. In general , the influence of strain hardening

on load capacity is not as sensitive as that of strain aging , due to the low strain hardening capacity of the ERW tube used. However , at lower values of (L/r) , the influence is relatively a little higher .

Table 4.10 Load Reduction of Prestrained Struts Compared with As-received Struts

Normalised Slenderness Ratios	Prestrained in Tension %	Condition	Reduction Up To
$(L/r)/(L/r)_T<0.63$	3	FA	11%
		NA	26%
	7	FA	15%
		NA	30%
$0.63\leq(L/r)/(L/r)_T<1.3$	3	FA	12%
		NA	38%
	7	FA	13%
		NA	38%

FA = Fully strain aged, NA = Not strain aged.

At slenderness ratio values higher than the transition length strut collapse occurs at low stress levels so material strength (0.2% offset values including any strain hardening) is expected to have little influence. However, the Bauschinger rounding of the stress-strain curve may cause a significant effect, leading to reductions in strength, and strain aging reduces this reduction, as seen in Fig.4.38.

Although it is difficult to separate the three material effects, the general trend of the influence can be summed to be that, in the range of slenderness ratios greater than 60, the Bauschinger effect plays a much more dominant role owing to the associated reduction in tangent modulus that leads to a greater propensity for buckling to occur, with load capacity reduction of up to 38% . Strain aging is more significant than strain hardening in enhancing the capacity of prestrained struts. Compared with the no aged condition, the load capacity increase with the fully aged condition is up to 31% for struts prestrained 7% and up to 32% for struts prestrained 3% . The combined effects of strain hardening, strain aging and the Bauschinger effect, therefore, have a substantial influence on strut carrying capacity.

It might be argued that the significant reduction of strut load capacity for prestrained tubes was due to the residual stresses induced in the tubemaking process (although it is expected that the influence of residual stresses had been swamped by the prestrains of 3% and 7%) instead of the Bauschinger loss. The SRA strut tests that were then prestrained explain this query.

From Fig.4.39, it is seen that the test results of SRA as-received struts for all slenderness ratios tested lie above those of the as-received struts, but without the SRA treatment. The exception to this case was the SRA as-received strut with slenderness ratio λ=36, which was slightly lower. The reason for this is probably due to the initial eccentricity of loading of the strut, which was beyond the given tolerance. The comparison of the test results of the as-received struts with those of the SRA as-received struts indicated that the existence of residual stresses set up during the tubemaking process reduced the load capacity for as-

received struts. This reduction was less than 5% for L/r=55; 9% for L/r=73 and 5.3 % for L/r=91.

As shown in Fig.4.39, it is seen that the agreement between the prestrained strut tests and the SRA prestrained strut tests is reasonably good, which implies that the residual stresses induced in tubemaking process for the ERW tube have little influence on strut load capacity of prestrained material whether fully aged or unaged. These test results give added strength to the observations mentioned above, i.e., it is clear that the loss of strut load capacity due to the Bauschinger effect on load reversal occurs for all the struts prestrained in tension. This loss is more sensitive to strain aging than strain hardening for the rimming steel used. The stress-relief-annealed strut tests carried out eliminate the effects of unknown residual stresses, it is therefore concluded that the influence of residual stresses on load capacity of prestrained struts is insignificant for prestrains of the order considered.

4.5.4.2 Post-Buckling Strength

The post-buckling strength will probably depend on the capability of the members to sustain secondary bending stresses. These stresses are a result of the bending moment due to the eccentricity of the axial load with respect to the deflected post-buckled shape. Therefore, it seems reasonable to assume that the post-buckling load capacities of circular struts will be significant in case of long struts where the initial buckling stresses are small.

As mentioned earlier, the Bauschinger rounding occurred for all the tubes that were prestrained in tension; strain aging reduced this rounding. Therefore, the behaviour of as-received tubes is closer to that of tubes that are prestrained in

tension and fully-aged than that of tubes which are prestrained in tension and unaged, as seen in Fig.4.17. Referring to Figs.4.40- 4.44 , it is seen that the behaviour for as-received struts is similar to that of prestrained in tension and fully-aged struts, but is different from that of prestrained in tension and unaged struts. The influence of post ultimate load shedding is evident in the load-axial shortening behaviour. For as-received and prestrained in tension and fully-aged struts, the inelastic post-buckling behaviour of struts is dependent on strut slenderness. Referring to Fig.3.13 (in Chapter three) once again, apart from the strain hardening behaviour of stub columns, three classes of behaviour are obvious, and these can be implied in Figs.4.40, 4.41 and 4.42. The zones are namely (I) gentle load shedding (λ=36), (II) rapid load shedding (λ=55-110), and (III) ductile (λ=146). The post-buckling behaviour follows one trend, i.e., (I) gentle load shedding. However, for prestrained in tension and unaged struts, it seems that only gentle load shedding behaviour exists, independently of the slenderness ratios of struts.

From Figs.4.45 - 4.50, it is seen that greater nonlinearity prior to buckling is demonstrated for the prestrained in tension and unaged struts, which shows a much lower buckling load while the post-buckling fall-off in load with increasing axial shortening is much less dramatic than with the as-received and prestrained in tension and fully-aged struts. However, this observation is not true in the case when the value of slenderness ratio is 146. In this case, all the struts (both as-received and prestrained in tension) are still in the elastic range before buckling. It is, therefore, more appropriate to use an unnormalised scale for this slenderness ratio, as shown in Fig.4.51. The significant difference between the as-received and the struts prestrained in tension at this slenderness ratio indicate that the Bauschinger rounding of the stress-strain curve causes significant reductions in strength, as strut collapse occurs at a low stress level so material strength (0.2%

offset value including strain hardening) is expected to have little influence, but the influence of strain aging is significant.

It is of interest to note that the difference between as-received and prestrained in tension and fully-aged struts is insignificant, whether in the pre-buckling or post-buckling range. However, the difference between as-received and prestrained in tension and unaged struts is significant in the pre-buckling range up to peak load. This difference is reduced in the post-buckling range particularly in the range of slenderness ratios from 55 -110.

To better understand and quantify the post-buckling behaviour, vertical lines are drawn at $\varepsilon_{peak}/\varepsilon_y$ and $2\varepsilon_{peak}/\varepsilon_y$ to intersect the curves representing different strut conditions. With respect to the as-received struts, the struts prestrained in tension and fully-aged, and the struts prestrained in tension and unaged respectively (Figs.4.45 - 4.50), the points of intersection between ordinates at $2\varepsilon_{peak}/\varepsilon_y$with the normalised critical stress vs axial strain curves are referred to as the residual load capacity (σ_{Re}/σ_y) after buckling, as afterwards the post-buckling behaviour is ductile.

Table 4.11 gives details of the maximum load capacity and the residual load capacity. The post-buckling loads drop dramatically (29% to 42%) for the as-received struts with slenderness ratios λ=55–110, and as expected the drop reduces with slenderness ratios smaller λ=36 (16%) and larger λ=146 (17%).

For the struts prestrained in tension and fully-aged, the post-buckling load drop is similar to that of the as-received struts. That is, the post-buckling loads drop more dramatic for struts with λ=55–110 (25% - 37%) than with λ=36 (10%) and λ=147 (11%).

The post-buckling load drop for the struts prestrained in tension and unaged, which belongs to the type of gentle load shedding behaviour, is much less (8% -17%) for all the slenderness ratios (λ=36 – 147) compared with the as-received struts and the struts prestrained in tension and fully-aged.

Figs.4.45 - 4.50 and Table 4.11 also indicate the significant post-buckling load capacities of the struts after reaching the ultimate load, 58% to 84% of maximum load capacities for the as-received struts, 63% to 90% of maximum load capacities for the struts prestrained in tension and fully-aged, and 83% to 92% of maximum load capacities for struts prestrained in tension and unaged.

Table 4.11 Summary of Failure and Post-Failure Condition (Experimental Results)

λ	Condition	σ_{peak}/σ_y	σ_{Re}/σ_y	$\sigma_{Re}/\sigma_{peak}$ %	$\frac{\sigma_{peak}-\sigma_{Re}}{\sigma_{peak}}$ %
36	AR	0.98	0.82	84	16
	FA	0.92	0.83	90	10
	NA	0.93	0.80	86	14
55	AR	0.89	0.60	67	33
	FA	0.84	0.63	75	25
	NA	0.75	0.62	83	17
73 (74)	AR	0.83	0.52	63	37
	FA	0.74	0.52	70	30
	NA	0.59	0.50	85	15
91 (92)	AR	0.71	0.41	58	42
	FA	0.64	0.40	63	37
	NA	0.45	0.39	87	13
110 (111)	AR	0.50	0.34	68	29
	FA	0.49	0.33	67	28
	NA	0.35	0.31	89	15
146 (147)	AR	0.29	0.24	83	17
	FA	0.27	0.24	89	11
	NA	0.24	0.22	92	8

FA=Fully-Aged. NA=Unaged, AR=As-Received.

σ_{peak}=Maximum load capacity, σ_{Re}=Residual load capacity.

4.5.5 Regression Results

On the basis of the least-squares criterion, regression analyses were used to provide an unbiased trend in the strut test results. Polynomial functions were adopted here to describe the relationship between the observed values of the tests .

The regression results of the first five series of strut tests mentioned before have been plotted with different scales . Raw results are given in Fig.4.52. To cater for the change of cross-section and of the length of the struts because of prestraining, normalised results with respect to both stress and the transition slenderness ratio are given in Fig.4.53. The equations adopted are given as follows:

Fig.4.52: As-received Tubes: $Y = 263 - 9.42X + 0.25X^2 - 0.0031X^3$

Prestrained 3% FA Tubes : $Y = 152 - 0.72X - 0.00038X^2$

Prestrained 3% NA Tubes : $Y = 167 - 1.96X + 0.0089X^2$

Prestrained 7% FA Tubes : $Y = 178 - 2.41X + 0.034X^2 + 0.0003X^3$

Prestrained 7% NA Tubes : $Y = 170 - 2.28X + 0.014X^2$

Where $X = (L/r)$, $Y = Pcr$

FA = Fully strain aged, NA = Not strain aged .

Fig.4.53: As-received Tubes: $Y=1.38-2.12X+4.62X^2 -5.12X^3 +2.43X^4 -0.41X^5$

Prestrained 3% FA Tubes : $Y=1.26-0.74X+0.23X^2 -0.059X^3$

Prestrained 3% NA Tubes : $Y=1.24-0.33X-1.45X^2 +1.57X^3 -0.63X^4 +0.092X^5$

Prestrained 7% FA Tubes : $Y=1.28-.88X+0.36X^2 -0.0093X^3$

Prestrained 7% NA Tubes : $Y=1.29-1.05X+0.26X^2 -0.0034X^3$

Where $X = \lambda/\lambda_T$, $Y = \sigma/\sigma_y$

4.5.6 Tangent Modulus Prediction

For comparative purposes, load capacities for all five series of struts were predicted using the tangent modulus method based on the compressive load-deformation plot of the stub column tests for each class of material. The tangent modulus formulae are shown in equation (4.3) and equation (4.4).

$$P_{cr} = \pi^2 E_t I / L^2 \qquad (4.3)$$

$$\sigma_{cr} = \pi^2 E_t / L^2 \qquad (4.4)$$

Using the tangent moduli found from stub column tests of the as-received tubes , and the prestrained 3% and 7% tubes under fully aged and no aging conditions , the theoretical curves derived from the tangent modulus theory and the regression results of the strut tests are shown in Fig.4.54 - Fig. 4.56 . It is seen that the agreement between the strut tests and the associated tangent modulus curves is reasonable, highlighting the significance of the loss of modulus associated with strain reversal. This aspect of the Bauschinger effect, viz., the reduction of the tangent modulus with increasing compressive strain is of prime significance in the tests . As indicated in the material tests, strain hardening and strain aging lead to an enhancement of strength when strains are of the same sign as the prestrain. On reversal of strain, however, the increasing curvature of the stress-strain plot means that the tangent modulus is reduced which, in turn, leads to a reduction in the ultimate carrying capacity of the struts. This reduction occurs even though the yield point of the material may have been increased on reversal relative to that of the virgin material.

In general , however, the tangent modulus calculation slightly underestimates the observed load capacity in the smaller slenderness ratio range and overestimates it in the larger range. Therefore , a more accurate theoretical model which includes geometrical imperfections and material effects , which has been described in Chapter 3, needs to be applied(see Section 3.6).

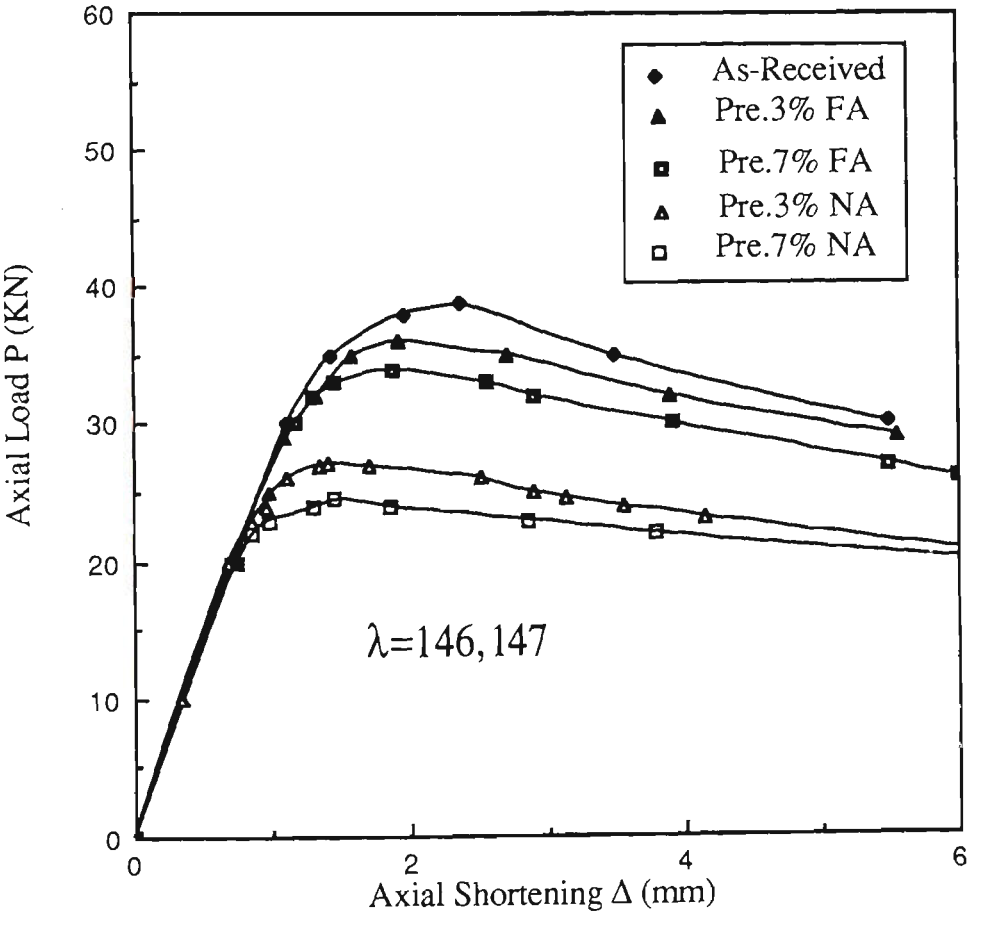

Fig.4.51 Test Results - All Conditions

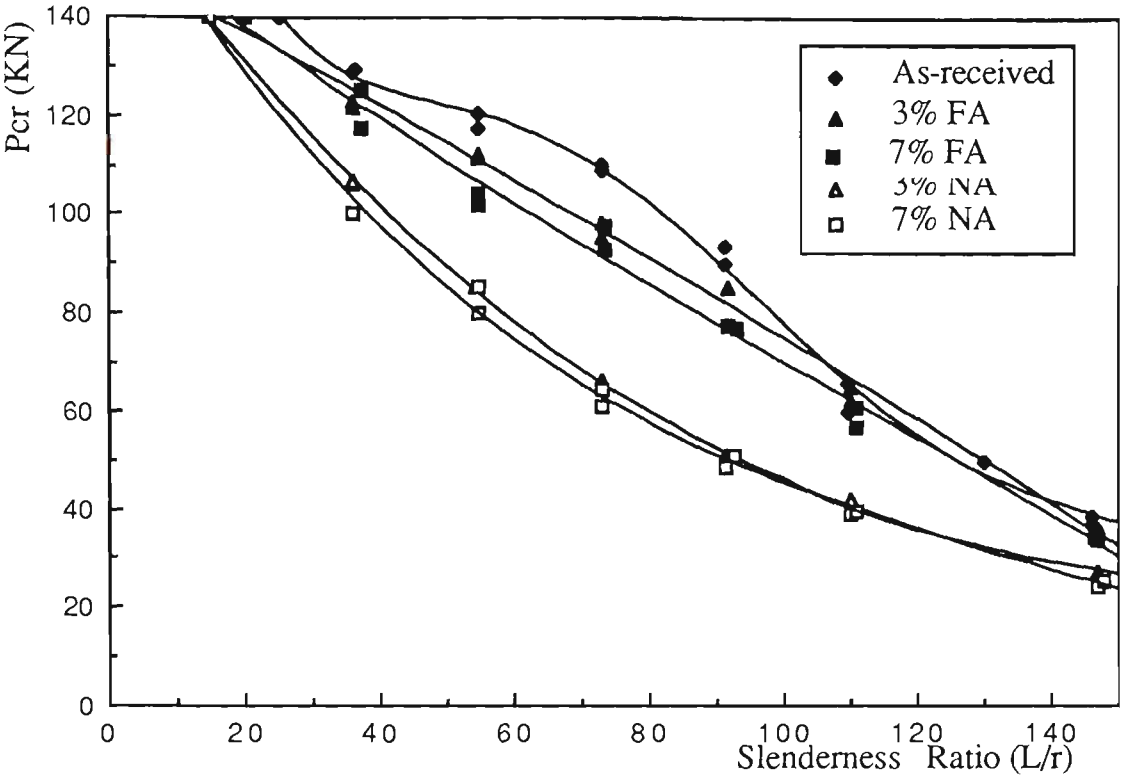

Fig.4.52 Strut Load Capacity vs Slenderness Ratio

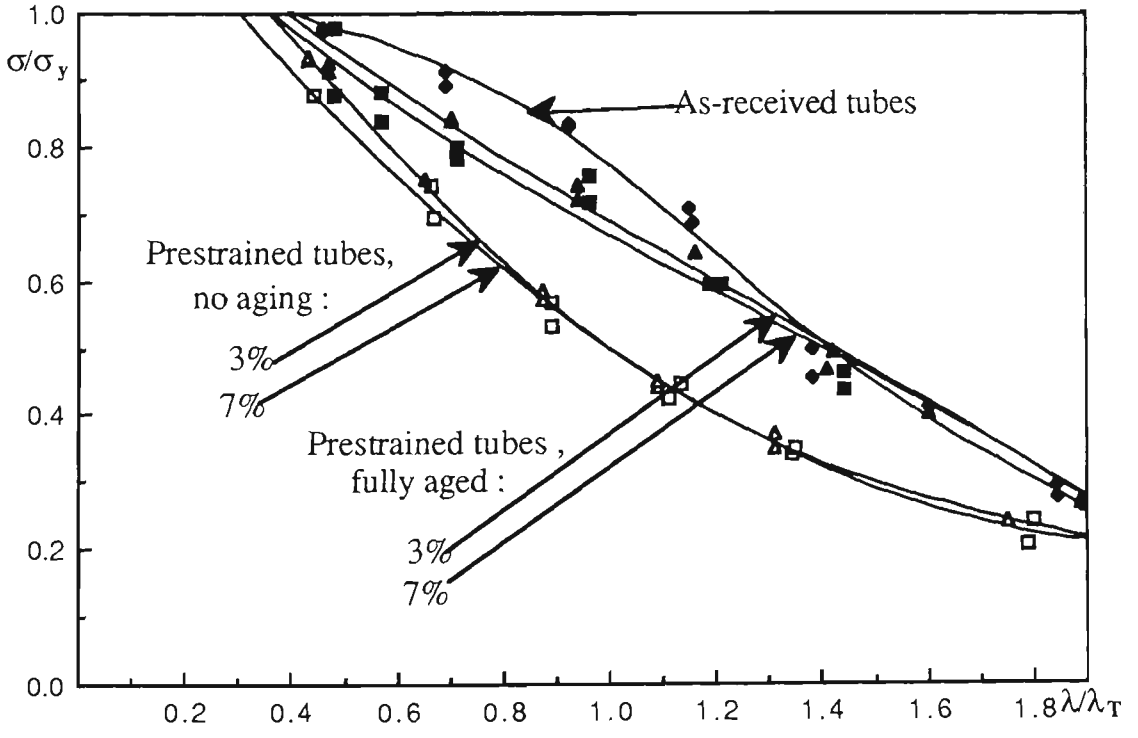

Fig.4.53 Normalised Critical Stress vs Normalised Slenderness Ratio

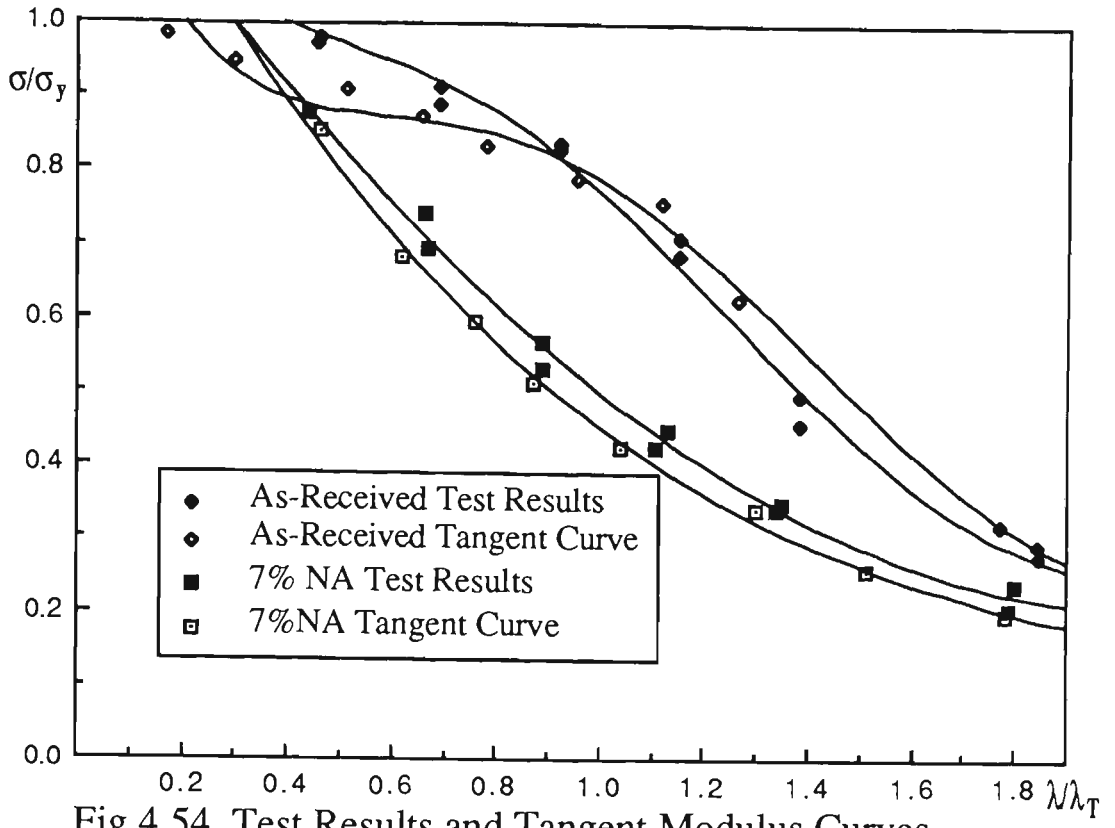

Fig.4.54 Test Results and Tangent Modulus Curves
- As-Received and 7% Prestrained

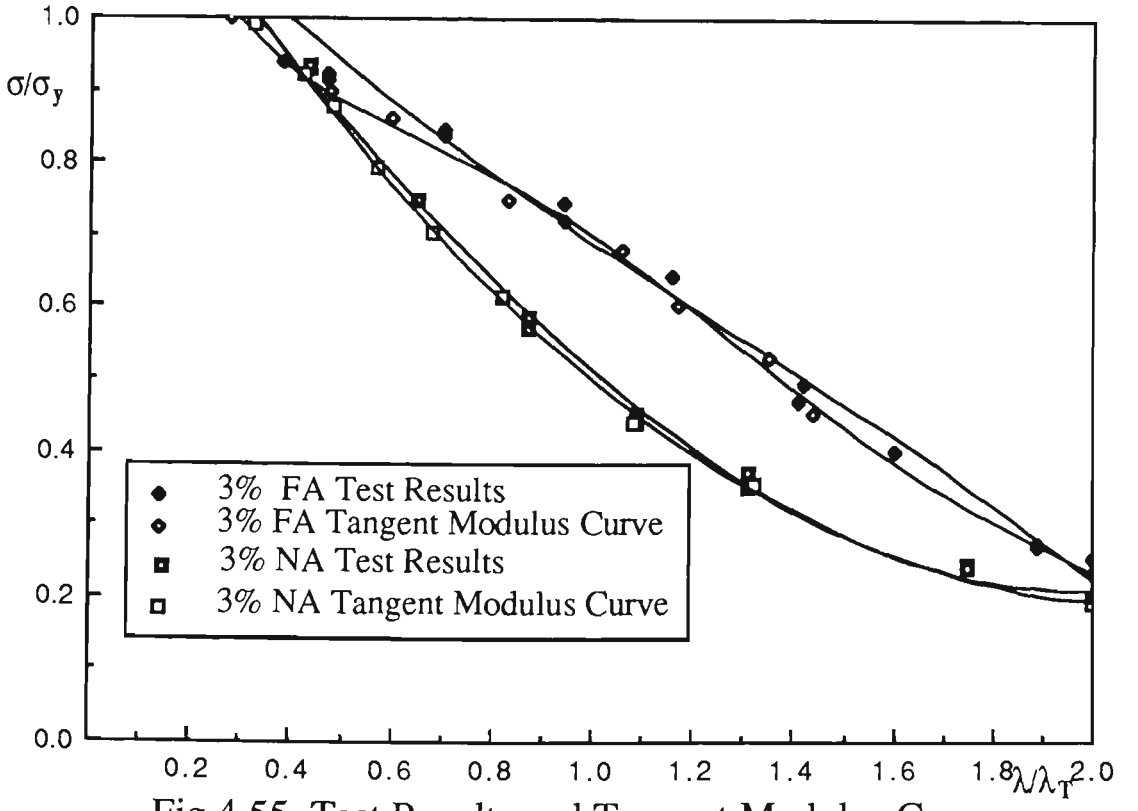

Fig.4.55 Test Results and Tangent Modulus Curves
- 3% prestrained

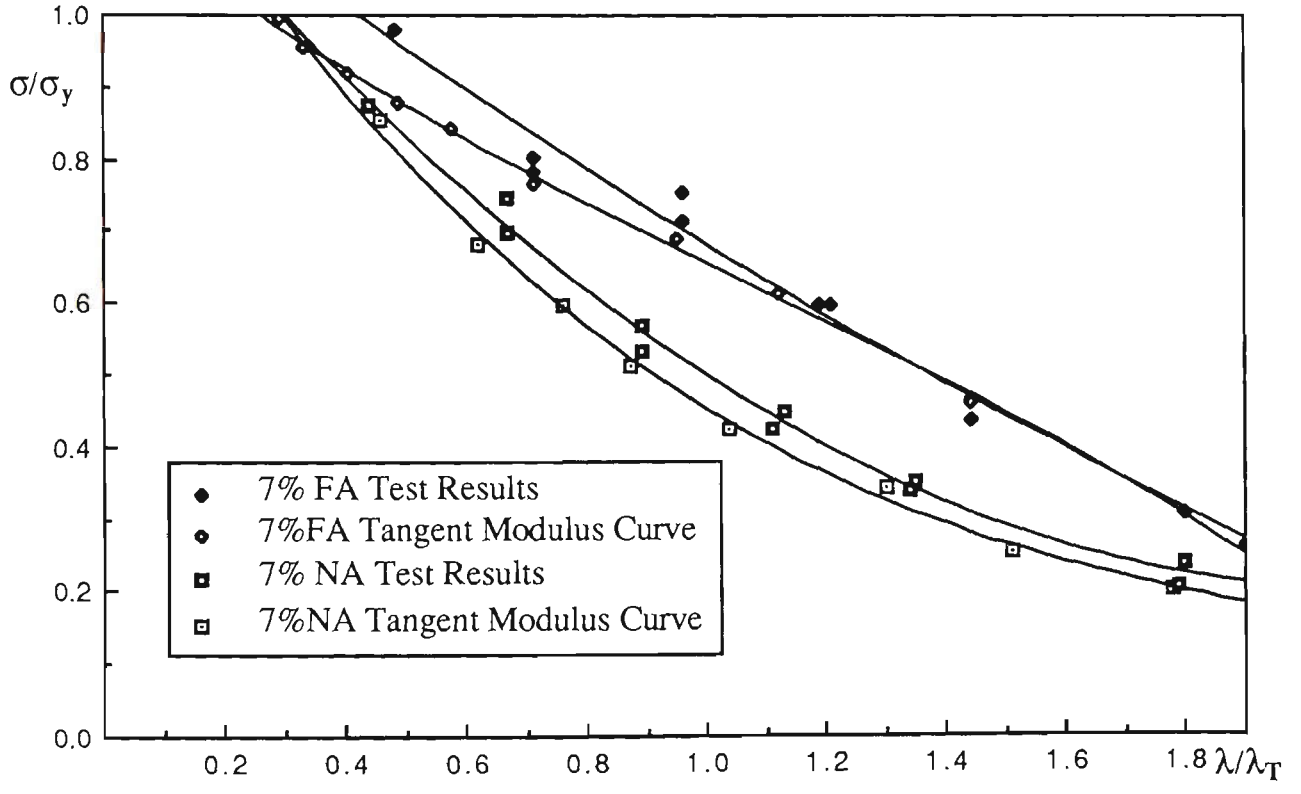

Fig.4.56 Test Results and Tangent Modulus Curves - 7% Prestrained

4.5.7 Comparison with Column Design Curves

4.5.7.1 European Column Curves

The European multiple column curves ECCS 'a', ECCS 'b' and ECCS 'c' (Dwight, 1975) shown in Fig.4.57. are based on an extensive program of theoretical and experimental studies. The maximum strength analytical model used for three curves assumes an initial sinusoidal out-of-straightness with a maximum value of L/1000 at mid span, together with material imperfections and residual stresses (Key and Hancock, 1985). An assumed average residual stress distribution was used as an input for the analytical model in the ECCS procedure. The ECCS description requires that all welded sections should be designed using a fictitious reduced yield stress approximately 6% below the parent material yield stress (Dwight, 1975). This provision affects stocky columns most.

Maximum loads for all the tested struts are compared with ECCS column design curves 'a', 'b' and 'c' in Fig.4.57. It is seen that all the column curves are conservative for as-received struts. The ECCS curve 'a' is the best fit to the maximum column strengths of struts that are prestrained in tension and fully-aged in the range of higher slenderness ($\lambda/\lambda_T \geq 0.94$) . The ECCS curve 'b' serves the best fit to the maximum column strengths of struts that are prestrained in tension and fully-aged in the range of lower slenderness ratios ($\lambda/\lambda_T < 0.94$). However, for struts that are prestrained in tension and unaged, even the bottom curve ECCS curve 'c' overestimates the ultimate strength in the generally commercially viable range of column slenderness.

4.5.7.2 SSRC Column Curves

The SSRC multiple column curves (in Fig.4.58) are described by a set of equations that have been empirically fitted to provide an approximate arithmetic mean to groups of column curves determined from precise analytical predictions of column strength . The SSRC maximum strength analytical model was based on statistical analyses of curve groupings with respect to fabrication and slope difference using measured residual stresses for each group of columns (Johnston, 1976). An initial out-of-straightness of L/1000 was assumed.

The experimental strut maximum strengths are given in Fig.4.58 and are compared with SSRC curves 1, 2 and 3. As ECCS curve 'b' and SSRC curve 2 match closely (Rotter, 1982), all the comments regarding ECCS curve 'b' compared with the test results in the previous section are applicable to SSRC curve 2 here. From Fig.4.58, it is seen that the experimental maximum strengths of the as-received struts all lie above SSRC curve 1, of struts that are prestrained in tension and fully-aged lie midway between curves 1 and 2. The SSRC curve 3 produces the best fit to the maximum strengths of struts that are prestrained in tension and unaged in the range of higher slenderness ($\lambda/\lambda_T \geq 0.64$).

4.5.7.3 Existing and Proposed Australian Column Curves

The current rule for the strength of axially loaded columns in the Australian Steel Structures Code AS1250-1981 is based on the work of Godfrey(1962). This work assumed that it is possible to define a single column strength curve which would be satisfactory for all sections(Rotter, 1982).

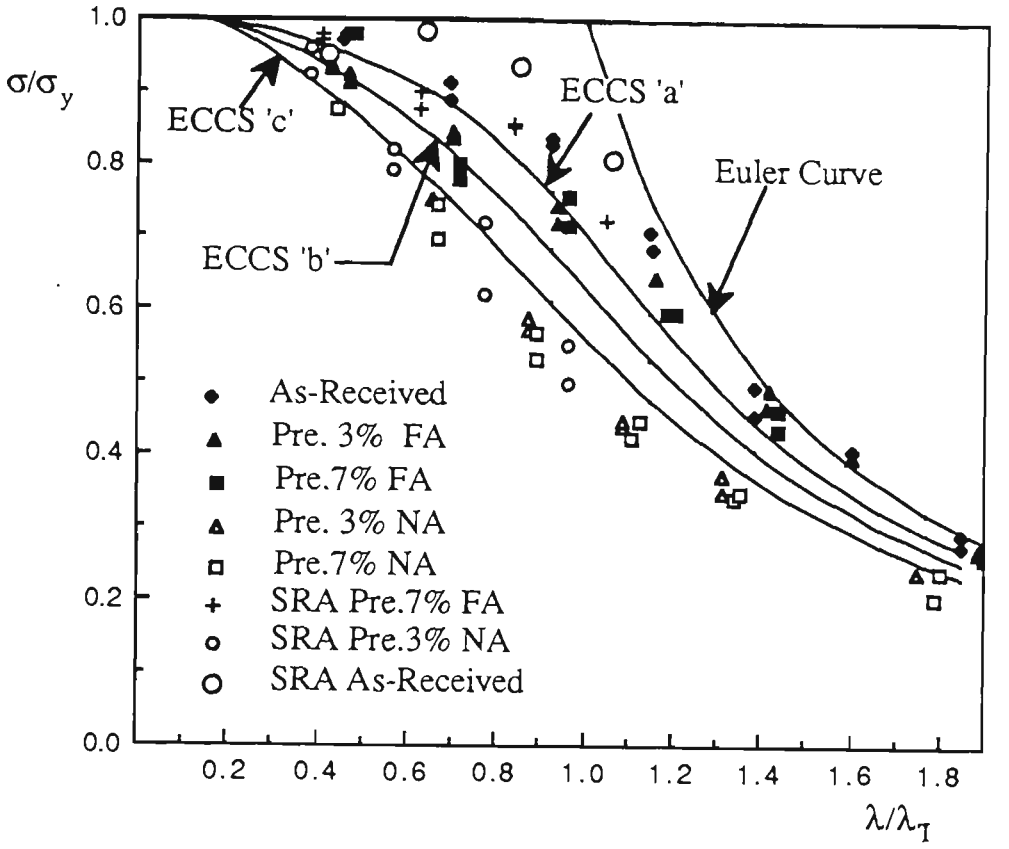

Fig.4.57 Comparison of ECCS Column Curves with Test Results

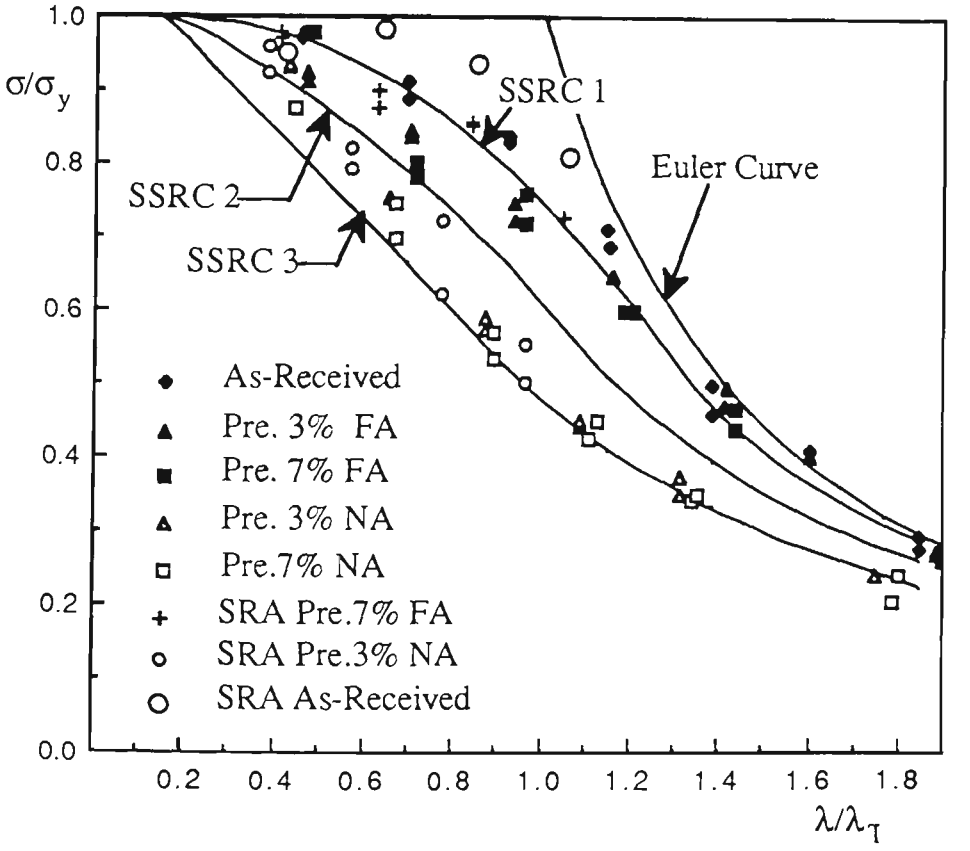

Fig.4.58 Comparison of SSRC Column Curves with Test Results

Fig.4.59 presents the existing AS1250-1981 column curve, together with the maximum strengths of the tested struts. The test results of the as-received struts lie above the AS1250 column curve, struts that were prestrained in tension and fully-aged lie close to the AS1250 column curve, and struts that were prestrained in tension and unaged lie below the AS1250 column curve. It is shown that the AS1250 column curve is conservative for as-received struts and safe for struts that were prestrained in tension and fully-aged in most of the cases, however, it is unsafe for struts that were prestrained in tension and unaged.

As indicated by Rotter(1982), if only one curve is used to represent columns of all classes, then it is difficult to decide where this curve should lie relative to the existing AS1250 description. Some heavy rolled I-sections and welded I-sections with slenderness ratios in the practical range have strengths up to 30% below the value predicted by the existing AS1250 code, giving a safety factor as low as 1.17 if designed according to AS1250.

Improved accuracy in the prediction of structural steel column strength by using multiple column curves (such as SSRC and ECCS column curves) can lead to greater design economy and greater uniformity for dependable safety margins.

Unfortunately, the form in which these multiple column curves are presented to designers in both Europe and the USA has made them relatively difficult to use. The ECCS curves were originally not defined by an equation at all, necessitating separate strength tables for each curve. The SSRC curves are defined by a series of polynomial curves each fitted over a range of slenderness values. The algebraic description needed in the SSRC curves has made them relatively awkward to use.

By examining the principal advantage and disadvantage of the use of a multiple column strength representation (ECCS and SSRC curves) with particular reference to Australian conditions, Rotter(1982) presented a simple method by deriving modifying factors which allowed a single central column curve to be used to represent any number of multiple column curves.

The formulation suggested by Rotter(1982) will be discussed and the design curves will be compared with the experimental results.

The central column curve is defined by :

$$\frac{P}{P_y}=\left[\left(\frac{\lambda^2+1+\eta}{2\lambda^2}\right)^2-\frac{1}{\lambda^2}\right]^{\frac{1}{2}} \qquad (4.5)$$

with an imperfection parameter, η, given by

$$\eta = 0.293(\lambda-0.15) \geq 0 \qquad (4.6)$$

and

$$\lambda=\frac{1}{90}\left[\frac{L}{r}\sqrt{\frac{\sigma_y}{250}}\right]_{mod} \qquad (4.7)$$

The modified slenderness to be used in the selection of other column curves is given by

$$\lambda=\frac{1}{90}[\frac{L}{r}\sqrt{\frac{\sigma_y}{250}}+c.a\,] \qquad (4.8)$$

where c is a constant determining the shift from the central curve (c=0) and a is the modify function.

The modifying function is given by

$$a=\frac{2100[\frac{L}{r}\sqrt{\frac{\sigma_y}{250}}-13.5]}{[\frac{L}{r}\sqrt{\frac{\sigma_y}{250}}\,]^2-15.3\frac{L}{r}\sqrt{\frac{\sigma_y}{250}}+2050}\geq 0 \qquad (4.9)$$

and the constant c has the value -1.0 corresponding to approximately SSRC curve 1, and has the value +1 corresponding approximately to SSRC curve 3.

The strut test results are plotted in Fig.4.60. and compared with the column curves of Rotter for values of c of -1.0, 0.0 and +1.0. The curve recommended by Key and Hancock, of adopting a mean curve between curve 1 and 2, using a value of c of -0.5 in Rotter's column curve formula (1982) is also plotted in Fig.4.60. For comparison purposes, the column curve of Rotter for a value of c of +0.5 is included in Fig.4.60 as well.

It can be seen that the maximum strengths of as-received struts all lie above the curve with c=-1.0 . Similar to ECCS curve 'a', the curve with c=-0.5 produces the best fit to the maximum column strength of struts that are prestrained in tension and fully-aged in the range of higher slenderness ($\lambda/\lambda_T\geq$ 0.94). Like SSRC curve 3, the curve with c=+1.0 provides the best fit to the maximum

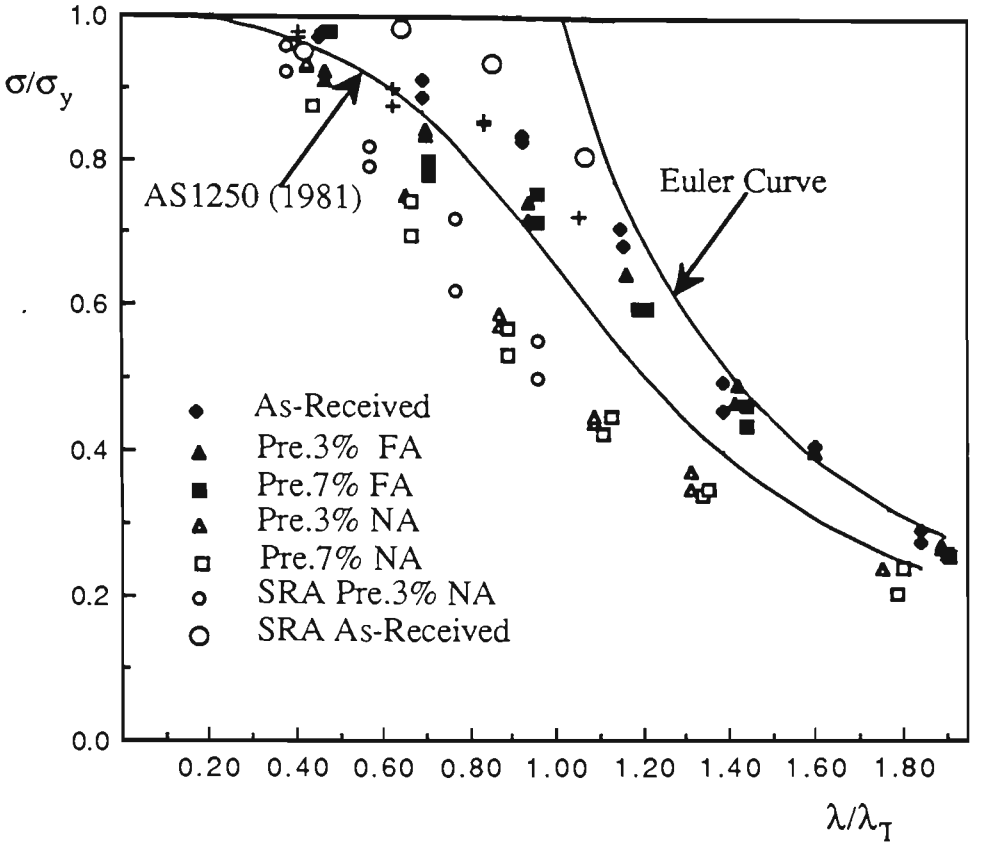

Fig.4.59 Comparison of AS1250(1981) Column Curves with Test Results

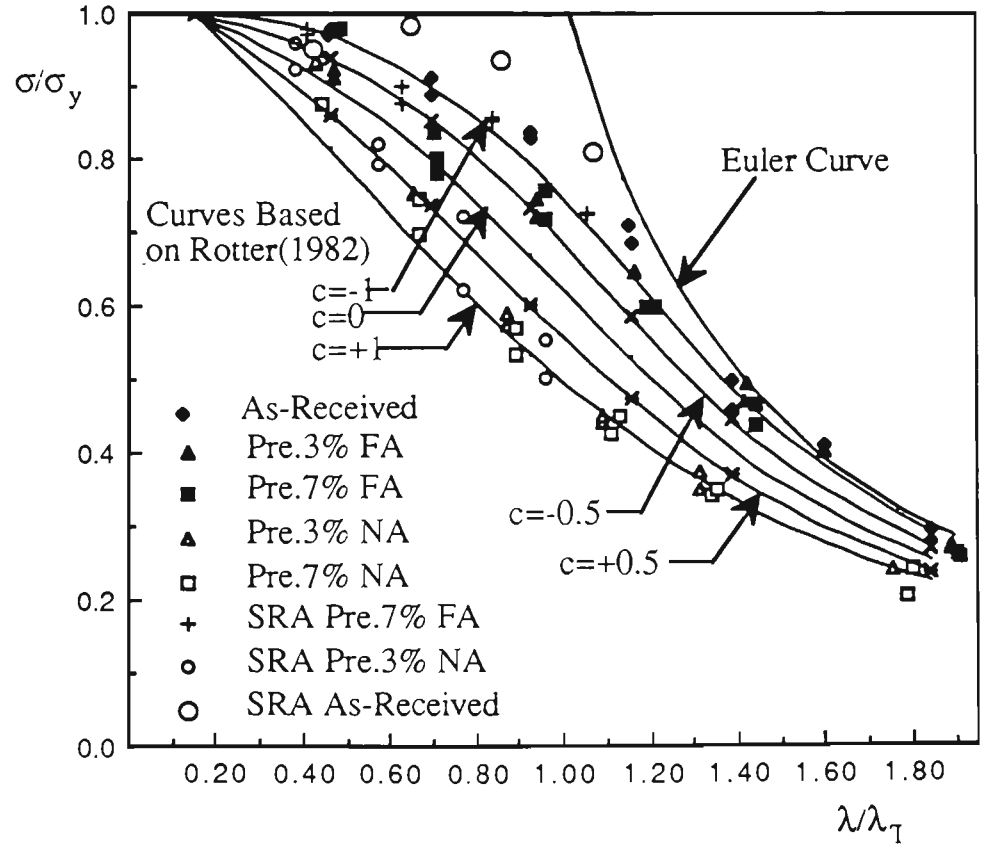

Fig.4.60 Comparison of Column Curves Based on Rotter(1982) with Test Results

strengths of struts that are prestrained in tension and unaged in the range of higher slenderness ($\lambda/\lambda_T \geq 0.64$). The curve with c=+0.5 is the best fit to struts that are prestrained in tension and unaged in the range of lower slenderness ($\lambda/\lambda_T < 0.64$).

4.6 SUMMARY

The primary objective of the experiment work was to report tests on tubular mild steel struts with variable influences of strain hardening , strain aging and the Bauschinger effect. The work follows the earlier investigations of tubular strut behaviour, that were confined to prestrains not more than 7% and differentiates between unaged and fully-aged material. The influence of strain aging is clearly seen. The work furnishes a benchmark for the theoretical model developed in Chapter 3, and therefore enables consideration to be given to the various material factors which influence the behaviour of steel (in ways which are individually well known), and to determine their influence on strut load capacity. The three material effects are active here. Strain aging interacts with strain hardening (beneficial) and the Bauschinger effect (deleterious). The combined influences of the factors exercise a significant effect on strut load capacity in additional to initial imperfections and residual stresses. The Bauschinger effect plays a dominant role in the test results referred herein, with load capacity reductions of up to 38% . Strain aging is seen to be more significant than strain hardening for the rimming steel used in enhancing the capacity of the prestrained struts.

The comparison of the present experimental results and the current column design curves shows that the simplified approximation to the SSRC column curves proposed by Rotter(1982), using the derived modifying factors to obtain

any number of intermediate curves from the central reference curve (corresponds approximately to SSRC curve 2), provides a flexible and easy to apply alternative to the existing column curve formulations.

CHAPTER FIVE

STATISTICAL ANALYSES OF EXPERIMENTAL RESULTS OF MATERIAL EFFECTS ON STEEL TUBULAR STRUT LOAD CAPACITY

5.1 GENERAL

The test results of the 92 tubular steel pin-ended struts tested under different conditions have been studied by statistical analysis. The significant influence of material effects such as strain aging, strain hardening and the Bauschinger effect on strut load capacity is investigated by applying a two-way analysis of variance test. It is found that the three material effects mentioned exercise a significant influence on strut load capacity for both the rimming steel and the semi-killed steel used. The Bauschinger effect plays a dominant role in reducing strut load capacity, while both strain hardening and strain aging have a significant influence on increasing load capacity.

5.2 BASIC DESCRIPTION OF ANALYSIS OF VARIANCE

From the previous description (Chapter Four), it is seen that there are significant differences between the normalised critical stress versus normalised slenderness ratio curves (see Fig.4.38). Some differences are large; some are small. However , it is necessary to be able to judge how large is "large" or how small is "small". This judgment is made by applying two-way analysis of variance tests. The analysis of variance procedure attempts to analyze the variation of a response and to assign portions of this variation to each of a set of

independent variables. It partitions the total sum of squares of deviations of the response measurements about their mean into portions associated with each independent variable and the experimental error. The former may be compared with the sum of squares for error, using mean squares and the F test, to see whether the mean squares for the independent variables are unusually large and thereby indicative of an effect on the response. The detailed description of the method may be found in standard texts (see for example, Freund 1962 and Mendenhall and Scheaffer 1973). A normal distribution of results is assumed in each case. While more refined statistical analysis techniques may be developed for this investigation, such techniques do not appear to be readily available at present.

To study whether there is any influence of steel types on strut load capacity, the test results conducted by Morgan and Schmidt (1985) are also included in the analysis.

The 92 tubular steel pin-ended struts have been tested in following categories:

(i) 12 HFW (Hot fusion welding, semi-killed steel) tube tests (Morgan and Schmidt, 1985) .

(ii) 20 ERW (Electric resistance welding, rimming steel) tube tests (Morgan and Schmidt, 1985).

(iii) 64 ERW (rimming steel) tube tests (this thesis).

Different conditions of material state to be tested by the analysis of variance procedure are listed as follows:

(1) 3% prestrained in tension and fully-aged and 7% prestrained in tension and fully-aged for ERW tubes (this thesis); test the difference between the different prestrains for fully-aged tubes.

(2) 3% prestrained in tension and unaged and 7% prestrained in tension and unaged for ERW tubes (this thesis); test the difference between different prestrains for unaged tubes.

(3) As-received ERW tubes (this thesis) and as-received tubes (Morgan and Schmidt, 1985); test the difference between the different yield stresses for the same steel.

(4) 7% prestrained in tension and fully-aged and 7% prestrained in tension and unaged for ERW tubes (this thesis); test the influence of strain aging.

(5) 3% prestrained in tension and fully-aged and 3% prestrained in tension and unaged for ERW tubes (this thesis); test the influence of strain aging.

(6) As-received and 3% prestrained in tension and fully-aged ERW tubes (Morgan and Schmidt, 1985); test the difference between as-received tubes and the tubes that were prestrained in tension and fully-aged for ERW tubes.

(7) As-received and 8% prestrain in tension and fully-aged HFW tubes (Morgan and Schmidt, 1985); test the difference between as-received tubes and the tubes that were prestrained in tension and fully-aged for HFW tubes.

(8) As-received and 3% prestrained in tension and fully-aged ERW tubes (this thesis); test the difference between as-received tubes and the tubes that were prestrained to 3% in tension and fully-aged for ERW tubes.

(9) As-received and 7% prestrained in tension and fully-aged ERW tubes (this thesis); test the difference between the as-received tubes and the tubes that were prestrained to 7% and fully-aged for ERW tubes.

(10) As-received and 3% prestrained in tension and unaged ERW tubes (this thesis); test the difference between the as-received tubes and the tubes that were prestrained to 3% in tension and unaged for ERW tubes.

(11) As-received and 7% prestrained in tension and unaged ERW tubes (this thesis); test the difference between the as-received tubes and the tubes that were prestrained to 7% in tension and unaged for ERW tubes.

(12) As-received HFW tubes and as-received ERW tubes (Morgan and Schmidt, 1985); test the difference between the different steels for as-received tubes.

In the problem considered here it is desired to investigate two effects on normalised load capacity : (1) different slenderness ratios, and (2), different conditions of material state. Referring to the slenderness ratios as Ai for i=1,2...k , and to the different conditions as Bj for j=1,2...n, suppose that x_{ij} is

the normalised ultimate load obtained with the ith slenderness ratio and jth condition. A possible model for this kind of problem is to look upon the x_{ij} as the values assumed by independent random variables having normal distributions with means μ_{ij} and common variance σ_2 , where ,

$$\mu_{ij} = \mu + \alpha_i + \beta_j + e_{ij} \qquad (5.1)$$

and

$$\sum_{i=1}^{k} \alpha_i = 0 \qquad \sum_{j=1}^{n} \beta_j = 0 \qquad (5.2)$$

in which μ is referred to as a grand mean, α_i and β_j , as the effects of the two variables , and the e_{ij} are values of independent random variables having normal distributions with zero means and common variance.

The null hypotheses to be tested are, (1), that the α_i are all equal to 0, and (2), that the β_j are all equal to 0; the corresponding alternative hypotheses are that the respective parameters are not all equal to 0 . The tests of these hypotheses are based on the following analysis of the total variability of the data, decomposing it into terms attributed to differences among the A's, differences among the B's, and chance (experimental error) :

$$\sum_{i=1}^{k}\sum_{j=1}^{n}(x_{ij} - \bar{x})^2 = n\sum_{i=1}^{k}(\bar{x}_{i.} - \bar{x})^2 + k\sum_{j=1}^{n}(\bar{x}_{.j} - \bar{x})^2$$
$$+ \sum_{i=1}^{k}\sum_{j=1}^{n}(x_{ij} - \bar{x}_{i.} - \bar{x}_{.j} + \bar{x})^2 \qquad (5.3)$$

Here $\overline{x_{i.}} = \frac{1}{n}\sum_{j=1}^{n} x_{ij}$ and $\overline{x_{.j}} = \frac{1}{k}\sum_{i=1}^{k} x_{ij}$

where $\overline{x_{i.}}$ is the mean of the sample from the ith population, in other words, i is held to be constant while summing over the jth factors; $\overline{x_{.j}}$ is the mean of the sample from jth population, i.e., j is held to be constant while summing over the ith factors.

The test of the null hypothesis concerning the α_i can be based on the following statistic,

$$F_A = \frac{SSA/(k-1)}{SSE/(n-1)(k-1)} = \frac{(n-1)\,SSA}{SSE} \qquad (5.4)$$

which , under the null hypothesis that the α_i are all equal to 0, is a value assumed by a random variable having the F distribution with k-1 and (n-1)(k-1) degrees of freedom (Where SSE is an error sum of squares, and SSA is a between sample sum of squares). This hypothesis is rejected if $F_A > F\alpha(k-1,(n-1)(k-1))$. $F\alpha(k-1,(n-1)(k-1))$ is the critical F for α percent significance level , and (k-1) and (n-1)(k-1) degrees of freedom on the numerator and denominator.

Similarly, the test of the null hypothesis that the β_j are all equal to 0 can be based on the statistic,

$$F_B = \frac{SSB/(n-1)}{SSE/(n-1)(k-1)} = \frac{(k-1)\,SSB}{SSE} \qquad (5.5)$$

which, under the null hypothesis that the β_j are all equal to 0, is a value assumed by a random variable having the F distribution with n-1 and (n-1)(k-1) degrees of freedom (where SSB is a between sample sum of squares). This hypothesis is rejected if $F_B > F\alpha(n-1, (n-1)(k-1))$.

Table 5.1 shows an analysis of variance table.

Table 5.1 The Analysis of Variance Table

Source of variation	Degrees of freedom	Sum of squares	Mean square	F
Between A's	k-1	SSA	MSA=SSA/(k-1)	MSA/MSE
Between B's	n-1	SSB	MSB=SSB/(n-1)	MSB/MSE
Error	(n-1)(k-1)	SSE	MSE=SSE/(n-1)(k-1)	
Total	nk-1	SST		

MSA and MSB are mean squares of between-sample sum,
ME is mean square of error sum.

5.3 APPLICATION OF ANALYSIS OF VARIANCE TO TEST RESULTS

As six slenderness ratios were used in the tests, therefore, let k equal to 6 to test the effect of slenderness ratios and n equal to 2 comparing two conditions each time to test the effect of strain aging, the amount of prestrain, strength of material, and so on in turn.

Table 5.2 summarises the observed values F_A and F_B. Also given is the critical $F_{0.05}$ for the 5 percent significance level, and the 5 and 5 degrees of freedom on the numerator and denominator, respectively (which is equal to 5.05 for all cases , from Table VIa in Freund 1962), together with $F_{0.05}$ for the 1 and 5 degrees of freedom on the numerator and denominator, respectively (which is equal to 6.61 for all cases, from Table VIa in Freund 1962).

Table 5.2 Observed and Critical Values of F

Case No.	Two Comparative Targets	F_A	$F_{A0.05}$	F_B	$F_{B0.05}$
1	3%, FA(ERW, 1987) & 7%, FA(ERW,1987)	152	5.05	0.02	6.61
2	3%, NA(ERW,1987) & 7%, NA(ERW,1987)	635	5.05	2.95	6.61
3	AR (ERW, 1987) & AR (ERW, 1984)	279	5.05	2.94	6.61
4	7%, FA (ERW, 1987) & 7%, NA(ERW,1987)	77	5.05	37.2	6.61
5	3%, FA(ERW, 1987) & 3%, NA(ERW, 1987)	31	5.05	14	6.61
6	AR(ERW,1984) & 3%, FA(ERW, 1984)	15	5.05	0.29	6.61
7	AR(HFW, 1983) & 8%, FA(HFW, 1983)	19	5.05	14	6.61
8	AR(ERW, 1987) & 3%, FA(ERW,1987)	126	5.05	4.24	6.61
9	AR(ERW, 1987) & 7%, FA(ERW, 1987)	93	5.05	3	6.61
10	AR(ERW, 1987) & 3%, NA(ERW, 1987)	28	5.05	18.3	6.61
11	AR(ERW, 1987) & 7%, NA(ERW, 1987)	31	5.05	25	6.61
12	AR(HFW, 1983) & AR (ERW, 1984)	53	5.05	3.4	6.61

5.4 DISCUSSION OF STATISTICAL TEST RESULTS

5.4.1 Influence of Slenderness Ratios

From Table 5.2 , it is seen that the F_A for all the different conditions are greater than $F_{A0.05}(5,5)$. Therefore the null hypothesis is rejected and it is concluded that there is a significant difference between the normalised load capacities of the struts at different slenderness ratios.

5.4.2 Influence of Strain Hardening, Strain Aging and the Bauschinger Effect

F_B for case 1 (3%+FA(ERW,1987) and 7% + F_A (ERW,1987)) and case 2 (3%+NA(ERW,1987) and 7% +NA (ERW,1987)) is less than $F_{B0.05}(1,5)$. Therefore the null hypothesis is accepted and it is concluded that there is no significant difference between the 3% tensile prestrained fully-aged struts and the 7% tensile prestrained fully-aged struts,and likewise for the 3% tensile prestrained unaged struts and 7% tensile prestrained unaged struts. In other words, there is no significant influence on strut load capacity between 3% and 7% prestrain .

In general , the influence of strain hardening on the load capacities of ERW struts is not as significant as strain aging, due to the low strain hardening capacity of the ERW tube, which had a strain hardening ratio,SHR, of 1.15 (SHR = ratio of the as-received ultimate stress to the as-received yield stress). From Fig.1, it seems that there is a higher normalised strut strength for the HFW tube than for the ERW tube in the as-received condition . Even though the SHR of the HFW tube (1.64) is significantly different from that for the ERW

tube(1.15), there is apparently no significant difference in normalised strut load capacity, as determined by the statistical test (case 12).

F_B for case 4 (7% + FA (ERW,1987) and 7% + NA (ERW,1987)), case 5 (3% + FA (ERW,1987) and 3% + NA (ERW,1987)), case 10 (AR(ERW,1987) and 3%+NA(ERW,1987)) and case 11 (AR(ERW,1987) and 7%+NA(ERW,1987)) is greater than $F_{B0.05}(1,5)$. Therefore the null hypothesis is rejected and it is concluded that the influence of strain aging on strut load capacity is significant at the 5 percent significance level .

The influence of strain aging on load capacity is evident. This influence depends largely on steel type; fully killed steels offering virtually no aging, rimming steels displaying significant strain aging, and semi-killed steels offering some intermediate degree of strain aging strength enhancement. The HFW tube material was semi-killed while the ERW tube was a rimming steel. The results presented in Figs.5.1 and 5.3 reflect this difference. The significant influence of strain aging is highlighted by comparison of Figs.5.3 and 5.4. Compared with the unaged condition, the load capacity increase with the fully-aged condition is up to 32% for ERW tubes.

5.4.3 Influence of Steel Type

F_B for case 12 (AR(HFW,1983) and AR(ERW,1984)) is less than $F_{B0.05}(1,5)$. Therefore the null hypothesis is accepted and it is concluded that the different steel as used herein has no significant influence on normalised strut load capacity.

F_B for case 3 (AR(ERW,1987) and AR(ERW,1984)) is less than $F_{B0.05}(1,5)$. Therefore the null hypothesis is accepted and it is concluded that the different yield stresses for as-received material have no significant influence on normalised strut load capacity .

F_B for case 6 (AR(ERW ,1984) and 3% + FA (ERW ,1984)), case 8 (AR(ERW,1987) and 3% + FA (ERW,1987)), case 9 (AR(ERW,1987) and 7% + FA (ERW,1987)) is less than $F_{B0.05}(1,19)$. Therefore the null hypothesis is accepted and it is concluded that the difference between as-received struts and prestrained fully-aged struts for ERW tubes is not significant.

F_B for case 7 (AR(HFW,1983) and 8% +FA (HFW,1983)) is greater than $F_{B0.05}(1,5)$. Therefore the null hypothesis is rejected and it is concluded that there is significant difference between as received struts and struts prestrained in tension for HFW tubes even when fully-aged .

5.5 SUMMARY

The results of the statistical analyses, which are summarised in Table 5.2, and which were discussed above, enable the following observations to be made on the regression results expressed in the Figs.5.1 to 5.5. The results of the statistical analyses give added strength to the observations made earlier (Morgan and Schmidt 1984;Morgan and Schmidt 1986; Morgan and Schmidt 1985; Schmidt and Morgan 1984; Schmidt and Morgan 1986; Schmidt et al.1989).

As shown in Figs.5.2, 5.3 and 5.4, except for ERW tube (1984) at slenderness ratios less than 60, all the struts prestrained in tension had lower

load capacities than the corresponding as-received struts due to the Bauschinger effect on load reversal.

All the struts prestrained in tension and fully aged (presented in Fig.5.5) followed the same general trend in behaviour. However, if compared with the as-received struts, the ERW tube differences were much less than those for the HFW tube, which is clearly seen in Fig.5.4. For the prestrained and fully-aged tubes the effect of steel type appeared to be significant , the test results in Fig.5.2 showing that the stress ratio (σ / σ_y) at collapse of the HFW tube (semi-killed steel) fell well below that of the ERW tube (rimmed steel).

Although it is difficult to separate the three material effects interacting with each other, the general trend of the influence, supported by the analysis of variance tests herein, can be summarised as follows, in the structurally more significant range of slenderness ratios (50-110) :

• The Bauschinger effect plays a dominant role on strut load capacity referred to the steel used herein. The Bauschinger loss on load reversal is greater than the strength gains due to the combined effects of strain aging and strain hardening.

• Strain aging has a significant influence on load capacity, and varies with different steel types. For a rimming steel, strain aging is more significant than strain hardening in enhancing the capacity of prestrained struts. For a fully killed steel, no strain aging occurs, therefore no gain in strength can follow.

• The combined effects of strain hardening, strain aging and the Bauschinger effect exercise a significant influence on strut load capacity for both rimming steel and semi-killed steels .

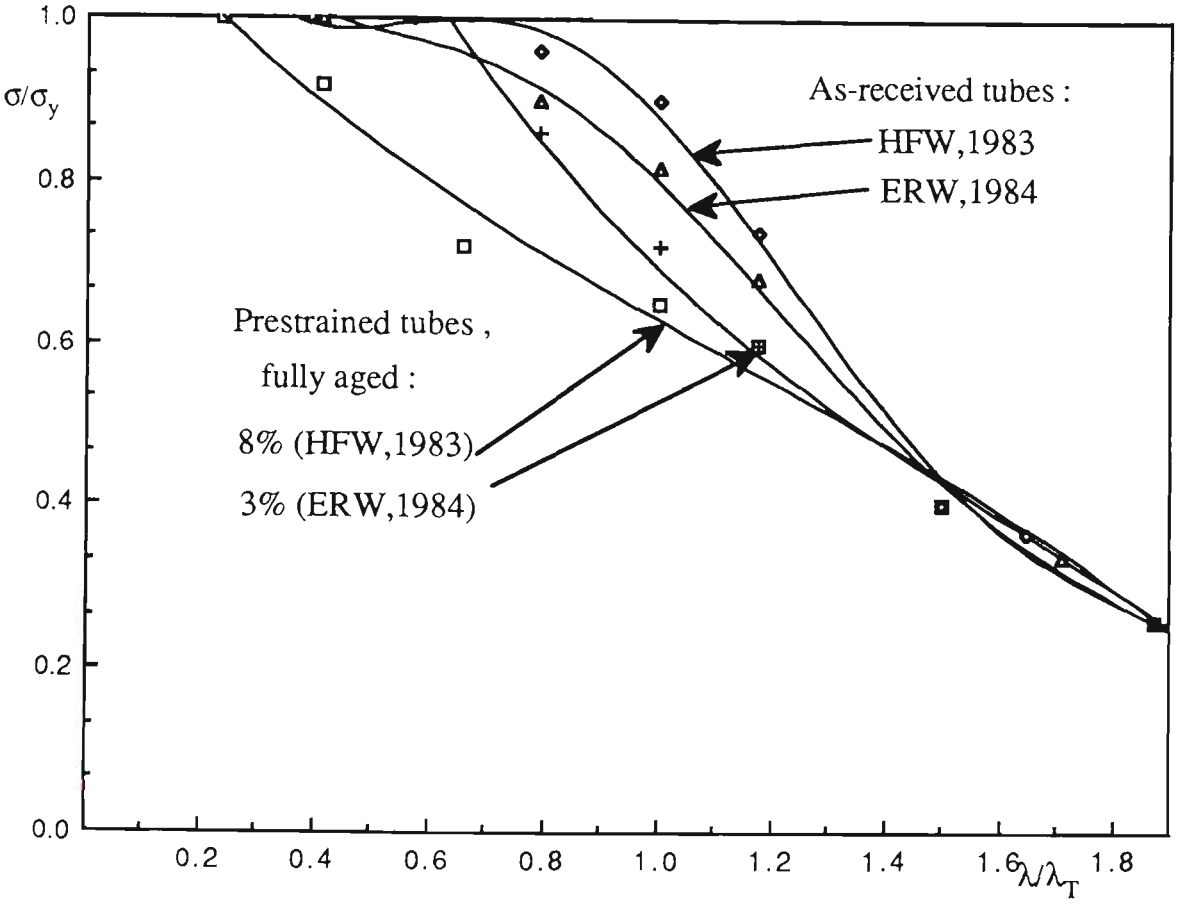

Fig.5.1 Normalised Test Results of 1983 and 1984 (ERW and HFW)

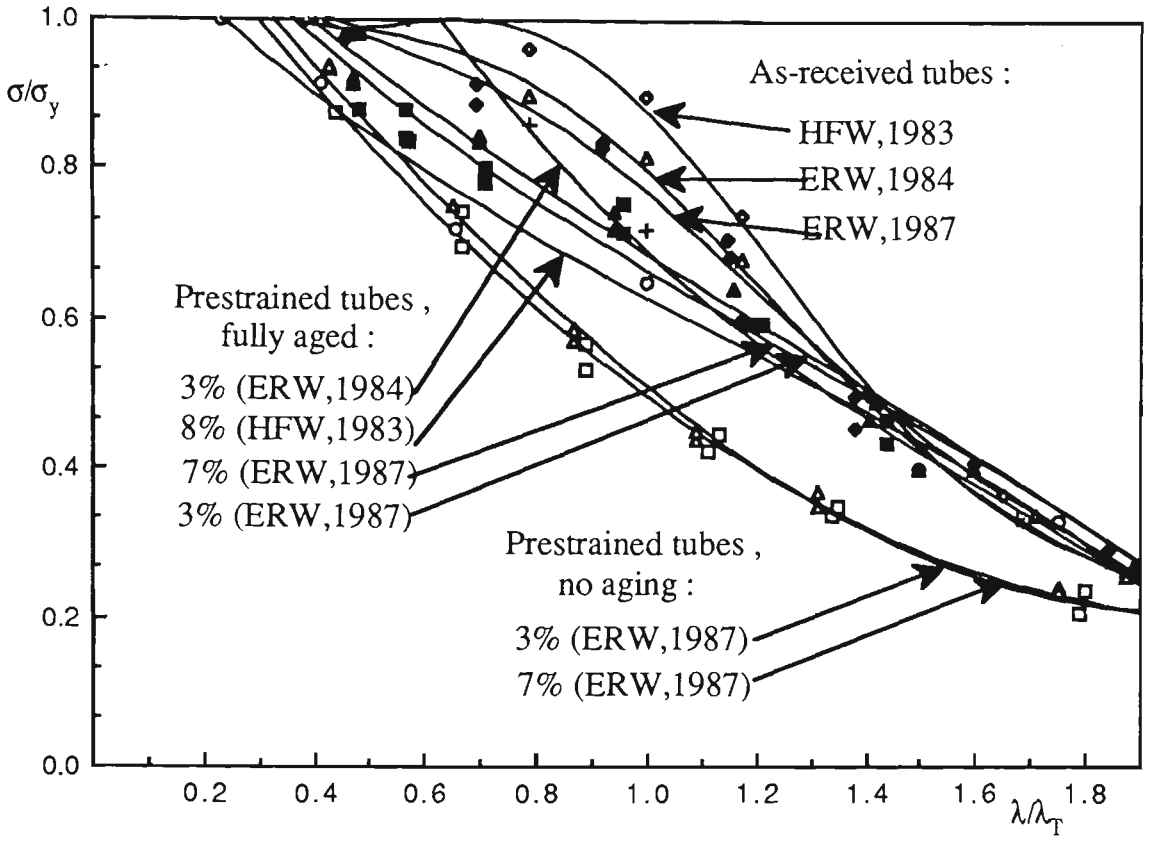

Fig.5.2 Combined Test Results 1983,1984 and 1987 (ERW and HFW)

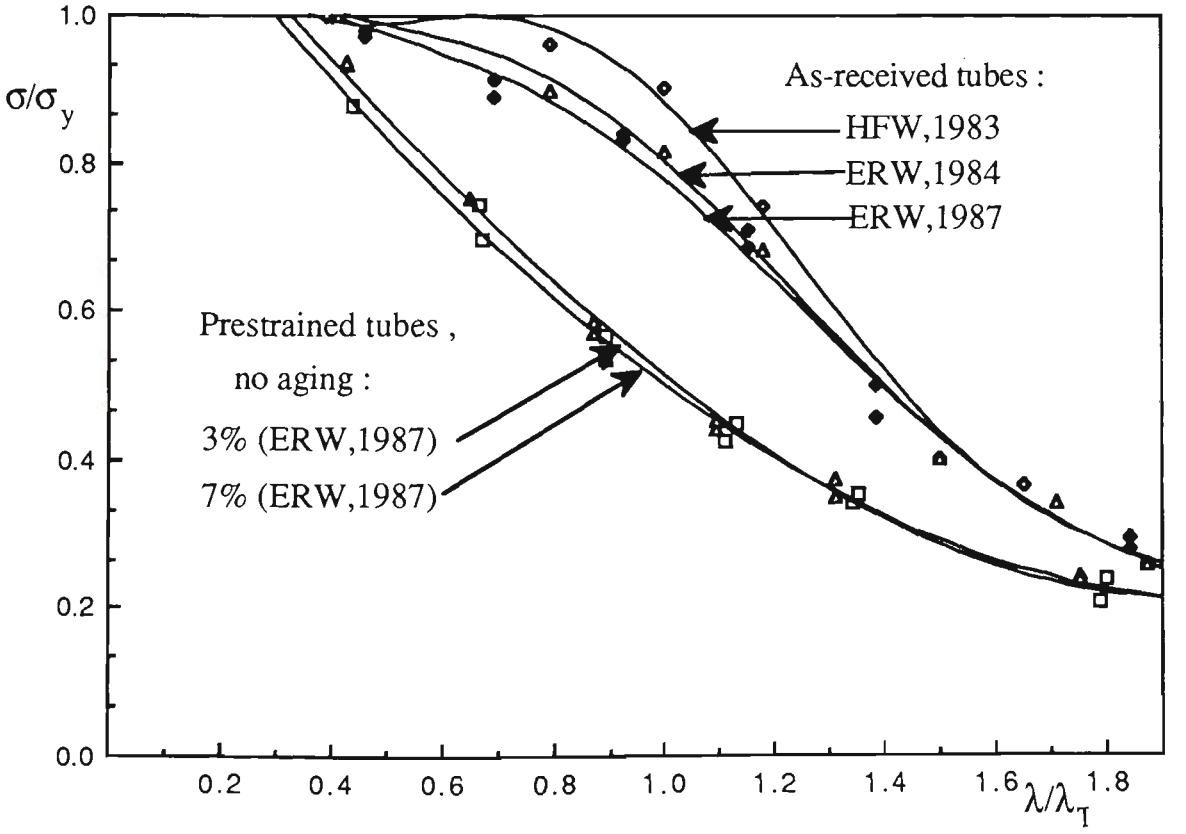

Fig.5.3 Test Results of As-Received and Prestrained Unaged Struts

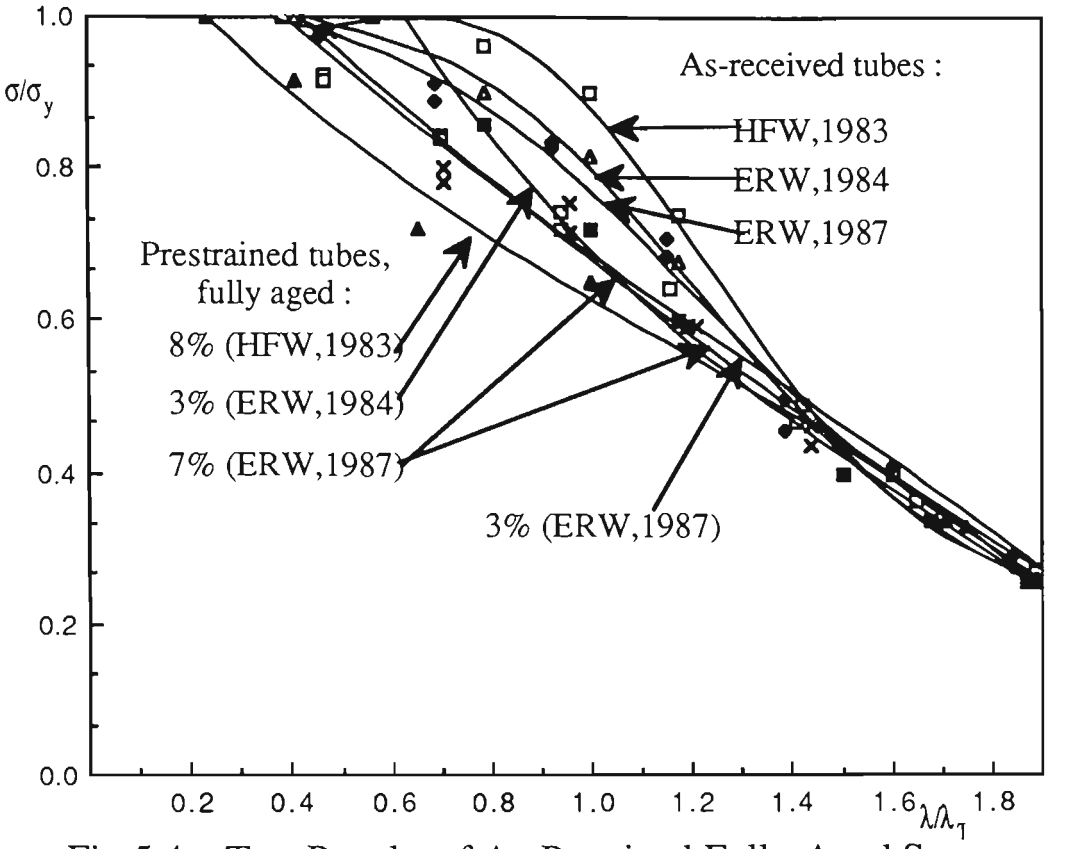

Fig.5.4 Test Results of As-Received Fully-Aged Struts

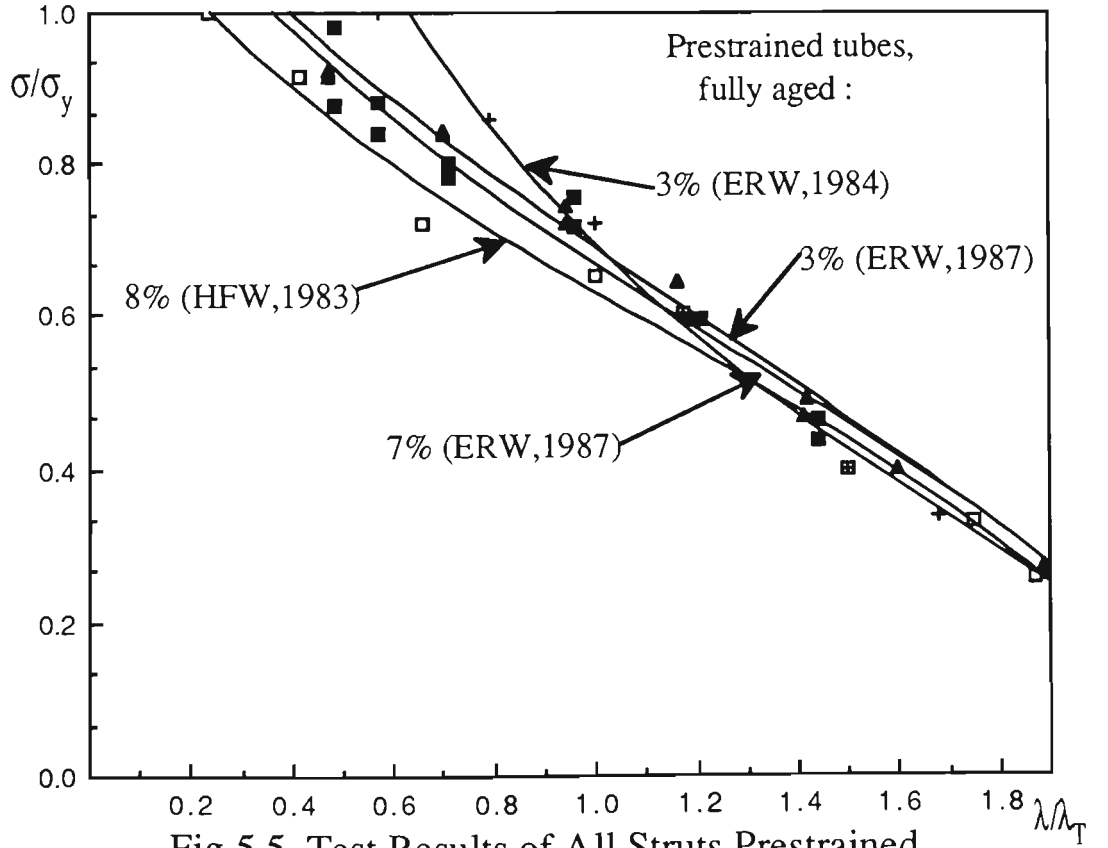

Fig.5.5 Test Results of All Struts Prestrained in Tension and Fully-Aged

CHAPTER SIX

COMPARISON AND DISCUSSION OF THEORETICAL AND EXPERIMENTAL RESULTS

6.1 GENERAL

The details of the theoretical development and the experimental program have been described in Chapters Three and Four, respectively. The following sections of this Chapter compare the theoretical and experimental results and give relevant discussion.

6.2 COMPARISON OF THEORETICAL AND EXPERIMENTAL LOAD-DEFORMATION CURVES

Using the computer program developed herein, the pre-buckling and post-buckling load-deflection paths of both as-received and prestrained tubular struts of different slenderness ratios have been obtained. As the test results of two sets of struts were reasonably close to each other, the specific dimensions of only one set of specimens for strut testing, which were listed in Table 4.3, were used to compute the theoretical curves.

As mentioned in Chapter Four, with the limitation of the facilities used, the initial geometrical imperfections of the test specimens were not known with great detail. The measurements of the out-of-straightness were used only as a reference. The initial imperfections adopted in the theoretical analysis were assumed as follows : $\delta_0/L=0.0015$ for slenderness ratios, λ = 36 and 55; 0.001

for λ = 73; 0.0005 for λ = 91, 110 and 150. These values are comparable to those observed in the as-received test specimens.

Figs. 6.1 to 6.6 compare theoretical and experimental average stress versus average strain curves, normalised with the yield stress/strain of the as-received struts with slenderness ratios L/r of 36, 55, 73, 91, 110 and 146 respectively. Figs.6.7 to 6.18 show results of the struts that were prestrained in tension and fully-aged; Figs.6.19 to 6.30 show results of the struts that were prestrained in tension and unaged. Fig.6.31 shows the comparison of theoretical and experimental curves for specimen No.18 that was prestrained in tension and fully-aged, with a large initial out-of-straightness (0.003L) because of an accidental machine reversal after prestraining cycle. For comparison purposes, the theoretical curves calculated for the various combinations of initial out-of-straightness, both above and below the measured value (0.003L), are also included in Fig.6.31.

It can be seen that the theoretical curves closely follow the experimental results, particularly for the as-received struts and the struts that are prestrained in tension and fully-aged. However, there is a relative large difference between theoretical and experimental curves for the struts with a slenderness ratio L/r of 36(37). As mentioned in Chapter Three, at this slenderness ratio, the strut strengths and the post-buckling behaviour are very sensitive to the value of Es (strain hardening modulus). The normalised curves pictured in Figs.6.1, 6.7, 6.13, 6.19 and 6.25 reflect this sensitivity. Dwight (1975) also mentioned that the stocky columns could exceed yield due to the effect of strain hardening.

It should be noted that the struts that are prestrained in tension and unaged should be tested in compression shortly after the prestraining to exclude strain

aging. However, the longest struts that were prestrained to 3% in tension (L/r=147) were tested in compression one day later (at an ambient temperature 23^0c) after the prestraining. It was believed that some strain aging occurred in this time and therefore the compressive strengths and the post-buckling capacities were higher than those computed from the theoretical model, as shown in Fig.6.24.

6.3 COMPARISON OF THEORETICAL AND EXPERIMENTAL MAXIMUM COLUMN LOADS

Theoretical maximum loads for one set of test struts described in Chapter Four have been obtained by using the theoretical model developed in Chapter Three to trace out the strut load-deflection curves. Theoretical and experimental maximum loads are compared in Tables 6.1 to 6.3 for the as-received struts, the struts that are prestrained in tension and fully-aged and the struts that are prestrained in tension and unaged, respectively. It can be seen that agreement between the present theoretical model and experiments for most cases is very good, and only in cases when the struts that were prestrained to 3% in tension and unaged with slenderness ratio (L/r=147) were the differences between theory and experiment relatively large, possibly for the reason mentioned previously.

The experimental maximum loads and the theoretical maximum loads calculated for all the as-received struts and the struts that are 7% prestrained in tension with the corresponding initial out-of-straightness are summarized in Fig.6.32. Fig.6.33 shows the corresponding results for 3% prestrained struts. Note that the tolerance for maximum initial out-of-straightness in the strut tests performed was 0.0015L. In fact, the maximum initial out-of-straightness for

most of struts were less than this. Figs.6.34 and 6.35 summarize the experimental maximum loads and the theoretical maximum loads computed for the various combinations of initial out-of-straightnesses for the as-received struts and the struts that were 3% prestrained in tension and unaged. It can be seen that all the test results lie on or above the theoretical curves with the given tolerance for maximum out-of-straightness 0.0015L. Most of the test results lie in the band between the theoretical curves with an initial out-of-straightnesses $\delta_0/L=0.0002$ and 0.002. The exceptions to this case were the struts that were prestrained in tension and unaged, with slenderness ratios of $\lambda=110$ ($\lambda/\lambda_T=1.31$), which was slightly over the upper limit line ($\delta_0/L=0.0002$). At least the theory presented may be considered as furnishing the minimum load capacity. In a structure, any errors due to use of this theory will be on the safe side.

Table 6.1 Comparison of Theoretical and Experimental Maximum Loads for As-Received Struts

Slenderness Ratio, L/r	Maximum Load Ratio Pmax/Py		
	Tests	Theory	% Diff.
36	0.979	0.948*	-3.2
55	0.889	0.916*	+3.0
73	0.829	0.804#	-3.0
91	0.709	0.685+	-3.4
110	0.497	0.494+	-0.6
146	0.293	0.289+	-1.4

*: $\delta_o/L=0.0015$ #: $\delta_o/L=0.001$

+: $\delta_o/L=0.0005$ Diff.=Difference

Table 6.2 Comparison of Theoretical and Experimental Maximum Loads For Prestrained and Fully-Aged Struts

Slenderness Ratio, L/r	Maximum Load Ratio Pmax/Py					
	3%			7%		
	Tests	Theory	% Diff.	Tests	Theory	% Diff.
36	0.923	0.900*	-2.5			
37				0.897	0.873*	-2.7
55	0.838	0.819*	-2.3	0.799	0.789*	-1.3
73	0.743	0.735#	-1.1			
74				0.712	0.710#	-0.3
92	0.643	0.639+	-0.6	0.592	0.571+	-3.5
110	0.492	0.470+	-4.5			
111				0.466	0.455+	-2.4
146	0.271	0.275+	+1.5	0.259	0.271+	+4.6

*: $\delta_o/L=0.0015$ #: $\delta_o/L=0.001$ +: $\delta_o/L=0.0005$ Diff.=Difference

Table 6.3 Comparison of Theoretical and Experimental Maximum Loads for Prestrained and Unaged Struts

Slenderness Ratio, L/r	Maximum Load Ratio Pmax/Py					
	3%			7%		
	Tests	Theory	% Diff.	Tests	Theory	% Diff.
36	0.934	0.975	+4.4	0.911	0.966*	+6.0
55	0.750	0.726	-3.2	0.744	0.710*	-4.6
73	0.587	0.572#	-2.6	0.566	0.559#	-1.2
91	0.45	0.443+	-1.6			
92				0.447	0.435+	-2.7
110	0.352	0.339+	-3.7	0.340	0.327+	-3.8
147	0.239	0.220+	-7.9	0.214	0.209+	-2.3

*: $\delta_o/L=0.0015$ #: $\delta_o/L=0.001$ +: $\delta_o/L=0.0005$ Diff.=Difference

6.4 DISCUSSION OF THEORETICAL AND EXPERIMENTAL RESULTS

6.4.1 The Influence of Strain Hardening, Strain Aging and the Bauschinger Effect

The most significant result is the difference in load capacities for different conditions which are clearly seen in Fig.3.18 (in Chapter Three) and Fig.4.38 (in Chapter Four). The loss of strut load capacity due to the Bauschinger effect on load reversal occurs for all the struts that are prestrained in tension (3% and 7%), whether fully-aged or not aged, and this loss is seen to be more sensitive to strain aging than strain hardening for the rimming steel used herein. The potential strength gains due to strain hardening have been outweighed by the combined effects of strain aging (beneficial) and the Bauschinger effect (deleterious).

It is seen that following plastic tensile prestrains the Bauschinger rounding reduces the tangent modulus in compression significantly, which in turn furnishes a significant reduction of strut load capacity, up to 38% (based on normalised results).

Regarding the struts that were prestrained in tension and fully-aged, it is seen that the strut behaviours are very similar to those for the as-received struts, whether in the pre-buckling or post-buckling range. Referring to Fig.3.13, it is illustrated schematically that the post-buckling behaviour falls into two different defined zones, A and B. Apart from the strain hardening behaviour of stub columns, there are three types of post-buckling behaviour in zone A, namely (I) gentle (moderate) load shedding, (II) rapid load shedding, (III) ductile

behaviour. Inzone B, the post-buckling behaviour follows one trend, i.e., (I) gentle load shedding (see Figs.3.12,3.14 and 3.15 in Chapter Three and Figs.4.40-4.42 in Chapter Four).

However, the difference between the as-received struts and the struts that are prestrained in tension and unaged is significant near the peak load area. This difference is reduced in the post-buckling range and eventually clusters around the curves of as-received struts after a certain deformation range. The post-buckling behaviour of the struts that are prestrained in tension and unaged follows the trend classified in Zone B, i.e., (I) gentle load shedding (see Figs.3.16 and 3.17 in Chapter Three, and Figs.4.43 and 4.44 in Chapter Four).

The little difference in the load capacities between 3% and 7% prestrained struts (see Figs.3.18 in Chapter Three and 4.38 in Chapter Four) implies that the influence of strain hardening on load capacity is not significant for the steel used. However, at lower values of slenderness ratios, the influence is relatively a little higher. This influence is mainly reflected in the post-buckling range (see Figs.3.27 to 3.32 in Chapter Three).

From the average stress versus average axial strain curves (Figs.3.19 to 3.24 in Chapter Three and Figs.4.45-4.50 in Chapter Four), normalised with respect to the yield stress/strain, it is seen that greater nonlinearity prior to buckling is demonstrated for the struts that are prestrained in tension and unaged. This nonlinearity is due to the Bauschinger rounding which shows lower buckling loads, while the post-buckling fall-off in load with increasing axial shortening is much less dramatic than with the as-received struts and the struts that are prestrained in tension and fully-aged.

The great difference between the struts that are prestrained in tension and fully-aged and the struts that are prestrained in tension and unaged near the peak load area indicates the significant influence of strain aging on strut load capacity. This influence is reduced in the post-buckling range.

The significant post-buckling load capacities of steel tubular struts (indicated in Figs.3.19 - 3.24 and Table 3.2 in Chapter Three and Figs.4.45 - 4.50 and Table 4.11 in Chapter Four) are important in consideration of the overall ultimate load capacities of large span space truss systems. Even if a few members have failed, those failed members still possess significant residual load-bearing capacity until an overall collapse of a space truss system occurs.

Although it is difficult to separate the three material effects, namely, strain aging, strain hardening and the Bauschinger effect, the general trend of the influence can be summed to be that the Bauschinger effect plays a more dominant role owing to the associated reduction in tangent modulus that leads to a greater propensity for buckling to occur. Strain aging is more significant than strain hardening in enhancing the capacity of prestrained struts for the steel considered herein.

6.4.2 The Influence of Initial Imperfections

The geometric imperfections for the strut tests reported herein were kept within a defined tolerance, but the material properties were varied. The amplitude of the central lateral imperfection, measured between knife edge fittings (length L), was kept $\leq 0.0015L$. The influence of the geometric imperfections on the variability of the strut strength was restricted, therefore, as the tolerance was reasonably severe.

The computer model developed enables the various amplitudes of initial deformations to be considered, therefore, to study the influence of initial out-of-straightness on stiffness and strength of steel tubular struts. Deviations from straightness of amplitude δ_o were considered, having the form : $y=\delta_o \sin(\pi z/L)$.

Calculations were carried out for the as-received struts and struts that are prestrained to 3% in tension and unaged, with different slenderness ratios in the range $36 \leq L/r \leq 146$, for the various combinations of initial out-of-straightnesses, both above and below the usual design tolerances (0.001L or 0.0015L). The effect of initial deformation on pre-buckling stiffness and post-buckling behaviour is indicated in Figs.6.36 to 6.47, which show complete load versus axial-shortening and load versus mid-length lateral deflection curves.

Referring to the two extremes of initial out-of-straightnesses, 0.0002L (smallest) and o.002L (largest) considered herein (see Figs.6.36 to 6.47), the percentages of peak load reduction with respect to different slenderness ratios are shown in Table 6.4.

As might be expected, for the as-received struts, the influence of initial imperfections on compressive strength is found to be greatest and the post-buckling load reductions are most severe in struts for which the elastic buckling and yield stress are approximately equal ($\lambda/\lambda_T \approx 1, \lambda=73$) (Fig.6.38). At this slenderness ratio, it can be seen that the increase in initial imperfection reduces the ultimate strength significantly, but after a certain deformation range the post-buckling behaviour follows a similar trend for all the values assumed for initial out-of-straightness. It is found that this observation is also true for struts with

slenderness ratio of λ=91. The influence is found to be smaller for the struts with other slenderness ratios.

For struts that are prestrained to 3% in tension and unaged, the influence of initial out-of-straightness on strut load capacity and post-buckling behaviour is not as significant as for the as-received struts, for all but the strut with slenderness ratio of λ=73. At this slenderness ratio (see Fig.6.44), it is seen that the influence of initial out-of-straightness on buckling load is not significant. However, with a small initial out-of-straightness (0.0002L) the post-buckling fall-off in strength is more dramatic than the other initial out-of-straightnesses assumed (0.0005L, 0.0015L and 0.002L).

The sensitivity of compressive strength to various amplitudes of initial deformations is indicated in Fig.6.48 for the as-received struts, Fig.6.49 for the struts that are prestrained to 3% in tension and unaged, with different slenderness ratios. It is seen that for the as-received struts, whether the compressive strength is sensitive to the amplitudes of initial deformation or not depends on the values of the slenderness ratios. The change with different amplitudes of initial deformation is almost kept constant for the lowest and highest slenderness ratios (λ/λ_T=0.459 and 1.844) in the slenderness ratio range considered here.

The curve with λ/λ_T=0.921(Fig.6.48) shows the severest change of compressive strength with increasing the initial deformation. With increasing or decreasing the slenderness ratios, this change is gradually reduced until reaching the two extremes - the lowest and highest λ/λ_T values (0.459 and 1.844), where the change of compressive strength with increasing the amplitudes of initial deformation is almost kept constant. However, this situation is not the case for struts that are prestrained in tension and unaged(Fig.6.49).

In general for struts that are prestrained in tension and unaged, the compressive strength is not as sensitive to different amplitudes of initial deformation as that for as-received struts. The change of compressive strength with increasing the amplitudes of initial deformation is gentle for all the values of λ/λ_T. The relatively smaller change is due to the fact that for struts that are prestrained in tension and unaged, the material reaches the proportional strength (inelastic range) earlier in which the order of magnitude of deformations is much larger than the order of magnitude of the initial out-of-straightness (see Table 6.5, in which δ_o is the initial out-of-straightness and δ_p is the mid-length lateral deflection at peak load).

Table 6.6 shows the peak load reductions (from as-received struts to struts that are prestrained in tension and unaged) due to the Bauschinger effect within the two extremes of initial out-of-straightnesses, 0.0002L (smallest) and 0.002L (largest) considered herein.

By comparing Tables 6.4 and 6.6, it is seen that the influence of the Bauschinger effect on strut load capacities is more significant than that of initial imperfections. Even considering the severest reduction owing to initial imperfections (24.4% for λ= 73 from 0.0002L to 0.002L, Table 6.4), the Bauschinger effect is still more dominant (reduction between 33.7% - 45%, Table 6.6). Apparently, the smaller the initial imperfections, the more significant the influence of the Bauschinger effect. In practical structures, all the members are expected to be produced to be closely straight within a reasonable given tolerance. In such cases the Bauschinger effect plays a significant role.

The effect of initial eccentricity of loading on the tubular struts is studied with: e/L=0.0002, 0.0015 and 0.002. The initial out-of-straightness is also considered in conjunction with variations in loading eccentricity. The cases where the initial out-of-straightness and eccentricity for load are in both the same directions ('positive' eccentricity) and in opposite directions ('negative' eccentricity) are investigated as well. These combinations of initial imperfections are shown in Table 6.7.

The results of analyses of a 60.3mm diameter by 2.3mm thick, 1.87m long as-received strut for the various combinations of initial imperfections are given in Figs.6.50 and 6.51, which show the axial shortening and the mid-length lateral deflection, in each case plotted against the load. As expected, the maximum load of the struts decreases with increasing load eccentricity and a more ductile post-buckling behaviour is exhibited. The case where an out-of-straightness (0.0015L) is combined with a loading eccentricity (0.0015L, in the same directions) shows a much lower buckling load, while the post-buckling curves are much flatter and do not show an immediate drop in load carrying capacity compared with the case where the initial out-of-straightness (0.0015L) and eccentricity for load (0.0015L) are in opposite directions (see Fig.6.51).

It can be seen that the effect of the 'negative' eccentricity is to raise the load level; and effect of the 'positive' eccentricity is to reduce the load level. However, after the peak, the load of the strut with 'negative' eccentricity falls off rapidly and the results tend to those for the case where the initial out-of-straightness and loading eccentricity are in the same direction ('positive' eccentricity).

6.5 SUMMARY

By comparing the theoretical results with the experimental results of as-received struts and the struts that are prestrained in tension, both fully-aged and unaged, it is shown that the developed theoretical model can accurately predict the experimental maximum loads and the post-buckling load-deformation curves of steel tubular struts. The comprehensive theoretical and experimental results have been discussed in the previous sections. The influence of strain aging, strain hardening, the Bauschinger effect and the effects of initial imperfections have been examined.

Table 6.4 Load Reduction due to Initial Imperfections (from 0.0002L to 0.002L)

Condition	λ	Load Reduction %
As-Received	36	6.8
	55	12.2
	73	24.4
	91	23.9
	110	18.3
	146	12.0
3% Prestrained Unaged	36	4.1
	55	9.0
	73	8.8
	91	11.1
	111	12.4
	147	15.8

Table 6.5 Magnitude of Deflections for Prestrained and Unaged Struts

λ=36		λ=55		λ=73		λ=91		λ=110		λ=147	
δ_o mm	δ_p mm	δ_o mm	δ_p mm	δ_o mm	δ_p mm	δ_o mm	δ_p mm	δ_o mm	δ_p mm	δ_o mm	δ_p mm
0.15	14.5	0.56	3.8	0.29	11.6	0.37	18.4	0.45	23.0	0.60	1.82
1.11	14.7	1.11	4.7	0.74	12.4	1.86	19.1	2.24	23.8	1.50	4.8
1.47	16.5	1.67	5.3	1.47	12.1	2.79	19.7	3.36	24.6	2.98	25.7
		2.22	5.8	2.21	13.3	3.72	19.8	4.48	25.5	4.47	26.6
				2.94	12.4					5.96	26.9

δ_p is the mid-length lateral deflection at peak load.

Table 6.6 Load Reduction due to the Bauschinger Effect

λ	Load Reduction %	
	δ_o=0.0002L	δ_o=0.002L
36	12.1	15.7
55	32.1	29.6
73	45.0	33.7
91	46.5	37.5
110	41.9	27.6
146	33.1	35.9

Table 6.7 Combination of Initial Imperfections

Case	Initial Out-of-Straightness	Loading Eccentricity
1	0.001L	0
2	0.0015L	0
3	0.0015L	0.0015L
4	0.0015L	-0.001L
5	0.0015L	-0.0015L
6	0	0.0002L
7	0	0.0015L
8	0	0.002L

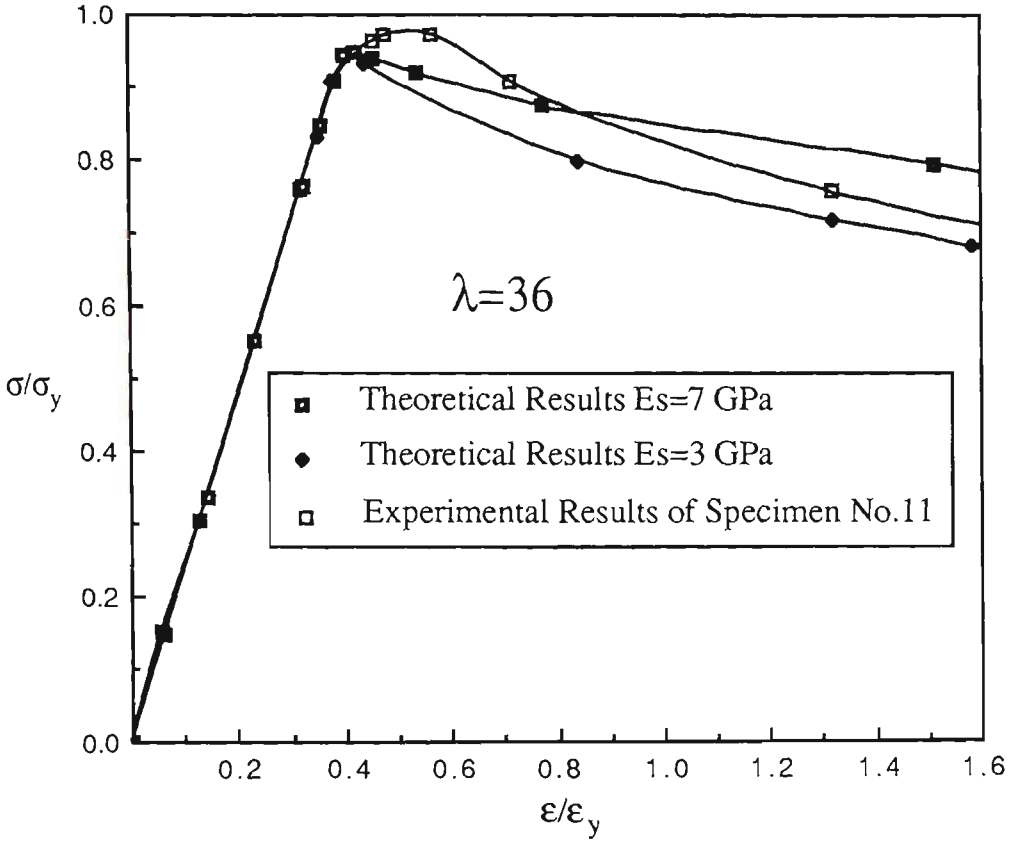

Fig.6.1 Comparison of Theoretical and Experimental Curves - As-Received Struts

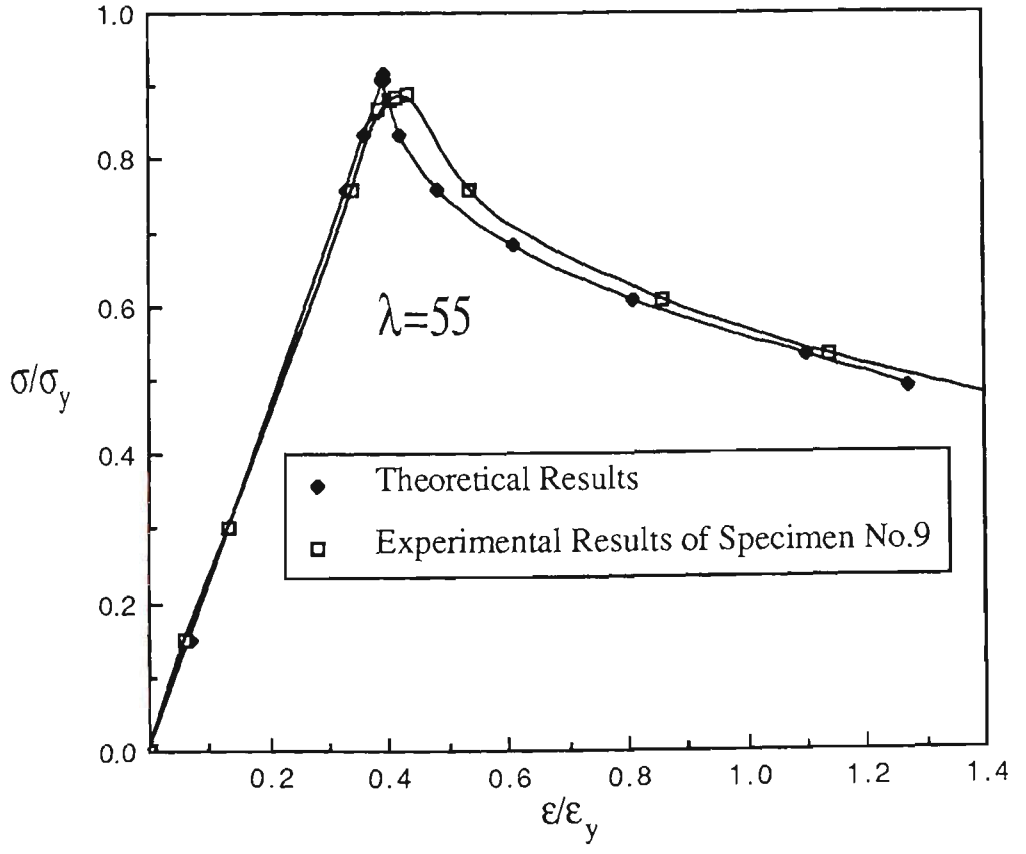

Fig.6.2 Comparison of Theoretical and Experimental Curves - As-Received

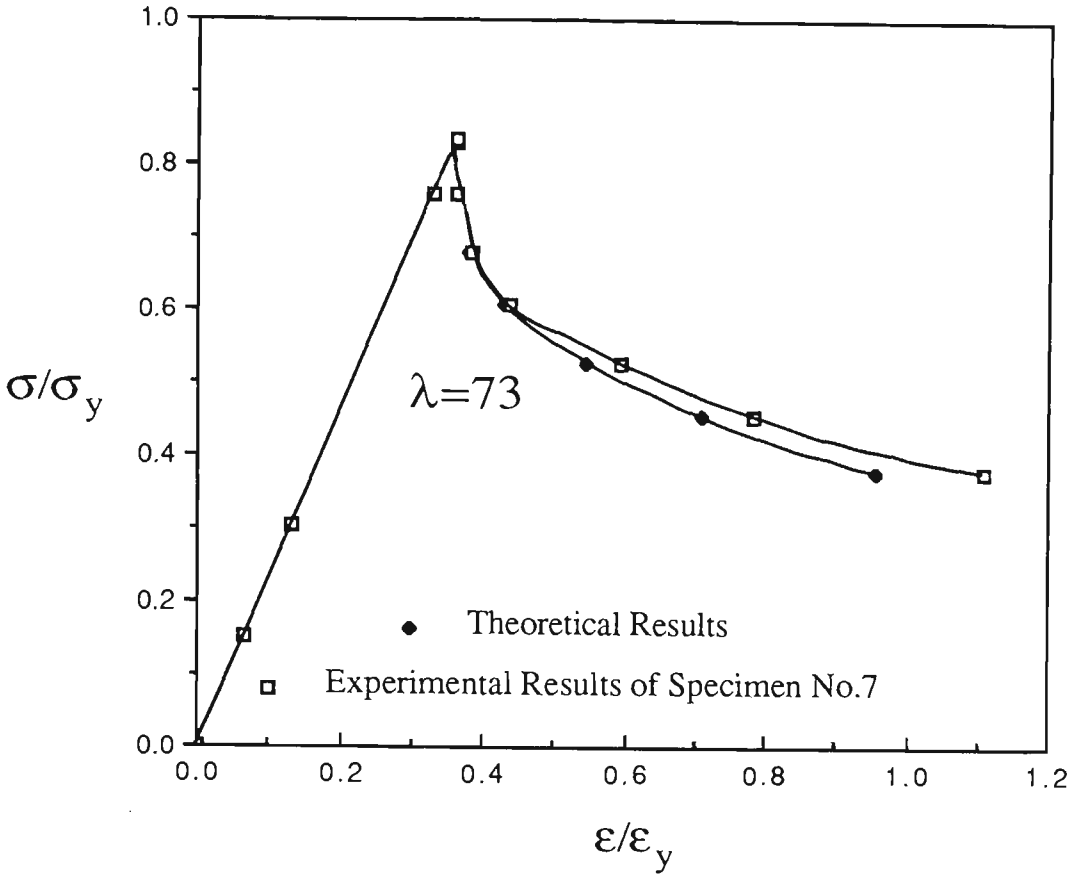

Fig.6.3 Comparison of Theoretical and Experimental Curves - As-Received

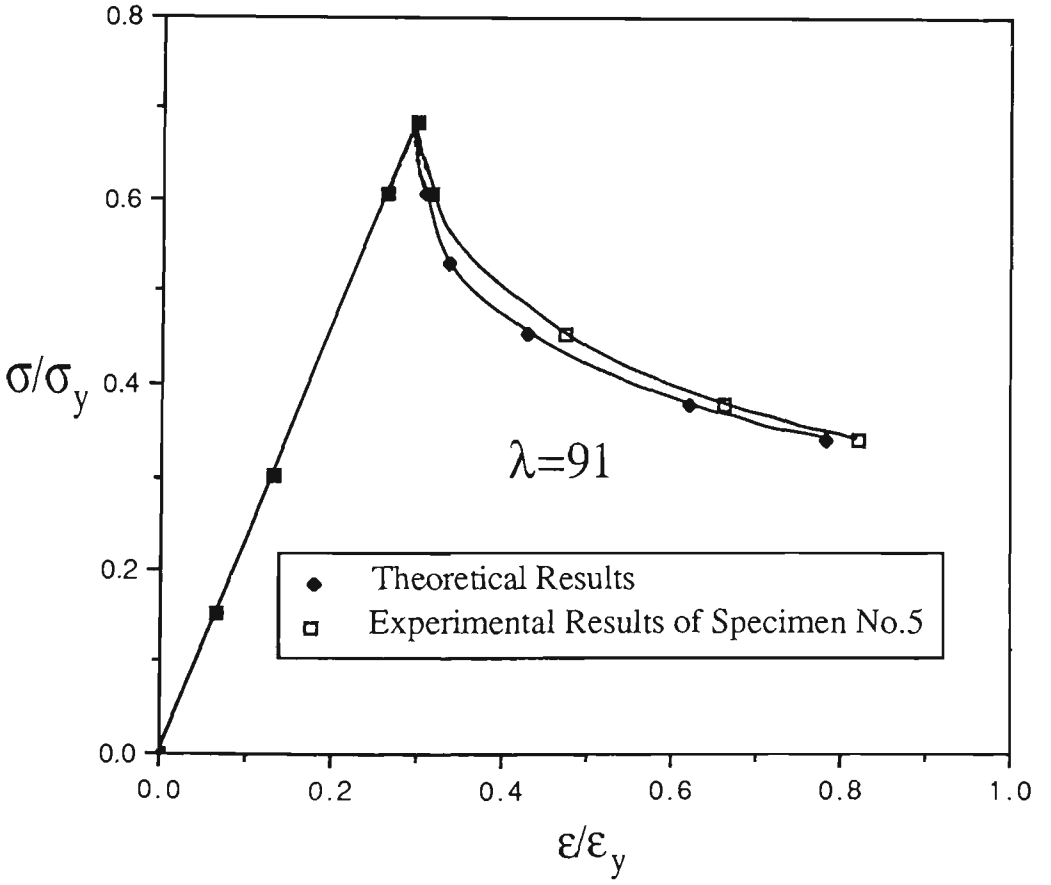

Fig.6.4 Comparison of Theoretical and Experimental Curves - As-Received

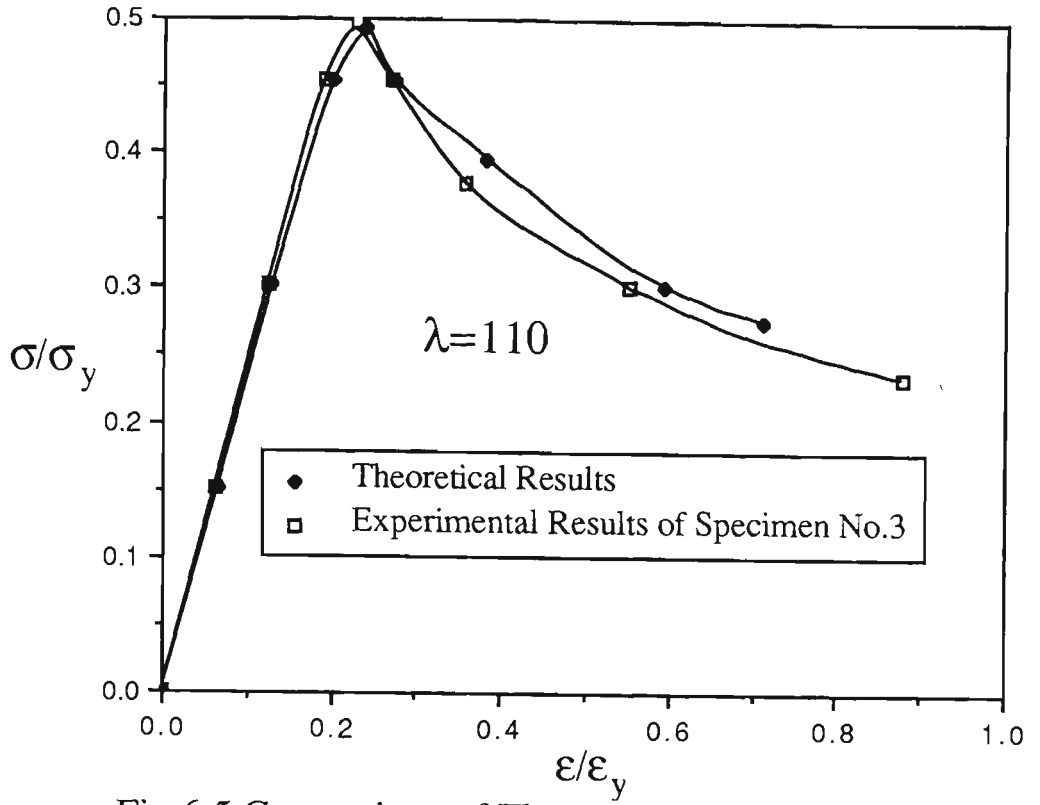

Fig.6.5 Comparison of Theoretical and Experimental Curves - As-Received

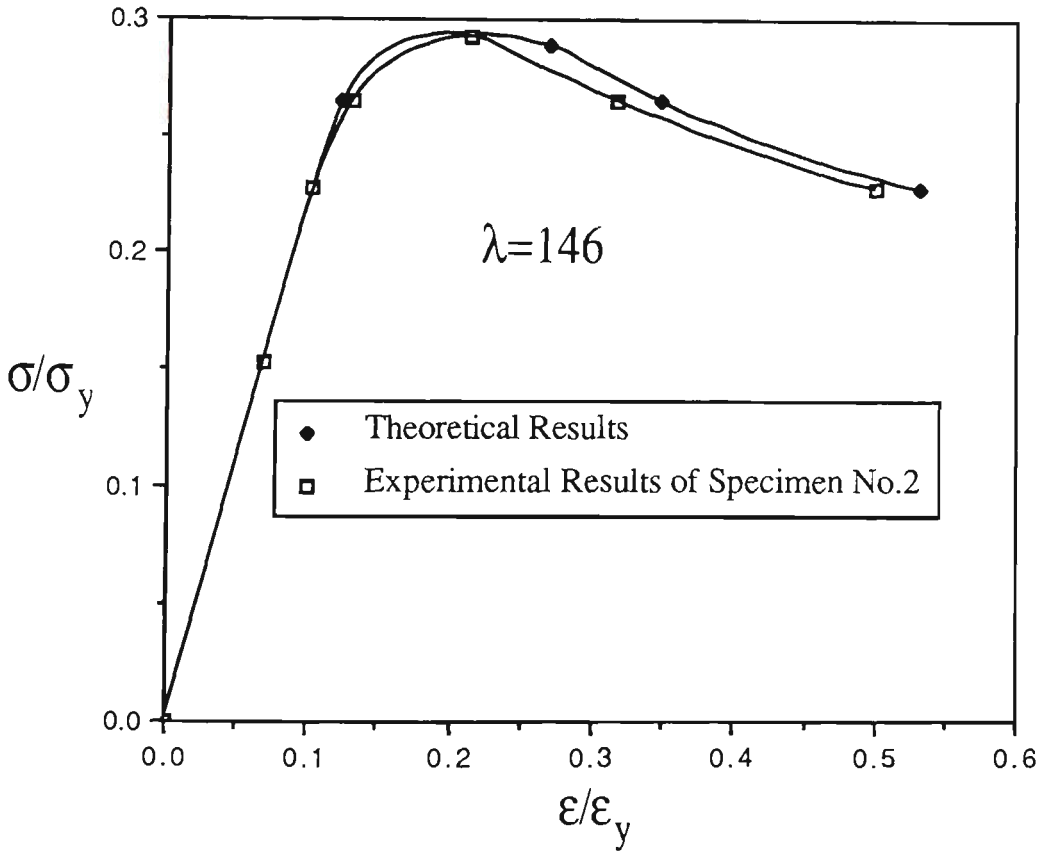

Fig.6.6 Comparison of Theoretical and Experimental Curves - As-Received

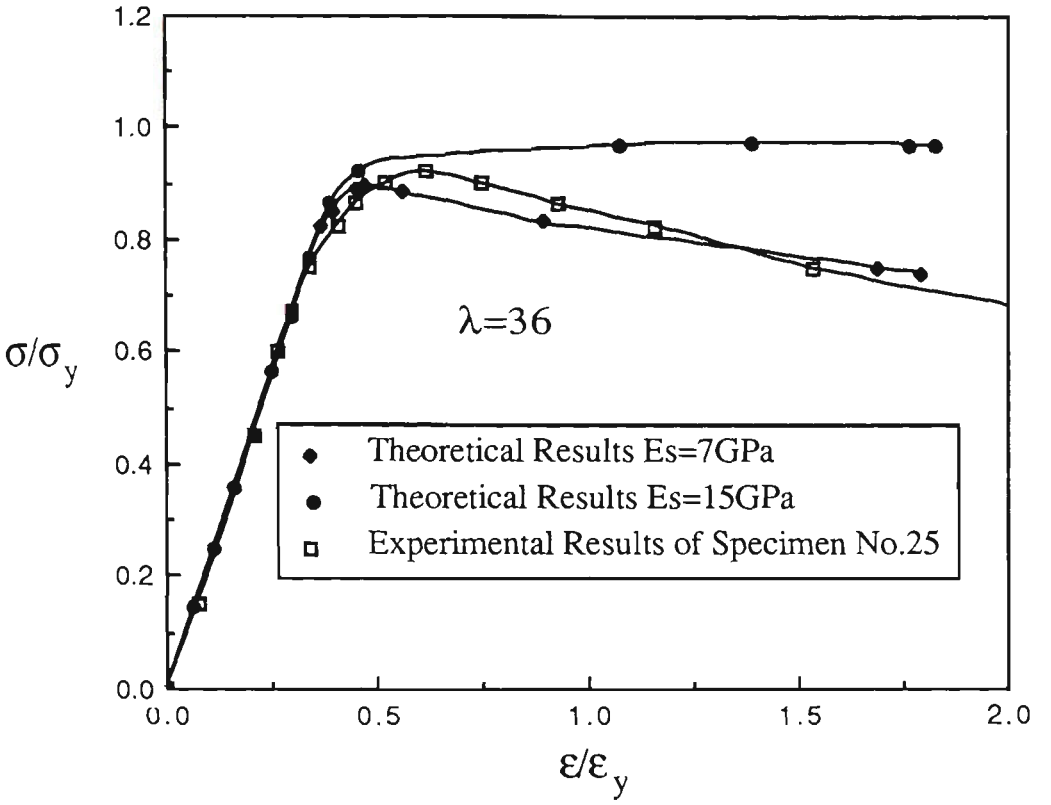

Fig.6.7 Comparison of Theoretical and Experimental Curves-3% Prestrained, Fully-Aged

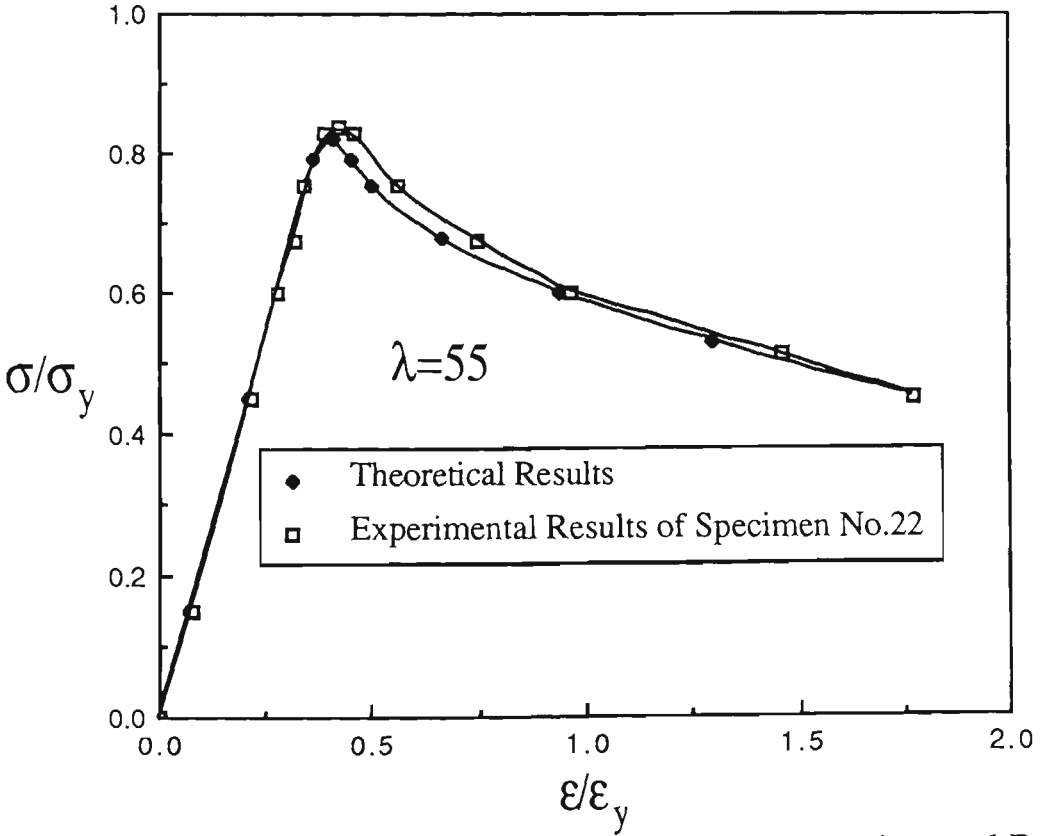

Fig.6.8 Comparison of Theoretical Results with Experimental Results 3% Prestrained, Fully-Aged

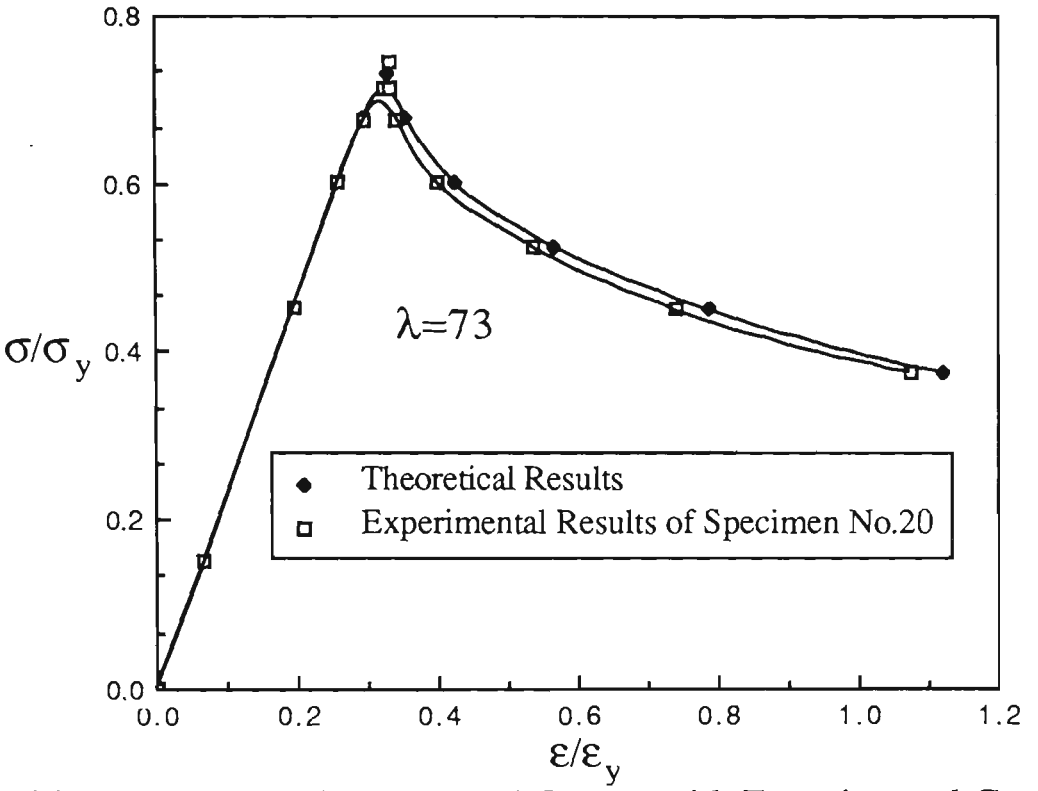

Fig.6.9 Comparison of Theoretical Curves with Experimental Curves 3% Prestrained, Fully-Aged

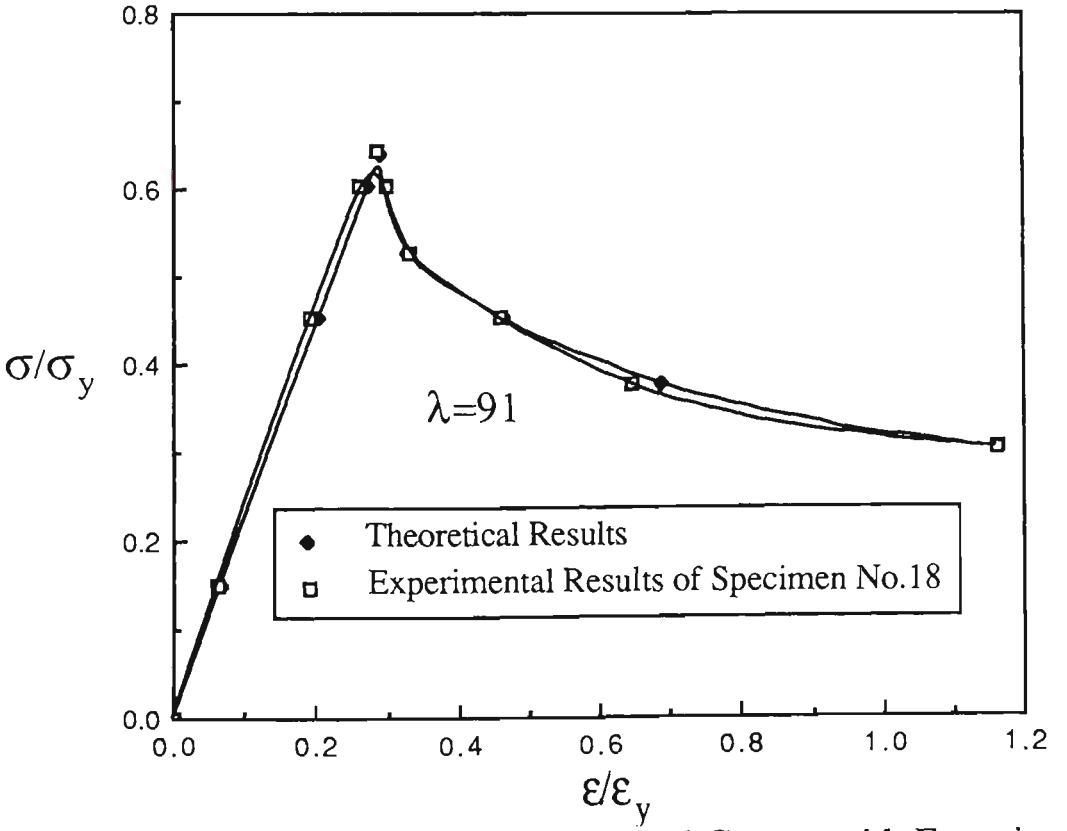

Fig.6.10 Comparison of Theoretical Curves with Experimental Curves - 3% Prestrained, Fully-Aged

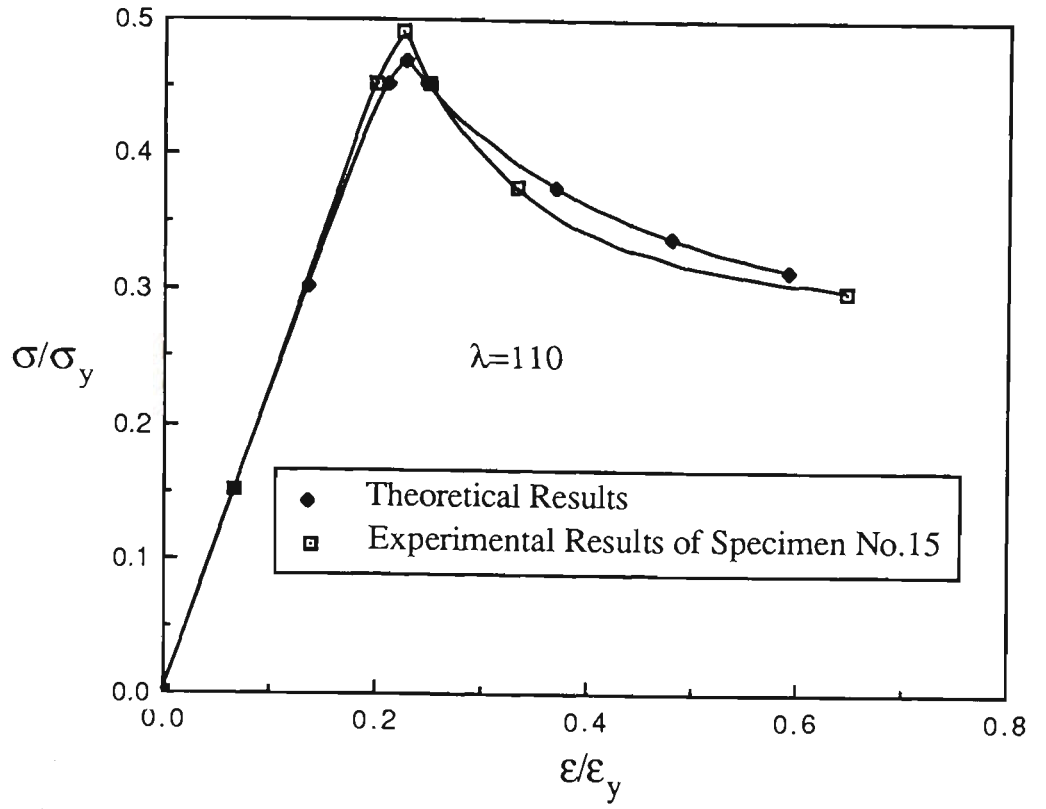

Fig.6.11 Comparison of Theoretical Curves with Experimental Curves 3% Prestrained, Fully-Aged

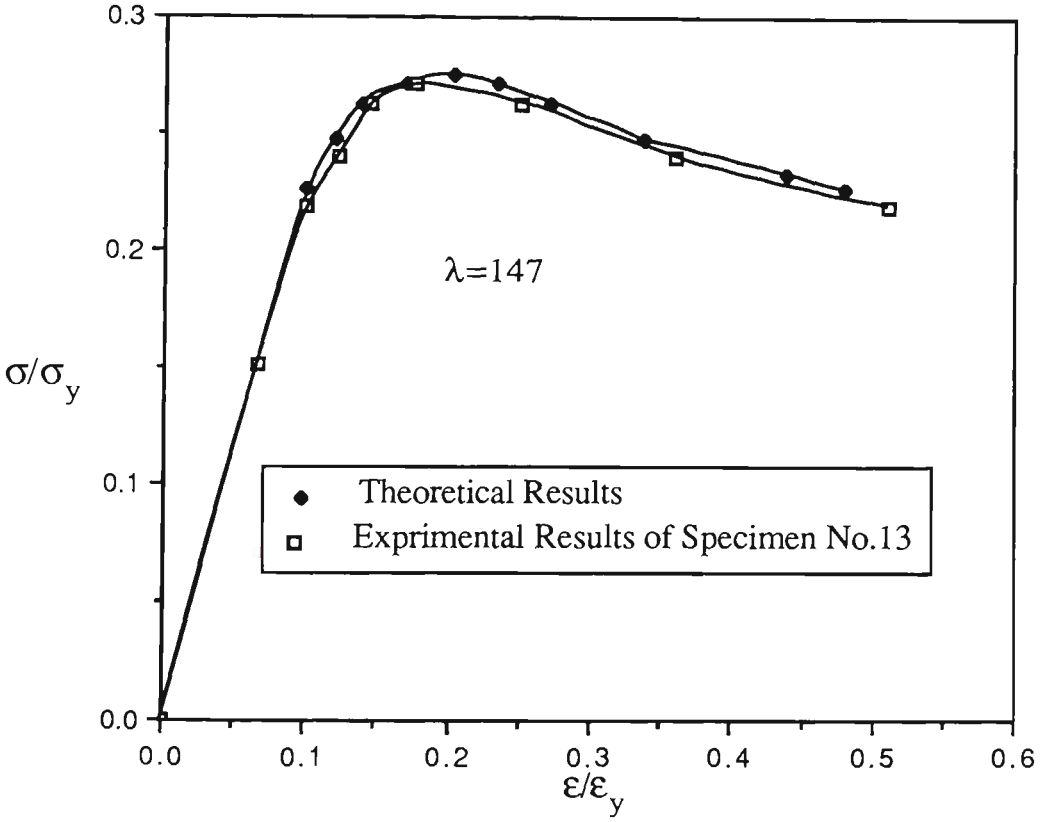

Fig.6.12 Comparison of Theoretical and Experimental Curves - 3% Prestrained, Fully-Aged

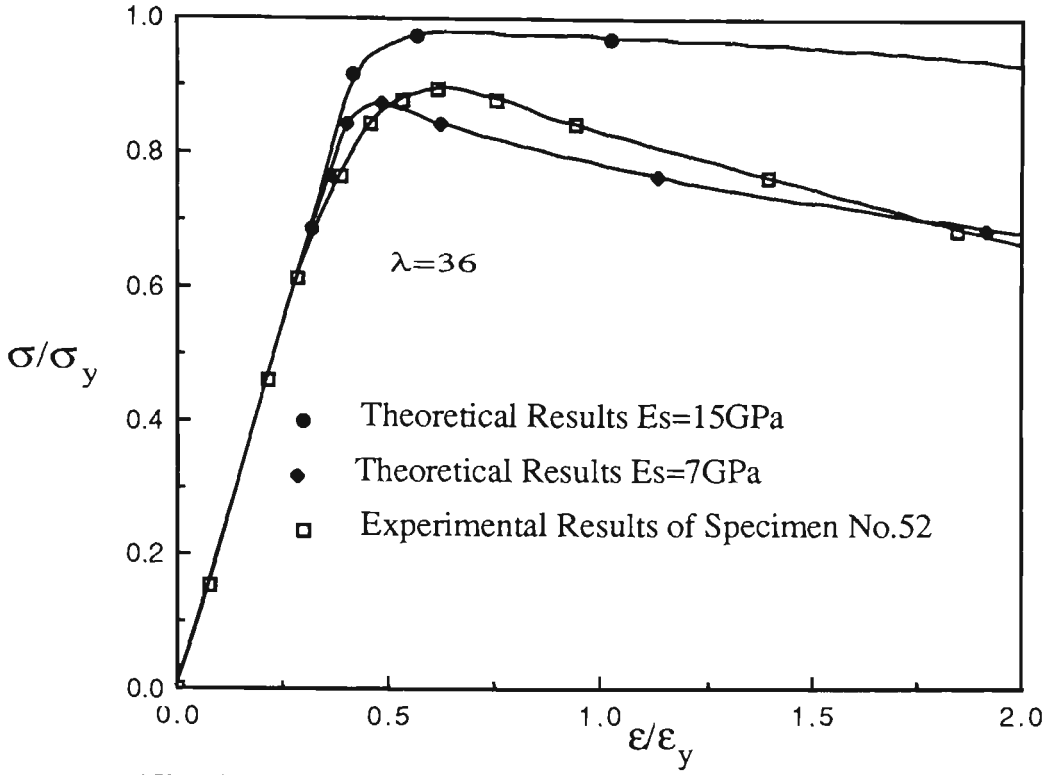

Fig.6.13 Comparison of Theoretical and Experimental Curves - 7% Prestrained, Fully-Aged

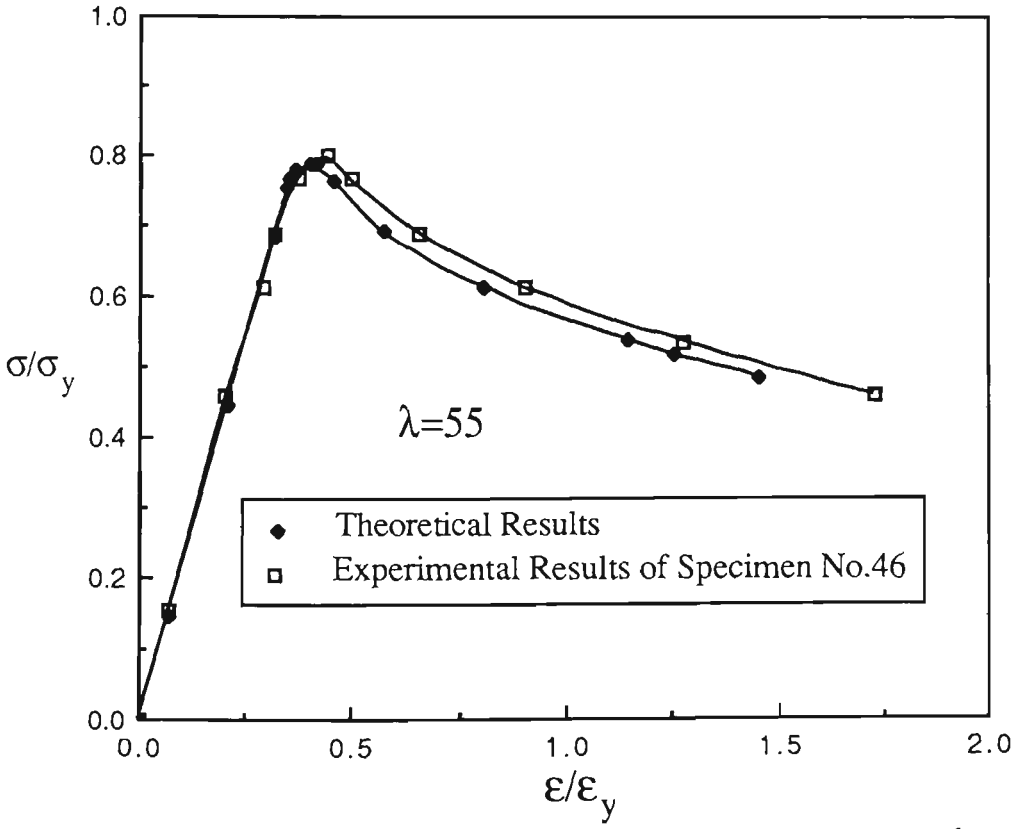

Fig.6.14 Comparison of Theoretical and Experimental Curves-7% Prestrained, Fully-Aged

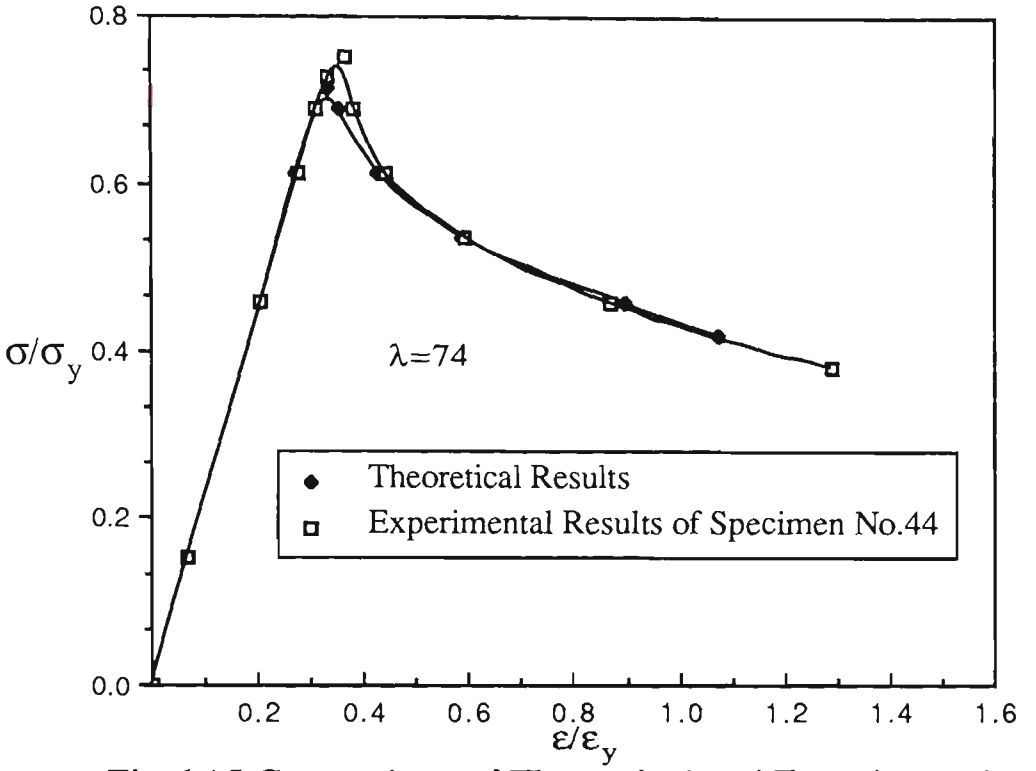

Fig.6.15 Comparison of Theoretical and Experimental Curves-7% Prestrained, Fully-Aged

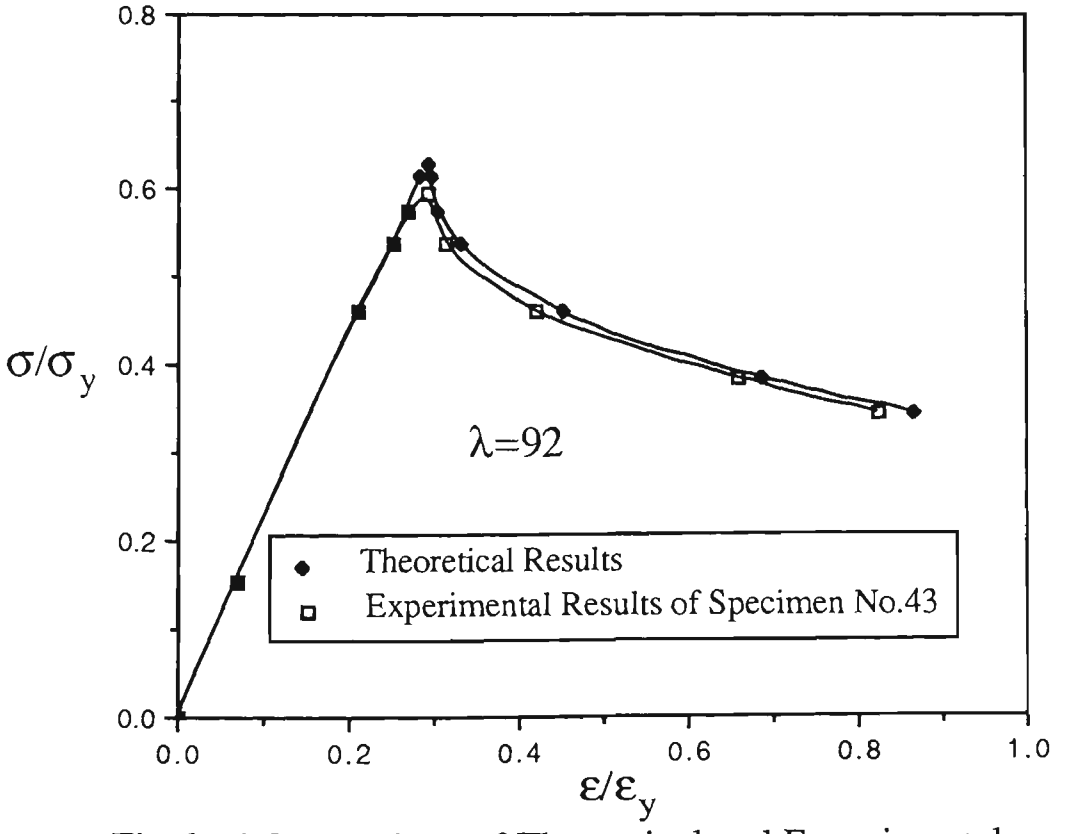

Fig.6.16 Comparison of Theoretical and Experimental Curves-7% Prestrained, Fully-Aged

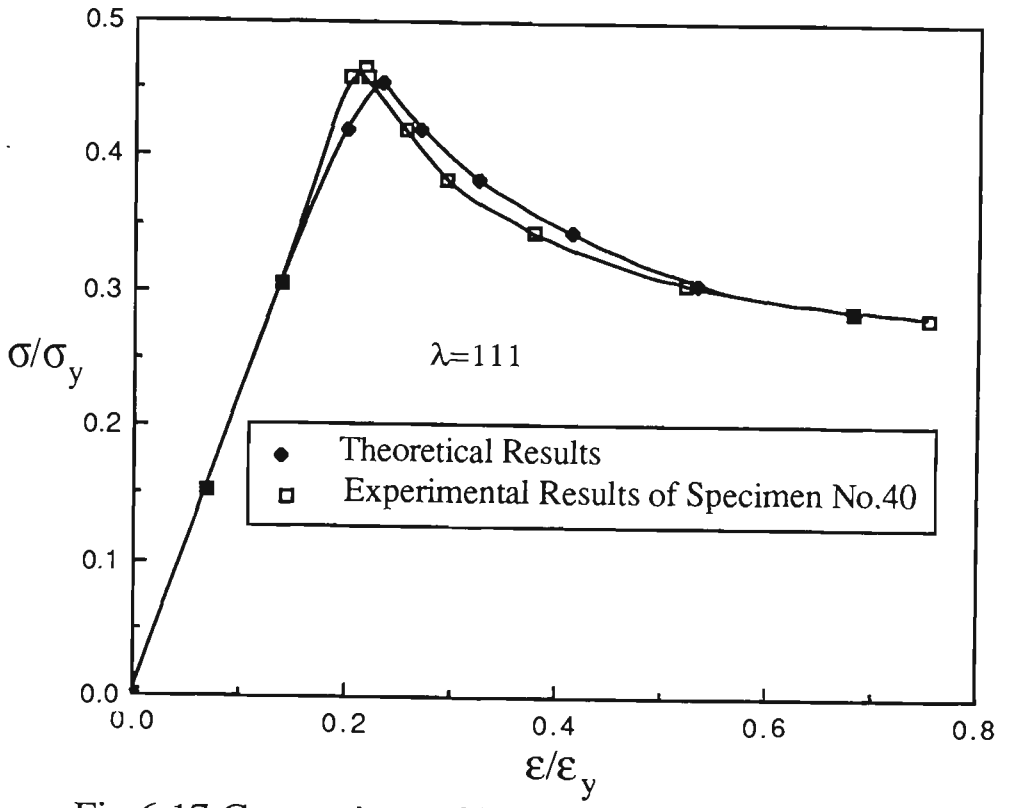

Fig.6.17 Comparison of Theoretical and Experimental Curves - 7% Prestrained, Fuly-Aged

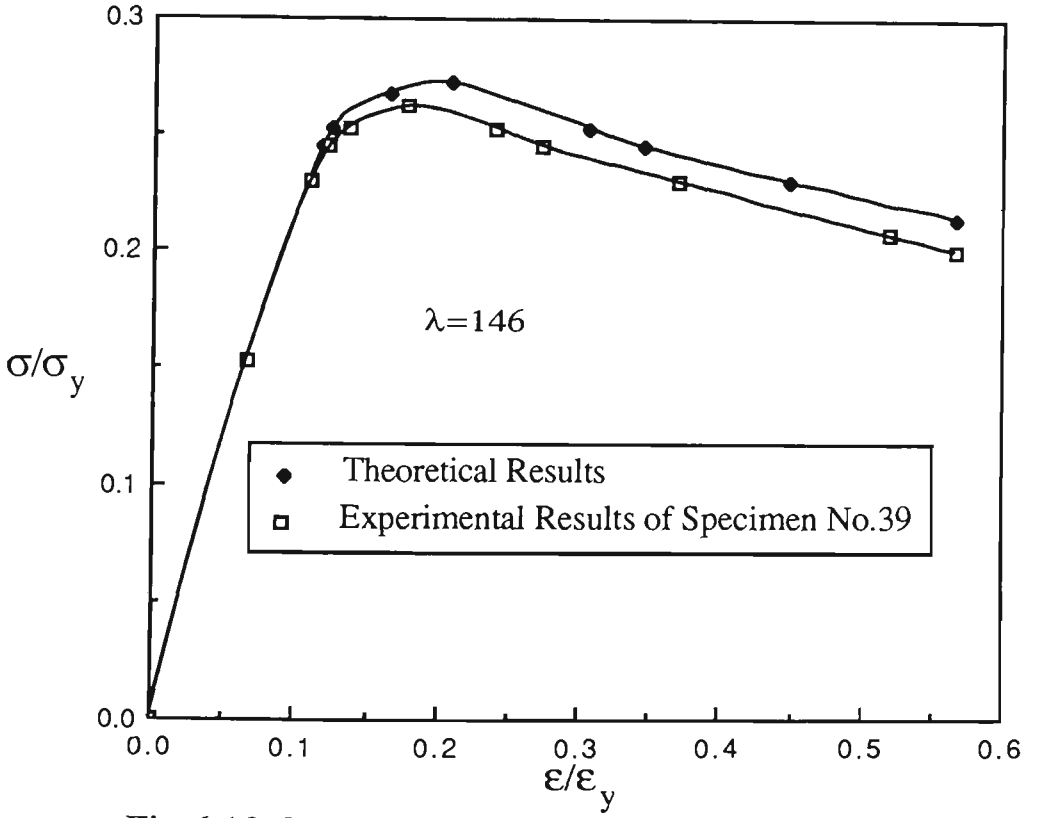

Fig.6.18 Comparison of Theoretical and Experimental Curves-7% Prestrained, Fully-Aged

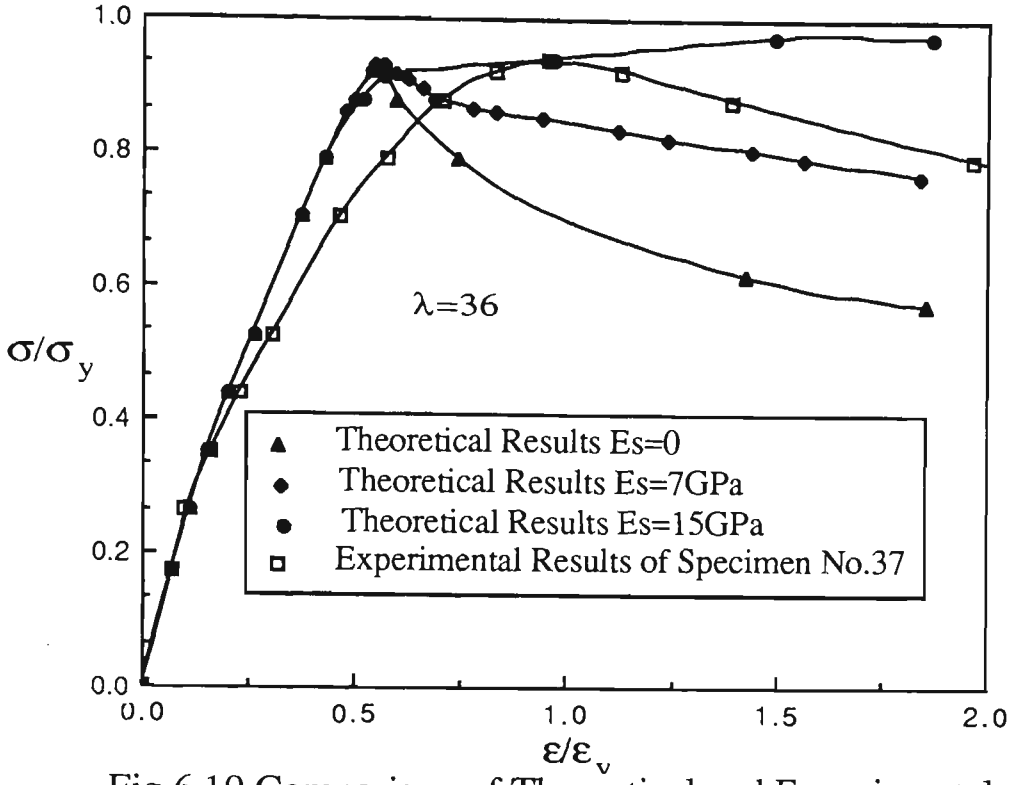

Fig.6.19 Comparison of Theoretical and Experimental Curves - 3% Prestrained, Unaged

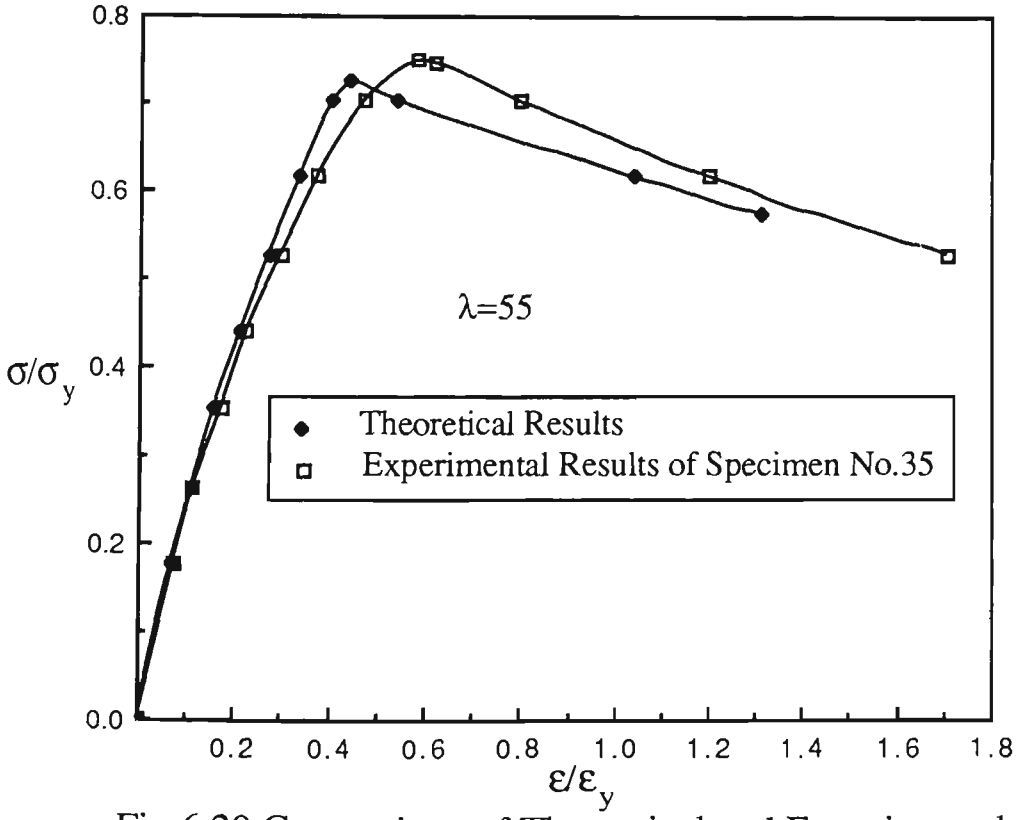

Fig.6.20 Comparison of Theoretical and Experimental Curves - 3% Prestrained, Unaged

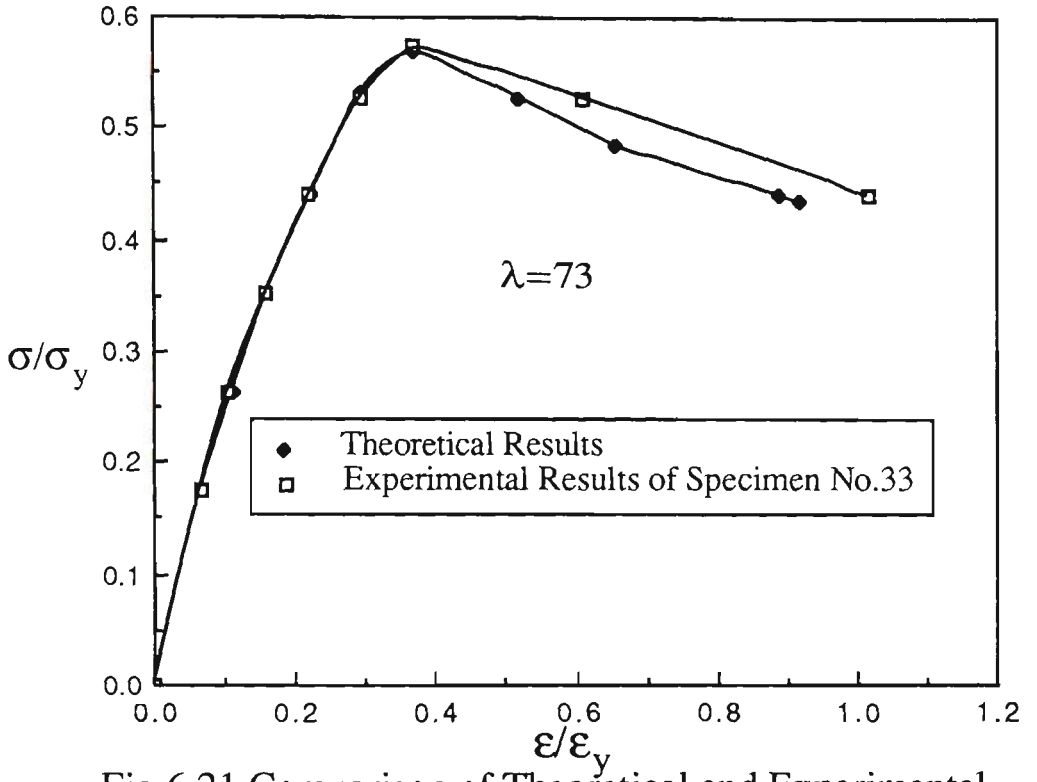

Fig.6.21 Comparison of Theoretical and Experimental Curves - 3% Prestraind, Unaged

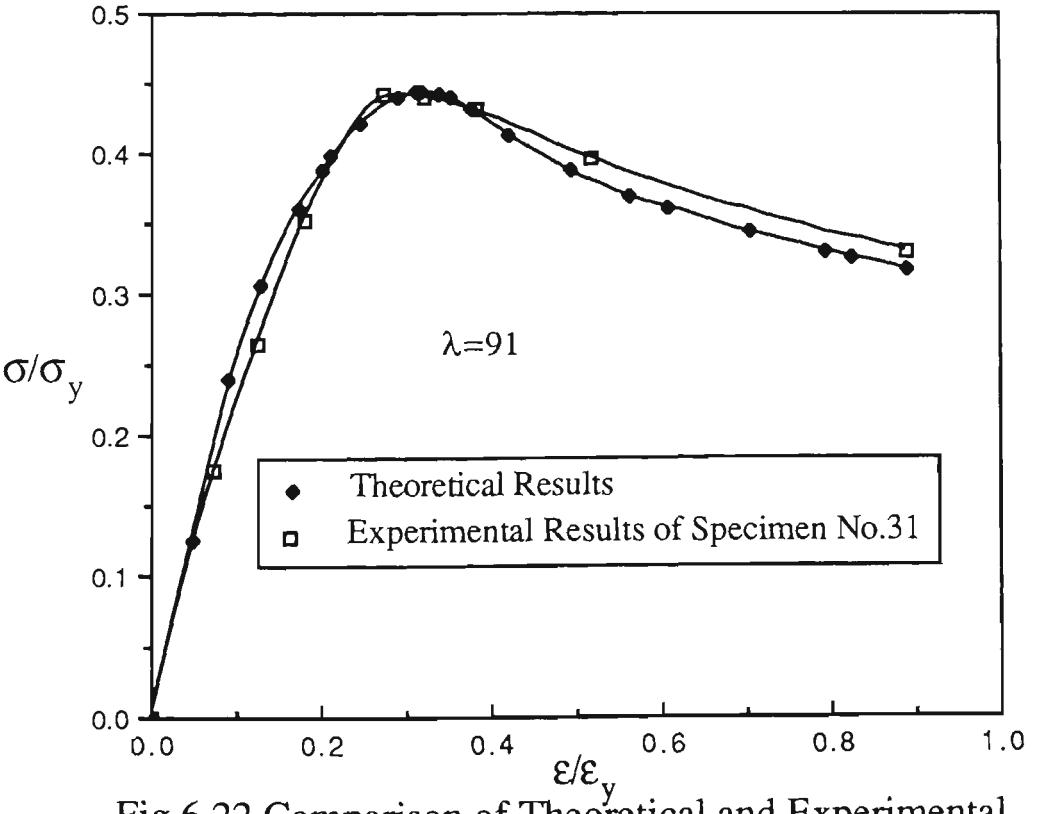

Fig.6.22 Comparison of Theoretical and Experimental Curves - 3% Prestrained, Unaged

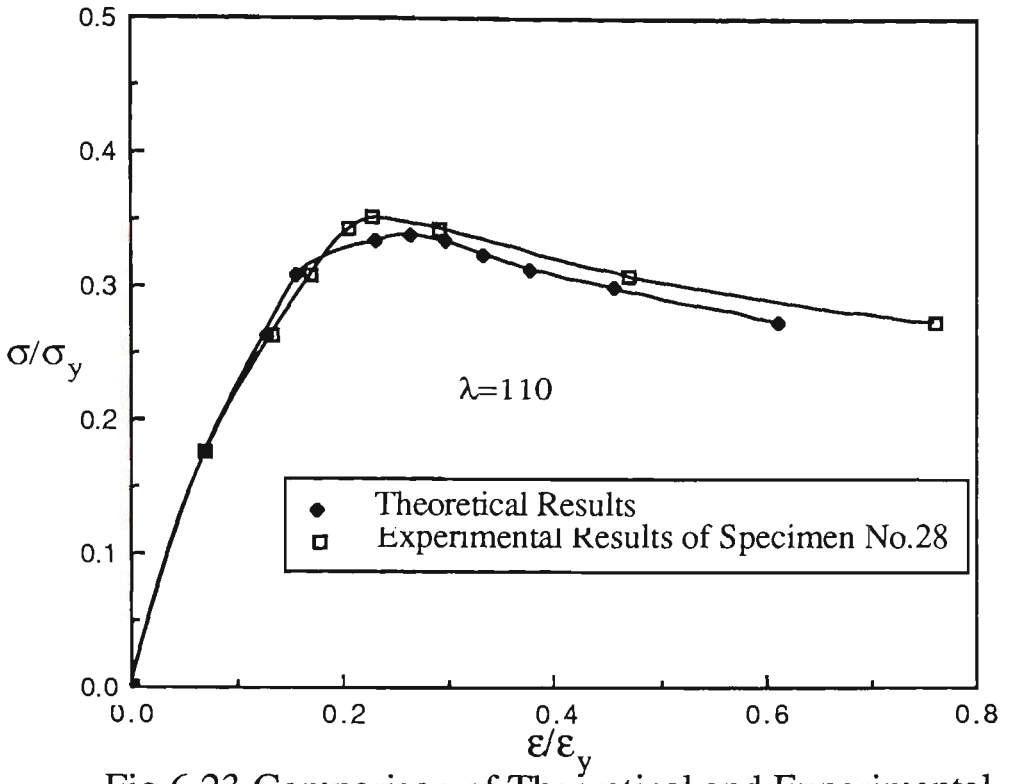

Fig.6.23 Comparison of Theoretical and Experimental Curves - 3% Prestrained, Unaged

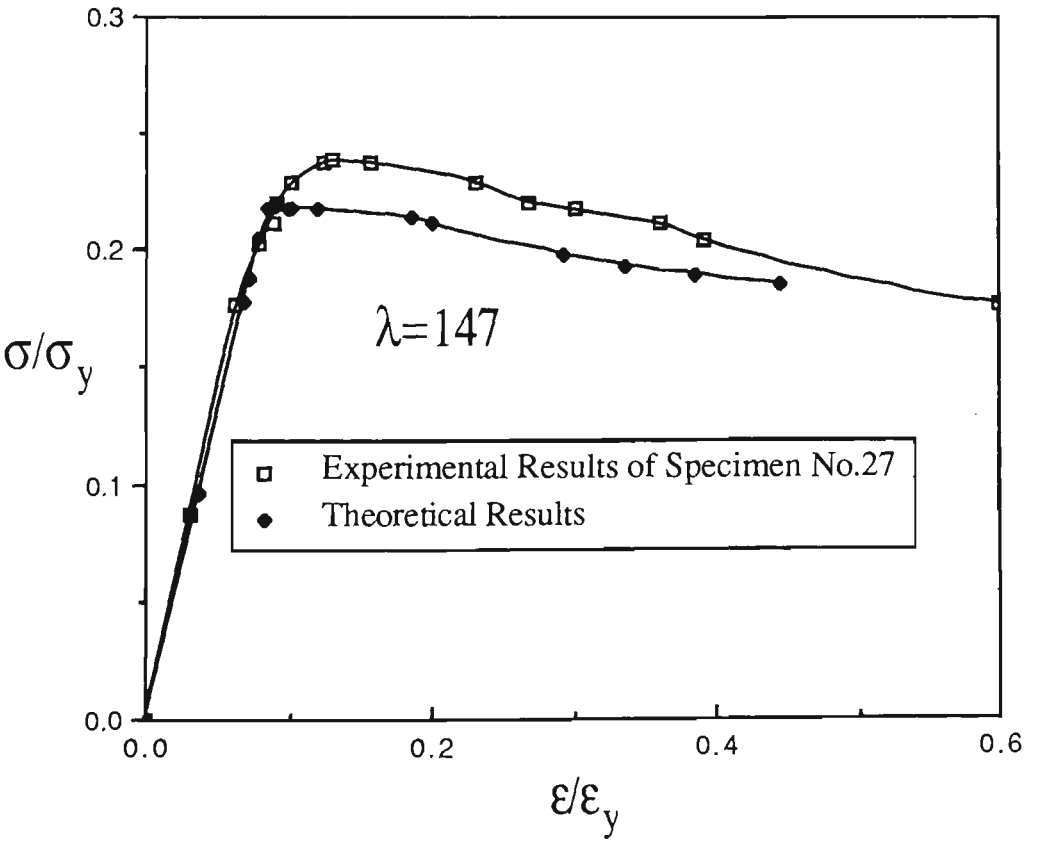

Fig.6.24 Comparison of Theoretical and Experimental Curves 3% Prestrained, Unaged

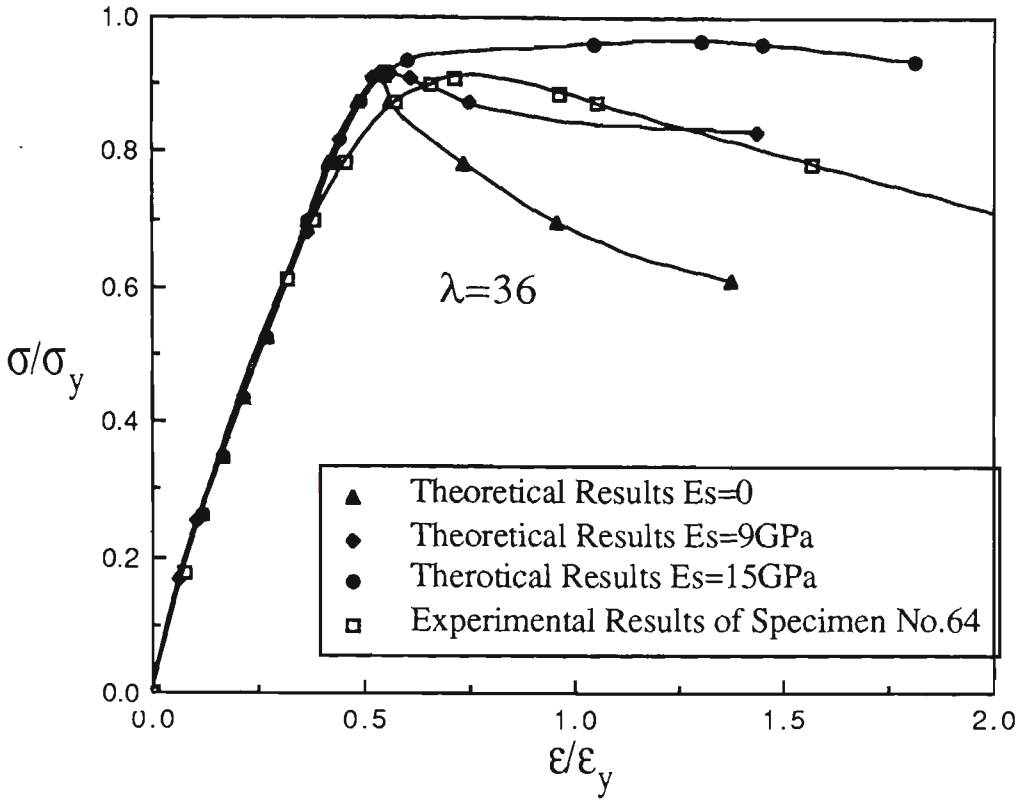

Fig.6.25 Comparison of Theoretical and Experimental Curves - 7% Prestrained, Unaged

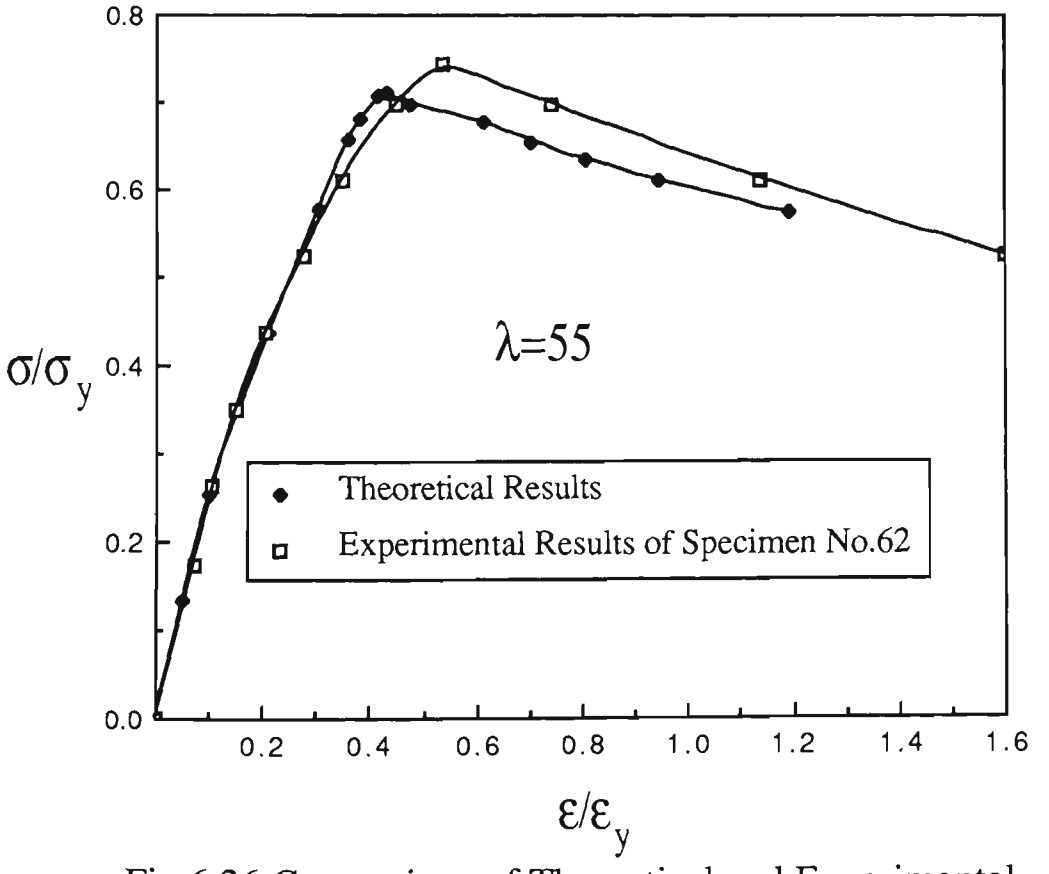

Fig.6.26 Comparison of Theoretical and Experimental Curves - 7% Prestrained, Unaged

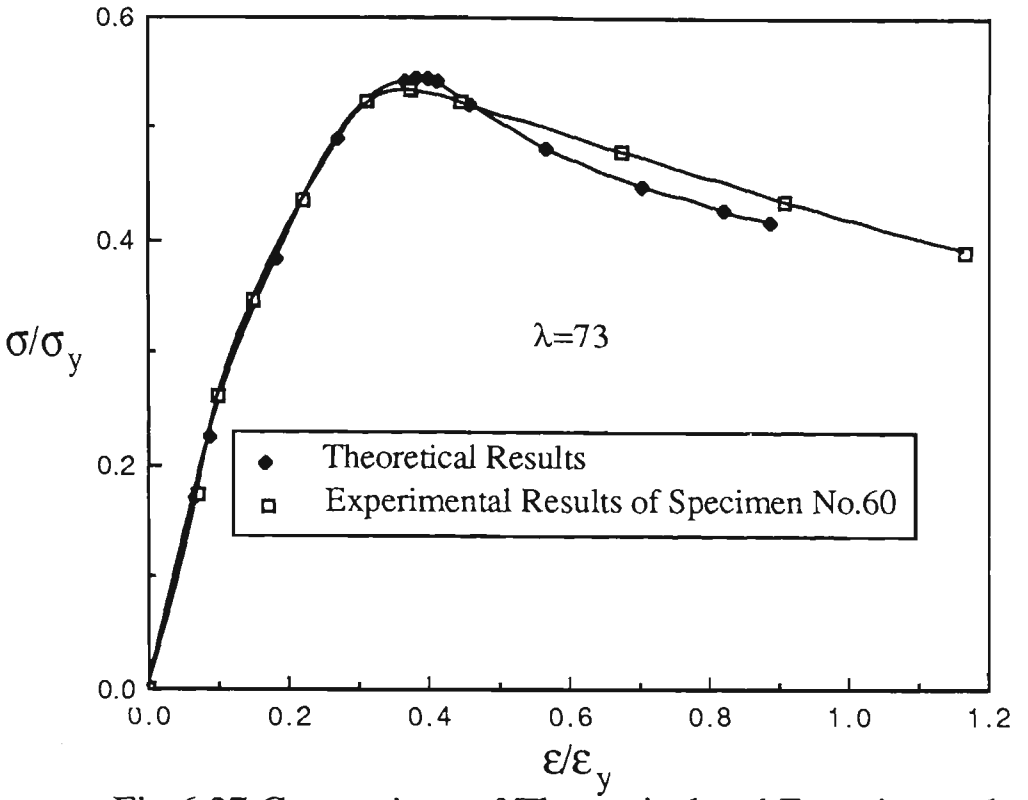

Fig.6.27 Comparison of Theoretical and Experimental Curves - 7% Prestrained, Unaged

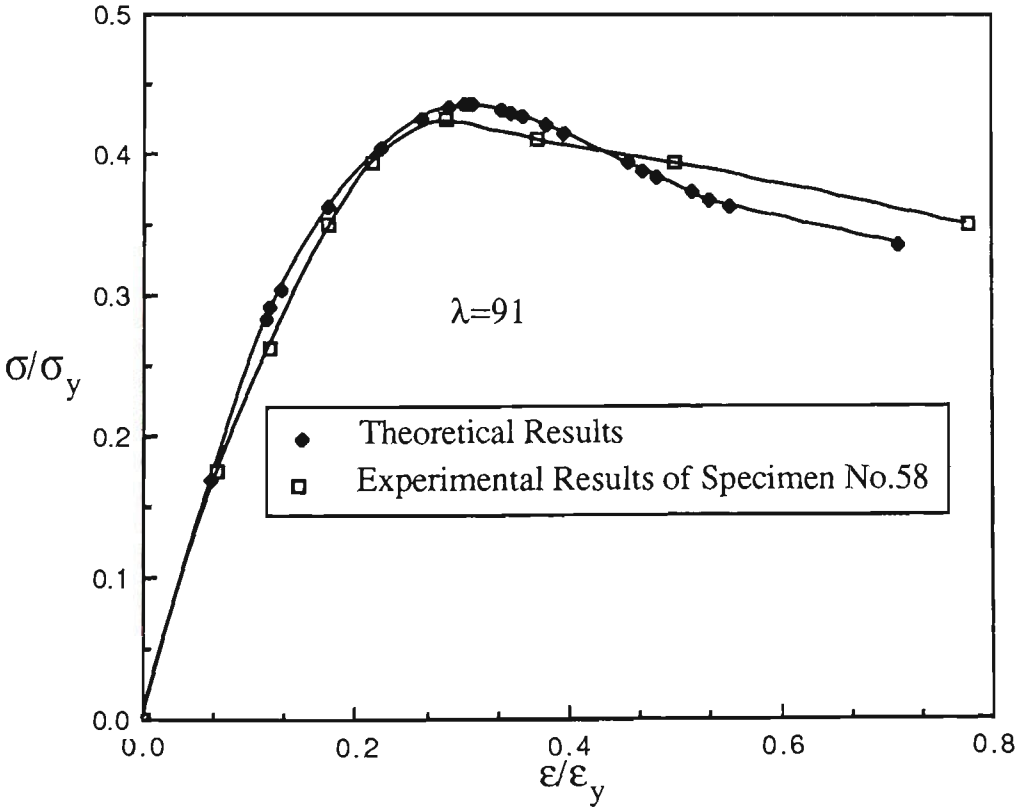

Fig.6.28 Comparison of Theoretical and Experimental curves - 7% Prestrained, Unaged

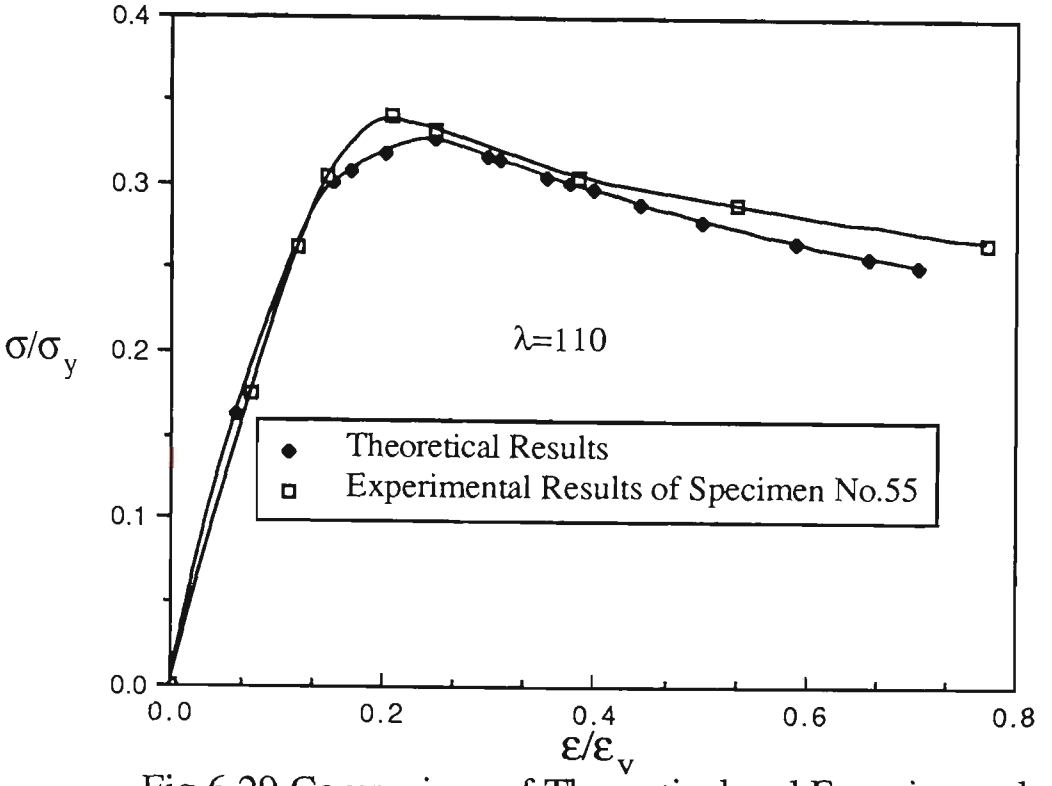

Fig.6.29 Comparison of Theoretical and Experimental Curves - 7% Prestrained, Unaged

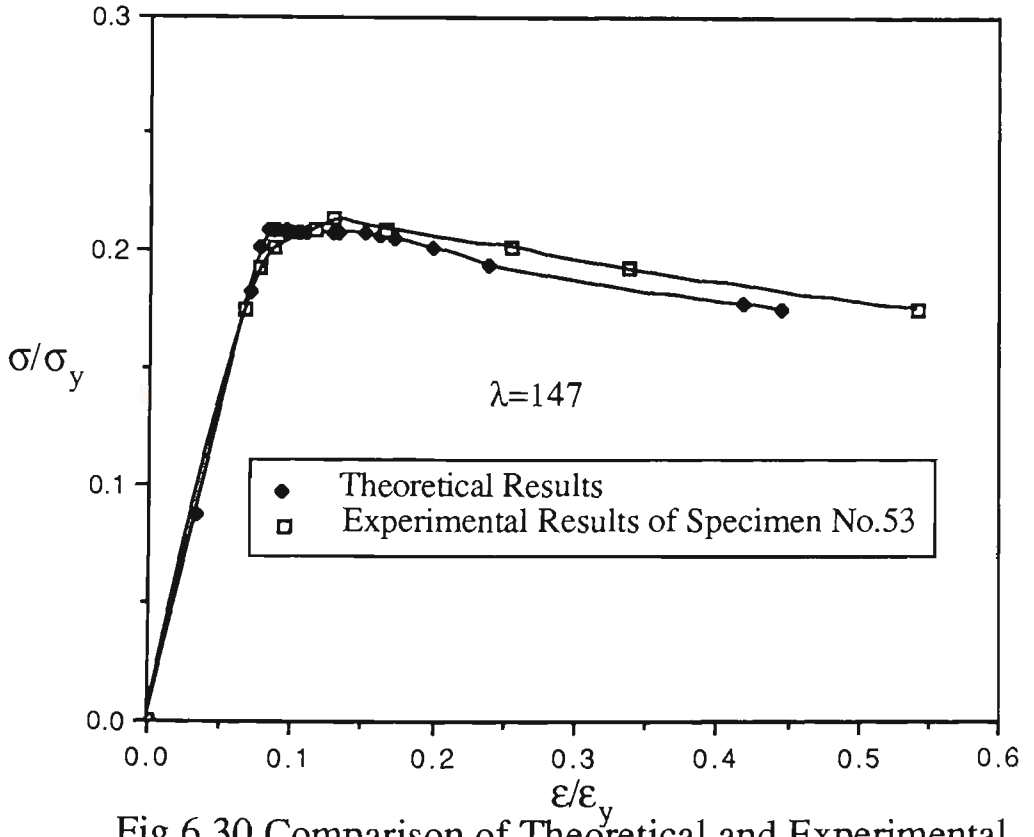

Fig.6.30 Comparison of Theoretical and Experimental Curves - 7% Prestrained, Unaged

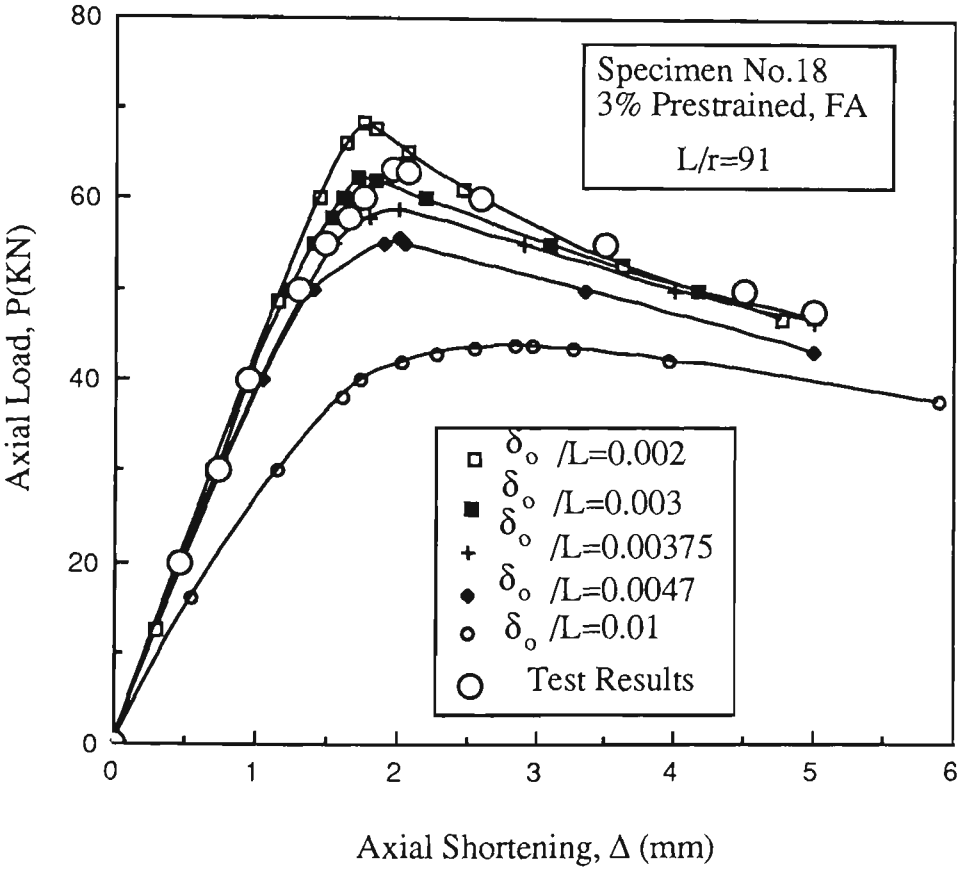

Fig.6.31 Comparison of Theoretical and Test Results

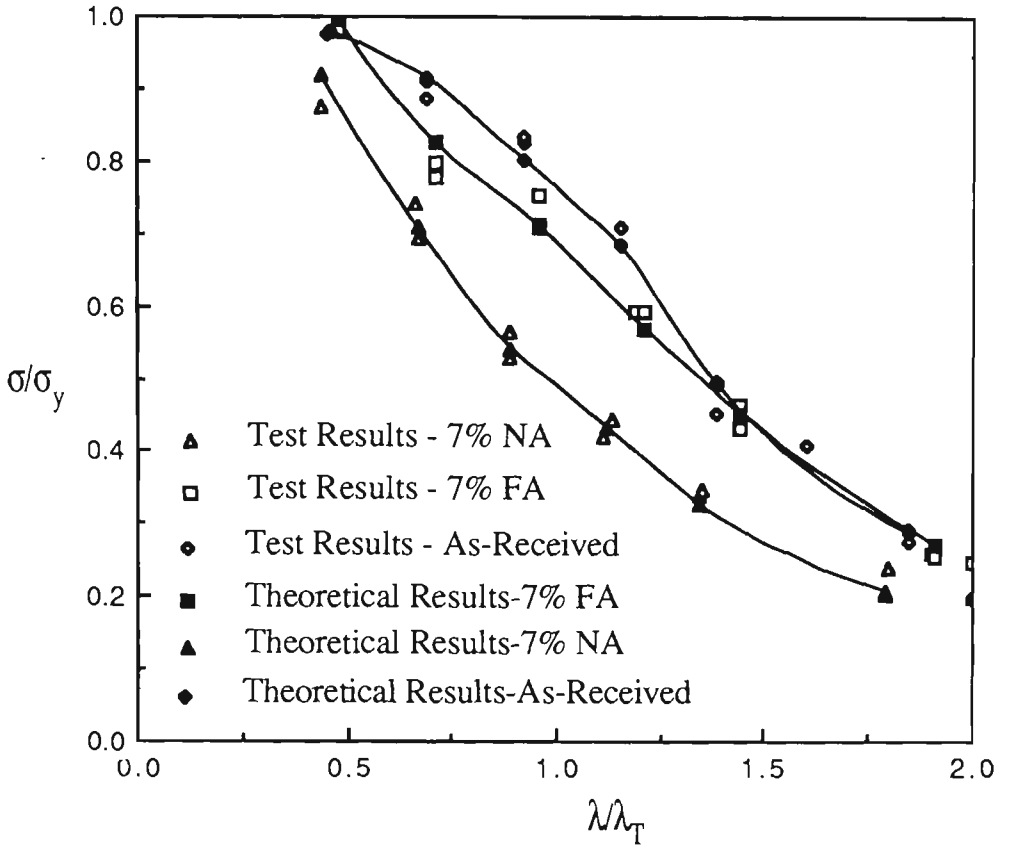

Fig.6.32 Comparison of Theoretical and Experimental Maximum Loads As-Received and 7% Prestrained

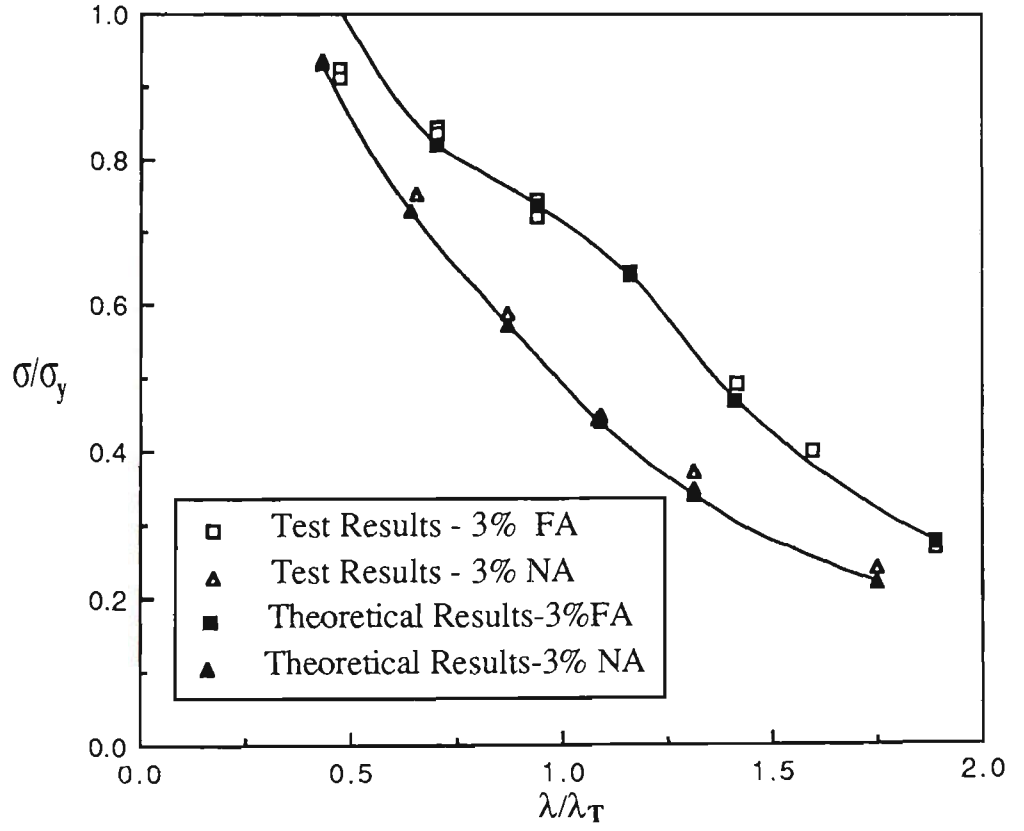

Fig.6.33 Comparison of Theoretical and Experimental Maximum Loads 3% Prestrained

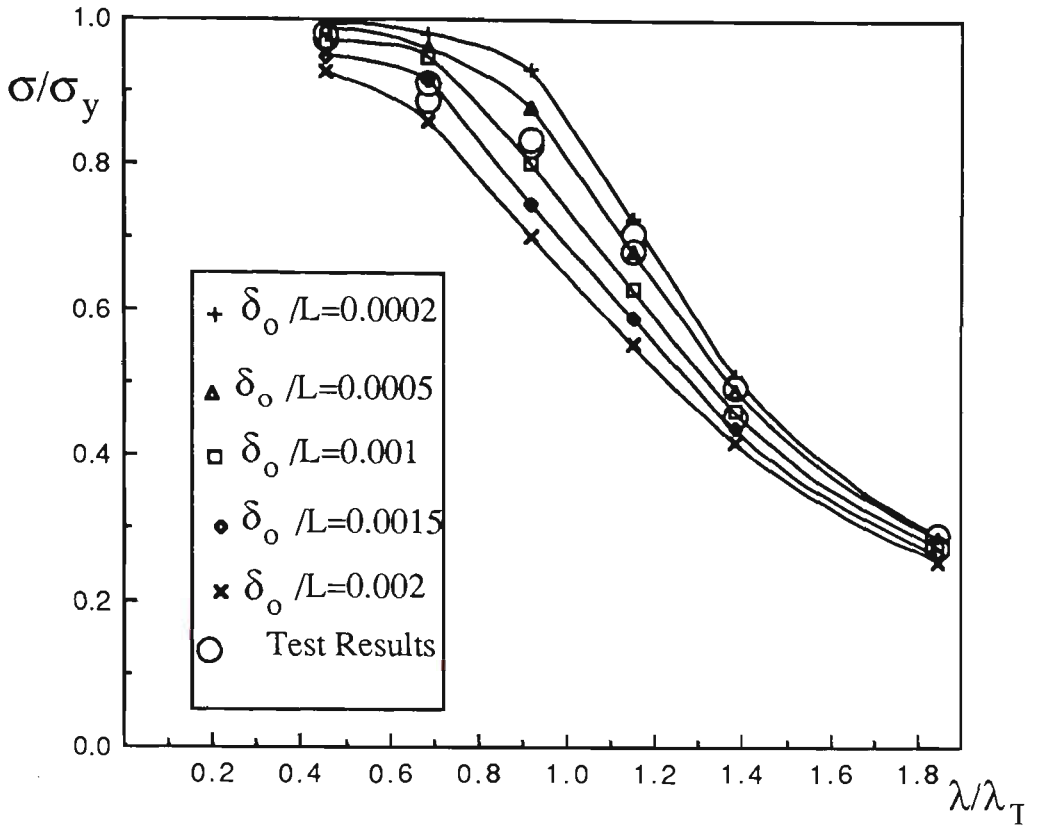

Fig.6.34 Theoretical Results with Different Initial Imperfections
As-Received

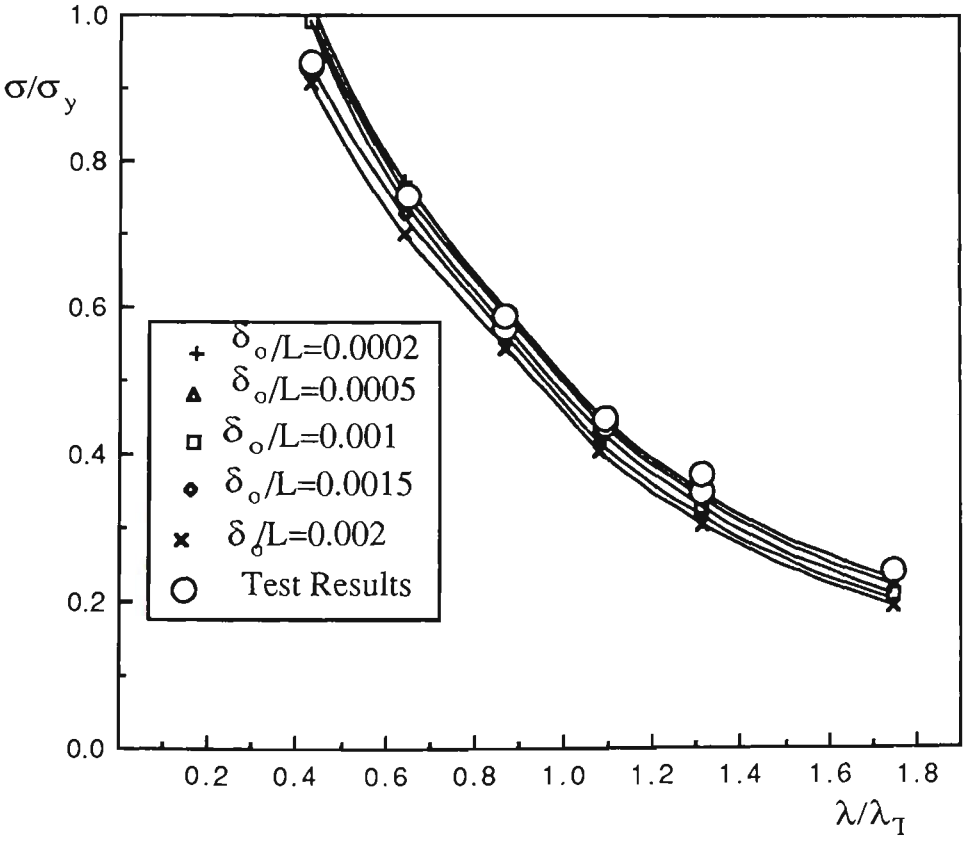

Fig.6.35 Theoretical Results with Different Initial Imperfections
Pre.3%, Unaged

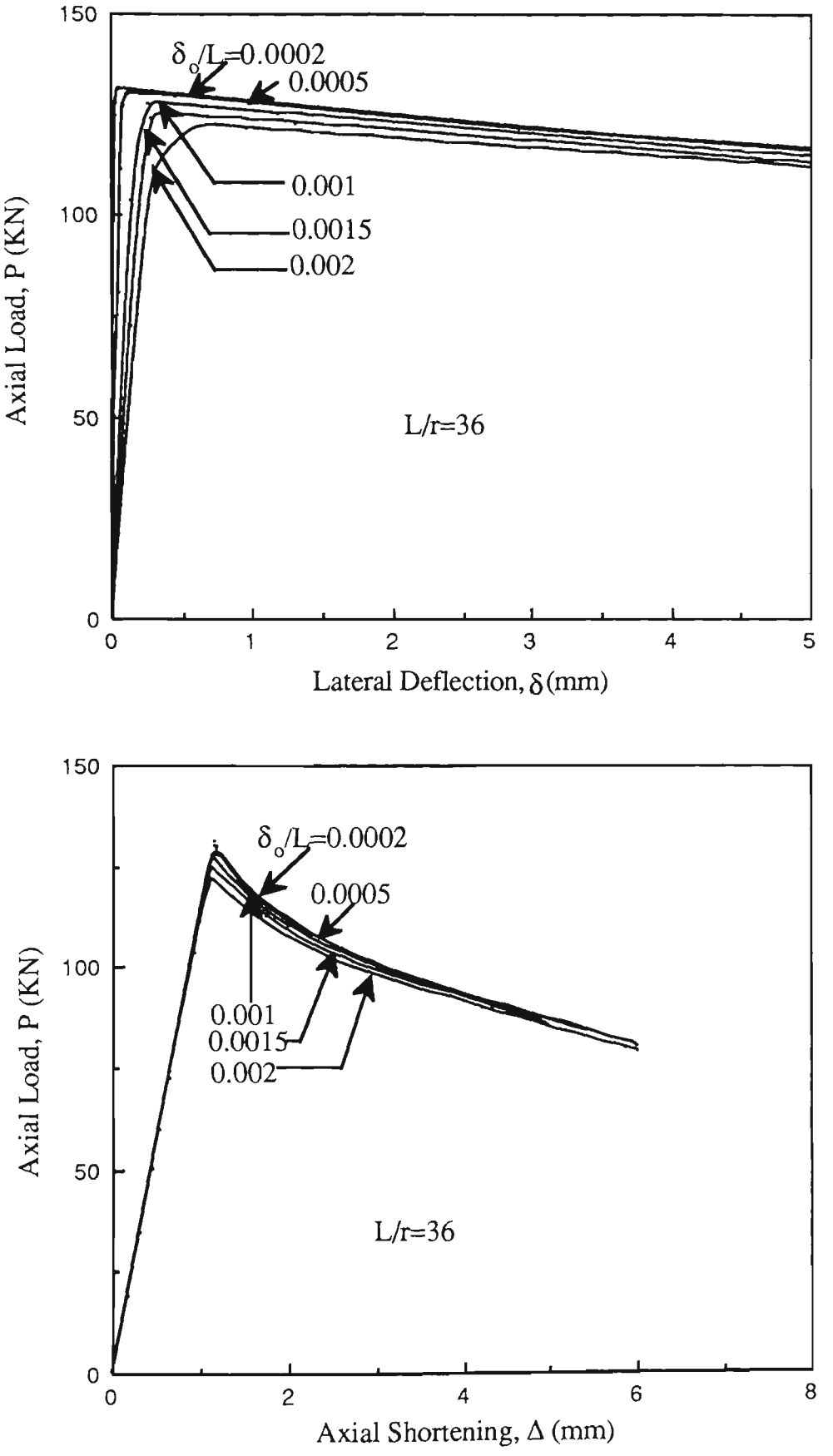

Fig.6.36 Theoretical Axial Load-Deflection Curves with Varying Initial Out-of-Straightness - As-Received Struts

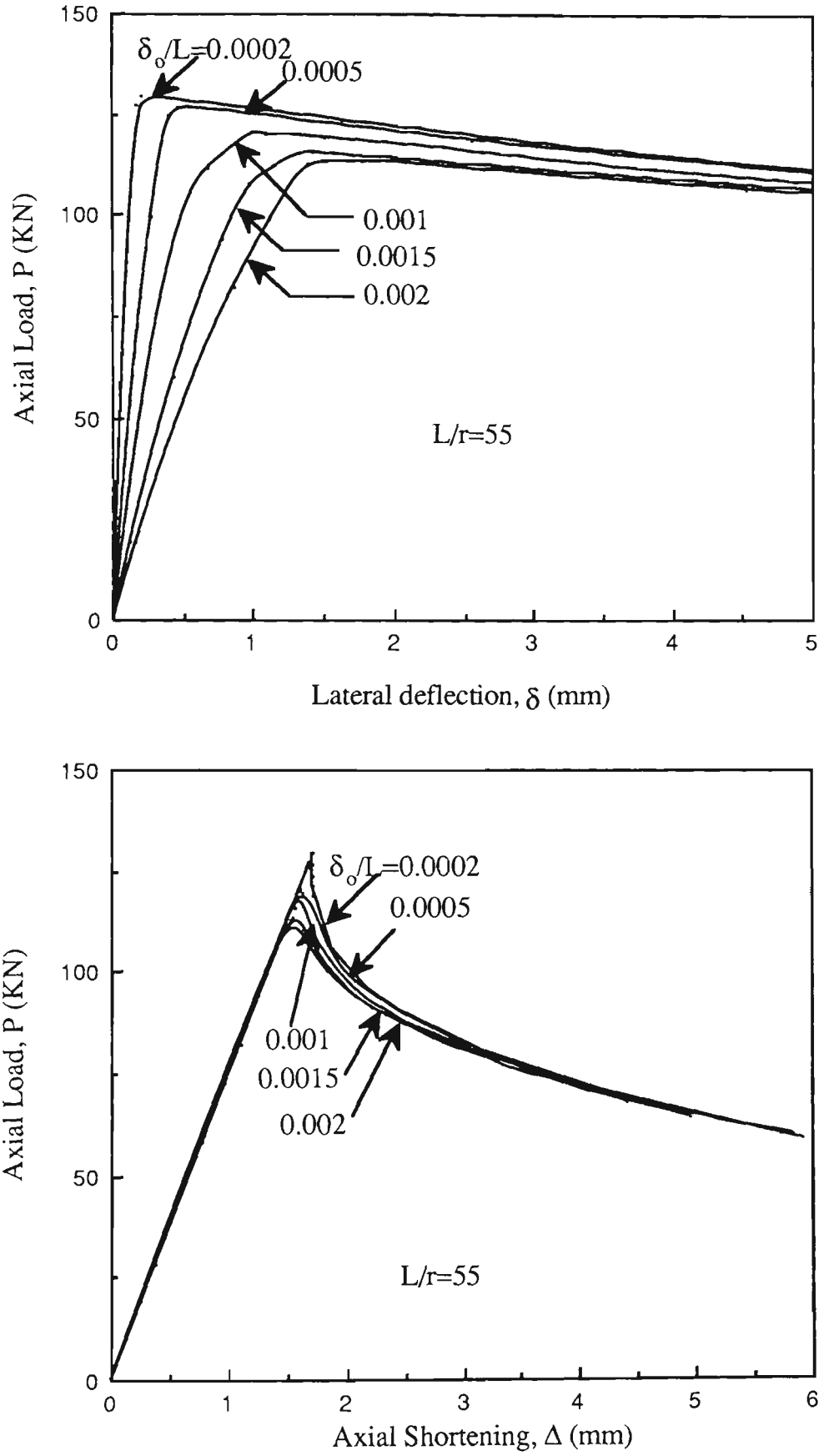

Fig.6.37 Theoretical Axial Load-Deflection Curves with Varying Initial Out-of-Straightness - As-Received Struts

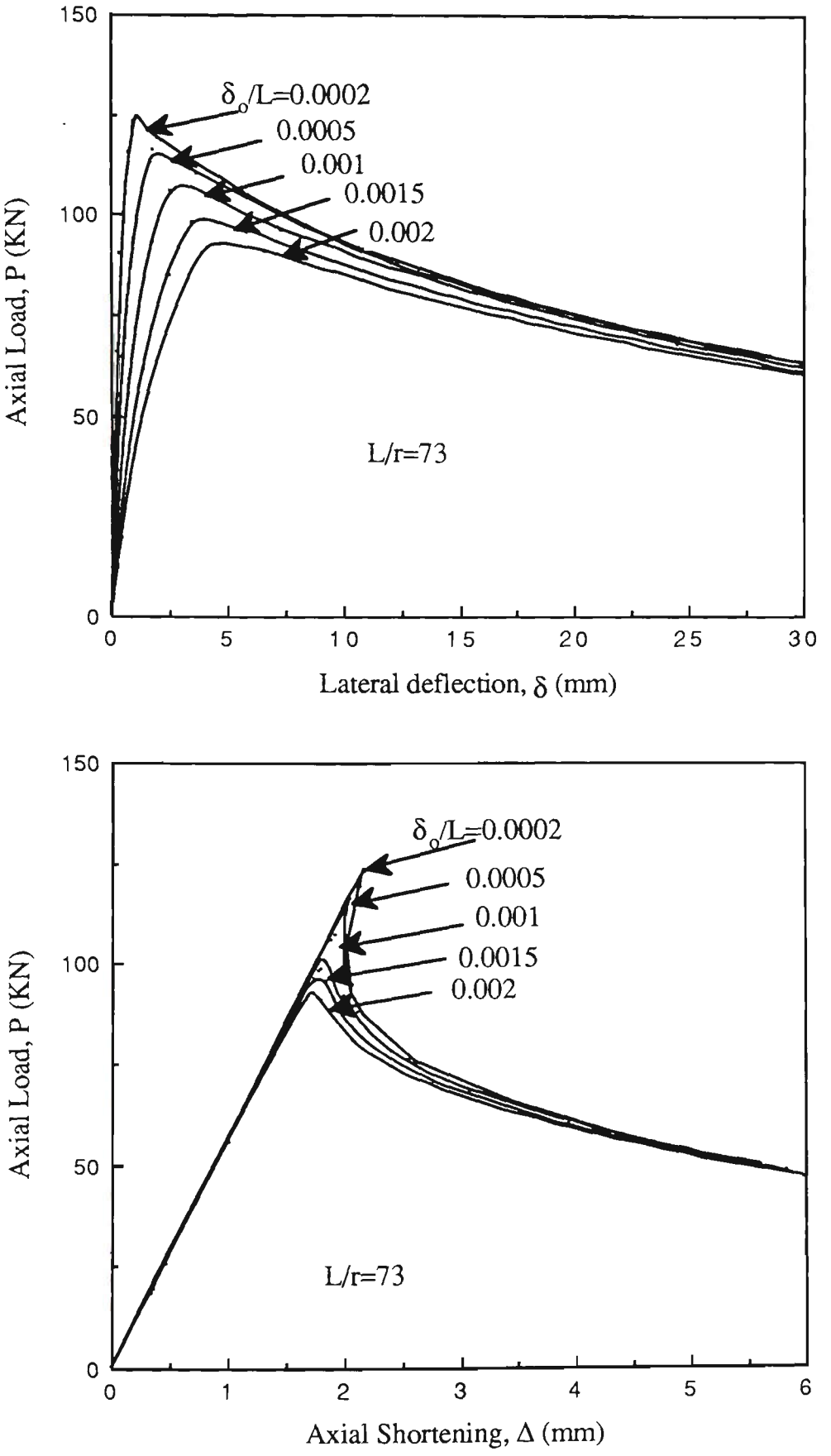

Fig.6.38 Theoretical Axial Load-Deflection Curves with Varying Initial Out-of-Straightness - As-Received Struts

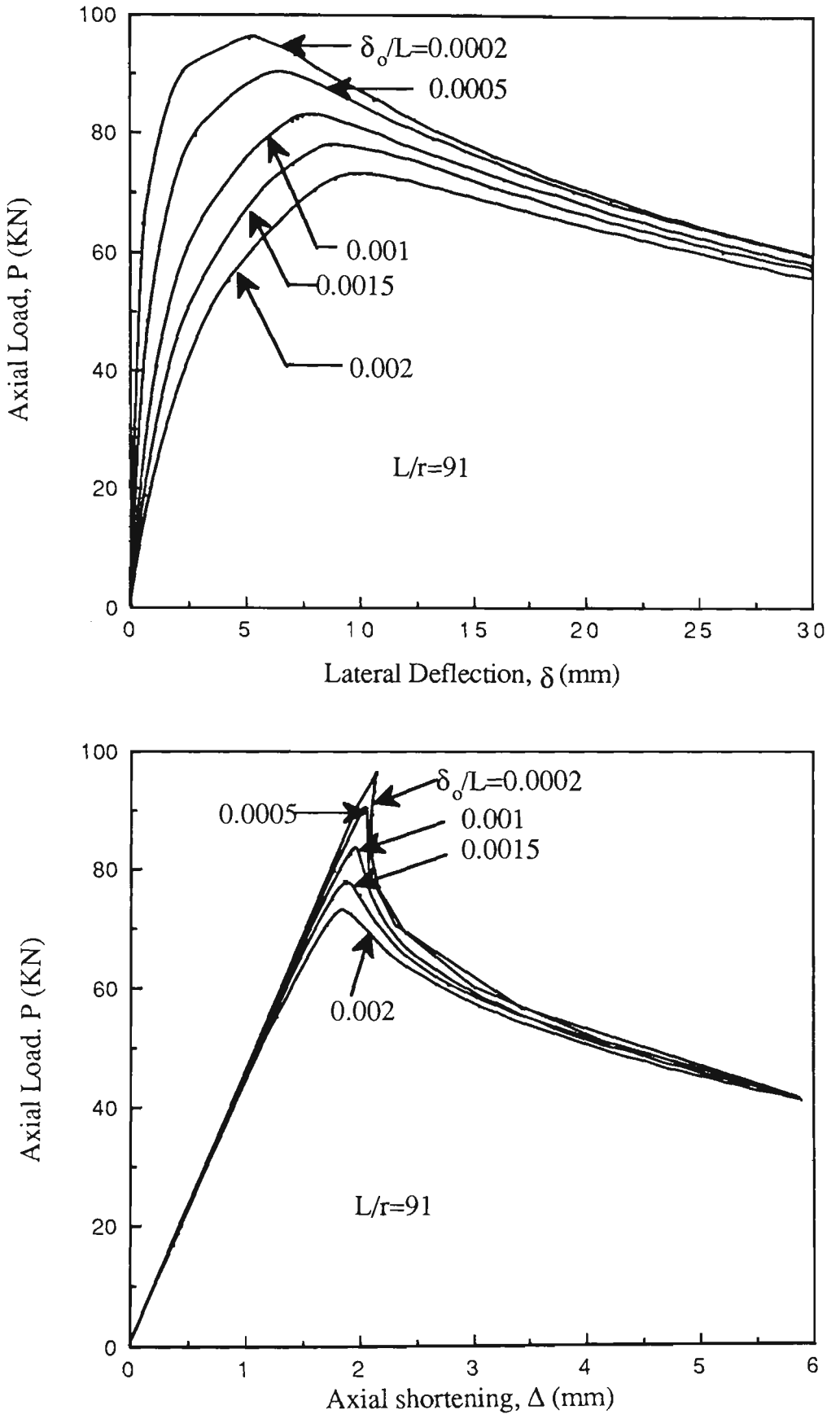

Fig.6.39 Theoretical Axial Load-Deflection Curves with Varying Initial Out-of-Straightness - As-Received Struts

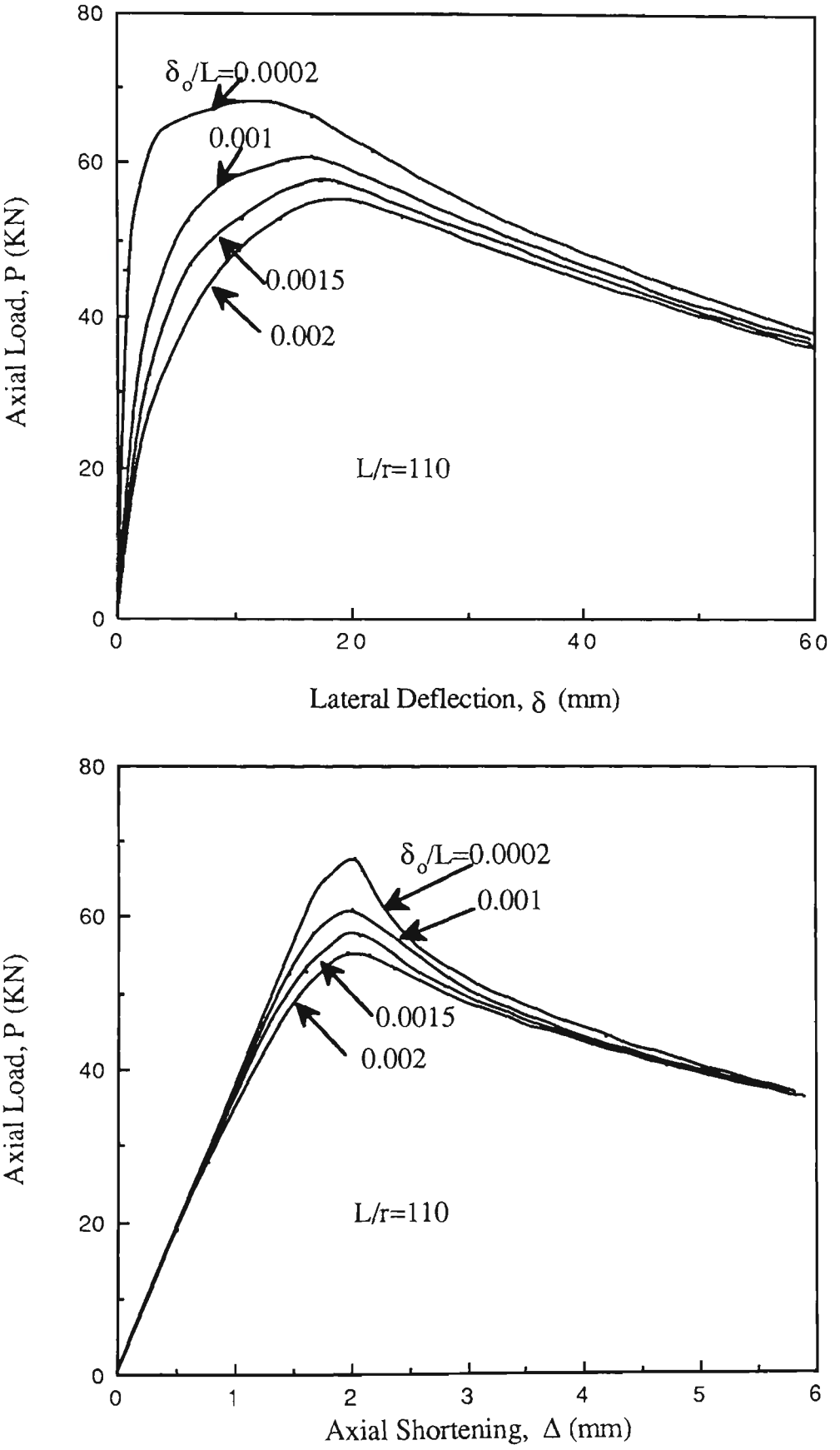

Fig.6.40 Theoretical Axial Load-Deflection Curves with Varying Initial Out-of-Straightness - As-Received Struts

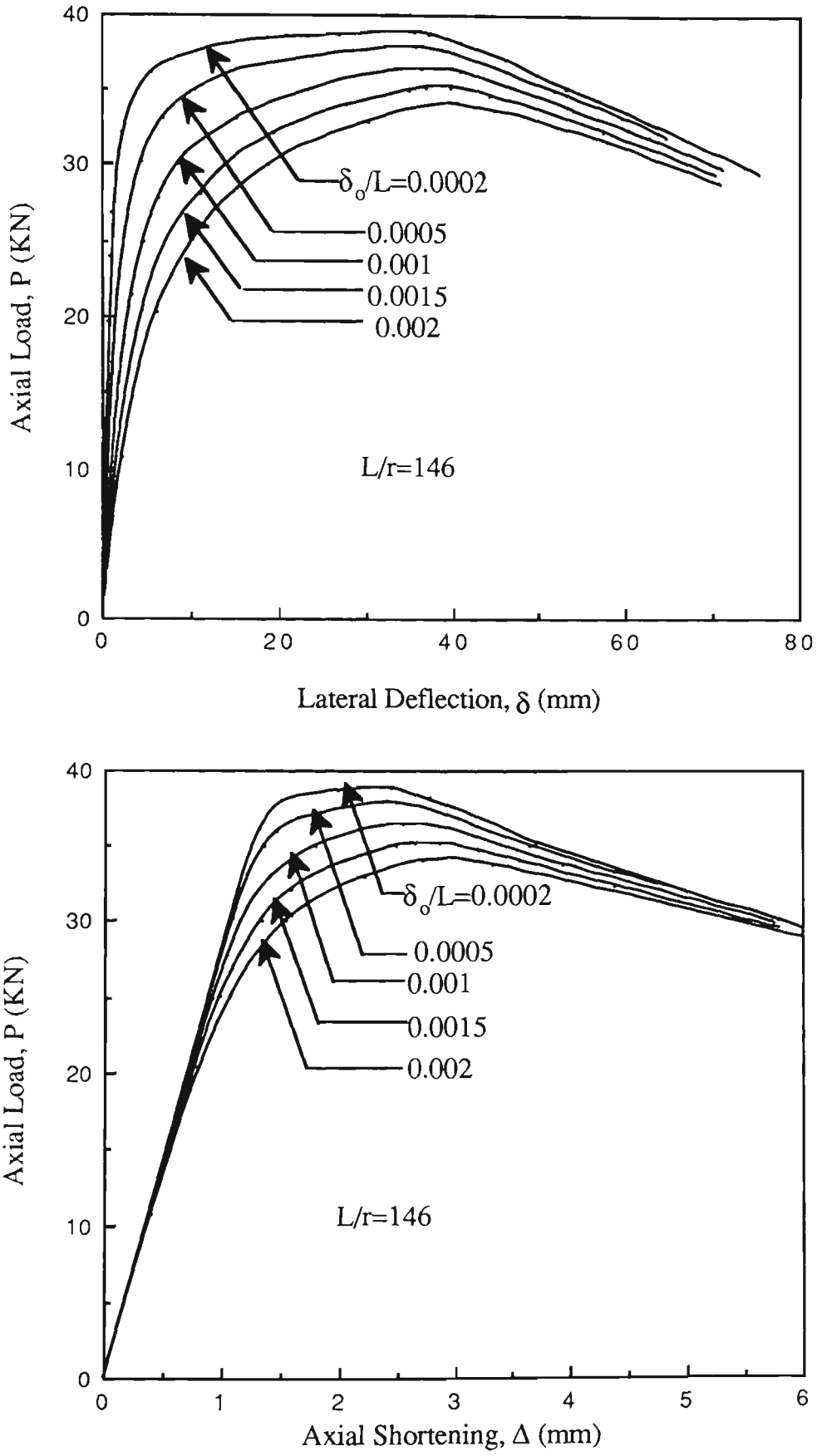

Fig.6.41 Theoretical Axial Load-Deflection Curves with Varying Initial Out-of-Straightness - As-Received Struts

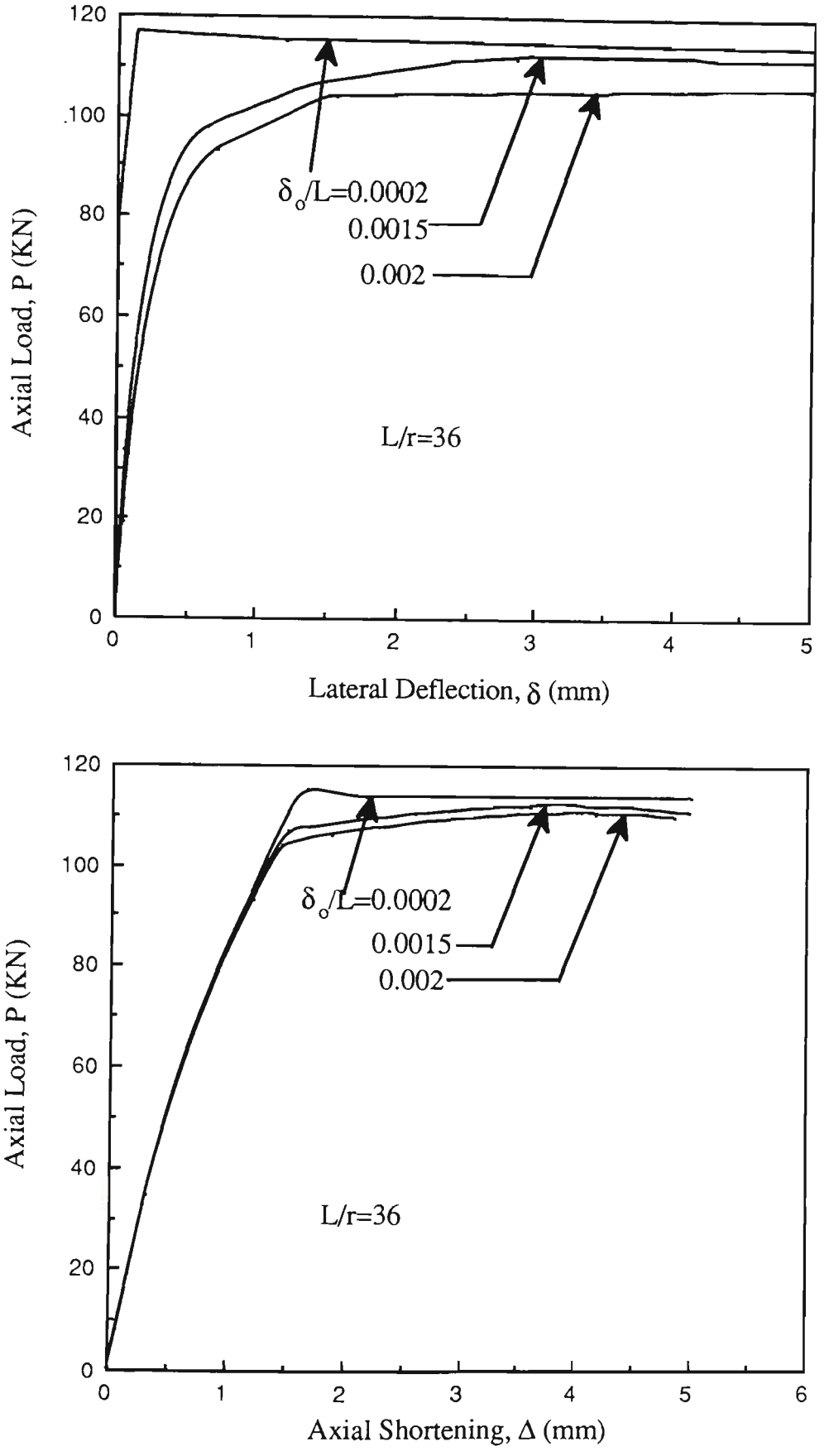

Fig.6.42 Theoretical Axial Load-Deflection Curves with Varying Initial Out-of-Straightness - 3% Prestrained Unaged Struts

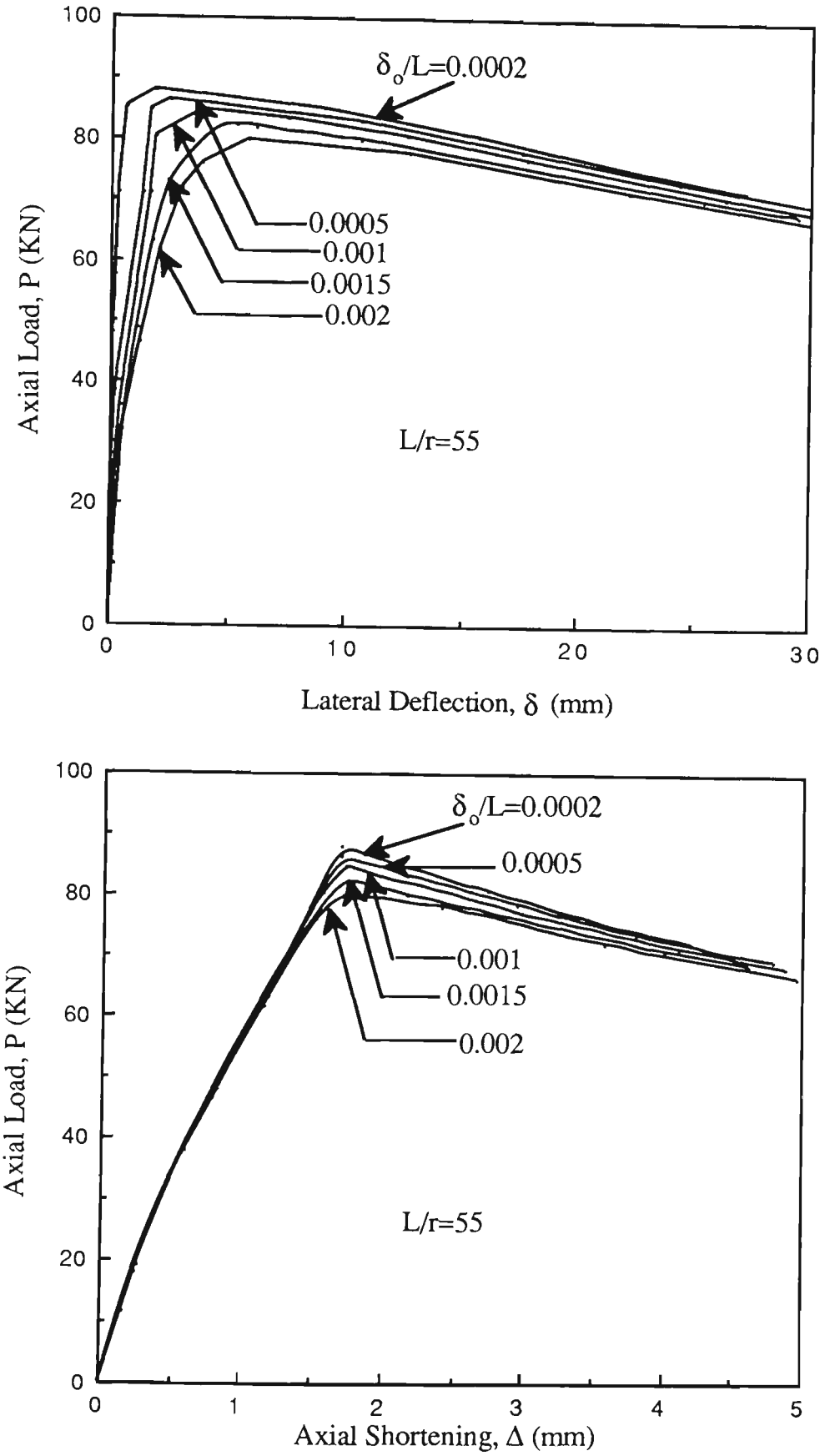

Fig.6.43 Theoretical Axial Load-Deflection Curves with Varying Initial Out-of-Straightness - 3% Prestrained Unaged Struts

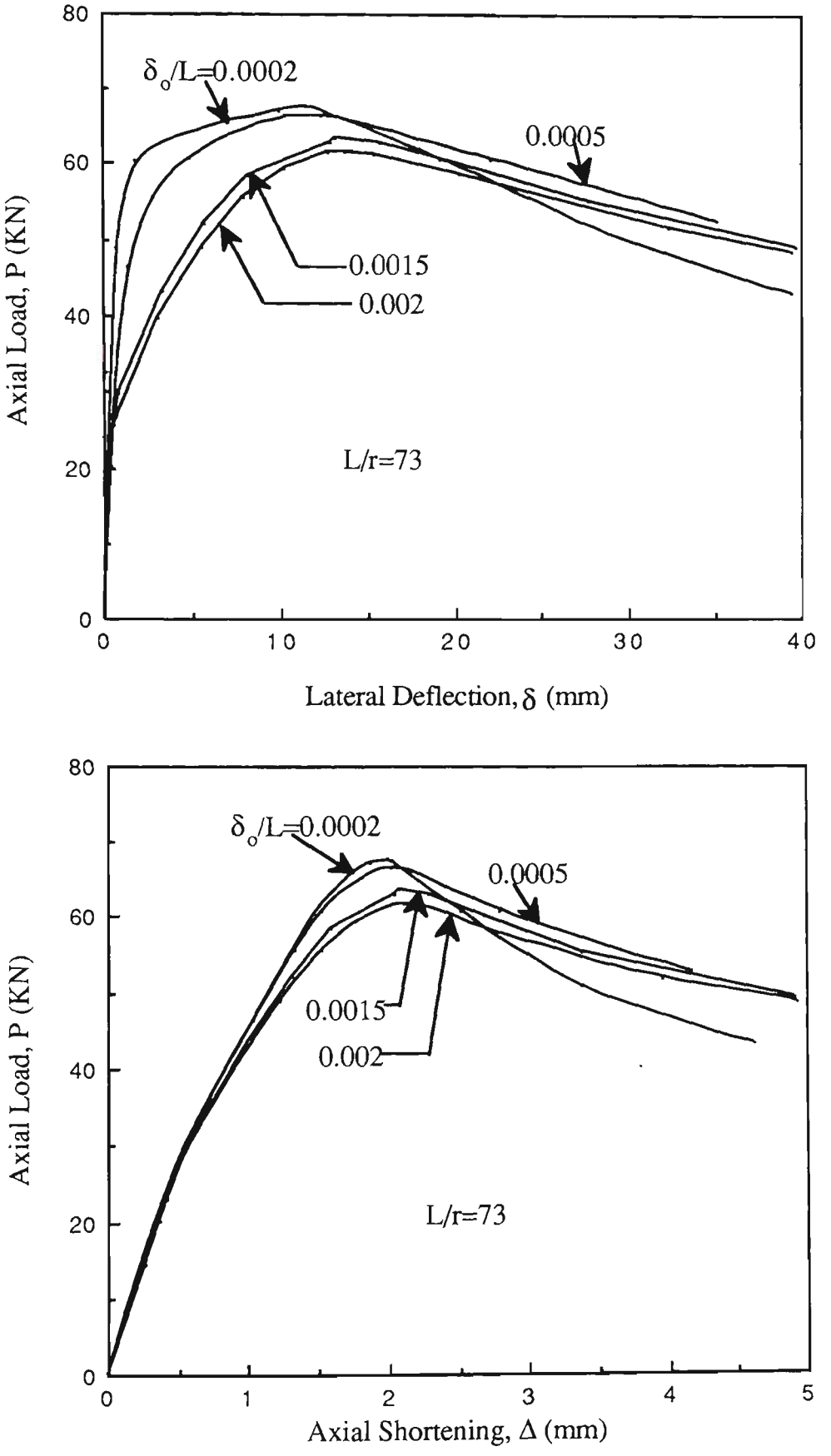

Fig.6.44 Theoretical Axial Load-Deflection Curves with Varying Initial Out-of-Straightness - 3% Prestrained Unaged Struts

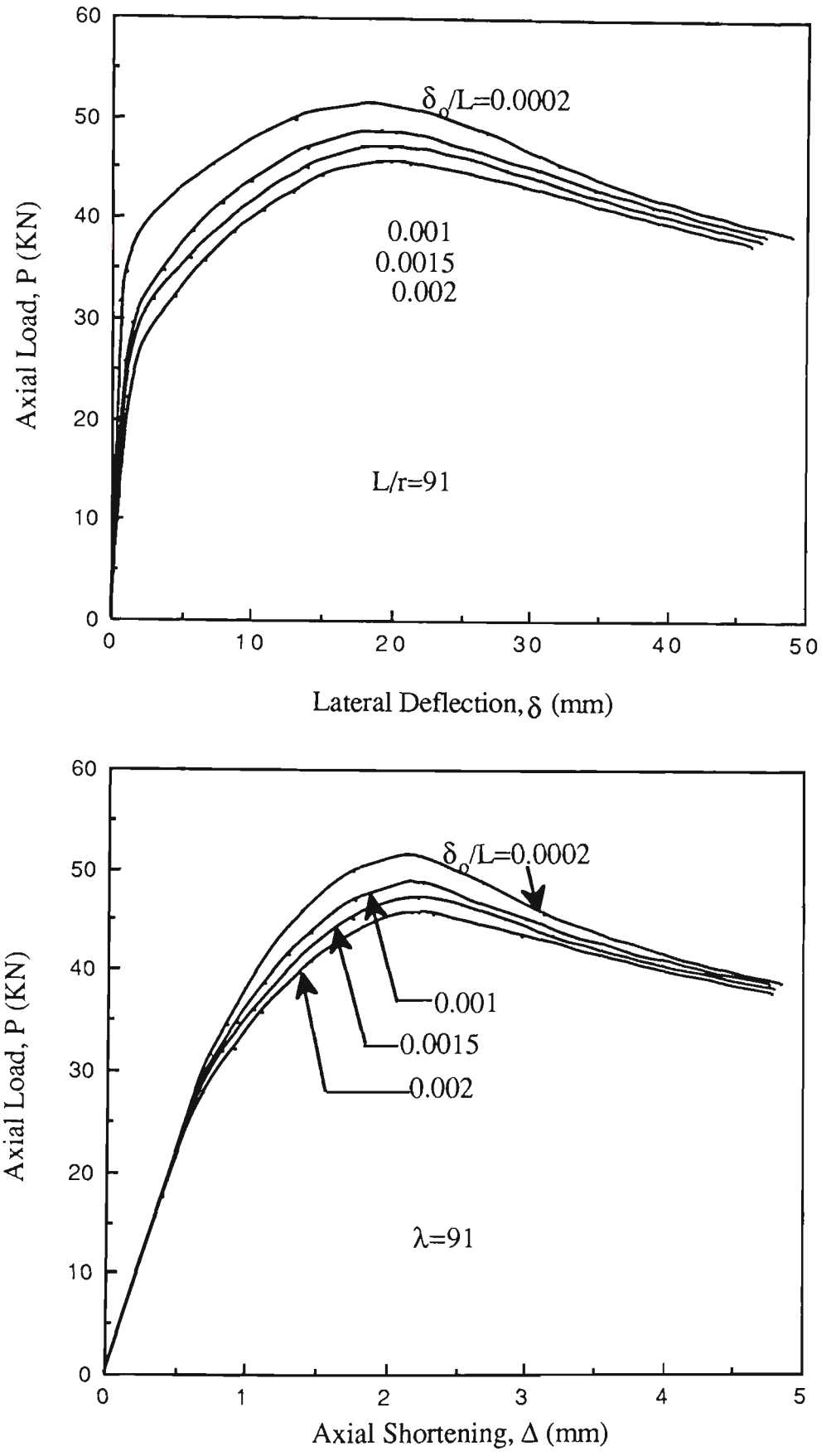

Fig.6.45 Theoretical Axial Load-Deflection Curves with Varying Initial Out-of-Straightness - 3% Prestrained Unaged Struts

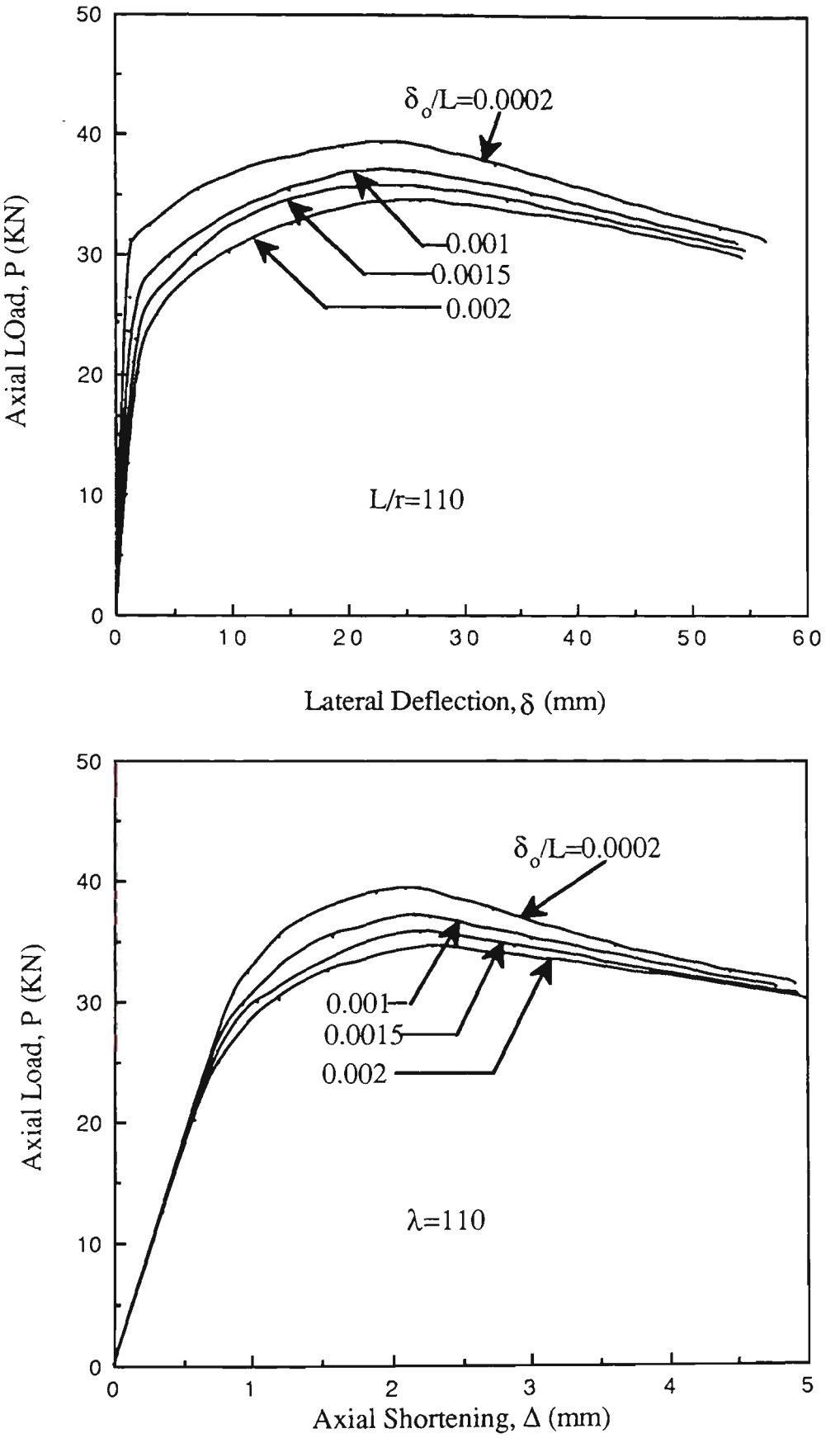

Fig.6.46 Theoretical Axial Load-Defelction Curves with Varying Initial Out-of-Straightness - 3% Prestrained Unaged Struts

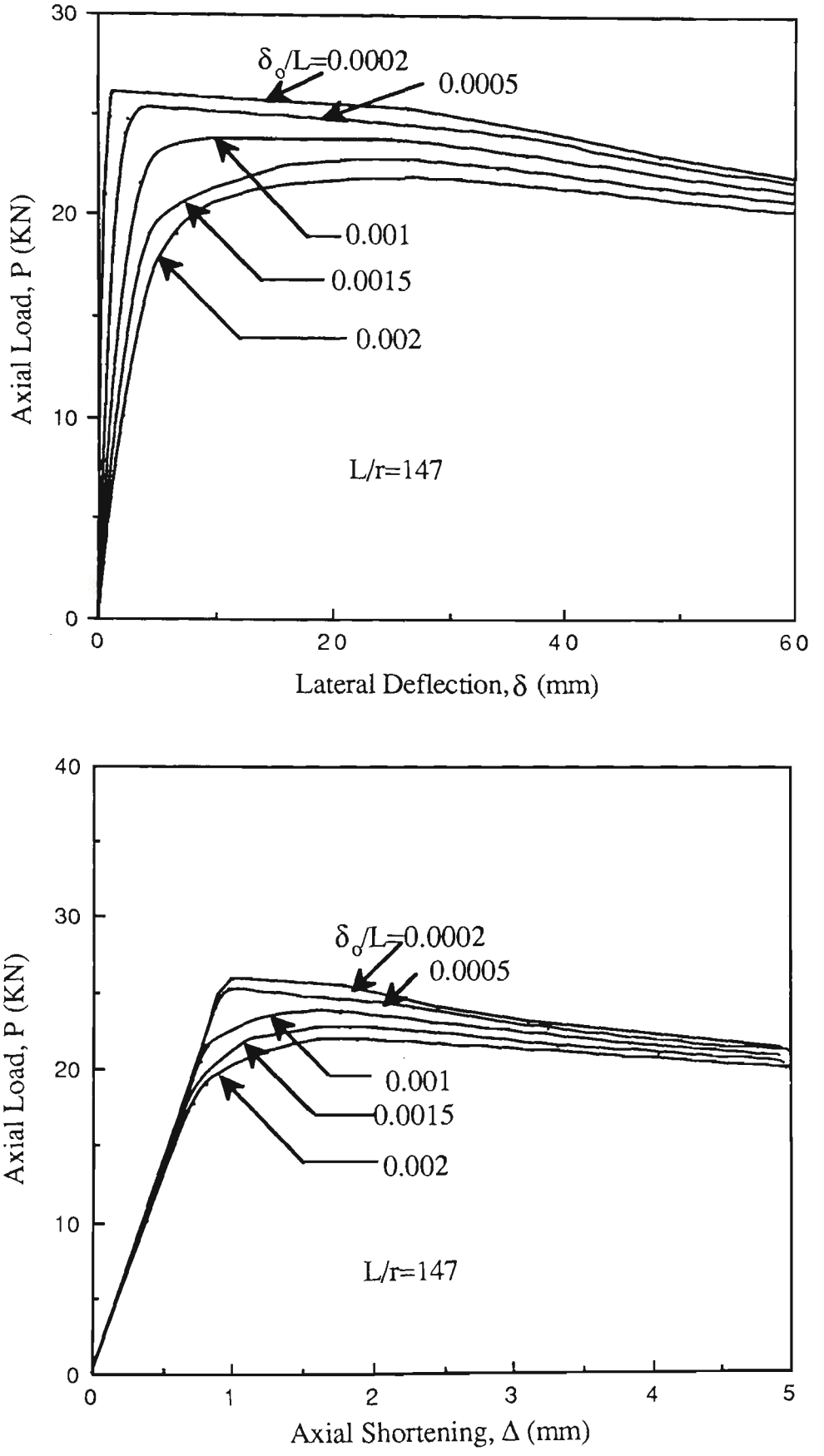

Fig.6.47 Theoretical Axial Load-Deflection Curves with Varying Initial Out-of-Straightness - 3% Prestrained Unaged Struts

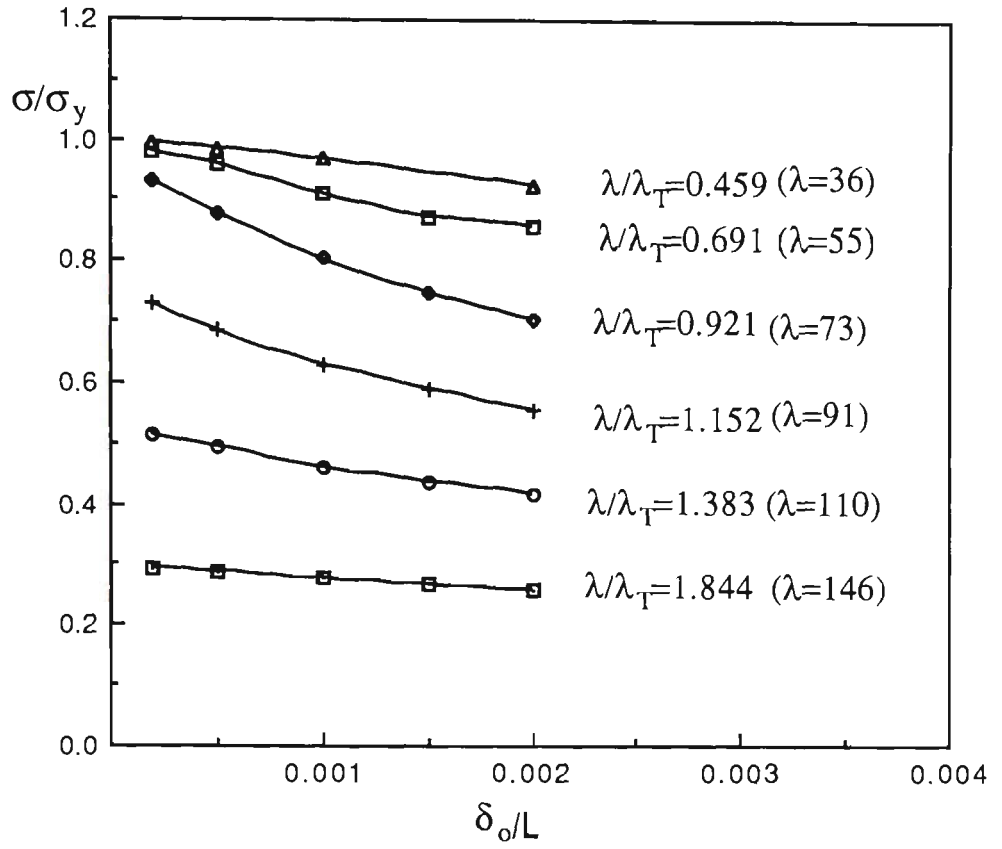

Fig.6.48 As-Received Struts

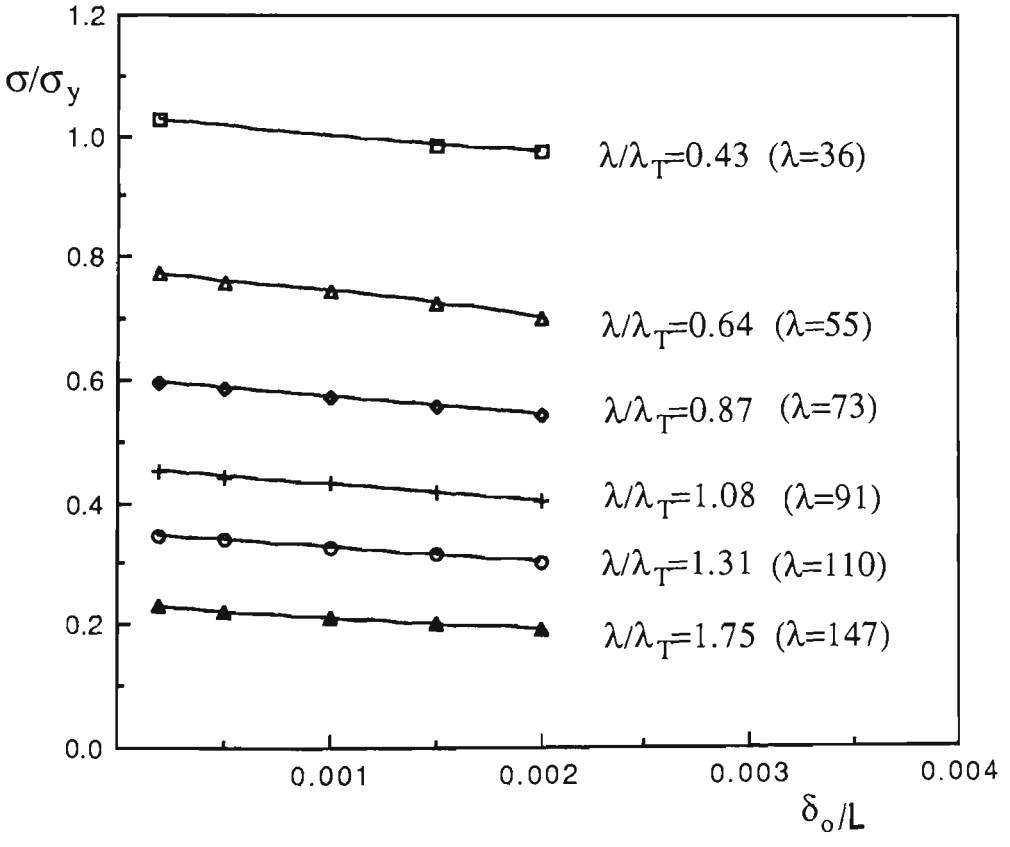

Fig.6.49 3% Prestrained Unaged Struts

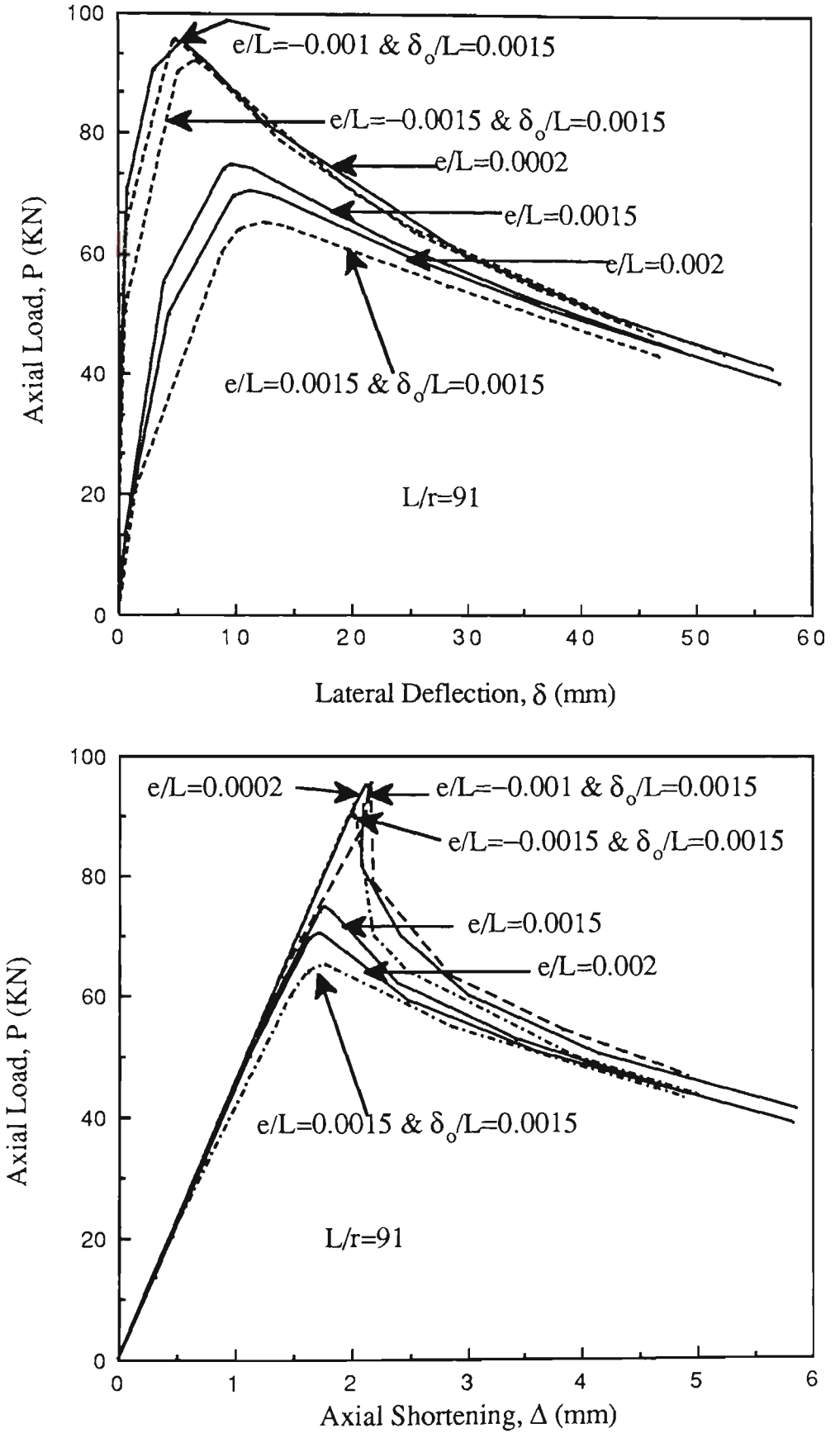

Fig.6.50 Theoretical Axial Load-Deflection Curves with Both Initial Out-of-Straightness and Load Eccentricity

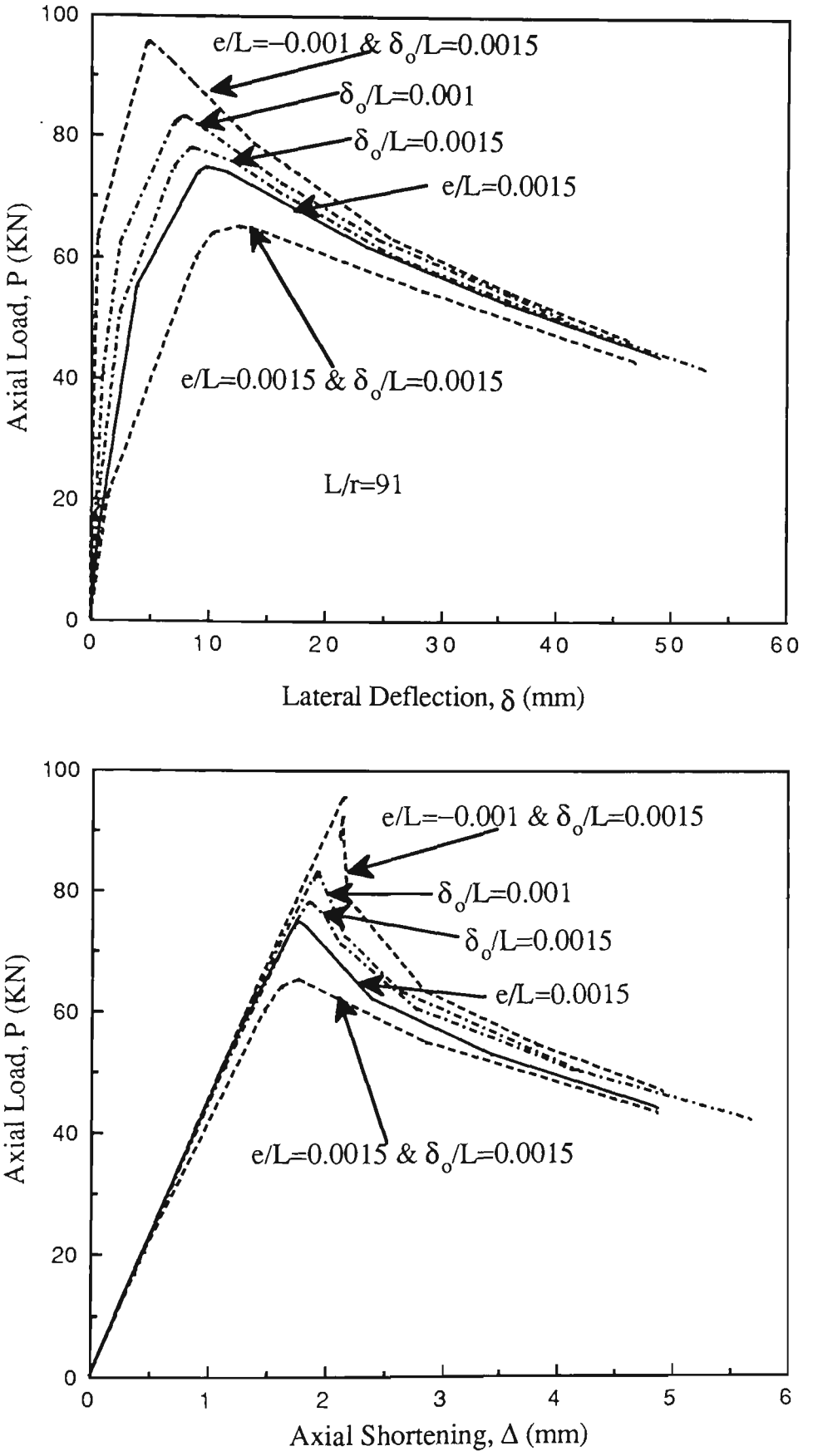

Fig.6.51 Theoretical Axial Load-Deflection Curves with Both Initial Out-of-Straightness and Load Eccentricity

CHAPTER SEVEN

CONCLUSIONS AND RECOMMENDATIONS

7.1 CONCLUSIONS

From the theoretical and the experimental studies outlined previously, the following results have been obtained and conclusions reached.

(a) A nonlinear finite element model for tracing the inelastic pre- and post-buckling load-deformation path of tubular struts has been developed. The analysis accounts simultaneously for both the geometrical and material nonlinearities. The influence of strain-unloading is included. In particular, the model takes into account a generalised stress-strain relationship and the influence of strain hardening. Several stress-strain relationships of the material are assumed, and these are a bilinear curve, a trilinear curve or a quadrilinear curve corresponding to as-received material, material that is prestrained in tension and fully-aged, or material that is prestrained in tension and unaged, respectively. In the analysis, the cross-section of the element is divided into a finite number of elementary areas. Allowance is made for the shift of the centroid and the rotation of the principal planes. The structure tangent stiffness matrix is obtained by using a series of transformation matrices to update the element geometry. A so-called arc-length iterative numerical procedure is combined with a modified Newton-Raphson method to obtain a solution to the incremental equations of equilibrium.

(b) The procedure has been applied to trace out the inelastic load-deflection paths of pin-ended struts with varying slenderness ratios and initial geometrical imperfections for both as-received and prestrained struts.

(c) Theoretical curves have been established defining the effects of initial imperfections both within and outside normal design tolerances, on the strut load capacities and the post-buckling behaviour. Theoretical results obtained for an elastic ideally-plastic stress-strain curve compared very well with available analytical results, such as those obtained from a commercial computer package and the other workers.

(d) The initial out-of-straightness is also considered in conjunction with variations in loading eccentricity. Cases where the initial out-of-straightness and eccentricity for load are in same the directions ('positive' eccentricity) and in the opposite directions ('negative' eccentricity) are investigated. It is found that the effect of the 'negative' eccentricity is to raise the load level; and the effect of the 'positive' eccentricity is to reduce the load level. However, after the peak, the loads of the struts with 'negative' eccentricity falls off rapidly and the load-deflection paths tend to those for the cases where the initial out-of-straightness and loading eccentricity are positive.

(e) By comparing the influence on ultimate load carrying capacity of the Bauschinger effect with that due to initial imperfections, it has been found that the smaller the initial imperfections, the more significant the influence of the Bauschinger effect. In the range of initial imperfections considered herein, the Bauschinger effect is more dominant.

(f) As the three stress-strain relationships of the steel assumed with respect to the as-received, prestrained in tension and fully-aged, and prestrained in tension and unaged material, consider the influence of strain aging, strain hardening and the Bauschinger effect, the difference in load capacities for the as-received and the prestrained struts is clearly seen. All the prestrained struts have lower capacities than the corresponding as-received struts. This loss of load capacity is due to the Bauschinger effect on load reversal . Strain aging reduces this reduction.

(g) The experimental work followed the earlier investigations of tubular strut behaviour with variable influences of strain aging, strain hardening and the Bauschinger effect (Morgan and Schmidt, 1985), that was confined to prestrains not more than 7% and differentiated between unaged and fully-aged material. The influence of strain aging is clearly seen. To furnish basic data in the elastic and inelastic ranges, material tests were conducted under tensile and compressive loading, including the above effects. The results showed that the reduction of material strength due to the Bauschinger effect on strain reversal occurred for all the tensile prestrained and unaged tubes, and the Bauschinger effect was interactive with both strain aging and strain hardening. The influence of strain aging on Bauschinger loss was significant. It should be observed that this result is true for rimming (ERW tube) and semi-killed steel (HFW tube, Morgan and Schmidt, 1985) . The loss should be more significant for fully-killed steels which display virtually no strain aging capacity. All of the factors mentioned affect the tangent modulus significantly, which in turn leads to a significant influence on the load capacity of struts.

(h) In order to determine the influence of strain aging, strain hardening, the Bauschinger effect and residual stresses on strut load capacity, 85 pin-ended steel tubular strut tests have been carried out under different conditions. To investigate

the influence of the residual stresses set up during the tubemaking process on the steel tubular strut capacity, tests on stress-relief-annealed tubes were performed on a total of 16 specimens.

(i) The strut test results showed that the combined influence of strain aging, strain hardening and the Bauschinger effect have a significant effect on strut load capacity. The Bauschinger effect plays a dominant role in the test results referred herein, with load capacity reduction up to 38%. Strain aging was seen to be more significant than strain hardening for the rimming steel used (Strain hardening ratio, SHR=1.15) in enhancing the capacity of the prestrained struts.

(j) On the basis of the least-squares criterion, regression analyses were used to provide an unbiased trend in the strut test results.

(k) The test results of 92 tubular steel pin-ended struts (including tests conducted by Morgan and Schmidt, 1985) under different conditions have been studied by statistical analysis. The significant influence of strain aging, strain hardening and the Bauschinger effect on strut load capacity is investigated by applying a two-way analysis of variance test. The results of statistical analyses give added strength to the observations made earlier. That is, the three material effects mentioned exercise a significant influence on strut load capacity for both the rimming steel (SHR=1.15) and the semi-killed steel (SHR=1.64) used. The Bauschinger effect plays a dominant role in reducing strut load capacity, while strain aging has a significant influence on increasing load capacity.

(l) A comparison is made between the observed strut load capacities and the tangent modulus predictions. It is found that the agreement is reasonable, highlighting the significance of the loss of modulus associated with strain reversal.

In general, however, the tangent modulus calculation slightly underestimates the observed load capacity in the smaller slenderness ratio range and overestimates it in the larger range.

(m) The experimental results are also compared with the current column design curves from ECCS, SSRC and existing and proposed Australian column curves. It is found that for struts that are prestrained in tension and unaged, even the bottom curve of ECCS, curve 'c' overestimates the ultimate strength in the generally commercially viable range of column slenderness. The current column design curve for the strength of axially loaded columns in the existing Australian Steel Structures Code AS1250-(1981) is conservative for the as-received struts and the struts that are prestrained in tension and fully-aged, but unsafe for struts that are prestrained in tension and unaged. The simplified approximation to the SSRC column curves proposed by Rotter (1982), using the derived modifying factors to obtain any number of intermediate curves from the central reference curve (corresponds approximately to SSRC curve 2), is found to provide a flexible and easy to apply alternative to the existing column curve formulations.

(n) By comparing the theoretical results with the experimental results of as-received struts and the struts that are prestrained in tension both fully-aged and unaged, it is shown that the developed theoretical model can accurately predict the experimental maximum loads and the post-buckling load-deformation paths of steel tubular struts.

(o) The significant post-buckling load capacities of steel tubular struts are important in consideration of the overall ultimate load capacities of large span space truss systems. Even if a few members have failed, those failed members

still possess significant residual load-bearing capacity until an overall collapse of a space truss system occurs.

(p) The results from the research are of relevance to a designer concerned with steel structures where elements may be cold formed during the fabrication and / or erection process. Under ultimate load conditions for such structures, members that were initially strained inelastically in tension may be subjected to compressive loading. Consequently, the material effects discussed herein will influence greatly the response of the structure. If the beneficial effects of strain aging are to be relied upon, then the designer would need to ensure that a rimmed or semi-killed steel is used, so that there would not be a serious deterioration of the ultimate load capacities of the struts. A designer needs to aware of these effects, as does the construction engineer who may be tempted to repair damaged members by cold straightening.

(q) The work indicates the potential dangers of utilizing, for struts, material that has been prestrained in tension in order to increase its yield point, without paying due regard to the associated reduction in tangent modulus upon strain reversal. Otherwise the significant loss in reduction of strut load capacity may be missed. Careful consideration needs to be given to the factors discussed, especially when utilizing structural sections formed by new or modified manufacturing processes. This caution is needed as the strength of such sections may be judged on tensile yield stress as the only relevant material property.

7.2 RECOMMENDATIONS FOR FUTURE WORK

The theoretical and experimental work completed has been confined to the pin-ended tubular struts which are prestrained in tension, with circular cross-sections.

More and more modern structures use arched chords in truss systems (cold formed or hot formed). In such cases, the arched compressive chords which have been prestrained in a bow shape may be subject to tension on the top fibre and compression on the bottom fibre of the chord. The state of the stress distribution and the deformation of these struts which are prestrained in flexure becomes more complicated than those prestrained in pure tension. When the chords are under axial loading the Bauschinger effect occurs at that part of the cross-section in which the tensile strains have been occurred, whereas the other part of the cross-section in which the compressive strains have occurred will experience the influence of strain aging and strain hardening. The combined influence of these effects on the load capacity of struts which are prestrained in this way is unclear at present.

It is therefore recommended that the theoretical model developed herein be extended to handle this more complicated problem. It is also suggested that further material and strut tests be performed in a continuing study into the influence of strain hardening, strain aging, and the Bauschinger effect on load capacity of struts which are prestrained inelastically in flexure.

REFERENCES

Abel, A. and Muir, H.(1972) " A New Look at the Bauschinger Effect ". Metals Australia; Sept., pp.267-271.

Abel, A. and Muir, H.(1972) "The Bauschinger Effect and Discontinuous Yielding". Philosophical Magazine.Vol.26, No.2, Aug., pp.489-504.

Baird, J.D.(1963) " Strain Aging Steel--A Critical Review ". Part I; Iron and Steel, May , pp.186-192. Part II; Iron and Steel, July and Aug., pp.400-405.

Bathe, K.J. and Dvorkin, E.N.(1983) " On the Automatic Solution of Nonlinear Finite Element Equations ", Vol.17, No.5-6, pp.871-879.

Belvin, W.K.(1984) " Analytical and Experimental Vibration and Buckling Characteristics of a Pretensioned Stayed Column", J. Spacecraft, Vol.21, No.5, Sep.-Oct., pp456 - pp462.

Bergan, P.G. (1978) " Solution Techniques for Non-Linear Finite Element Problems", Int.J.for Numerical Methods in Engineering, Vol.12, pp.1677-1696.

Bouwkamp, J.G. (1975) "Buckling and Post-Buckling Strength of Circular Tubular Sections ", Proceedings of Seventh Annual Offshore Technology Conference, Houston, Texas, May.

Bradford, M.A., Bridge, R.Q., Hancock, G.J., Rotter, J.M. and Trahair, N.S.(1987) " Australia Limit State Design Rules for the Stability of Steel

Structures", Proceedings of the International Conference on Steel and Aluminium Structures, Cardiff, UK, 8-10 July.

Camotim, D. and Roorda, J. (1985) " On the Effect of Residual Stresses in the Plastic Building of Columns - A Model Study". Transactions, Canadian Society for Mechanical Engineering, Vol.9, Part 4, pp.210-223.

Chajes, A., Britvec, S.J.,and Winter, G.(1963) "Effects of Cold-Straining on Structural Sheet Steels." Proc.ASCE, Journal of Structural Division, Vol.89, No.2, April , pp.1-32.

Chan, S.L. and Kitipornchai, S.(1986) "Inelastic Post-Buckling Behaviour of Tubular Struts", Research Report , Dept. of Civil Eng., University of Qld., CE75.

Chan, S.L.(1988) "Geometric and Material Non-linear Analysis of Beam-columns and Frames Using the Minimum Residual Displacement Method", International Journal for Numerical Methods in Engineering, Vol.26, pp.2657-2669.

Chan, S.L. (1989) " Inelastic Post-buckling Analysis of Tubular Beam-columns and Frames", Engineering Structures, Vol.11, pp.23-30.

Chen, W.F. and Atsutta, T. (1977) " Theory of Beam-Columns", Volume 2: Space Behaviour and Design. McGraw - Hill, N.Y..

Chen, W.F. and Han, D.J.(1985) "Tubular Members in Off-shore Structures", Pitman press, Bath.

Crisfield, M.A. (1981) " A Fast Incremental Iteration Procedure That Handles Snap-Through " Computer and Structures, 13, 55.

Dwight, J.B.(1975) " Adaption of Perry Formula to Represent the New European Steel Column-Curves" Steel Construction, Vol.9, No.1.

Freund, J.E.(1962) Mathematical Statistics, Prentice-Hall, Inc., Englewood Cliffs, N.J..

Gere, J.M. and Weaver, W.J. (1965) " Analysis of Framed Structures", Van Nostrand Reinhoold, New York.

Godfrey, G.B. (1962) " The Allowable Stresses in Axially Loaded Steel Struts". The Structural Engineer, Vol. 40, No.3.

Han, D.J. and Chen, W.F. (1983) " Behaviour of Portal and Strut Types of Beam-columns" , Engineering Structures, 5(1), pp.15-25.

Han, D.J. and Chen, W.F. (1983) " Buckling and Cyclic Inelastic Analysis of Steel Tubular Beam-Columns ", Engineering Structures, 5(2), pp.119-132.

Hasegawa, A., Liyanage, K.K. Noda, M. and Nishino, F.(1987) "An Inelastic Finite Displacement Formulation of Thin-Walled Members", Structural Eng./ Earthquake Eng., Vol.4, No.2, 269s-276s, October, Japan Society of Civil Engineers (Proc. of JSCE No.386/I-8).

Hays, C.D.Jr. and Santhanan, T.K.(1979) " Inelastic Section Response by Tangent Stiffness ", Journal of the Structural Division, ASCE, 105 (ST7), pp.1241-1259.

HP Manuals : Operating and Service Manual, System Voltmeter 3437A, Vol III; Operating and Service Manual, Digital Voltmeter 3456A, Vol III; 3497A, Main Frame, Installation and Service Manual, Vol III; Plug-in, Assemblies Service Manual; 1982.

Johnston, B.G. (1976) " Structural Stability Research Council Guide to Stability Design Criteria for Metal Structures", 3rd Ed., Wiley, New York.

Karren, K.W.,and Gohil, M.M.(1975) "Strain Hardening and Aging in Cold-Formed Steel." Proc.ASCE, Journal of Structural Division , Vol.101, No.1, Jan., pp.187-200.

Key, P.W. and Hancock, G.J. (1985)" Strength Tests of Cold Formed Square Hollow Section Columns", Metal Structures Conference, I.E.Australia, Melbourne.

Kitipornchai, S. and Chan, S.L. (1986) " Geometric Nonlinear Analysis of Asymmetric Thin-Walled Members", Research Report , Dept. of Civil Eng., University of Qld., CE73.

Kitipornchai, S., Al-bermani, F.G.A. and Chan, S.L. (1987) " Geometric and Material Nonlinear Analysis of Structures Comprising Rectangular Hollow Sections", Research Report , Dept. of Civil Eng., University of Qld., CE79.

Lu, L.W., Shen, S.Z., Shen, Z.Y. and Hu, X.R.(1983)"Stability Theory of Steel Structural Members", Beijing, China Building and Industry Publishing House.

Mendenhall, W. and Scheaffer, R.L.(1973) Mathematical Statistics with Applications. Duxnury Press, North Scituate, Massachusetts.

Morgan, P.R.,Schmidt, L.C. and Rhodes, W.A.(1984) "Material Effects on Mild Steel Strut Stability". Third Int. Conf. on Space Structures. Ed. H. Nooshin, Elsevier, London, pp. 388-393.

Morgan, P.R. and Schmidt, L.C.(1985) " The Influence of Material Effects on Tubular Steel Strut Capacity". RR/Strut/11/1985. Department of Civil Engineering, University of Melbourne.

Morgan, P.R. and Schmidt, L.C., (1986) "Strut Capacity after Repeated Tests to Failure ". Tenth Australasian Conf. Mech. Struct. and Materials, Univ. of Adelaide, Adelaide, Australia, August, pp.521-526.

Morgan, P.R. and Schmidt, L.C.(1986) "Material Effects and Tubular Steel Strut Capacity. " Proc.ASCE, Journal of Structural Engineering, Vol.112, No.10,Oct., pp.2299-2313.

MSC / Nastran, Application Manual, Vol.II, The Macneal - Schwendler Corporation Univac edition, edited by Terrard A. Joseph, April 1982.

Pascoe, K.J.(1971) "Strength of Cold-Formed Cylindrical Steel Plates." J.Strain Analysis, Vol.6, No.3 , pp.167-176.

Pascoe,K.J.(1971) "Directional Effects of Prestrain in Steel ." J.Strain Analysis, Vol.6, No.3 ,pp.181-189.

Paris, P.C.(1956) "The Bauschinger Effect on Columns", J. Applied Mech..

Pavlovic, M.N., and Stevens, L.K.(1981) "The Effect of Prior Flexural Prestrain on the Stability of Structural Steel Columns." Engineering Structures, Vol.3, No.2, April, pp.66-70.

Perry, S.H. and Chilver, A.H.(1976) "The Statistical Variation of the Buckling Strengths of Columns. " Proc.I.C.E., London , Vol.61, Part 2, March, 109-125.

Polakowski, N.K. and Ripling, E.J.(1966) " Strength and Structure of Engineering Material ", Prentic-Hall Inc..

Ramm, E. (1981) " Strategies for Tracing Nonlinear Responses Near Limit Points", In nonlinear Finite Element Analysis in Structural Mechanics (Edited by Wunderlich et al.), Soringer-Verlag, New York, pp.63-89.

Rhodes, J. (1987) " Cold Formed Steel Sections - State of the Art in Great Britain",
Proceedings of the International Conference on Steel and Aluminium Structures, Cardiff, UK, 8-10 July.

Riks, E.(1972) " The Application of Newton's Method to the Problem of Elastic Stability ", J.Appl. Mech., 39, pp1060-1066.

Riks, E. (1979) " An Incremental Approach to the Solution of Snapping and Buckling Problems", Int. J. Solids Struct., 15, pp529-551.

Rolfe, S.T., Haak, R.P.and Gross, J.H.(1968)"Effect of State-of-Stress and Yield Criterion on the Bauschinger Effect". Journal of Basic Engineering, Transactions of the ASME, Sept., pp.403-408.

Rotter, J.M.(1982) " A Simple Approach to Multiple Column Curves." Civil Engineering Transactions.

Saleeb, A.F. and Chen, W.F. (1981) " Elastic-plastic Large Displacement Analysis of Pipes", Journal of the Structural Division, ASCE, 107(ST4), pp.605-626.

Schmidt, L.C.and Morgan, P.R., (1984)"Influence of Tensile Prestraining on the Ultimate Load Capacity of Mild Steel Tubular Struts ". Ninth Australasian Conference Mechanics of Structures and Materials, Univ. of Sydney, Australia. Aug. pp.326-331.

Schmidt, L.C. and Morgan, P.R.(1986) " E_T For Tensile Prestrained Tubular Struts. " Proc. ASCE, Journal of Structural Engineering, Vol.112, No.5, May , pp.1115-1124.

Schmidt, L.C., LU, J.P. and Morgan, P.R.(1989) "The Influence on Steel Tubular Strut Load Capacity of Strain Hardening , Strain Aging and the Bauschinger Effect". 14, Journal of Constructional Steel Research, pp.107-109.

Schmidt, L.C., Lu, J.P. and Morgan, P.R. Material effects-statistics of steel tube strut , Submitted for publication.

Series 8000 Servo-Hydraulic Testing Systems, Operating Instructions, Instron Limited, Coronation Road, High Wycombe, Buckinghamshire, England, 1981. Operating and Service Manual, System Voltmeter 3437A Vol III; Operating and Service Manual, Digital Voltmeter 3456A Vol III; 3497A Main Frame, Installation and Service Manual, Vol III.

Smith, C.S., Kirkwood, W. and Swan, J.W. (1979) "Buckling Strength and Post-Collapse Behaviour of Tubular Bracing Members Including Damage Effects", Second International Conference on Behaviour of Off-Shore Structures, Imperial College, England, pp.303-326.

Smith, C.S., Somerville, W.L. and Swan, J.W. (1981) "Residual Strength and Stiffness of Damaged Steel Bracing Members", Proceedings of 13th Annual Offshore Technology Conference, Houston, Texas, May.

Standards Association of Australia (1981) "Steel Structures Code", AS1250, Sydney.

Sugimoto, H. and Chen, W.F. (1985) " Inelastic Post-Buckling Behaviour of Tubular Members", Journal of Structural Engineering, ASCE, 111(9), pp1965-1978.

Supple, W.J. and Collins, I. (1982) " Post-Critical Behaviour of Tubular Struts", Engineering Structures, 2(3),pp225-229.

Szilard, R. (1985) " Critical Load and Post-Buckling Analysis by FEM Using Energy Balancing Technique", Computers & Structures, Vol.20, No.1-3, pp277-286.

Taby, J. and Moan, T. (1981) "Theoretical and Experimental Study of the Behaviour of Damaged Tubular Members in Offshore Structures", Norwegian Maritime Research, No.2,pp26-33.

Toma, S. and Chen, W.F. (1983) " Post-buckling Behaviour of Tubular Beam-Columns", J.Struct.Eng., ASCE, 109,pp.1918-1932.

Wempner, G.A. (1971) " Discrete Approximations Related to Non-linear Theories of Solids", Int. J. Solids Struct., 7, pp.1581-1599.

Zienkiewicz, O.C. (1977) " The Finite Element Method", 3rd Ed., McGraw-Hill, New York.

APPENDICES

APPENDIX I DEFINATION OF MATRICES

Matrices [N1], [N2], [S1], [S2], [T1] and [T2] are defined as:

$$[N1] = \begin{bmatrix} \frac{6}{5L_e} & & \text{symm.} & \\ \frac{-1}{10} & \frac{2L_e}{15} & & \\ \frac{-6}{5L_e} & \frac{1}{10} & \frac{6}{5L_e} & \\ \frac{-1}{10} & \frac{L_e}{30} & \frac{1}{10} & \frac{2L_e}{15} \end{bmatrix}$$

$$[N2] = \begin{bmatrix} \frac{-1}{10L_e} & \frac{1}{5} & \frac{1}{10L_e} & \frac{-1}{10} \\ 0 & \frac{-L_e}{30} & 0 & \frac{L_e}{30} \\ \frac{11}{10L_e} & \frac{-1}{5} & \frac{-11}{10L_e} & \frac{-9}{10} \\ \frac{1}{10} & 0 & \frac{-1}{10} & \frac{-L_e}{10} \end{bmatrix}$$

$$[S1] = \begin{bmatrix} \frac{12}{L_e^3} & & \text{Symm.} & \\ \frac{-6}{L_e^2} & \frac{4}{L_e} & & \\ \frac{-12}{L_e^3} & \frac{6}{L_e^2} & \frac{12}{L_e^3} & \\ \frac{-6}{L_e^2} & \frac{2}{L_e} & \frac{6}{L_e^2} & \frac{4}{L_e} \end{bmatrix}$$

$$[S2] = \begin{bmatrix} \frac{-6}{5L_e} & \frac{11}{10} & \frac{6}{5L_e} & \frac{1}{10} \\ \frac{1}{10} & \frac{-2L_e}{15} & \frac{-1}{10} & \frac{L_e}{30} \\ \frac{6}{5L_e} & \frac{-1}{10} & \frac{-6}{5L_e} & \frac{-11}{10} \\ \frac{1}{10} & \frac{L_e}{30} & \frac{-1}{10} & \frac{-2L_e}{15} \end{bmatrix}$$

$$[T1] = \begin{bmatrix} \frac{1}{L_e} & \frac{-1}{L_e} \\ \frac{-1}{L_e} & \frac{1}{L_e} \end{bmatrix}$$

$$[T2] = \begin{bmatrix} \frac{-1}{2} & \frac{-L_e}{10} & \frac{1}{2} & \frac{L_e}{10} \\ \frac{L_e}{10} & 0 & \frac{-L_e}{10} & \frac{-L_e^2}{60} \\ \frac{-1}{2} & \frac{-L_e}{10} & \frac{1}{2} & \frac{-L_e}{10} \\ \frac{-L_e}{10} & \frac{L_e^2}{60} & \frac{L_e}{10} & 0 \end{bmatrix}$$

APPENDIX II EXECUTIVE CONTROL DECK, CASE CONTROL DECK AND BULK DATA DECK IN NASTRAN PACKAGE

```
$ Executive Control Deck Follows:

ID MSC
SOL 66
TIME 60
CEND

$ CASE CONTROL DECK FOLLOWS:

TITLE=ULTIMATE LOAD OF PIN-ENDED STRUT
SPC=5
SEALL=ALL
DISPLACEMENT=ALL
SPECFORCES=ALL
GPSTRESS=ALL
SUBCASE 1
LOAD=10
NLPARM=10
SUBCASE 2
LOAD=20
NLPARM=20
SPCFORCES=ALL
SUBCASE 3
LOAD=30
NLPARM=30
SUBCASE 4
```

```
LOAD=40
NLPARM=40
SUBCASE 5
LOAD=50
NLPARM=50
SUBCASE 6
LOAD=60
NLPARM=60
SUBCASE 7
LOAD=70
NLPARM=70
SUBCASE 8
LOAD=80
NLPARM=80
SUBCASE 9
LOAD=90
NLPARM=90
SUBCASE 10
LOAD=10
NLPARM=100
SUBCASE 11
LOAD=11
NLPARM=110
SUBCASE 12
LOAD=12
NLPARM=120
SUBCASE 13
LOAD=13
NLPARM=130

$BULK DATA FOLLOWS:

CBEAM   101     10      1       2       1.      1.      0.
CBEAM   102     10      2       3       1.      1.      0.
CBEAM   103     10      3       4       1.      1.      0.
CBEAM   104     10      4       5       1.      1.      0.
CBEAM   105     10      5       6       1.      1.      0.
```

```
FORCE   10      1       0       0.0     -1.     0.      0.
FORCE   20      1       0       0.0     -1.     0.      0.
FORCE   30      1       0       0.0     -1.     0.      0.
FORCE   40      1       0       0.0     -1.     0.      0.
FORCE   50      1       0       0.0     -1.     0.      0.
FORCE   60      1       0       0.0     -1.     0.      0.
FORCE   70      1       0       0.0     -1.     0.      0.
FORCE   80      1       0       0.0     -1.     0.      0.
FORCE   90      1       0       0.0     -1.     0.      0.
FORCE   100     1       0       0.0     -1.     0.      0.
FORCE   110     1       0       0.0     -1.     0.      0.
FORCE   120     1       0       0.0     -1.     0.      0.
FORCE   130     1       0       0.0     -1.     0.      0.
GRID    1       0       0.0     0.187   0.              345
GRID    2       0       18.7    0.129   0.              345
GRID    3       0       37.4    0.077   0.              345
GRID    1       0       56.1    0.036   0.              345
GRID    1       0       74.8    0.009   0.              345
GRID    1       0       93.5    0.      0.              123456
MAT1    10      +2.9+4          0.3
MATS1   20              PLASTIC 1.-5    1       1       3.6+3
NLPARM  10      1               AUTO            15      UP
NLPARM  20      1               AUTO            15      UP
NLPARM  30      1               AUTO            15      U
NLPARM  40      1               AUTO            15      U
NLPARM  50      1               AUTO            15      U
NLPARM  60      2               SEMI            15      U
NLPARM  70      1               SEMI            15      U
NLPARM  80      1               SEMI            15      U
NLPARM  90      1               SEMI            15      U
NLPARM  100     2               SEMI            15      U
NLPARM  110     1               SEMI            15      U
NLPARM  120     2               SEMI            15      U
NLPARM  130     2               SEMI            15      U
PARAM   LGDISP  1
PARAM   NLDISP  1
PARAM   POST    0
```

```
PBEAM      10                10          1.3          3.151     3.151
+Z1
+Z1                                      YES                    1.0
+Z4
+Z4        0.0       0.0
SPC        5         1       1345
SPCD       10        1       1         .032825
SPCD       20        1       1         .037274
SPCD       30        1       1         .054503
SPCD       40        1       1         .055
SPCD       50        1       1         .07
SPCD       60        1       1         .0725
SPCD       70        1       1         .075
SPCD       80        1       1         .0775
SPCD       90        1       1         .08
SPCD       100       1       1         .09
SPCD       110       1       1         .11
SPCD       120       1       1         .15
SPCD       130       1       1         .2
ENDDATA
```